AMINOPHENYL DOUBLE DECKER SILSESQUIOXANES: SPECTROSCOPIC ELUCIDATION, PHYSICAL AND THERMAL CHARACTERIZATION, AND THEIR APPLICATIONS

By

Beth Whitney Schoen

A DISSERTATION

Submitted to
Michigan State University
in partial fulfillment of the requirements
for the degree of

Chemical Engineering – Doctor of Philosophy

2013

ABSTRACT

AMINOPHENYL DOUBLE DECKER SILSESQUIOXANES: SPECTROSCOPIC ELUCIDATION, PHYSICAL AND THERMAL CHARACTERIZATION, AND THEIR APPLICATIONS

By

Beth Whitney Schoen

The incorporation of cage-like silsesquioxanes (SQ) to form polymers has demonstrated property enhancements in areas such as: thermal and mechanical characteristics, flame retardance, dielectric properties, and oxidative resistance. However, with most hybrid polymers investigated, the attached SQs are pendant with respect to the polymer backbone. A recently developed class of these nano-structured, cage-like silsesquioxanes, formally known as double decker silsesquioxanes (DDSQ), offers the opportunity to form hybrid polymers with SQ cages as a part of the polymer backbone. However, during the capping reaction, these functionalized DDSQs generate *cis* and *trans* isomers with respect to the 3D Si-O core. Therefore, it is logical to characterize properties, which will allow for optimization of capping reaction parameters, particularly if one isomer is favored over the other. Moreover, these characteristics are also relevant when reacting or incorporating these isomers, or mixtures thereof, with other molecules to form novel materials.

In this dissertation, three aminophenyl DDSQs were synthesized. More specifically, two meta- aminophenyl DDSQs, which were differentiated according to the moiety attached to the D-Si (methyl or cyclohexyl), and one para-aminophenyl DDSQ with a methyl moiety were used. Chemical, physical, and thermal characteristics were evaluated for individual isomers as well as binary mixtures of different *cis/trans* ratios.

The ^{1}H NMR spectra of the *cis* and *trans* isomers of these DDSQ had not previously

been assigned to a degree that allowed for quantification, which was necessary for these studies. Thus, ^{1}H–^{29}Si HMBC correlations were applied to facilitate ^{1}H spectral assignments and also to confirm previous ^{29}Si assignments. Using ^{1}H NMR not only saves time and material over ^{29}Si NMR, but also provides a more accurate quantification, thus allowing for the ratio of *cis* and *trans* isomers present in each compound to be determined.

Solubility behavior was investigated for the individual isomers, such that separation techniques could be developed. It was found that *cis* isomers were 33 times more soluble than *trans* isomers for para-aminophenyl (R = methyl), and 22 times more soluble for the analogous meta-aminophenyl in a solution of THF and hexanes. For a more sterically hindered meta-aminophenyl (R = cyclohexyl), *cis* isomers were only 3.5 times more soluble, and the overall solubility was also the lowest.

Phase diagrams representing solid-liquid melt equilibria of the binary *cis/trans* mixtures were developed. Single crystal x-ray diffraction data of isolated isomers helped to interpret the phase behavior. Both compounds with a methyl moiety exhibited eutectic phase diagrams. Their *trans* isomers were higher melting and exhibited larger packing density. Changing from para- to meta-aminophenyl shifted the solid-liquid equilibrium further from ideal, with decreased activity coefficients. Cyclohexyl DDSQ exhibited an isomorphic phase diagram (a complete solid-solution), attributed to cyclohexyl being more similar in size to the phenyl moieties.

A specific application that was chosen for these DDSQ was high performance thermosetting oligoimides. They displayed advantages over their organic counterparts in areas such as the liquid to solid transition and viscosity, which improves the processing window. Additionally, they increased the overall degree of cross-linking leading to improved oxidative stability at elevated temperatures.

This doctoral dissertation is dedicated to my Father, Howard Gilbert Schoen (05.14.1943-11.27.1999). His love for science was instilled in me. May his memory be a blessing to all.
זכרונו לברכה

ACKNOWLEDGMENTS

The completion of my doctoral dissertation would not have been possible without the help and guidance of so many individuals. First, and foremost I would like to thank my advisor, Professor Andre Lee. When I began working for him, just four years ago, I was not the researcher that I have become today. Throughout these years, he has sought to create an environment of independence and critical-thinking, which has allowed me to take ownership of my research and pursue experiments that I find to be important.

I would also like to thank each person on my guidance committee individually, beginning with Professor Melissa Baumann, who was my co-advisor for 3.5 years of my dissertation. She was always there to push me forward and provide additional insight on research problems. She also introduced me to other facets of research, encouraging me to expand my area of expertise and think outside the box.

Next, I would like to thank my committee member, Professor Robert Maleczka Jr., for his incessant encouragement in organic chemistry. Without his help and guidance, I would not have had access to so many organic chemists, chemistry facilities, and learning opportunities. I like to think of his class that I took as one of the turning points in my Ph.D studies. It encouraged me to continue taking and succeeding in the organic chemistry doctoral courses, although they were not easy and I was already finished with my course requirements, throughout my Ph.D studies. Additionally, I cannot express my gratitude towards him allowing me to attend and take part in presenting at his weekly group meetings. His encouragement for all that I have mentioned contributed greatly towards the understanding necessary for the synthetic aspect of my dissertation, and opened doors to observe research outside my area that would not have been available otherwise.

I would also like to thank my committee member, Professor Carl Lira, for his persistent reassurance and instruction with MatLab and computer programming. He has spent endless hours with me teaching me how to use MatLab for modeling purposes and even more time going over the results for our recently submitted paper for publication. As a teaching assistant for him in thermodynamics, I was able to further expand my thermodynamics knowledge and apply this to my dissertation. I appreciate all the time he took out of his already busy schedule for me and how he was able to make very difficult problems seem easy. His contributions to the thermodynamics portion of my dissertation are innumerable.

My final committee member is Professor Dennis Miller. I would like to thank him for his positive reinforcement and encouragement throughout my Ph.D studies. His door was always open for any questions that I had. I also learned a great deal from him as a teaching assistant, and would seek advice from him regarding my teaching experiences in the last four years. Outside of academia, Professor Miller was also available and I would like to express my deepest gratitude towards him for this. Specifically, I would like to thank him for playing volleyball with me and several other graduate students throughout my time at Michigan State University; we could not have won the intramural championship without you!

I would also like to thank Daniel Holmes, Ph.D for the countless hours he spent teaching me about Nuclear Magnetic Resonance and his assistance in interpreting my results. Basically, I could not have completed my chapter 2 without his help, and greatly appreciate all the time he spent reviewing my paper for our publication. I would also like to thank him for his help with my cover letters for my post-doctoral applications, and any other writing assignments that I requested.

I would also like to express gratitude for the numerous hours that Richard Staples, Ph.D spent with me teaching me the ins and outs of single crystal X-ray Diffraction. His assistance with growing crystals and interpreting the results has contributed tremendously to my chapter 4 and the current article we are working on for publication. Additionally, he was always available for my myriad of questions and helped me gain an understanding for the structural implications of my molecules.

I would also like to thank Professor Aaron Odom and his research group for allowing me to use space in his laboratory and graduate student office to complete my dissertation studies. This helped me tremendously to finish my synthetic work and was especially beneficial to have access to his group members when I had questions regarding specific synthetic procedures.

Additionally, I would like to thank Tim Haddad (Ph.D, AFRL), Air Force Research Labs (Edwards, Air Force Base), and my funders the Air Force Office of Scientific Research (grant number FA9550-08-1-0213. I would not have developed my foundation in organic chemistry had it not been for the countless hours that Tim spent with me teaching me the basics of the synthetic procedures for my reactions.

I would also like to thank several other people; including Gina Comiskey for taking time out of her busy schedule in the final two years of her dissertation to teach me how to synthesize polymers. Also, I would to thank Brad Seurer for introducing me to my project and teaching me the basics during his time as a postdoctoral researcher in my research group. Additionally, I would like to thank several other friends and undergraduate research assistants that at some point helped me with various aspects of my dissertation including: thermodynamics, MatLab, reviewing chapters, and learning experimental procedures. These people are: Annie Lown, Arati Santhanakrishnan, David Olson, Nate Leonard, Bria Kamdem, and Jake Finkbiner. I would like

to thank all my other friends and my research group for their continuous support and encouragement throughout this time period, and for lack of space I cannot mention all your names, but I am sure you know who you are.

Last, but certainly not least, I would like to thank my family, specifically my sisters (Jill, Leah, and Marly) and my mother (Shelley Schoen) for their unremitting support and encouragement throughout my Ph.D. I thank them all for understanding why I could not come on all the family vacations and home for the holidays, especially during my last year of my doctoral studies. Most of all, I would like to thank my mother for just being herself. Without her I would not have gotten as far as I have today. Throughout my life, she has always been there for me and supported me in everything I endeavor to achieve.

TABLE OF CONTENTS

LIST OF TABLES

LIST OF FIGURES

LIST OF SCHEMES

KEY TO SYMBOLS AND ABBREVIATIONS

Common Acronyms

SQ silsesquioxane

- sil silicon
- sesqui each silicon atom is bound to an average of 1.5 oxygen atoms
- ox oxygen
- ane each silicon atom is bound to one hydrocarbon group

DDSQ	double decker silsesquioxane
SLE	solid-liquid equilibrium
LLE	liquid-liquid equilibrium
MW	molecular weight
NRTL	non-random two liquid
HPM	high performance material
PEPA	phenylethynylphthalic anhydride
PEPI	phenylethynylphthalic imide
PETI	phenylethynyl-terminated polyimide oligomer
Mmv	minimum viscosity
PPD-T	poly(para-phenylene terephthalamide); Kevlar®
MPD-I	poly(meta-phenylene isophthalamide); Nomex®
MDA	meta-diamines
PDA	para-diamines
PCL	phthaloyl chloride

H-bond	hydrogen bond
IL	ionic liquid

Common Apparatuses

DSC	differential scanning calorimetry
XRD	x-ray diffraction
NMR	nuclear magnetic resonance
TGA	thermal gravimetric analysis
GPC	gel permeation chromatography

Common Symbols

T_g	glass transition temperature
T_m	crystalline melting transition temperature
T_d	degradation temperature
T_r	recrystallization temperature upon heating
T_c	crystallization temperature upon cooling
T_E	eutectic temperature
$T_{m\text{-}E}$	meta-stable eutectic temperature
T_P	peritectic temperature
γ	activity coefficient
ΔC_p	heat capacity
ΔH_m	heat of fusion; enthalpy of the melt transition
ΔS_m	entropy of fusion

ΔH_c enthalpy of the crystallization transition

CHAPTER 1

INTRODUCTION

Keywords
double decker silsesquioxane, cis/trans isomers

1. Introduction

1.1 Overall goal

The goal of this Ph.D. dissertation was to develop a fundamental understanding of a class of double decker silsesquioxane (DDSQ). This understanding was obtained through examining how configurational and structural modifications to these macromolecules influence chemical and physical characteristics. An appropriate structure to property relationship was established for the selected DDSQ (Figure 1-1) and was ultimately applied to create novel engineering designs.

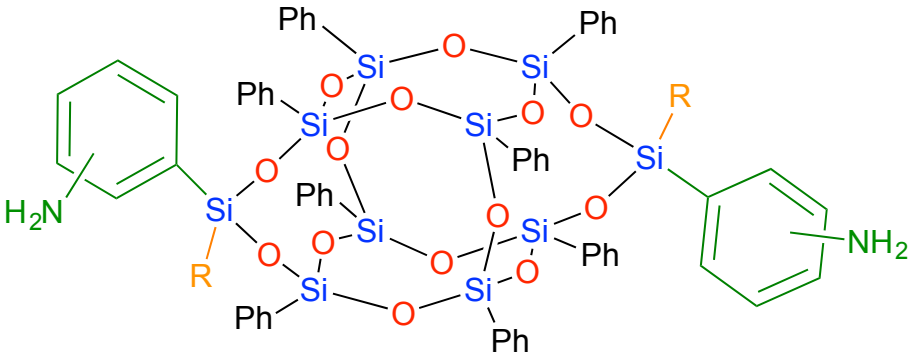

Figure 1-1. Double Decker Silsesquioxane (DDSQ). For interpretation of the references to color in this and all other figures, the reader is referred the reader is referred to the electronic version of this dissertation.

1.2 Motivation

Hybrid inorganic/organic nano-structures play a significant role in the advancement of new technology through the development of a large variety of new materials, such as: polymers,[1] sensors,[2] fuel cells,[3] semi-conductors,[4] catalysts,[5] and biological materials.[6] Furthermore, they provide a synergistic combination of the flexibility and reactivity of organic networks with the excellent thermal and mechanical properties of inorganics. Three-dimensional (3D) nano-structures such as fullerenes,[7] oxo/alkoxide transition metal clusters,[8] and cage-like

silsesquioxanes[9] increase the surface area of the hybrid segments when incorporated into any of these materials, which can enhance these hybrid affects. Of these 3D architectures, cage-like silsesquioxanes are the easiest to functionalize and purify, do not contain toxic transition metals, and display mono-dispersed physical and chemical characteristics.[9] Superior properties over their organic polymers have been displayed by these cage-like silsesquioxanes in areas such as: solubility,[10-12] thermal and mechanical properties,[13-15] flame retardance,[16-18] dielectric properties,[19-21] and oxidative resistance[22-24]. However, with most hybrid polymers investigated, the attached SQs are pendant with respect to the polymer backbone. A recently developed class of these nano-structured cage-like silsesquioxanes, formally known as double decker silsesquioxanes (DDSQ) offers the opportunity to form hybrid polymers with SQ cages as a part of the polymer backbone.[25] During the capping reaction, these functionalized DDSQs generate *cis* and *trans* isomers with respect to the 3D Si-O core (Figure 1-2). Therefore, it is logical to

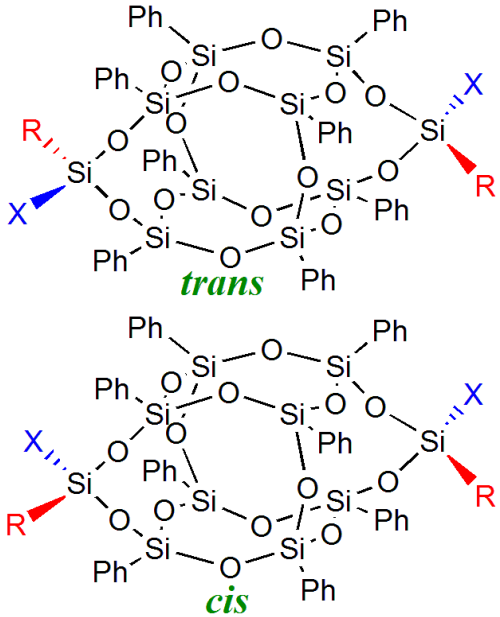

Figure 1-2. *Trans* and *cis* isomers of DDSQ.

derive explicit understandings for the characteristics of the individual isomers, which will allow for optimization of capping reaction parameters, particularly if one isomer is favored over the other. Moreover, these characteristics are also relevant when reacting or incorporating these isomers, or mixtures thereof, with other molecules to form novel materials. Consequently, a structure/property relationship becomes essential. Therefore, the motivation of this thesis was to develop an appropriate structure/property relationship for these DDSQ, thus making it possible to systematically enhance material properties from a bottom-up approach.

The particular reactive moiety (X) in Figure 2 of these DDSQ not only has a significant impact on the characteristics of the molecule itself, but it also limits the applications. An aminophenyl moiety (Figure 1-1) was selected for this dissertation as the specific reactive moiety for the following reasons:

1. The aminophenyl moiety can be thought of as a reactive version of the phenyl moieties attached to each silicon atom.
2. The amine is particularly reactive and has been used in the development for a variety of applications of engineering importance in areas such as: high performance polymers,[26] ionic-liquids,[19] photochemistry,[27] and catalysis[28].

1.3 Fundamental Idea and Specific Aims

The fundamental idea of this dissertation was to use a thermally stable, functionalized double-decker silsesquioxane (DDSQ) that can be chemically modified, and develop a structure/property relationship based upon the altered properties of the modified structure. This study has addressed fundamental questions regarding how the isomers of functionalized DDSQ monomers impact their chemical, physical, and structural properties, thus allowing for the logical

introduction of regio- and diastereo-isomeric functionality, providing for novel engineering designs. Specific aims of this project include:

1. Careful design and analysis of the synthetic procedures of selected DDSQ.
2. Spectroscopic elucidation of the stereoisomers of each DDSQ for quantification.
3. Determining solubility limits and investigating solubility behavior of the individual isomers, such that concise separation techniques could be developed.
4. Development of phase diagrams representing the solid-liquid melt equilibria of the individual isomers and binary mixtures.
5. Exploring material applications based on the DDSQ from this work.

Quantifiable structure-property-performance relationships of DDSQ molecules were developed based on the specific regio- and diastereo-isomers. This research endeavored to advance the general understanding of how introducing isomerism influences three-dimensional macromolecular assemblies: including fullerenes, carboranes, and oxo/alkoxide transition metal clusters. After this work was completed, a fundamental structure/property relationship was developed from this bottom-up approach to chemical engineering and materials science.

REFERENCES

REFERENCES

(1) Allcock, H. R. *Advanced Materials* **1994**, *6*, 106.

(2) Wang, S.; Kang, Y.; Wang, L.; Zhang, H.; Wang, Y.; Wang, Y. *Sensors and Actuators B-Chemical* **2013**, *182*, 467.

(3) Laberty-Robert, C.; Valle, K.; Pereira, F.; Sanchez, C. *Chemical Society Reviews* **2011**, *40*, 961.

(4) Zhao, L.; Lin, Z. *Advanced Materials* **2012**, *24*, 4353.

(5) Diaz, U.; Brunel, D.; Corma, A. *Chemical Society Reviews* **2013**, *42*, 4083.

(6) Kellermeier, M.; Coelfen, H.; Manuel Garcia-Ruiz, J. *European Journal of Inorganic Chemistry* **2012**, 5123.

(7) Sergio, M.; Behzadi, H.; Otto, A.; van der Spoel, D. *Environmental Chemistry Letters* **2013**, *11*, 105.

(8) Turova, N. Y. *Uspekhi Khimii* **2004**, *73*, 1131.

(9) Hartmann-Thompson, C.; SpringerLink (Online service) In *Advances in Silicon Science,*; Springer Netherlands,: Dordrecht, 2011, p XXVII.

(10) Gnanasekaran, D.; Reddy, B. S. R. *Polymer Composites* **2012**, *33*, 1197.

(11) Guenthner, A. J.; Lamison, K. R.; Lubin, L. M.; Haddad, T. S.; Mabry, J. M. *Industrial & Engineering Chemistry Research* **2012**, *51*, 12282.

(12) Rizvi, S. B.; Yildirimer, L.; Ghaderi, S.; Ramesh, B.; Seifalian, A. M.; Keshtgar, M. *International journal of nanomedicine* **2012**, *7*, 3915.

(13) Yang, B.; Li, M.; Wu, Y.; Wan, X. *Polymers & Polymer Composites* **2013**, *21*, 37.

(14) Wu, S.; Hayakawa, T.; Kakimoto, M.; Oikawa, H. *Macromolecules* **2008**, *41*, 3481.

(15) Wu, J.; Mather, P. T. *Polymer Reviews* **2009**, *49*, 25.

(16) Fan, H.; Yang, R. *Industrial & Engineering Chemistry Research* **2013**, *52*, 2493.

(17) Rakesh, S.; Dharan, C. P. S.; Selladurai, M.; Sudha, V.; Sundararajan, P. R.; Sarojadevi, M. *High Performance Polymers* **2013**, *25*, 87.

(18) Vahabi, H.; Eterradossi, O.; Ferry, L.; Longuet, C.; Sonnier, R.; Lopez-Cuesta, J. M. *European Polymer Journal* **2013**, *49*, 319.

(19) Cardiano, P.; Lazzara, G.; Manickam, S.; Mineo, P.; Milioto, S.; Lo Schiavo, S. *European Journal of Inorganic Chemistry* **2012**, 5668.

(20) Geng, Z.; Ba, J.; Zhang, S.; Luan, J.; Jiang, X.; Huo, P.; Wang, G. *Journal of Materials Chemistry* **2012**, *22*, 23534.

(21) Ke, F.; Zhang, C.; Guang, S.; Xu, H. *Journal of Applied Polymer Science* **2013**, *127*, 2628.

(22) Vila Ramirez, N.; Sanchez-Soto, M. *Polymer Composites* **2012**, *33*, 1707.

(23) Jin, L.; Ishida, H. *Polymer Composites* **2011**, *32*, 1164.

(24) Blanco, I.; Abate, L.; Bottino, F. A.; Bottino, P. *Polymer Degradation and Stability* **2012**, *97*, 849.

(25) Takashi, K.; Takashi, K.; Masaya, I.; Kazuhiro, Y.; Yasuhiro, Y. Japan, 2006.

(26) Garcia, J. M.; Garcia, F. C.; Serna, F.; de la Pena, J. L. *Progress in Polymer Science* **2010**, *35*, 623.

(27) Slegt, M.; Overkleeft, H. S.; Lodder, G. *European Journal of Organic Chemistry* **2007**, 5364.

(28) Wang, L.; Du, W.; Wu, Y.; Xu, R.; Yu, D. *Journal of Applied Polymer Science* **2012**, *126*, 150.

CHAPTER 2

BACKGROUND INFORMATION

Keywords

double decker silsesquioxane, NMR, cis/trans isomers, separations, phase diagrams, eutectic, isomorphous, polyamide, polyimide

2. Background Information

This section includes information on the following topics: *section 2.1* outlines general information on silsesquioxane (SQ) macromolecules. *Section 2.2* discusses the necessity of spectroscopic elucidation using ^{1}H-NMR spectra. *Section 2.3* examines information relevant to isomer separation techniques. *Section 2.4* explores the impact of molecular structure on melting temperatures, melting enthalpies, solidification, crystallization, and solubility. Finally, *section 2.5* highlights the motivation for the selected material applications.

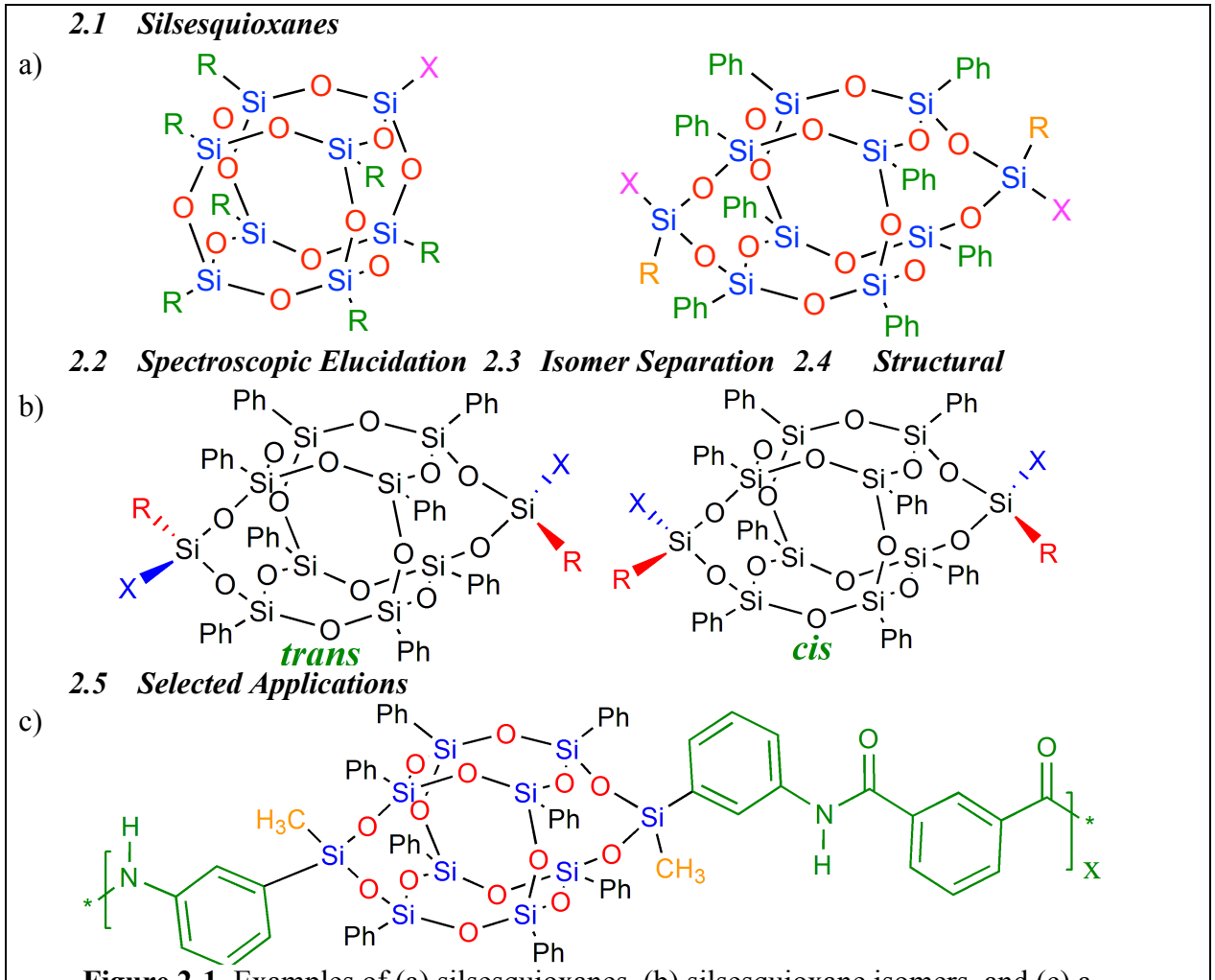

Figure 2-1. Examples of (a) silsesquioxanes, (b) silsesquioxane isomers, and (c) a silsesquioxane application.

2.1 Silsesquioxanes

Fully condensed cage-like SQs with different functionalities have revealed superior performance over their organic counterparts in areas such as: thermal and mechanical properties,[1-4] flame retardance,[5-13] solubility,[14-16] oxidation resistance,[17-20] and dielectric properties.[21-23] These benefits are mostly attributed to molecular level reinforcement, and the ceramic-like properties of the inorganic cage.[24] SQs are comprised of covalently bonded oxygen to silicon atoms in a three to two (sesqui) ratio. Additionally, each silicon atom is covalently bonded to an organic peripheral group (R), which allows these molecules to interact with themselves, or other organics in the medium (Figure 2-2).[25] Additionally, one or more of these peripheral groups can be modified to make the molecule reactive.

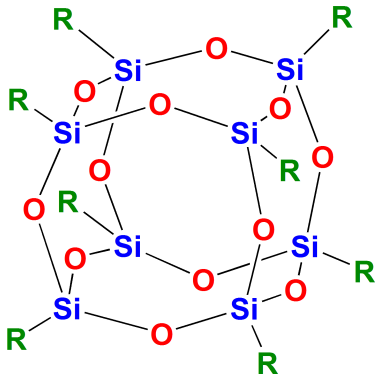

Figure 2-2. Cage-like silsesquioxane.

It has been demonstrated that the incorporation of SQs into material systems decouples strength from toughness, while simultaneously providing the same or better thermal and mechanical properties, as a result of the inherent flexibility of the Si-O cage.[26,27] This feature has been exploited to decrease stiffness in brittle polymers. Furthermore, SQs are easy to functionalize, and incorporate into material systems. The combination of all these features distinguishes SQs from other three-dimensional macromolecular assemblies, which tend to be

stiff and/or difficult to functionalize, including: fullerenes, carboranes, and oxo/alkoxide transition metal clusters.

An entire background in the field of SQs would require a published volume, and is beyond the scope of this dissertation. Therefore, several SQs have been selected to demonstrate advances in this field and are presented in the following sections. For a more detailed review, the reader is encouraged to refer to a recently published volume on cage-like SQs.[28]

2.1.1 Monofunctionalized

2.1.1.1 Corner-capped SQ

Corner capping is the most common method for modifying one of the peripheral groups on a cage-like SQ. Corner capping is accomplished through reacting a trisilanol SQ with a trichlorosilane, dimethoxysilane, diethoxysilane, or a silane with two similar leaving groups (Scheme 2-1).[29] In a corner-capped SQ, an R-moiety is replaced by an X- (or reactive) moiety. These structures are also known as a monofunctionalized SQ, since only one R-moiety is replaced. Specific R-moieties that have been functionalized by corner capping include:

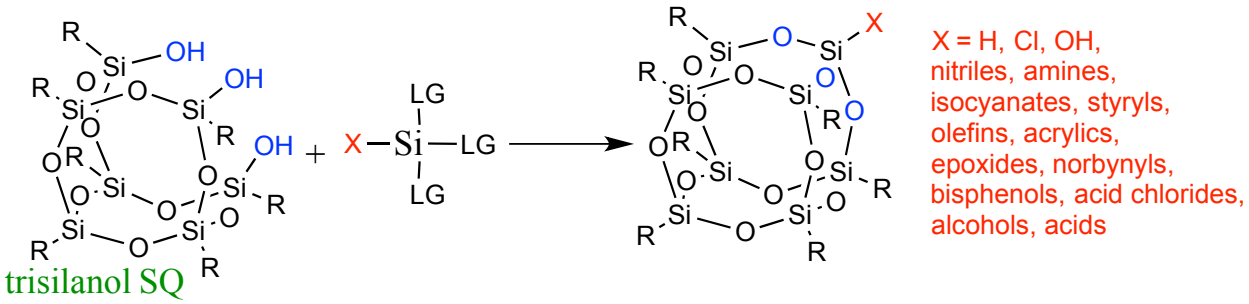

Scheme 2-1. Synthetic Scheme for corner capping a trisilanol SQ; LG can be a variety of leaving groups including: Cl, OMe, OEt; R can be: Phenyl, cyclohexyl, cyclopentyl, isobutyl, isooctyl.

hydride, chloride, hydroxide, nitriles, amines, isocyanates, styryls, olefins, acrylics, epoxides, norbornyls, bisphenols, acid chlorides, alcohols, acids.[29] Specific functionalized corner-capped SQs have been used in many applications (Table 2-1, Figure 2-3). Particularly, the addition of corner-capped SQs into organic monomers and polymers has realized an increase in glass transition (T_g), melting (T_m), and decomposition (T_d) temperatures, and increases in the shear storage modulus (E′) (Table 2-1, Figure 2-3). It has been suggested that the bulky, inorganic SQ cages retard segmental motion of the polymers through interchain interaction.[29]

Table 2-1. Thermal-mechanical data for examples of monofunctionalized, corner-capped SQs.

	Compound	Mol % SQ	T_g (°C)	T_m (°C)	T_d (°C)	E' (Pa)
Homopolymer	A[30]	-	396	-	445	-
Copolymer	B[30]	9	132	-	402	> 1000*
Organic Polymer	poly(4-methylstyrene)	-	116	-	-	14.45*
Homopolymer	C[31]	-	None[+]	None[+]	388	-
Organic Polymer	PMMA	-	43-163	-	200	-
Copolymer	D[32]	7.7	81	-	-	-
Organic Polymer	polynorbornene	-	52.3	-	-	-
Copolymer	E[33]	0.7	-	125	410[^]	-
Organic Polymer	polyethylene	-	-	132	313	-
Monomer	F[34]	-	None	270	-	-
Organic Monomer	propyl amine	-	None	- 83	-	-
Copolymer	F[34]	2.5	80	~ 200	-	> 300[#]
Organic Polymer	Nylon 6	-	65	~ 200	-	225
Copolymer	G[35]	20	-45	-	355[**]	-
Organic Polymer	poly(ethylene imine)	-	- 51	-	355	-
Copolymer	H[36]	3.2	245.3	-	-	-
Organic Polymer	PHS-PVP	-	194.9	-	-	-

* Frequency = 0.1 rad/s and T = 180 °C. [+] None observed between 0 – 400 °C. [^] 30 % weight loss under air. [#]Frequency = 1 Hz and T = 100 °C. ** Although Td is similar, the rate for the SQ containing polymer is much lower. [^^]PHS-PVP: poly(hydroxystyrene-co -vinylpyrrolidone-co isobutylstyryl. For additional examples please see the following reference: [28]

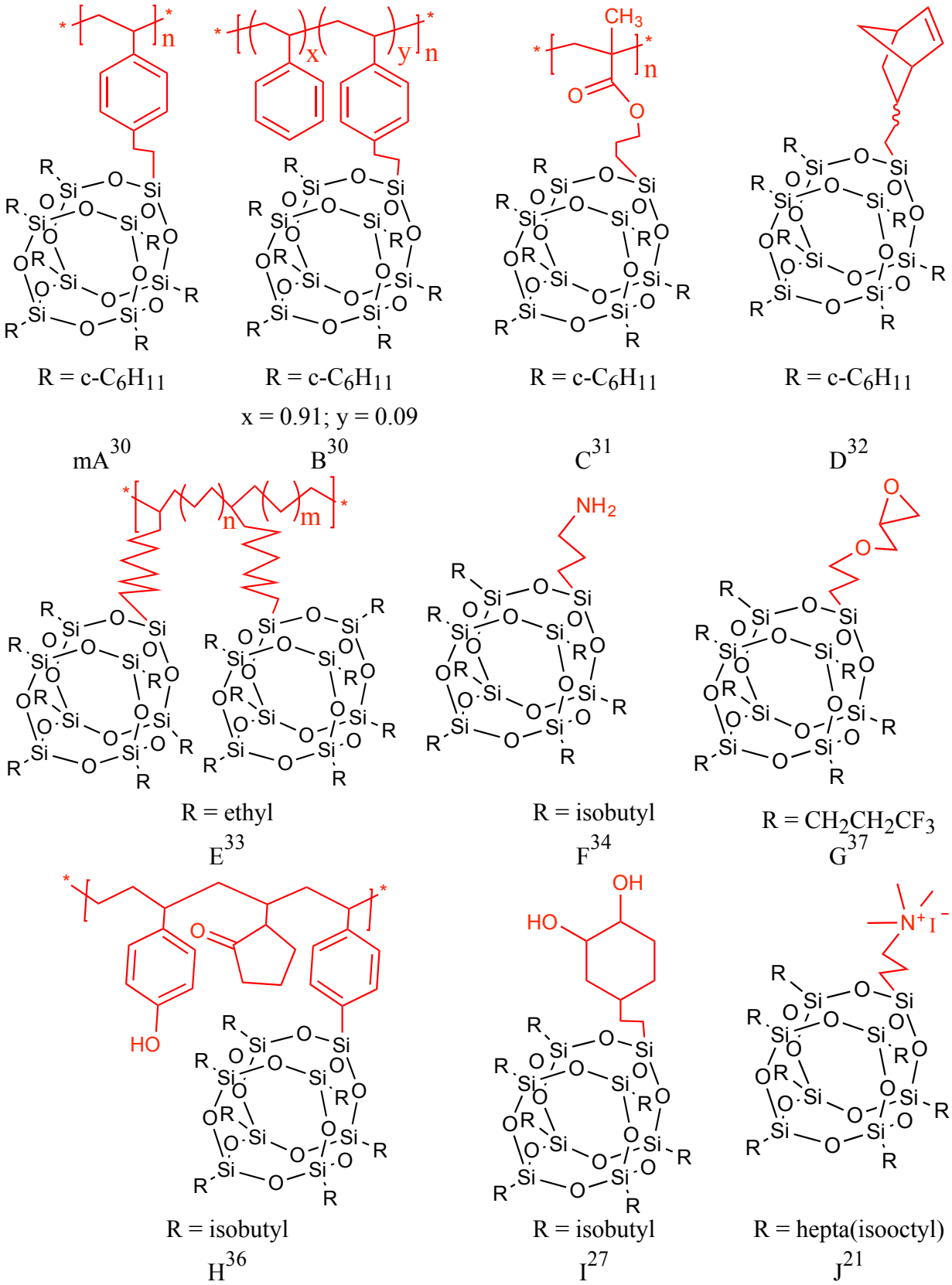

Figure 2-3. Selected examples of monofunctionalized, corner-capped SQs.

In addition to have a higher decomposition temperature, polymers with corner-capped SQs also exhibit a decrease in decomposition rate. Upon degradation, the organic groups of SQs initially degrade rapidly, but do not volatize (Table 2-1, Figure 2-3). Instead, they form an effective char-like coating on top of the still intact Si-O cage, providing extra protection.[38] This is specifically useful in increasing the limiting oxygen intake (LOI), or the volume fraction of oxygen necessary for a material to sustain combustion,[39] for flame retardant applications.

SQs have also been incorporated into polyurethane (PU) polymers (e.g. I, Figure 2-3) for use in vascular prostheses.[27] These SQ-PUs have demonstrated increased endothelial cell adhesion, proliferation, and growth, while displaying no significant increase in toxicity. Moreover, these SQs provide flexibility and further stabilize the prostheses. Additional biomedical applications include, but are not limited to: SQs for drug delivery[40,41] and scaffolds for tissue engineering.[42-47]

Furthermore, SQs have low dielectric constants. This feature has been exploited in applications relating to electronics and energy.[28] Recently, these latter properties have been advantageous in the design of a corner-capped SQ for potential use in fuel cells, which displays characteristics of an ionic liquid (e.g. J, Figure 2-3).[21]

2.1.1.2 Side-capped SQs

Another form of monofunctionalized cage-like SQs are side-capped SQs. These are synthesized through the reaction of a disilanol and a dichlorosilane (Scheme 2-2). Although the potential of side-capped SQs have been reported in the literature, there have not been significant applications based on this synthetic method.[28]

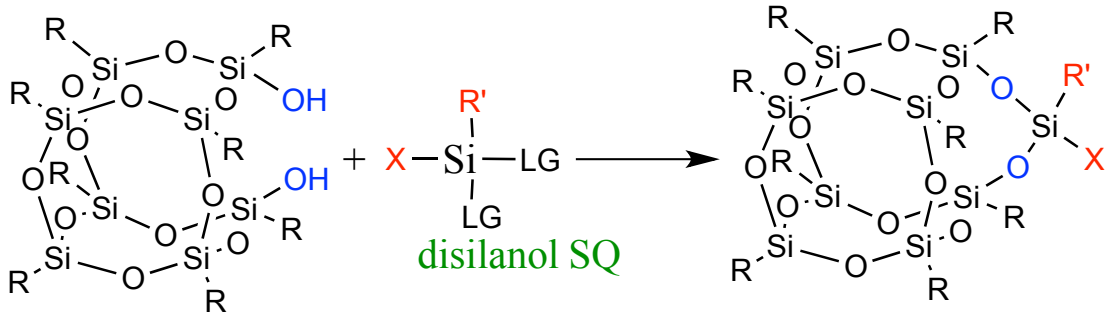

Scheme 2-2. Synthetic pathway to a side-capped SQ through the reaction of disilanol and silane with two LGs.

2.1.2 Difunctionalized SQs

Difunctionalized SQs have appeared more recently in the literature.[2,3,48-54] There are three major silanol starting materials that have been used to synthesize difunctional SQs, including: two types of disilanol SQs,[48,54] and one type of tetrasilanol[25] (Scheme 2-3).

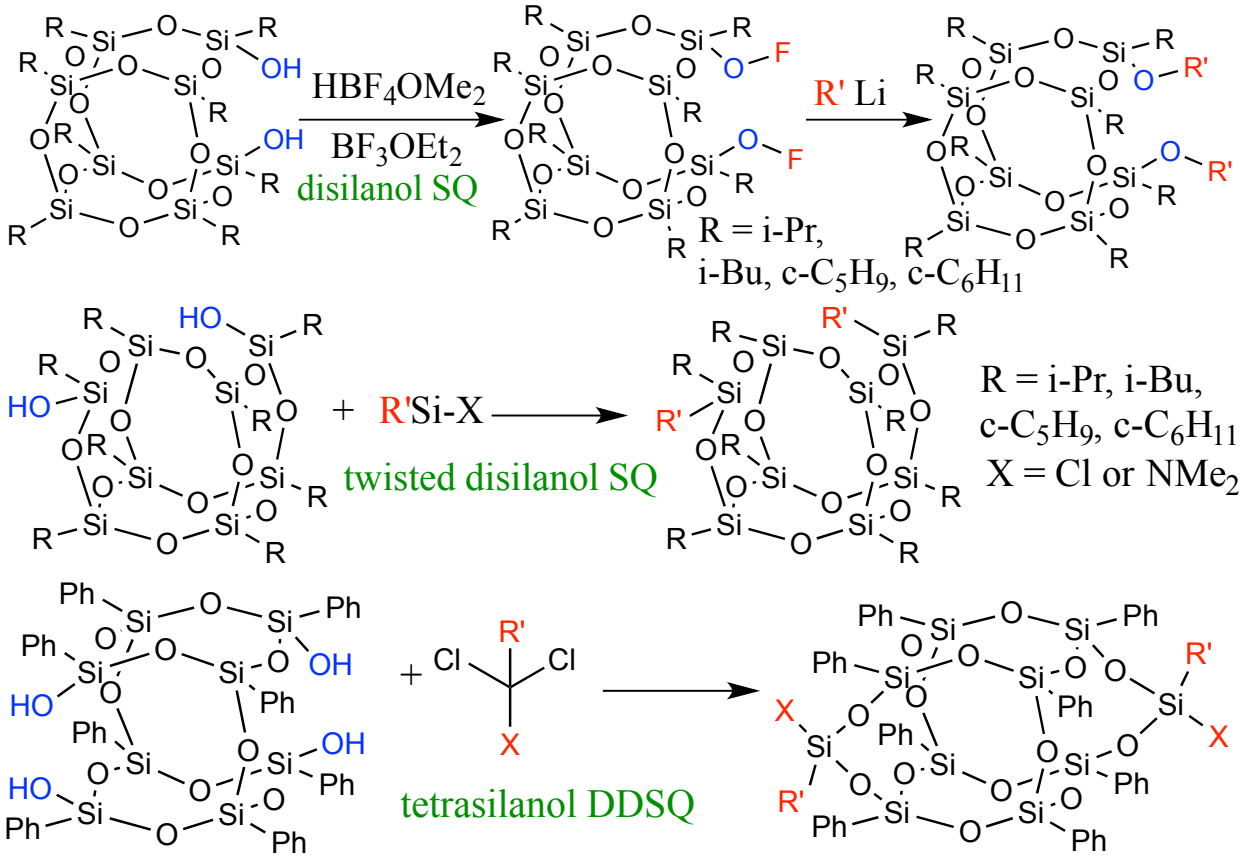

Scheme 2-3. Synthetic schemes for difunctionalized SQs.

Difunctional SQs are unique for their ability to become part of the main chain of a polymer, and have been called "beads" on a chain when polymerized,[54] whereas monofunctional SQs are pendant to the backbone of a polymer chain.

Difunctional SQs synthesized from disilanol SQ have mostly been used for space applications (Figure 2-4).[28] These SQs have been incorporated into the polyimide Kapton ® to provide additional protection in lower Earth orbit to atomic oxygen (AO) for spacecraft applications. Polymers based on SQs have demonstrated 10 times higher durability than neat Kapton ®, which has the highest resistance of conventional polymers towards active AO. Similarly to thermal degradation, when these SQs are exposed to AO their organic groups degrade and a silica (SiO_2) layer is preserved, providing protection from degradation to the

degrade and a silica (SiO_2) layer is preserved, providing protection from degradation to the

underlying polymer.[50] The erosion yield of the SQ-Kapton ® is as low as ~ 0.01 that of neat Kapton ®, depending on the weight % of SQ in the polymer.

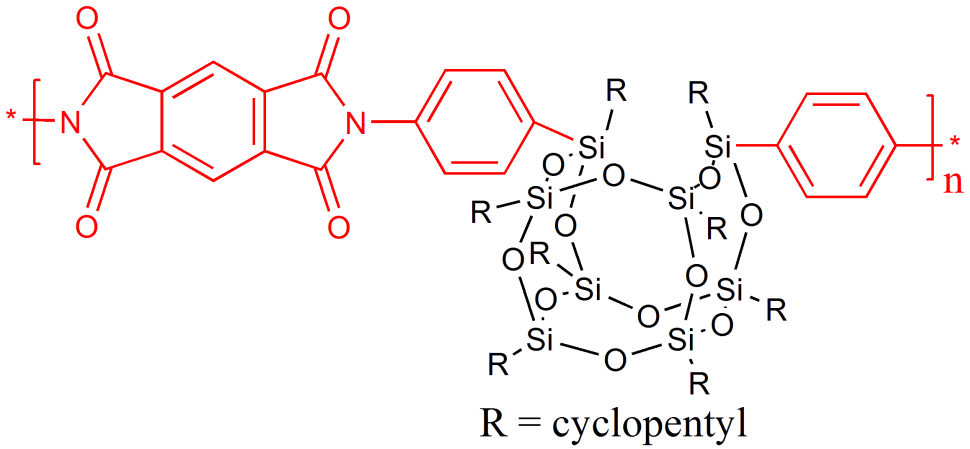

Figure 2-4. Example of a difunctionalized SQ from a disilanol.

The remaining two difunctionalized SQs are unique when compared to all other SQs mentioned so far. They are the only SQs capable of having isomers about the Si-O cage (Figure

2-5). The first is called “twisted SQ” since the cage itself is twisted when compared to the other disilanol, and there is an extra oxygen atom linking two silicon atoms that were not previously bounded to one another. The second is formally known as double decker silsesquioxane (DDSQ)

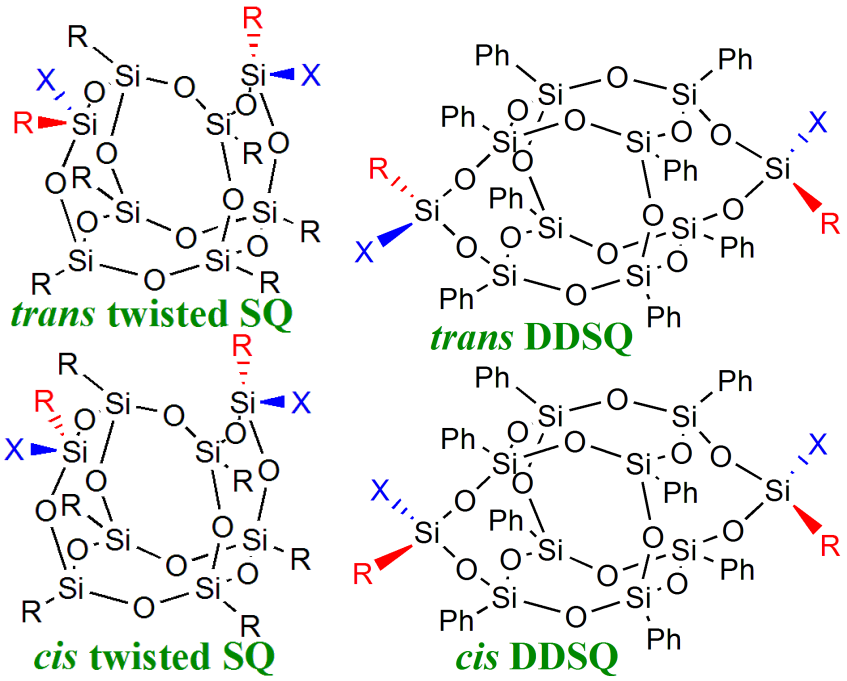

Figure 2-5. Isomers of difunctionalized SQs.

because it is comprised of two “decks” of silsesquioxanes stacked on top of one another.[55] Twisted SQs are difficult to synthesize in large quantities. However, there have been a few functionalized twisted SQ polymers that have been synthesized (Figure 2-6). The T_d was significantly increased for A, T_d = 490 °C, as compared to poly(dimethyl)siloxane where the T_d = 350 °C.[56] Twisted SQs have mostly been synthesized to contain organometallic, or inorganic segments (e.g. B). This demonstrates the first rational synthetic construction of SQ polymers to linearly contain transition metals in the structure, and proved that air/moisture stable materials could be designed. However, due to the difficulty of scale-up for twisted SQs, research in this area is not prevalent.

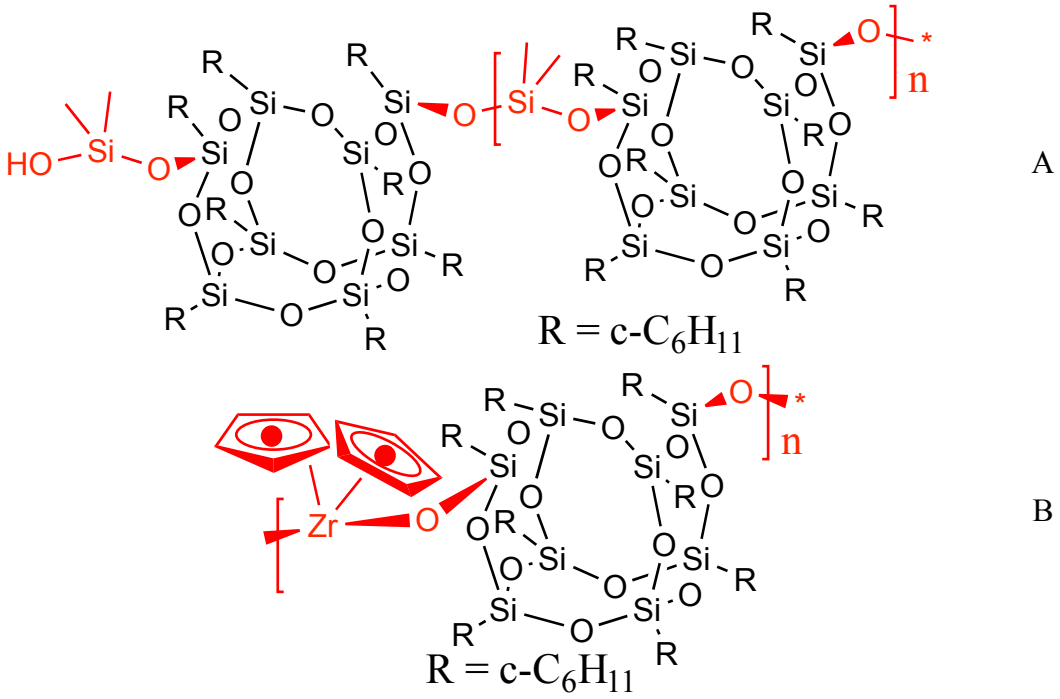

Figure 2-6. Twisted SQ polymers.

2.1.2.1 Double decker silsesquioxanes (DDSQ)

DDSQs can be easily synthesized in large quantities, incorporated into a polymer backbone, and have *cis* and *trans* isomers about the Si-O cage. These attributes make it attractive for material applications where rational control of properties is desired. Several fully condensed DDSQs have been synthesized (Figure 2-7) according to the previous schematic (Scheme 2-3).

Currently, only tetrasilanol with phenyl (Ph) moieties is synthetically available. DDSQs have also been synthesized to encapsulate metal nanoparticles similar to twisted SQs structures; however, that is beyond the scope of this dissertation and interested persons are encouraged to consult the literature for information regarding these materials.[57,58]

These DDSQ structures (A-D) were further reacted in order to incorporate into co-polymer systems (Figure 2-8 through Figure 2-17). Compound A (Figure 2-7) was used to synthesize polymer AA (Figure 2-8) as a potential substrate for lightweight, microelectronic devices.[59] However, in order for this application to be feasible, the hydrophobic surface of films

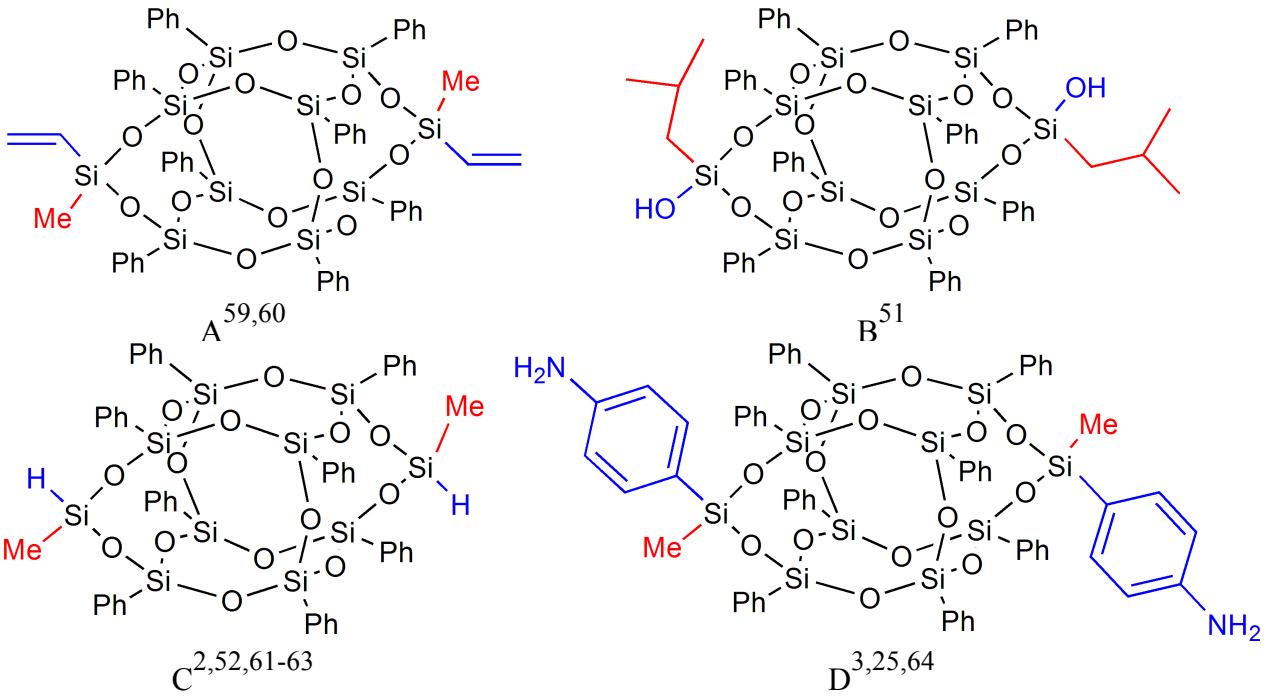

Figure 2-7. Fully condensed DDSQ structures.

made from polymer BA had to be made hydrophilic. This was accomplished by exposure to deep UV light, which allowed the formation of silanol (Si-OH) groups, making a hydrophilic surface. Thus, polymer BA provides a novel material in the field of flexible printed electronics.

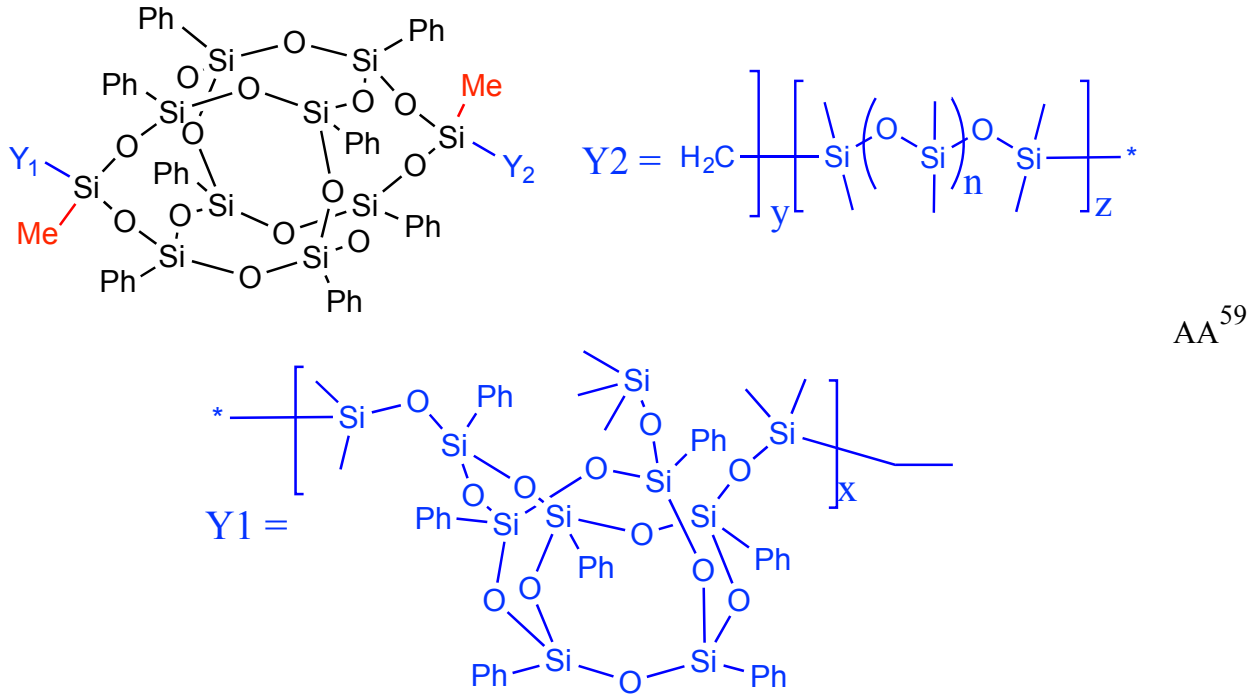

Figure 2-8. Polymer AA from DDSQ A.

Additionally, compound A was used to synthesize polymer AB (Figure 2-9) for developing new fluorinated functional materials.[60] Polymer BB did not exhibit a clear weight loss until T > 800 °C, much higher than that of the parent compounds: R_F-$(ACMO)_n$-R_F, R_F-$(DMAA)_n$-R_F and R_F-$(DOBAA)_n$-R_F, which exhibited a clear weight loss at only 250 – 350 °C. It was also determined that light absorbance was enhanced in BB and the fluorescent ability was good when compared to the parent polymer. Therefore, polymer BB not only has surface-active properties from the fluorine, but also possesses light emitting characteristics, and can potentially be used in fluorinated functional materials.

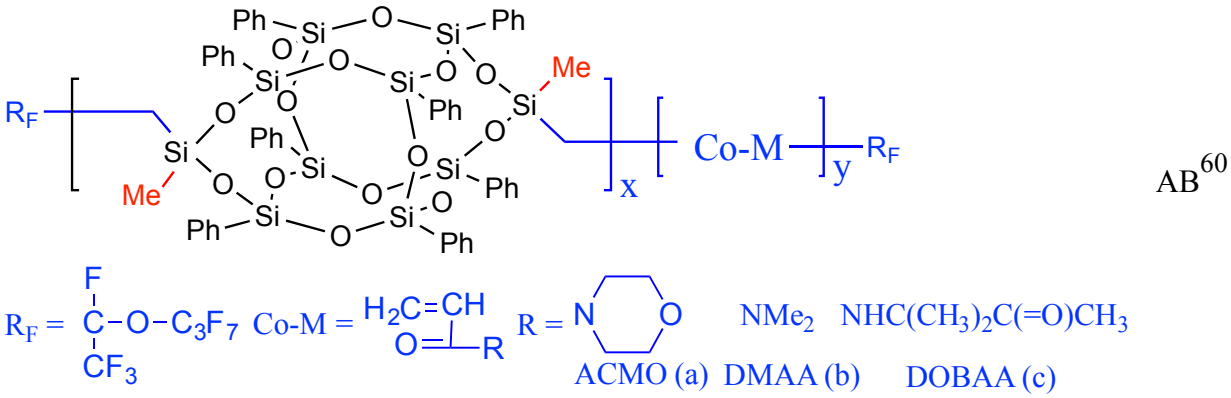

Figure 2-9. Polymer AB from DDSQ A.

Compound B (Figure 2-7) was used to synthesize polymer BA (Figure 2-10) in order to increase the T_g of polysiloxanes and expand their applications. Additionally, the *cis* and *trans* isomers were separated so that polymers of each isomer and an equivalent mixture of isomers could be synthesized. The T_m of each isomer and mixture was evaluated before polymerization and increased in the following order: mix (295 °C), *cis* (304 °C), and then *trans* (357 °C). T_g values were determined by DSC at a heating rate of 30 °C /min, and the softening temperature (T_s) was determeined by TMA at a heating rate of 10 °C /min. The T_g and T_s were highest for the *trans*

polymer (35 and 82 °C, respectively). These values were lowest for the *cis* polymer (30 and 39 °C, respectively). The mixed isomer had T_g and T_s values that were in between these values (34 and 45 °C, respectively). The neat polymer has a T_g at approximately -120 °C. Under nitrogen, 5 % weight loss at 10 °C /min was at T_d = 500 °C for both isomers, whereas T_d = 450 °C for the mixture of isomers. Under air, 5 % weight loss occurred at 400 °C (mix), 460 °C (*cis*), and 470 °C (*trans*), with a heating rate of 10 °C /min. This study demonstrated that the incorporation of DDSQ C significantly increased the T_g of polysiloxane, and the individual isomeric state could provide additional control over the polymeric system.

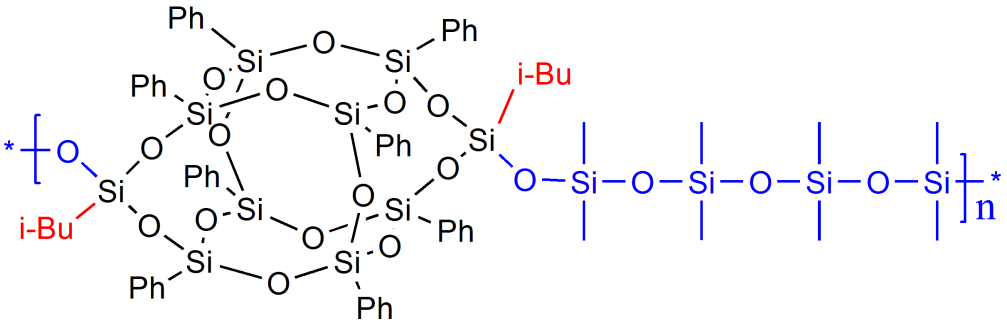

BA[51]

Figure 2-10. Polymer BA from DDSQ B.

Compound C (Figure 2-7) was used to synthesize compound CA and polymers CB and CC (Figure 2-11) in order to further enhance the thermal resistance, mechanical and dielectric properties of polyimide (PI) materials.[2] These polymers can be applied as interlayer dielectrics in integrated circuit fabrication.[65,66] Monofunctionalized SQs have been incorporated into PIs as side chains, for the purpose of decreasing dielectric constants; however, there was not a significant effect on the mechanical properties.[67-69] Material CA provides linear DDSQ co-polymerized with PIs and thermomechanical improvements were realized for these PIs over the neat PI, PMDA/ODA (Table 2-2). Generally, T_g was decreased and T_d was increased for the

majority of these PIs. Only CBc exhibited a decrease in T_d. There was no significant change in density. The initial modulus increased for all DDSQ/PIs; however, the tensile strength only increased for CBb. Percent elongation increased only for CBb and CBc. Material CBb also exhibited lower water absorption (< 1 %), when compared to the neat PI film.

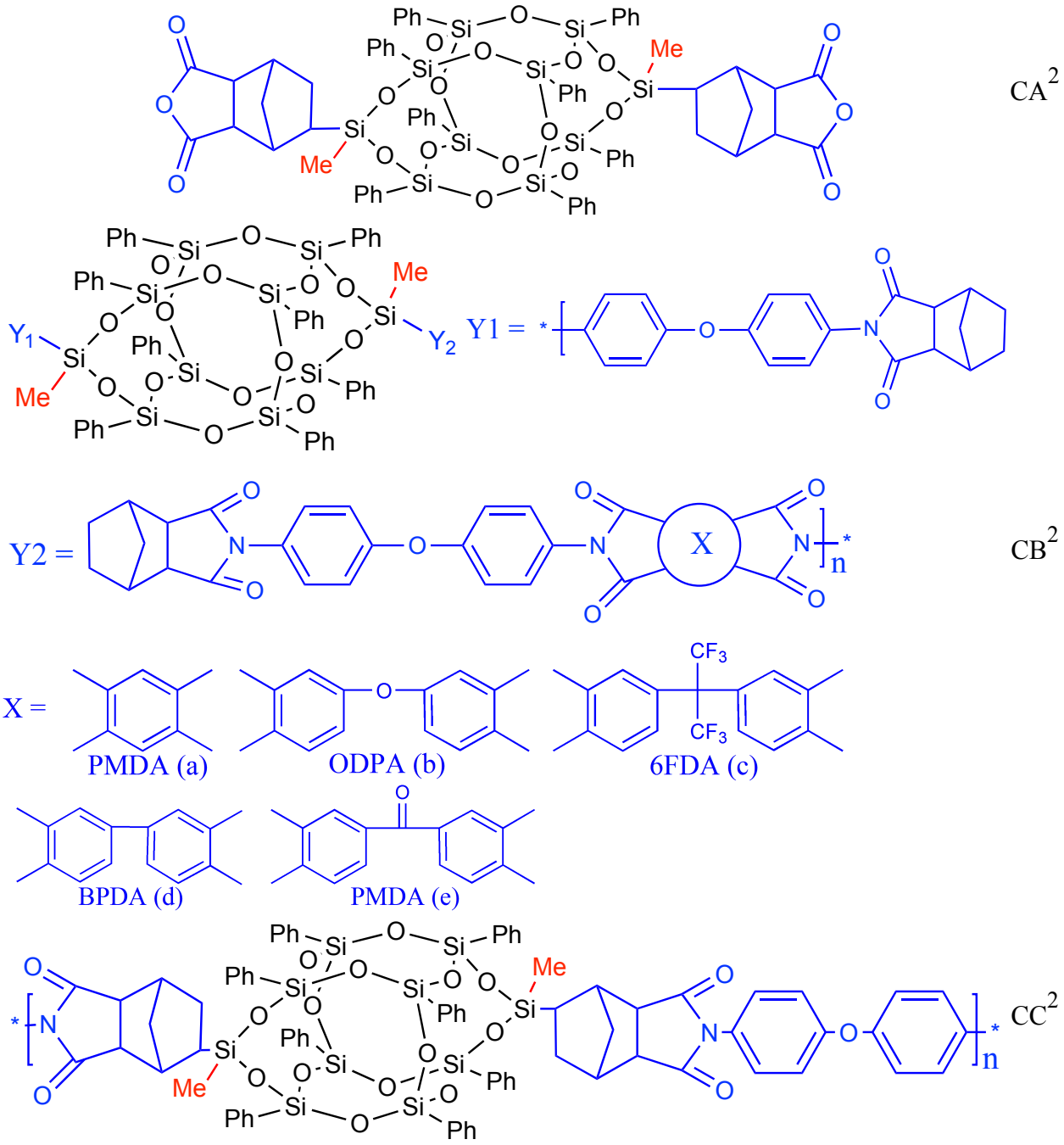

Figure 2-11. Material applications from fully condsensed C.

Table 2-2. Properties of materials CB and CC.[2]

Polymer	T_g (°C)+	T_d (°C)*	ρ (g/cm^3)#	ε (10 kHz)^	Tensile strength (MPa)	Elongation (%)	Initial modulus (GPa)
CBa	264	541	1.41	2.43	42.1	2.9	2.32
CBb	261	538	1.42	2.69	74.1	6.0	2.15
CBc	255	521	1.43	2.39	58.0	5.9	2.15
CBd	262	537	1.42	2.59	52.3	5.0	1.82
CBe	267	551	1.44	2.79	65.8	5.4	1.51
CB	248	537	1.40	-	-	-	-
PMDA/ODA	362	530	1.44	3.46	-	-	-

+ 2nd heating at a heating rate of 30 °C/min. * 10 % weight loss at a heating rate of 10 °C/min in air. # density. ^ dielectric constant.

Compound C (Figure 2-7) was also used to synthesize compound CD and polymer CE (Figure 2-12).[70] Compound CD was synthesized as a model reaction and demonstrated that the reaction formed quantitatively with almost no side reactions or further hydrosilylation. Polymers CEa and CEb were soluble in a large variety of common organic solvents, whereas polymer CEc was not. CEa and CEb showed a T_g just over 150 °C, whereas CEc showed no T_g. Under N_2, at a heating rate of 10 °C/min, CEa showed an onset of degradation at 518 °C. The other polymers

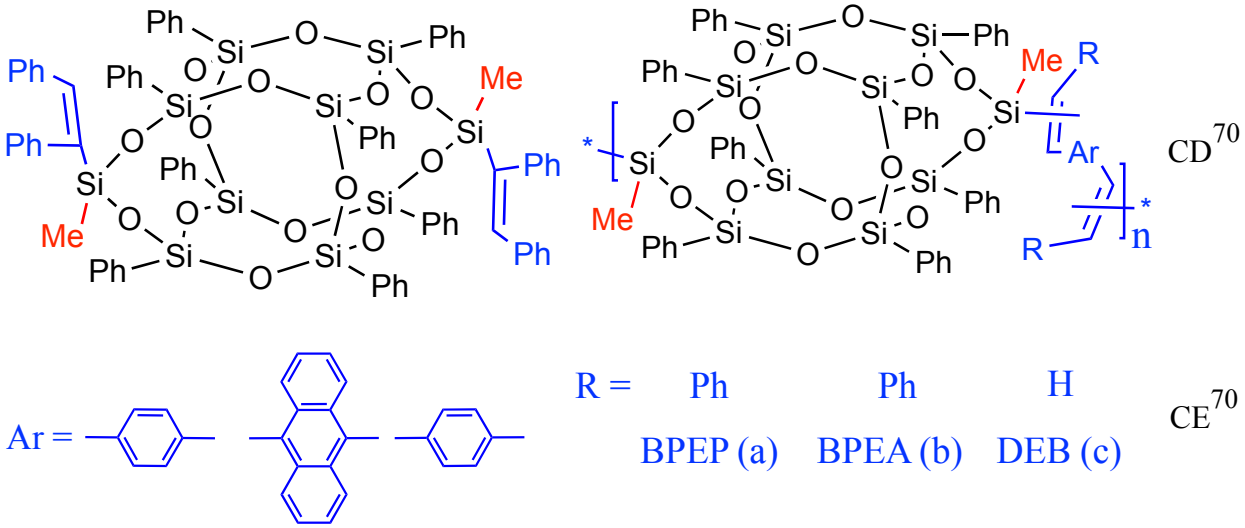

Figure 2-12. Structure CD and polymer CE from DDSQ C.

had considerably lower degradation onset temperatures. Again, the incorporation of DDSQ into the polymer backbone demonstrated high thermal stability.

Additionally, compound C was used to synthesize polymer CF (Figure 2-13) for preparing Langmuir-Blodgett (LB) films, or amphiphilic hybrid polymer nano-sheets, with a well-defined molecular structure and uniform molecular weight.[61] Previous studies have incorporated monofunctionalized SQs into LB films, but showed molecular weight distributions since they used SQ co-polymers or mixed SQs as a core.[71-73] Studies involving compound C, demonstrated that the DDSQ core with di(ethylene glycol) coronae formed a stable and uniform monolayer. Additionally, this structure demonstrated an amphiphile in which the core was hydrophobic and the coronae were hydrophilic. This is unique when compared to typical amphiphilic structures, with a polar/hydrophilic head and tail comprised of a hydrocarbon chain. Thus, the "core-coronae" type molecule is a potential candidate for LB film forming materials.

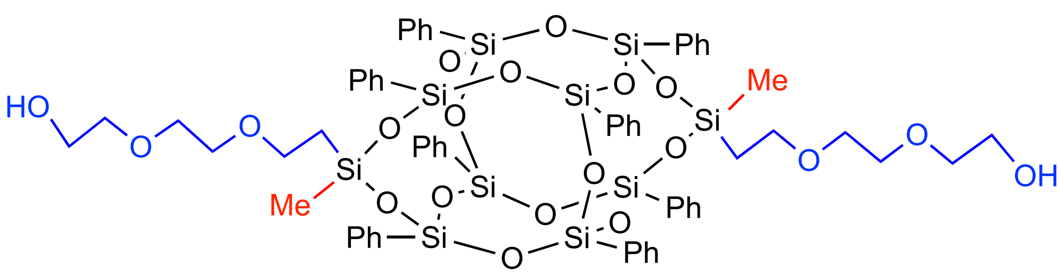

CF[61]

Figure 2-13. Polymer CF from DDSQ C.

Compound C was also used to synthesize compound CG (Figure 2-14) for the purpose of improving thermomechanical properties of polyurethanes (PU).[62] Generally, the Tg increased with increasing weight % of DDSQ in the PU backbone. Overall, the T_g increased to 7 °C (48 weight % DDSQ) from -28 °C for neat PU. The temperature at the maximum degradation rate and the yield of degradation temperatures were also improved with the addition of DDSQ. Moreover, DDSQ-PU displayed increased surface hydrophobicity when compared to neat PU.

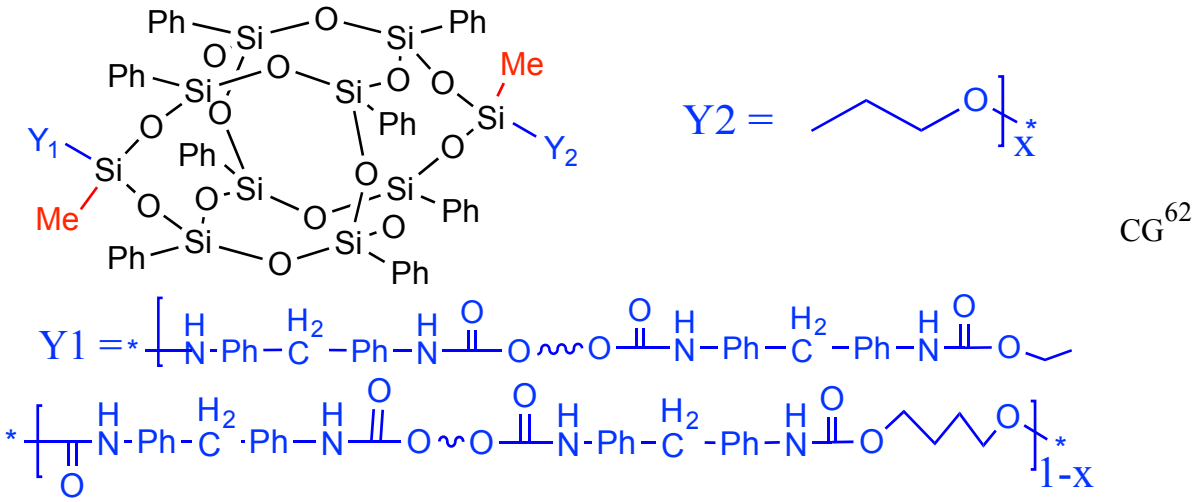

Figure 2-14. Co-polymer CG from DDSQ C.

Furthermore, compound C (Figure 2-7) was used to synthesize structure CH and polymer CI (Figure 2-15) to improve thermomechanical properties of poly(hydroxyether of bisphenol A).[63] This polymerization proceeded with a 1:1 ratio of bisphenol A hydroxyl groups to epoxide groups (combine for both compound CH and diglycidyl ether of bisphenol A, DGEBA).

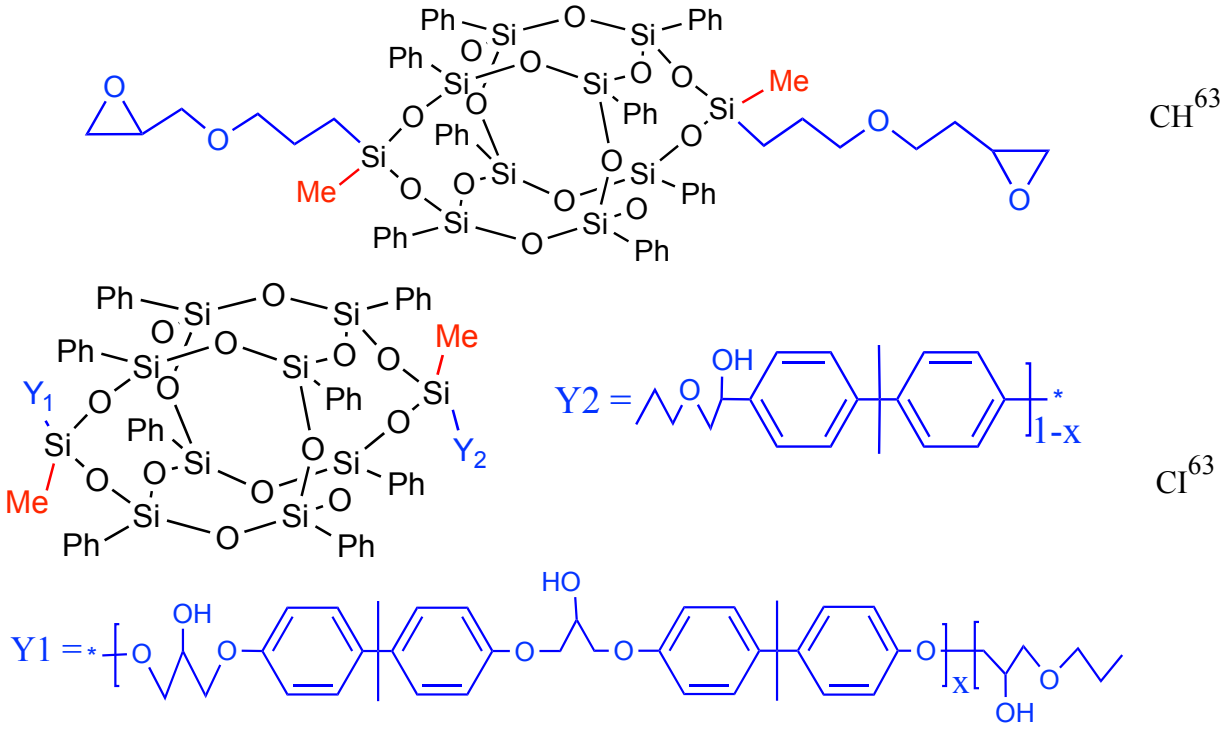

Figure 2-15. Compound CH and Polymer CI from DDSQ C.

It was determined that the T_g was dependent on the composition of the copolymers (Table 2-3). Although the onset of degradation temperature decreased with the addition of DDSQ, the maximum rate of degradation and the yield of degradation residues significantly increased. Similar to other polymers, the surface hydrophobicity was increased for DDSQ-PH polymers when compared to neat PH. This is yet another example where DDSQ incorporated into the backbone of a polymer improved thermomechanical properties of the neat polymer.

Compound D (Figure 2-7) was selected as the primary structure in this dissertation for several reasons: first, DDSQ was selected over other cage-like SQs since it can easily be difunctionalized in gram quantities, and be incorporated into the main chain of a polymer system.

Table 2-3.[63] Thermal properties of polymer CI with different wt % of CH.

Compound	CH (wt %)	DGEBA:DE (wt)	T_g (°C)*	T_d (°C)^	Residue (%)$^+$
Neat PH	0	10:0	91.5	424.3	2.2
PH9DDSQ1	6.4	9:1	94.5	424.4	7.9
PH7DDSQ3	20.3	7:3	94.1	418.4	13.7
PH5DDSQ5	35.9	5:5	83.6	385.2	25.3
PH3DDSQ7	53.5	3:7	57.4	385.1	36.9
PDDSQ	84.6	0:10	58.6	318.3	46.4

* DSC heating rate of 20 °C/min. ^ 5 % mass loss and a heating rate of 20 °C/min.

Additionally, DDSQ incorporates *cis* and *trans* isomers about the Si-O cage. Secondly, the particular reactive moiety (X) of these DDSQ not only has a significant impact on the characteristics of the molecule itself, but it also limits the applications. The aminophenyl moiety of compound D (Figure 2-7) can be thought of as a reactive version of the phenyl moieties attached to each silicon atom. Furthermore, the amine is particularly reactive and can be used in a large variety of potential applications in areas such as: aromatic polyamides,[74] polyimides,[75] ionic-liquids,[21] photochemistry,[76] and catalysis[77].

In previous work, compound D was used to synthesize polymer DA (Figure 2-16) in order to increase thermal stability, and mechanical properties while maintaining low dielectric constants of PIs. Good thermal stability was observed up to 500 °C (Table 2-4). At 700 °C in air, residual weights range from 64 – 76 %. The polymers also displayed good mechanical properties

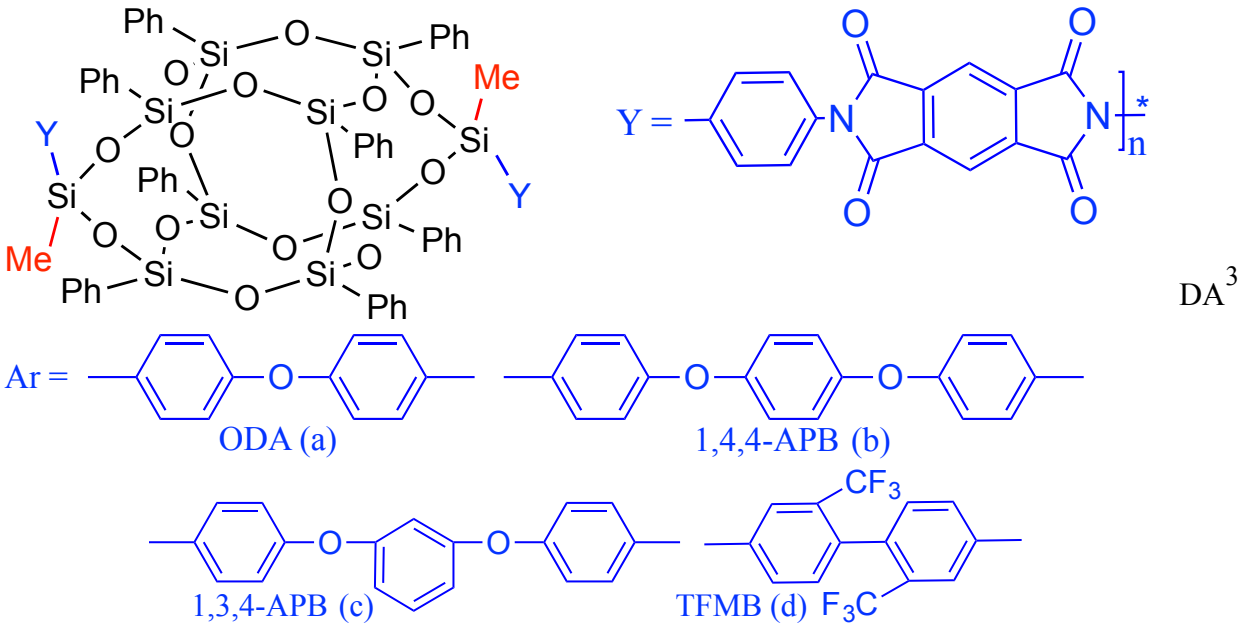

Figure 2-16. Polymer DA from DDSQ D.

and solubility in common organic solvents. These high thermomechanical properties coupled with low dielectric constants make DA a suitable candidate for polymeric materials in advanced microelectronic applications.

Table 2-4.[3] Thermal and mechanical properties of polymers DA.

Polymer	T_g (°C)$^+$	T_d (°C)*	ε (1 MHz)	Tensile strength (MPa)	Elongation (%)	Initial modulus (GPa)
DAa	None	555	2.56	82.1	10.9	2.6
DAb	None	550	2.59	78.1	13.6	2.4
DAc	325	540	2.65	76.0	15.9	1.9
DAd	None	553	2.43	72.3	8.0	1.8

+ 2nd heating at a heating rate of 30 °C/min. * 10 % weight loss at a heating rate of 10 °C/min

Additionally, compound D (Figure 2-7) was used to synthesize polymer DB (Figure 2-17) to form a thermosetting material based on phenylethynylphthalic anhydride (PEPA). The onset of the crosslinking reaction of neat phenylethynylphthalimide (PEPI) is above 300 °C. For DDSQ-PEPI, the onset temperature was raised to 343 °C with a heating rate of 2 °C/min and to 395 °C with a heating rate of 20 °C/min. Additionally the DDSQ cage impacted the activation energy of the reaction, the heat of fusion, and the overall reaction profile. This study demonstrated that these DDSQ-PIs could be materials used in fiber-reinforced composites.

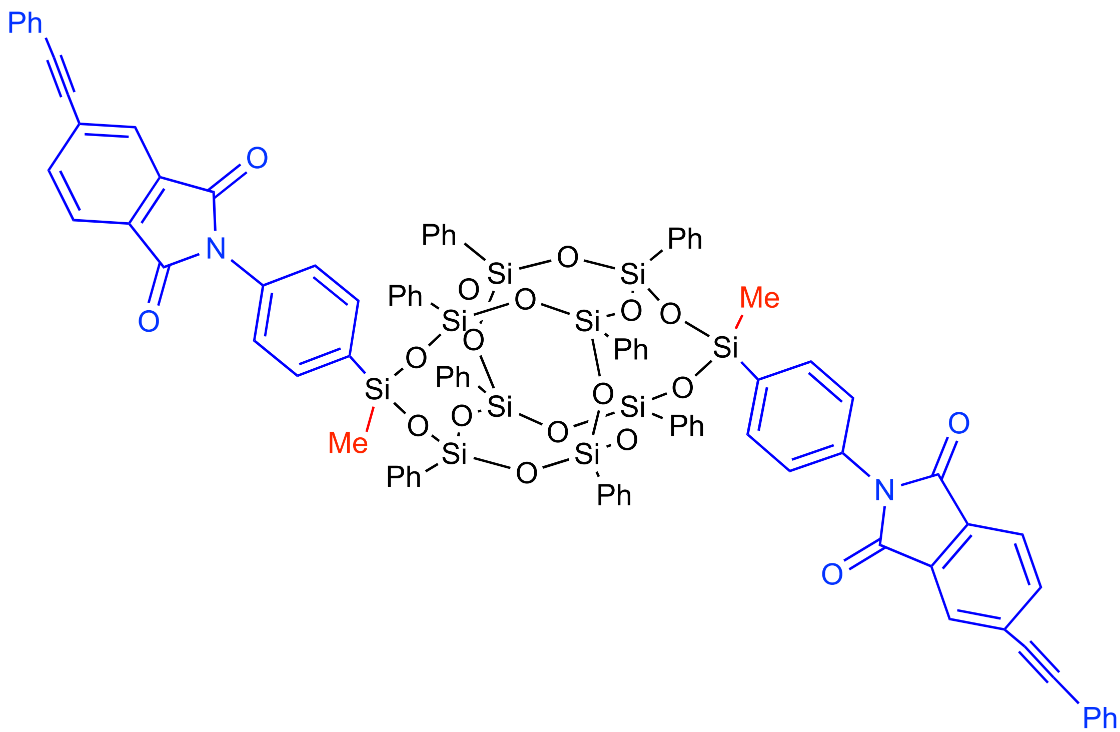

DB[25]

Figure 2-17. Polymer DB from DDSQ D.

2.2 Spectroscopic Elucidation

2.2.1 ^{29}Si NMR

As described above, DDSQ with various chemical moieties, including aminophenyls and 2-methylpropyl-hydroxyl have been synthesized and their *cis* and *trans* isomers partially isolated.[25,51] These isomers have been identified using one-dimensional ^{29}Si NMR spectroscopy.[2,3,25,51,52,64] Specifically ^{29}Si NMR spectra of DDSQ D (Figure 2-7), since it is the primary structure for this dissertation, were previously determined (Figure 2-18).[25] Mixed

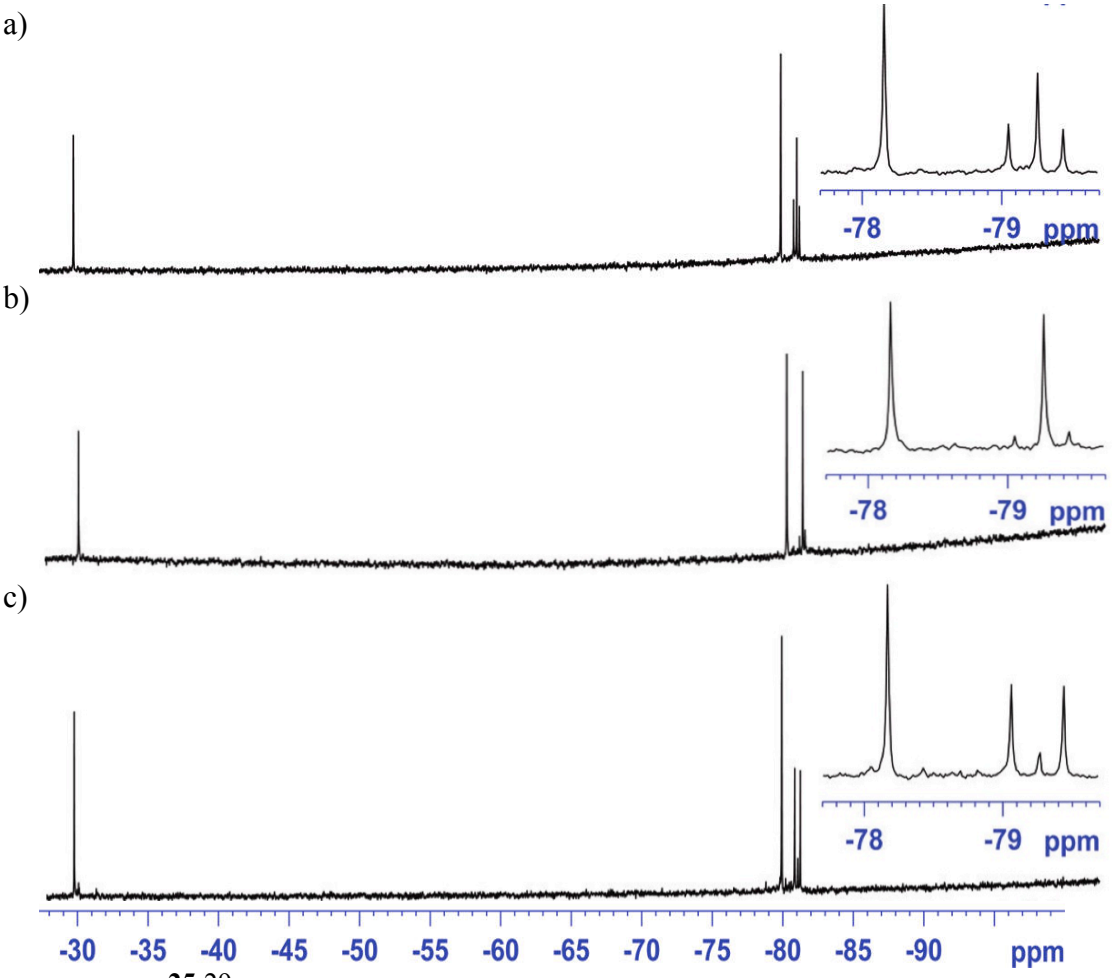

Figure 2-18.[25] ^{29}Si NMR spectra of (a) *cis* and *trans*, (b) majority *trans*, and (c) majority *cis* DDSQ D.

isomers from DDSQ D show ^{29}Si resonances at δ -29.9, -78.4, -79.3, -79.5, -79.7 in a ratio of 2:4:1:2:1 (Figure 2-18a). Majority *trans* isomers show characteristic ^{29}Si resonances at δ -29.9, -78.4, -79.5 in a ratio of 2:4:4 (Figure 2-18b). Majority *cis* isomers show characteristic ^{29}Si resonances at δ -29.9, -78.4, -79.3, -79.7 in a ratio of 2:4:2:2 (Figure 2-18c). It was initially expected that the ^{29}Si NMR spectra of the mixed isomers (Figure 2-18a) would display seven resonances representing all seven silicon environments in DDSQ D. However, since environments between the *cis* and *trans* isomers are very similar, some of the resonances are isochronus, or overlapping. Symmetry arguments were used to determine peak assignments of the individual silicon atoms. The ^{29}Si resonance at δ -29.9 has been assigned to the D-group silicon atoms, silicon atoms bonded to 2 oxygen atoms (Figure 2-19).[78] The ^{29}Si resonance at δ -78.4 has been assigned to the T-group silicon atoms, silicon atoms bonded to 3 oxygen atoms, nearest the D-group silicon atoms. ^{29}Si resonances at δ -79.4 (*cis*), -79.6 (*trans*), and -79.8 (*cis*) have been assigned to the internal T-group silicon atoms.

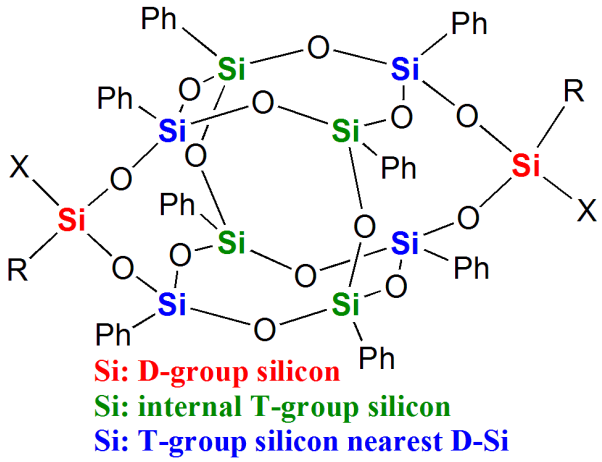

Figure 2-19. DDSQ silicon atom labels.

2.2.2 ^{1}H NMR

While ^{29}Si NMR does benefit from large chemical shift dispersion typically leading to reduced spectral congestion, the technique is not ideal.[79] ^{29}Si NMR delivers lower relative sensitivity when compared to that of ^{1}H NMR; requires a longer recycle delay and experimental time for quantitative measurements, more concentrated samples, and a broadband probe with appropriate hardware (i.e. broadband amplifier, RF filters, and specific capacitor sticks for tuning) for accurate results. These factors make ^{29}Si NMR less desirable when compared to the higher sensitivity, shorter relaxation and acquisition times, more dilute samples, and standard NMR equipment required for ^{1}H NMR. The ability to identify the isomeric ratio of DDSQ molecules using ^{1}H NMR spectroscopy would save time and material, and ultimately provide a more accurate quantification of the isomeric ratio than utilizing ^{29}Si NMR spectroscopy. In order to unambiguously assign the proton resonances and use them for quantitation, two-dimensional (2D) NMR techniques are necessary. Specifically, proton correlations to the silicon nuclei of the silsesquioxane core not only facilitates ^{1}H spectral assignment but also confirms previous ^{29}Si assignments for this class of DDSQ.

Heteronuclear multiple bond coherence (HMBC) provides a 2D inverse correlation of hydrogen connectivity to specific carbon atoms, or other heteroatoms (X) (Figure 2-20). Additionally, using a gradient-selected version (gHMBC) reduces unwanted signal artifacts.[80] A gHMBC will provide couplings that are in the range of 2-4 bonds. On a 2D heteronuclear plot, cross-peaks appear at the intersection of X-H peaks. These cross-peaks are displayed as a

contour plot, which is similar to a topographical map.[81] The correlations peaks are in actuality a cross-section (slice) of a 3-dimensional image of an NMR spectrum.

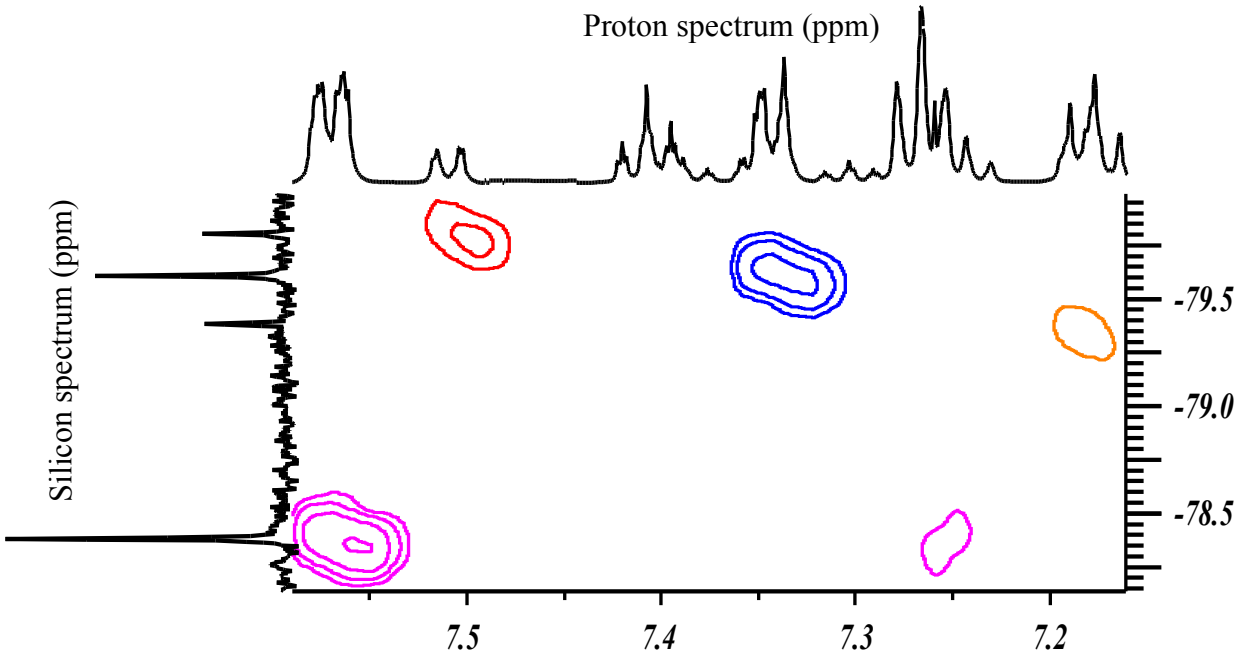

Figure 2-20. Representation of a hetereonuclear spectrum.

^{29}Si-^{1}H gHMBC NMR has been used to correlate Si-H atoms.[82,83] For these DDSQ, gHMBC can be used to correlated atoms that are separated by 2- or 3-bonds, $^{2}J_{Si-H}$ or $^{3}J_{Si-H}$ (Figure 2-21). Proton atoms that have a larger separation than 3 bonds from a silicon atom can be spectroscopically determined from ^{1}H-^{1}H correlation spectroscopy (COSY) experiments

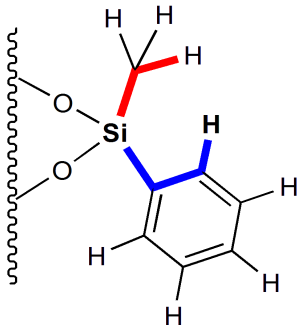

Figure 2-21. ^{2}J-coupled Si-H atoms (red, top), and ^{3}J-coupled Si-H atoms (blue, bottom).

(Figure 2-22). Unlike gHMBC, a gCOSY contour plot displays the 1D spectrum traced on the diagonal of the plot.[81] Peaks that do not appear on the diagonal are cross-peaks, or correlations peaks resulting from J-coupling.

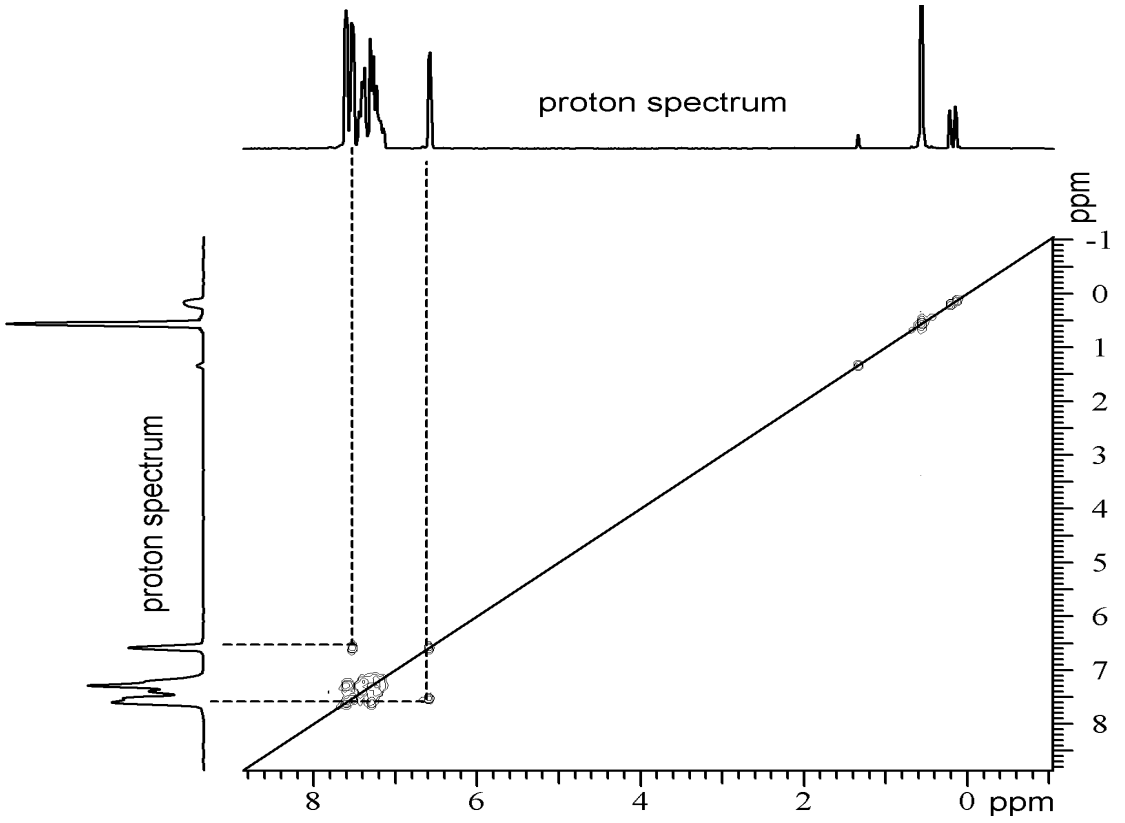

Figure 2-22. ^{1}H-^{1}H COSY spectrum. Correlation peaks that are not on the diagonal represent J-coupled peaks.

2.3 Isomer Separation

Fractional crystallization provides a platform for larger quantities of material to be separated into fewer fractions, as compared to other methods such as chromatography.[84-87] Furthermore, fractional crystallization provides a much lower energy demand as opposed to an energy-intensive thermal separation method such as distillation. Hence, it is accepted as an appropriate economic approach for an industrial scale.[87]

DDSQ B[51] and D[25] isomers have been separated in previous studies (Figure 2-7) through methods of fractional crystallization that exploit differences in the solubility of the two isomers, and through chromatography columns. However, these studies do not provide a means to accurately quantify the purity of the isomer after isolation. They also lack models representing the solubility behavior and thermodynamic properties of these isomers.

Solid-liquid equilibria (SLE) measurements allow for thermodynamic properties of multiple component mixtures to be measured. Simultaneously, solubility behavior of the individual components in these multicomponent mixtures can be determined. A common method for experimentally measuring SLE is through sampling a saturated solution and analyzing the sample with spectroscopy or chromatography.[88,89] Experimental data obtained through this method can then be modeled using common thermodynamic equations.

2.3.1 Thermodynamic Modeling of SLE

A criteria for phase equilibria is for the Gibbs energy to be equivalent in each phase at equilibrium (Equation 2-1):[90-92]

$$G_i^S = G_i^L \qquad (2-1)$$

where G is the Gibbs energy of component (i) the solid (S) and liquid (L) phases. For a pure component, Gibbs energy is the same as the chemical potential of the liquid, μ (Equation 2-2):[92]

$$G_i^S = \mu_i^L \quad or \quad G_i^S - \mu_i^L = 0 \qquad (2-2)$$

To form a liquid, the Gibbs energy change is (Equation 2-3):[92]

$$\Delta G_i^{fus} = G_i^{hypL} - G_i^S \qquad (2-3)$$

The pure liquid is a hypothetical pure liquid at the equilibrium temperature because it is typically below the pure component melting point. Manipulating equation 2-2 to account for the hypothetical Gibbs energy, gives (Equation 2-3):[92]

$$G_i^S - G_i^{hypL} + G_i^{hypL} - \mu_i^L = 0 \qquad (2-3)$$

With thermodynamic manipulations, equation 2-3 becomes (Equation 2-4):[92]

$$\Delta H_i^{fus} - T\Delta S_i^{fus} + G_i^{hypL} - \mu_i^L = 0 \qquad (2-4)$$

where ΔH_{fus} and ΔS_{fus} are the heat and entropy of fusion based on its melting transition (T_m). The difference between the hypothetical Gibbs energy and the chemical potential is the change in the chemical potential for mixing a component. For a mixture, equation 2-5 can be used: [92]

$$G_i^{mixing} = G - \sum G_i = \sum(\mu_i - G_i) = RT \sum [ln(x_i\gamma_i)] \qquad (2-5)$$

where x is the mole fraction of component (i) and γ is the activity coefficient. Thus for a single component this becomes (Equation 2-6):[92]

$$\mu_i^L - G_i^{hypL} = RTln(x_i\gamma_i) \qquad (2-6)$$

Combining equations 2-4 and 2-6 results in the general equation for predicting the saturation mole fraction of a solid in a liquid, known as the Schröder-van Laar equation (Equation 2-7):[92]

$$ln\left(x_i^l \gamma_i^l\right) = \frac{\Delta H_{m,i}}{RT_i}\left[1 - \frac{T_i}{T_{m,i}}\right] \qquad (2-7)$$

where x is the mole fraction of solute (i) that remains in solution (liquid phase) at a given temperature (T), based on its melting transition (T_m) and heat of fusion (ΔH_m), R is the ideal gas constant, and γ is the activity coefficient in the liquid phase.

The activity coefficient (γ) quantifies deviations from an ideal solution due to molecular interactions. An ideal solution is a solution formed with no accompanying energy or volume change on mixing and no excess entropy; the intermolecular attractive/repulsive forces (or intermolecular interactions) between the various pair types are all similar, and $\gamma = 1$. When $\gamma > 1$, the solubility is lower than an ideal solution (an unfavorable interaction), and when $\gamma < 1$, the solubility is greater (a favorable interaction).[92]

The structures of the solid material are generally large in comparison to the molecules of many common organic solvents. This will present a solution with non-uniformities and energetic interactions between molecules of the mixture and will give rise to non-idealities. There are many plausible activity coefficient models to be considered that demonstrate these non-idealities.

A multicomponent model is necessary when considering two isomers and the solvent system. Additionally, when modeling the solubility based on the fully saturated mole fractions of the solvent and the solute, the activity coefficients will be determined in the liquid state. The selected activity coefficient model will then be combined with equation 2-7 to calculate the SLE.

Several models based on the idea of local compositions that can be easily extended from a binary to multicomponent system and can be used for liquid activity coefficients are the universal quasi-chemical (UNIQUAC), the Wilson, and the nonrandom-two-liquid (NRTL) models.[90] The UNIQUAC activity coefficient model accounts for different molecular sizes and intermolecular forces through structural factors proportional to external surface area of the molecule (q) and the radius of the molecule (r). For many functional groups q and r are tabulated. However, they are not tabulated for silsesquioxane derivatives and would need to be estimated from experimental data, or by molecular group contribution methods.[90]

The Wilson activity coefficient model also accounts for different molecular sizes between solvent and solute and intermolecular forces, but does not rely on values of q and r. Instead, it relies only on the idea of local composition is used to capture these effects. Local mole fractions (x_{ij}) are scaled with bulk mole fractions (x_i) and a Boltzman factor that is proportional to the probability of finding a molecule of type i in the vicinity of a molecule of type j (P_{ij}). Considering a binary (1-2) mixture provides a depiction of this idea (Figure 2-23).[90] Ratios of the local mole fractions are analogous to ratios of the P_{ij}s and are expressed as a product of the bulk mole fractions and the Boltzmann factors in terms of g_{ij}'s. For a more detailed explanation of local composition and to understand how it is used in the derivation of the Wilson model, the

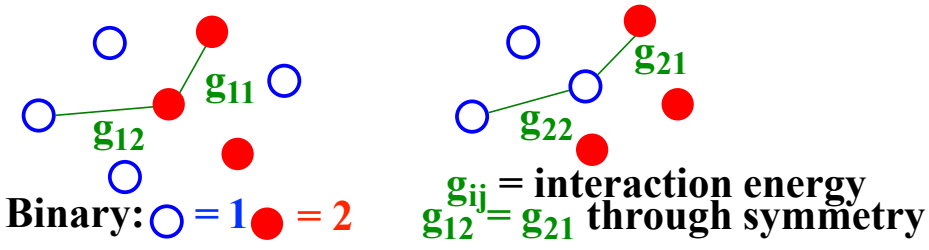

Figure 2-23.[90] Interaction energy of the molecules in the Wilson activity coefficient model, a central molecule of type 1 (left), and a central molecules of type 2 (right).

reader is encouraged to consult the literature.[90] A disadvantage of the Wilson model, however, is that it is applicable only to systems that are completely miscible.

The NRTL activity coefficient model is based on the same theory as the Wilson model, but can be used for systems that are partially immiscible, and far from ideality. Additionally the NRTL model provides a parameter, α_{ij}, to account for binary interaction characteristics of the non-randomness of the mixture. This will provide a more flexible model for the system in this dissertation. When $\alpha_{ij} = 0$, the solution is completely random. Generally α_{ij} is approximately in the range of 0.2 to 0.4 and Prausnitz has provided guidelines for specifying the magnitude of α_{ij} by considering comparisons to other classes of mixtures.[90] The NRTL activity coefficient model is (Equation 2-8):[93]

$$\ln\gamma_i = \frac{\sum_j x_j \tau_{ji} G_{ji}}{\sum_k x_k G_{ki}} + \sum_j \frac{x_j G_{ij}}{\sum_k x_k}\left[\tau_{ij} - \frac{\sum_m x_m \tau_{mj} G_{mj}}{\sum_k x_k G_{kj}}\right] \qquad (2-8)$$

$$G_{ij} = \exp(-\alpha_{ij}\tau_{ij}); \quad \tau_{ij} = a_{ij} + \frac{b_{ij}}{T}; \quad \tau_{ii} = 0; \quad G_{ii} = 1;$$

where γ is the activity coefficient of solute (i), x represents the mole fraction of each of the remaining constituents in this quarternary system, α represents the non-randomness parameter, and τ represents a binary interaction parameter characteristic of the difference between the binary energy parameters for the $i + j$ and $i + i$ interactions which is developed from the idea of local compositions.

In order to use the above models for determining SLE behavior, there are several steps that need to be taken. First, the solubility limit of the solute in a selected solvent solution will be determined experimentally. The solvent solution is generally comprised of two solvents. The

solute will be completely soluble in one solvent and insoluble in the other solvent, designated the anti-solvent. As the ratio of the solvent to anti-solvent is varied, the solubility limit of the solid material changes, and data points are generated for each ratio. The thermophysical properties of each isomer, T_m and ΔH_m, will also be determined at this step.

Secondly, the behavior will be modeled using the experimental data and equations 2-7 and 2-8 in order to determine the theoretical solubility limit at any solvent ratio. Since there are multiple unknown variables, this is generally accomplished numerically through a regression. For simplification, a binary system has been modeled in a flow chart selected (Figure 2-24). Generally, an initial value of γ_1 is selected, usually 1.0, and is used in equation 2-7 along with the thermophysical data. This provides a value of x_1 for that component. Other component mole fractions are determined through material balances; i.e. $x_2 = 1 - x_1$ in a binary. The initial values of x_1 and x_2 are then used in equation 2-8 with guessed values for the interaction parameters, which will generate a new value of γ_1 and γ_2. The new values of γ_1 and γ_2 are used again in equation 2-7 and the process is repeated until the change in x_1 is minimized.

Interaction parameters are continuously adjusted in order to satisfy the minimization. Simultaneously the differences in the calculated and experimental values for x_1 are minimized. After the minimization is complete, calculated values of x^1 and γ^1 can be compared with experimental values. Experimental values of γ^1 are determined by inputting experimental mole fractions and thermophysical data into equation 2-7.

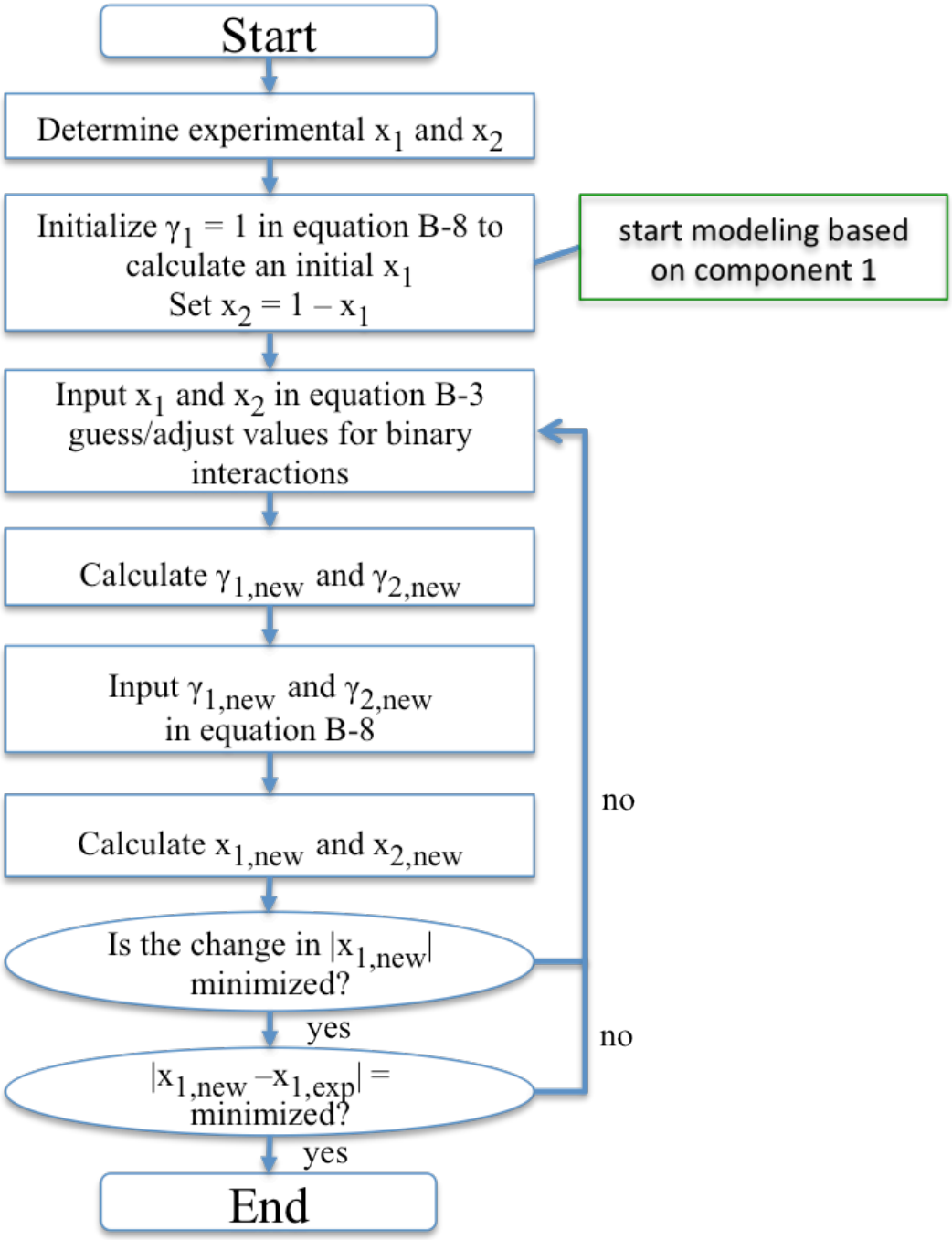

Figure 2-24. Flow chart for determining calculated xl and γl.

2.4 Structural Characterization

Configurational modifications, such as varying the conformation of a small organic molecule, tend to have large effects on the thermodynamic, physical, and structural properties.[94] Para-di-substituted benzenes typically have a higher symmetry than meta-di-substituted benzenes and thus can more easily pack in a three-dimensional crystal lattice, forming more stable, densely packed crystals that exhibit a higher T_m (Table 2-5).[94-97] The difference in the T_m for these

Table 2-5. T_m of meta vs. para isomers.

Compound	T_m (K)	
	meta	para
$C_6H_4Et_2$	189	230
$C_6H_4I_2$	310	403
$C_6H_4(CN)_2$	434	495
$C_6H_4(NC)_2$	377*	439
$C_6H_4(Cl)NO_2$	319	357
$C_6H_4(Br)NO_2$	329	400
$C_6H_4(OH)(NO)_2$	370	387
$C_6H_4(OH)Cl$	306	317
$C_6H_4(OH)Br$	306	339
$C_6H_4(Br)COOH$	428	527
$C_6H_4(I)COOH$	461	543
$C_6H_4(Me)COOH$	385	455
$C_6H_4(Br)CONH_2$	429	463
$C_6H_4(I)CONH_2$	458	488

* Inconsistent data also seen as 350

disubstituted benzenes is as large as 99 K ($C_6H_4(Br)COOH$) and as small as 9 K ($C_6H_4(OH)Cl$). Furthermore, many organic para- structures (*p*) that exhibit a higher symmetry number (σ), also exhibit a higher ΔH_m and ΔS_m than their meta-counterparts (*m*) (Table 2-6). Moreover,

compounds that are more symmetric and higher melting generally exhibit lower solubility.[94] For additional examples, the reader is encouraged to consult the literature.[94,95]

Table 2-6. Melting transitions based on meta- and para- substituted benzenes.

Compound	σ	ΔH_m (kJ/mol)	T_m (K)	ΔS_m (J/mol*K)
m-Dichlorobenzene	2	12.56	248.3	50.6
p-Dichlorobenzene	4	19.92	326.1	61.1
m-Xylene	2	11.55	225.2	51.3
p-Xylene	4	17.09	286.3	59.7

Similarly, *trans* isomers typically exhibit a higher order of symmetry over their *cis* counterparts; which also provides them with higher melting temperatures.[97-99] *Trans* isomers of disubstituted ethylenes have a higher T_m than their *cis* counterparts.[100] Specifically, *trans* dichloroethylene has a T_m at approximately 225 K, whereas *cis* dichloroethylene has a T_m below 200 K. Additionally, *trans* dimethylethylene has a T_m above 160 K, and *cis* dimethylethylene has a T_m below 150 K. Other *cis* and *trans* isomers demonstrate similar behavior (Table 2-7). Extensive studies on melting points of geometrical and constitutional isomers have been accomplished and the interested reader is encouraged to consult this literature.[97]

Table 2-7. T_m of cis/trans isomers.

Compound	P	T_m (K)
cis-But-2-ene	C_2	134
trans-But-2-ene	C_{2h}	167
cis-Pent-2-ene	C_1	122
trans-Pent-2-ene	C_1	137

Additionally, increasing the molecular weight (MW), while maintaining the same geometry, can also affect the symmetry, molecular packing, and the T_m of a small organic molecule.[95,101] This has been demonstrated using alkane chains (Table 2-8).[97] Increased MW

Table 2-8. T_m of increasing MW.

Compound	MW	T_m (K)
C_3H_8	44	83
C_4H_{10}	58	137
C_5H_{12}	72	146
C_6H_{14}	86	181
C_7H_{16}	100	188
C_8H_{18}	114	213
C_9H_{20}	128	219
$C_{10}H_{22}$	142	240
$C_{11}H_{24}$	156	249
$C_{12}H_{26}$	170	264
$C_{13}H_{28}$	184	270
$C_{14}H_{30}$	198	282
$C_{15}H_{32}$	212	289

provides increased number of site-site interactions per molecule, which increase the T_m. However, increasing the MW of substituted benzene by introducing a larger substituent, or branching of an alkane chain may actually lower the T_m. For example, adding a bulky moiety such as tert-butyl, cyclohexyl, or phenyl could interrupt the symmetry and distort the lattice for steric reasons, and would decrease T_m. Changing a moiety from hydrogen to a propyl group of an azopyridine carboxylic acid demonstrated such a decrease in T_m (Table 2-9).

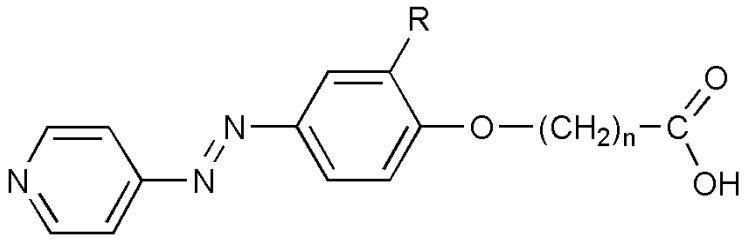

Table 2-9. T_m for altered moiety.

Compound	n	R	T_m (°C)
1a	5	H	229
1b	5	C_3H_7	172
2a	10	H	173
2b	10	C_3H_7	152

Moreover, the way molecules pack and their affinity for hydrogen bonding can also provide thermodynamic and structural modifications.[94,101-103] Molecules that exhibit hydrogen bonding in the crystal lattice have the potential to form stable dimers and exhibit an increase in T_m over a more symmetric isomer.[104,105] For example, meta-anisylpinacolone exhibits a T_m of 58 °C, whereas para-anisylpinacolone exhibits a T_m of 39.5 °C (Figure 2-25).[105] The higher T_m of the meta-structure was determined to be a result of its hydrogen bonding potential. The crystal structure shows two methoxy hydrogen atoms that exhibit hydrogen bonding with the carbonyl oxygen. Additionally, the methoxy oxygen atom shows hydrogen bonding with one methylene hydrogen and one aromatic hydrogen. Other reports demonstrate that a completely different crystal structure can be obtained from deuterating hydrogen bonding protons, which could potentially change the T_m along with other physical and chemical characteristics.

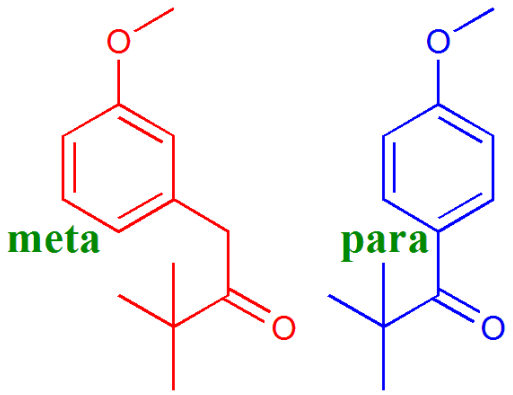

Figure 2-25. Meta- and para- anisylpinacolone.

2.4.1 Melting behavior and phase diagrams of mixed isomers

Melting points can be altered when a "guest" molecule is able to substitute or diffuse into the crystal lattice of a "host" molecule.[106] Lattice defects and solid solutions result in lower melting temperature, but are not necessary for melting depression, which can occur in mixtures where the solid and liquid compositions differ. This type of "melting point depression" is indicative of a eutectic melting system in which the solid phases are immiscible and the liquid phases are completely miscible. Binary mixtures that exhibit melting point depression can be classified as a general, congruent or incongruent-melting eutectic, and can be portrayed in phase diagrams.[107] General eutectic phase diagrams display two immiscible solid phases in equilibrium with a single liquid phase at the melting temperature (Figure 2-26).[108] The eutectic temperature (T_E) represents the temperature at which the first drop of liquid is observed. On a

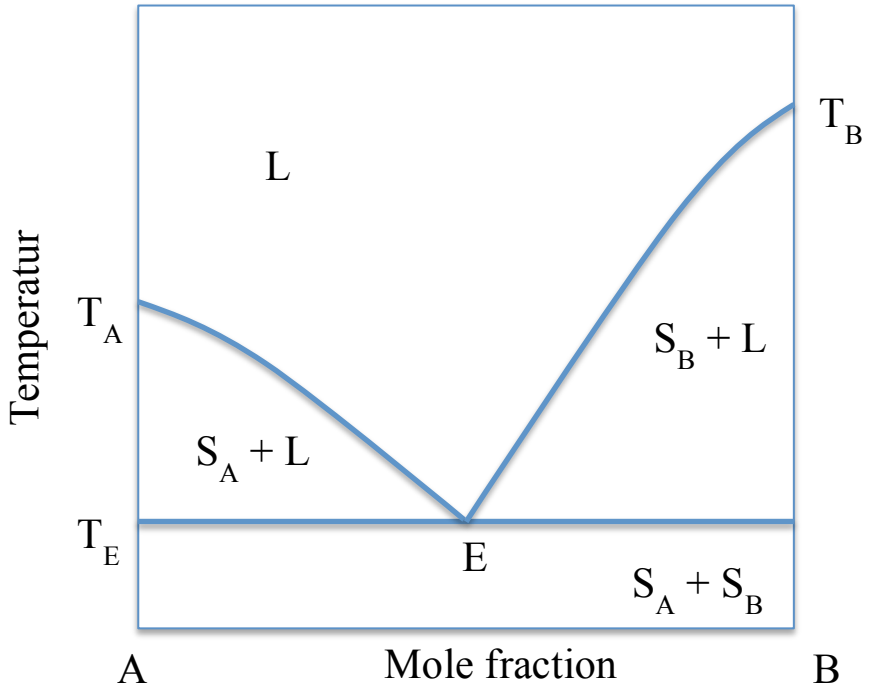

Figure 2-26.[107] Binary phase diagram of solids A and B.

differential scanning calorimetry (DSC) trace, this is sometimes observed as a change in the slope of the baseline (not to be confused with T_g), or an endothermic transition prior to the melt. T_E is constant regardless of composition. The composition at which the T_m is equivalent to T_E is the eutectic composition.

On a congruent melting eutectic phase diagram, the liquid and solid phases have identical compositions at the equilibrium melting temperature, T_m (Figure 2-27).[109] When a sample of mole fraction C (Figure 2-27) is heated, all of solid A (S_A) and part of solid B (S_B) will melt at the metastable eutectic temperature.[107] The melted portion will then recrystallize to form a co-crystal solid (S_C) and then S_C and the remainder of S_B completely melts at the congruent melting point T_c. A DSC trace will show an endothermic transition representing melting at $T_{m\text{-}E}$, which is immediately followed by an exothermic transition, representing co-crystal formation. A final endothermic transition then occurs representative of the T_c.

On an incongruent melting eutectic phase diagram, the liquid and solid phases have different compositions at the peritectic, or incongruent, melting point, T_p (Figure 2-27).[109,110] Similar to a congruent system, when a sample of mole fraction C is heated, all of S_A and part of S_B will melt at the metastable eutectic temperature, and the melted portion will then recrystallize to form a co-crystal solid (S_C).[107] Different from the congruent system, S_C will melt at the incongruent melting point, T_p, followed by a recrystallization of S_B that finally melts at T_B. A DSC trace will show an endothermic transition representing melting at $T_{m\text{-}E}$, which is

immediately followed by an exothermic transition, representing co-crystal formation. This is followed by another endothermic transition representative of the co-crystal melting, and an exothermic transition associated with the recrystallization of S_B at T_p. Finally, a broad endothermic transition follows at T_B.

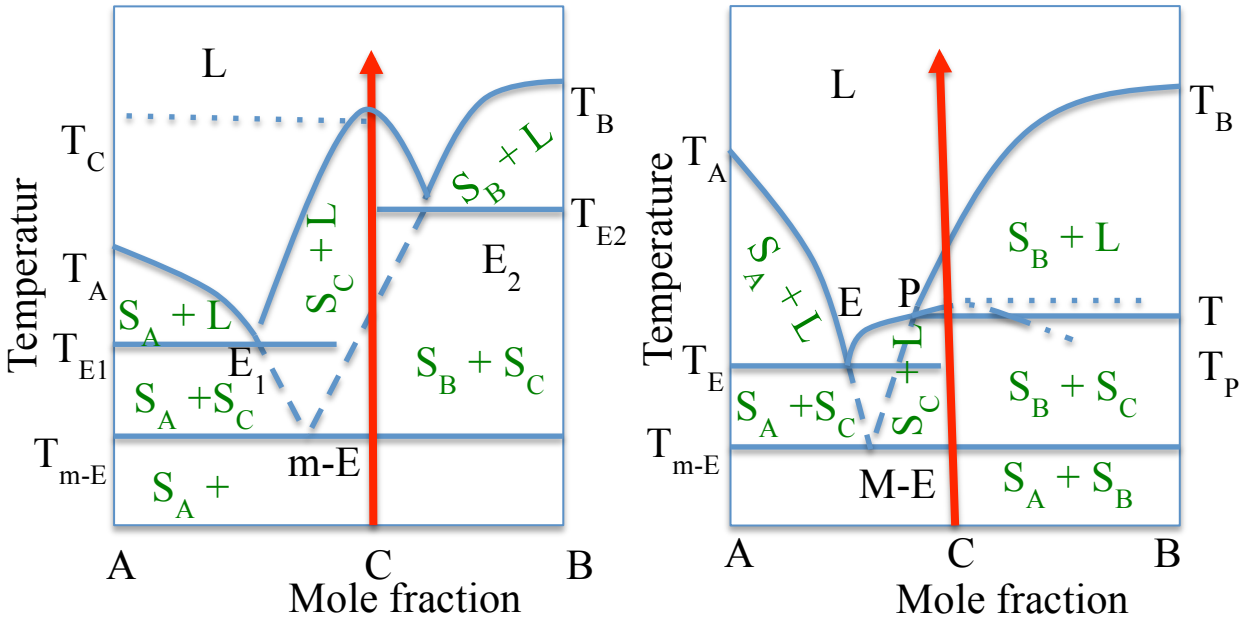

Figure 2-27. Phase diagram representing two systems of co-crystallization, congruent melting system (left), and incongruent melting system (right).

Both congruent and incongruent eutectic-type binary mixtures are capable of co-crystal formation. A co-crystal is a crystalline solid containing at least two unique solid components.[111-113] Co-crystal formation is particularly appealing in the pharmaceutical industry because it has been seen to improve physiochemical properties such as solubility, physical stability, mechanical properties, and bioavailability.[107]

A phase diagram in which both the solid and thee liquid phases are completely miscible is known as an isomorphous melting system, or a homogeneous solid-state solution.[109] In order

for a system to be isomorphous, both components must solidify in the same crystal system, with similar lattice dimensions, and related chemical constitution.[109] Solid solutions may be substitutional, where "guest" molecules replace "host" molecules in the crystal lattice, or interstitial, where "guest" molecules occupy empty spaces in the "host" lattice. Ideal behavior of an isomorphous system is achieved when the lattice dimensions of both components match and the compounds are chemically similar. Additionally, the "guest" molecule cannot interrupt the attractive-repulsive forces within the crystal lattice of the "host" component. Positive deviations from ideality would result from disruption and negative deviations from large attractive forces. A typical phase diagram for an isomorphous solution has liquidus and solidus curves that represent the onset of melting and the onset of cooling of the sample (Figure 2-28). Above the liquidus curve is a miscible liquid of A and B, and below the solidus curve is a solid solution of A and B. The area between the curves is the two-phase region. A smaller two-phase region is suggests a

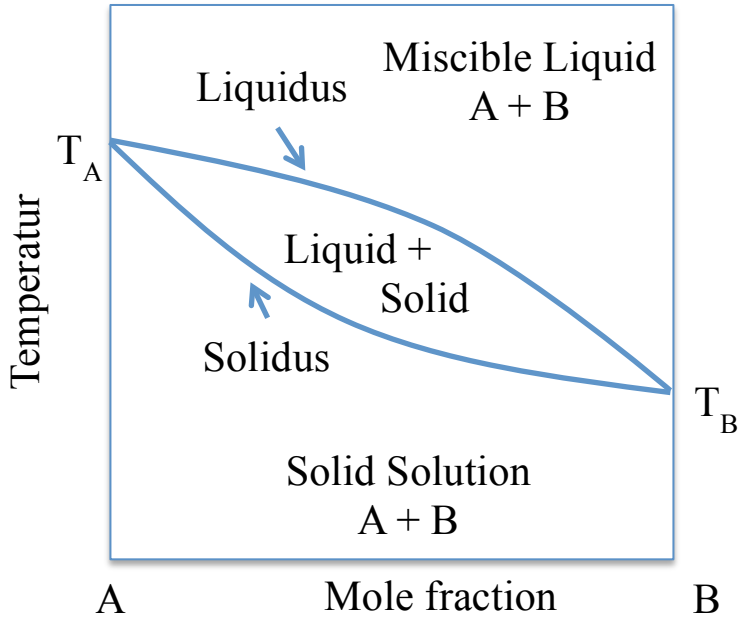

Figure 2-28. Phase diagram of an isomorphous, solid-solution melting system.

mixture that is nearer to ideal.[109] The DSC trace of a solid solution is represented by a single endothermic melting transition upon heating. Typically, as the composition moves further from a pure component, the endotherm gets broader. The broadness is indicative of the distance between the solidus and liquidus curves.

SLE methods that were discussed previously can also be used to model experimental melting point depression and determine a phase diagram.[114-116] For all three eutectic-type systems, the Schröder-van Laar equation (Equation 2-7) and the NRTL activity coefficient model (Equation 2-8) can both be used to determine the solid-liquid melt equilibria. However, for an isomorphous system; activity coefficients have to be considered in both the solid and the liquid phases if the system is not ideal. Thus a correction can be made to the Schröder-van Laar equation that accounts for this (Equation 2-9):[109]

$$ln\left(\frac{x_i^L \gamma_i^L}{x_i^S \gamma_i^S}\right) = \frac{\Delta H^\circ_{m,i}}{RT_i}\left[1 - \frac{T_{m,i}}{T^\circ_{m,i}}\right] \qquad (2-9)$$

where x is the mole fraction of (i) in the liquid (L) or solid (S) phase, $T\,^\circ_m$ and $\Delta H\,^\circ_m$ refer to the melting transition of the pure component, T_m refers to the depressed melting point at a specified mole fraction, R is the ideal gas constant, and γ is the activity coefficient. This equation relates the composition in both phases with the non-ideality of each phase and the thermophysical properties of the pure components.[117]

The thermodynamic, physical, and structural implications of configurational modifications discussed in this background section have been well established and can be easily predicted for small organic molecules. However, the same implications are much more complex

for larger molecules, especially for compounds containing a large inorganic portion. Previous to this dissertation, there have not been any structured studies on the implications of configurational modifications to these DDSQ molecules and their phase diagrams.

2.5 Selected Applications

2.5.1. Thermosets

Thermally cured polyimides are known as high performance materials (HPM) due to their excellent thermal and mechanical properties, in addition to their thermo-oxidative stability.[118] In light of their remarkable properties, polyimides have been applied to a wide variety of applications such as: matrices for high performance advanced composite materials, membranes for gas separation, thin films in electronic devices, structural adhesives and sealants, and high temperature indicators for aircraft wire coatings.[119] However, polyimides exhibit high viscosity, which requires high pressure to be used in order to process and fabricate the structural composites and adhesive joints. Therefore, research on polyimides has been directed towards decreasing the viscosity without sacrificing HPM characteristics.[120-124] Phenylethynyl groups are commonly used as polyimide thermosetting materials (Figure 2-29). Upon heating, the triple bond undergoes a polymerization through a cross-linking, curing reaction to form thermosets. In order to achieve a reduction in the viscosity phenylethynyl groups are placed on the terminal end of a molecule. Efforts in overcoming this complication include structural modifications to the bridging molecule, which involve adding noncoplanar phenylene moieties, kinked comonomers, and bulky lateral groups.

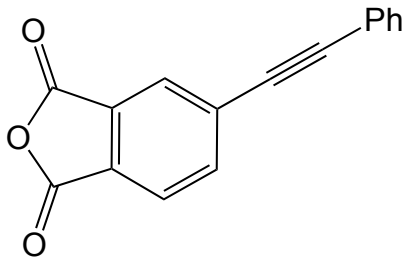

Figure 2-29. An example of a phenylethynyl group.

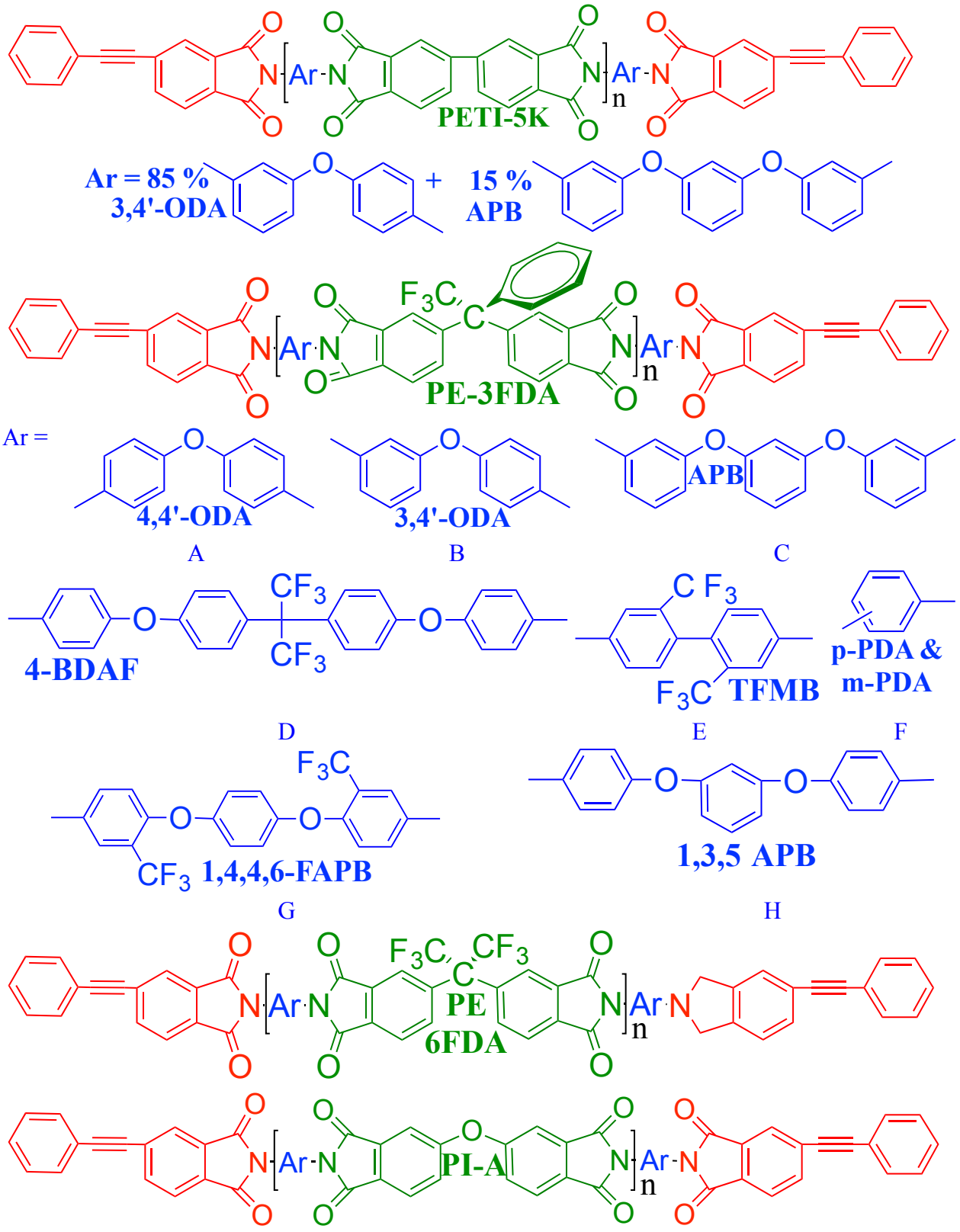

Figure 2-30.[119] Oligoimide structures used to reduce viscosity.

For PETI-3K and PETI-5K (Figure 2-30), minimum viscosity occurs over 350 °C. Additionally, these oligomers do not fully melt until 319 and 349 °C, respectively. Since the curing reaction occurs at approximately 350 – 371 °C, this make the processing window very small. Due to this, the initial viscosity may vary each time it is measured because the extent of melting and curing will vary. A reduction of viscosity was achieved through substitutions to the structures of PETI-5K and PETI-3K, where the 3 and 5 represent the number average MW (M_n) as 3000 and 5000 g/mol, respectively (Figure 2-30, Table 2-10).[119] The minimum viscosity was decreased for all oligomers when compared to their corresponding PETI-3K and -5K oligoimides. Thus, it was concluded that the replacement of the planar, biphenylene dianhydride (s-BPDA) with a bulkier group causes minimum viscosity to decrease. Furthermore, the crystalline melting transition no longer exists, and all oligomers only exhibit a T_g. As the T_g

Table 2-10.[119] Complex viscosity.

	Complex viscosity (Pa S) at the following T (°C)						
Compound	290	300	310	350	Mmv* (Pa s, °C)	T_g (°C)	T_m (°C)
PETI-3K	1823	1170	302	14	9 at 353	195	319
PETI-5K	71057	134770	161050	3353	2237 at 354	225	349
PE-3F-PETI-3K	27	17	7	29	6 at 314	190	
PE-3F-PETI-5K	860	350	154	65	51 at 339	218	
PE-3F-5K-A	1192	230576	230	347	91 at 328	235	
PE-3F-5K-B	22	18	16	21	14 at 330	226	
PE-3F-5K-C	38	32	31	19	11 at 355	184	
PE-3F-3K-D	--	--	7	--	--	--	
PE-3F-5K-D	367	165	99	312	68 at 325	237	
PE-3F-5K-E	161	53	21	260	14 at 328	213	
PE-3F-5K-F	1135	602	218	149	87 at 329	221	
PE-6F-PETI-3K	26	14	7	16	3.5 at 324	195	
PE-6F-PETI-5K	255	129	77	61	48 at 337	212	

*MMV: minimum viscosity

decrease for compounds that do not exhibit a melting transition, the minimum viscosity value and temperature appear to decrease. It was also recognized that at higher MW, there are more considerable influences on viscosity from the structural changes. When compound PI-A was used with different Ar moieties, a definitive trend in M_n was determined (Table 2-11).[125,126] As the M_n decreased, the minimum viscosity and T_g both decreased.

Table 2-11.[125,126] Complex viscosity according to MW of PI-A.

PI-A		Complex viscosity (Pa S) at the following T (°C)						
G:H[a]	M_n (g/mol)	250	275	300	325	350	Mmv (Pa s, °C)	T_g (°C)
1	10000[b]	27010	8349	1389	392.6	418.8	328.1 at 334	183
1	3234	3801	491.8	121.3	70.48	1162	69.88 at 322	187
1	2093	63.31	15.37	7.17	7.18	29.61	6.39 at 313	161
3	2200	0.61	0.36	0.30	0.33	1.78	0.28 at 308	126
1	2139	0.58	0.32	0.31	0.36	0.44	0.25 at 288	124
0.3	1762	54.1	0.60	0.50	0.57	0.69	0.50 at 300	124
G:B								
1	10000[b]	N/A	27590	12475	3030	1472	1451 at 351	208
1	3173	12430	1421	323	135	3449	131 at 327	197
1	2569	156	32.0	10.9	7.54	10.2	7.54 at 325	169
3	2200	1.0	0.70	0.71	0.64	0.70	0.60 at 301	129-132
1	1991	1.0	0.39	0.29	0.33	0.57	0.27 at 299	132
0.3	1272	19.8	0.84	0.69	0.82	1173	0.67 at 294	129-132

[a] Ratio of Ar moieties used [b] This is a calculated value, experimental was not determined

Isothermal viscosity measurements at 310 °C also demonstrated a decrease after holding for a 30 and 60 minutes (Table 2-12 and Table 2-13). It was suggested that the bulkier groups from 3FDA and 6FDA make the structure amorphous, providing weaker intermolecular interactions. Additionally, these units stabilize the phenylethynyl end caps, which will reduce the

rate of cross-linking at the minimum viscosity temperature. For PI-A, the variation in the viscosity, when isothermed at 280 °C for 2 hours, decreased as the M_n decreased (Table 2-14).

These studies depict the shortcomings of this class of polyimide thermosets; the minimum melt viscosity needs to be reduced in value and in temperature, and the solid-liquid phase transition needs to occur at a lower temperature in order to increase the processing window. Additionally, the MW for the oligomers is not constant, since *n* varies, and therefore the properties such as the melt viscosity are not constant (Figure 2-30). Thus, in addition to decreasing the viscosity and processing window, current research efforts have been directed towards developing a monodispersed oligomer to eliminate variation in MW.

Table 2-12.[119] Viscosity stability of PETI-3K and PE-3F.

	Viscosity (Pa s) at 310 °C			Rate of viscosity increase	
Compound	initial	30 min	60 min	30 min	60 min
PETI-3K	1501	9913	>27500	280	>433
PE-3F-5K-B	1781	8528	>14000	5.5	>286
PE-3F-5K-C	53	207	978	5.1	15.4
PE-3F-PETI-3K	60	298	2098	7.9	33.9
PE-3F-PETI-5K	1433	4620	16791	106	256
PE-3F-3K-D	821	3269	10266	81	255
PE-3F-5K-D	72	147	2610	2.5	42.3

Table 2-13.[119] Viscosity stability of PE 6F.

	Viscosity (Pa s) at 310 °C	
Compound	initial	60 min
PETI-3K	899	22500
PE-3F-PETI-3K	9	15
PE-6F-PETI-3K	17	28
PETI-5K	20759	412205
PE-3F-PETI-5K	321	527
PE-6F-PETI-5K	199	348

Table 2-14.[125,126] Viscosity stability for samples PI-A held at 280 °C for 2 hours.

PI-A G:H	M_n (g/mol)	Variation (Pa s)
1	10000	896.4 – 5379 [a]
1	3234	264.8 – 1563 [b]
1	2093	11.56 – 81.79
3	2200	0.48 – 3.30
1	2139	0.38 – 0.95
0.3	1762	0.57 – 4.01
G:B		
1	10000[b]	8268 – 59300 [a]
1	3173	479 – 3145 [b]
1	2569	25.0 – 178.6
3	2200	0.35 – 1.25
1	1991	0.56 – 2.09
0.3	1272	0.65 – 11.9

[a] 290 °C [b] 310 °C

A variety of cage like SQs have been end-capped with phenylethynyl groups (Figure 2-31). All SQ-based oligoimides displayed monodispersed MW. It was revealed that changing the R-group from isobutyl to phenyl resulted in a retardation of the phenylethynyl reactions. Additionally, changing the spacer group from propyl to phenyl effected the initial curing with the monofunctionalized, and octafunctionalized compounds. The DDSQ cage, in chain structure provided an increase in the extent of cure reaction. These studies also revealed that SQs end-capped with phenylethynyl groups are comparable with their organic counterparts and can be used for fiber-reinforced composites. Additionally, the solid to liquid phase transition of these materials was decreased. Studies based on how the SQ cage has affected the viscosity were not accomplished prior to this dissertation.

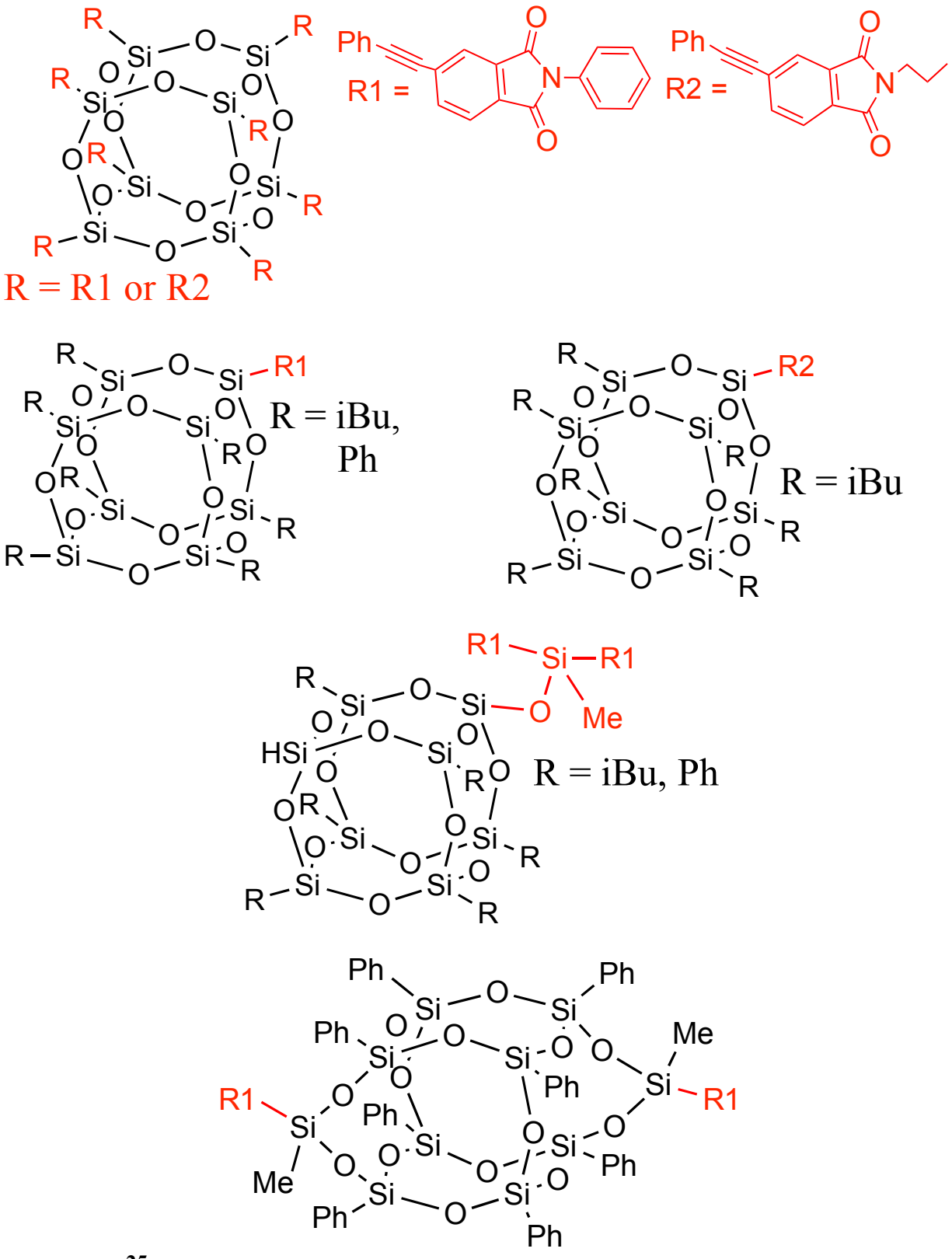

Figure 2-31.[25] Phenylethynyl end-capped SQs.

2.5.2 Thermoplastics

Aromatic polyamides, or polyaramids, are also considered to be HPMs due to their excellent thermomechanical properties, making them suitable for advanced engineering technologies.[74] The most common polyaramids are Kevlar ® and Nomex ®, or poly(*p*-phenylene terephthalamide) (PPD-T) and poly(*m*-phenylene isophthalamide) (MPD-I), respectively (Figure 2-32). There are three common polymerization methods for synthesizing

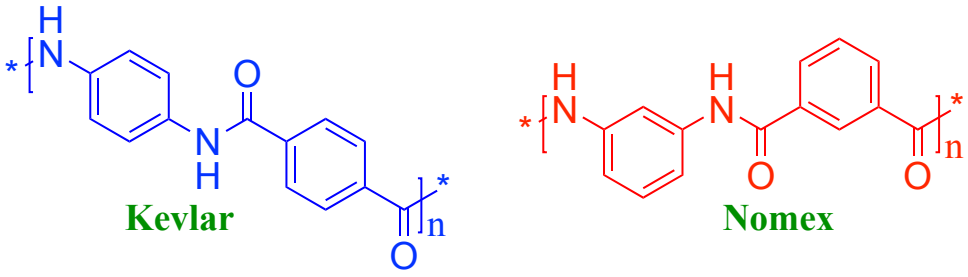

Figure 2-32. Kevlar ® (PPD-T) and Nomex ® (MPD-I) polymer structures.

these polymers: (1) interfacial polymerization with M/P-DA and PCL, (2) low temperature solution polymerization with a diamine (DA) and a phthaloyl chloride (PCL)[127-130], and (3) low temperature solution polymerization with N-silylated DA and PCL[131-133] (Scheme 2-4). The method producing the highest molecular weight (MW) polymer is generally preferred.[127]

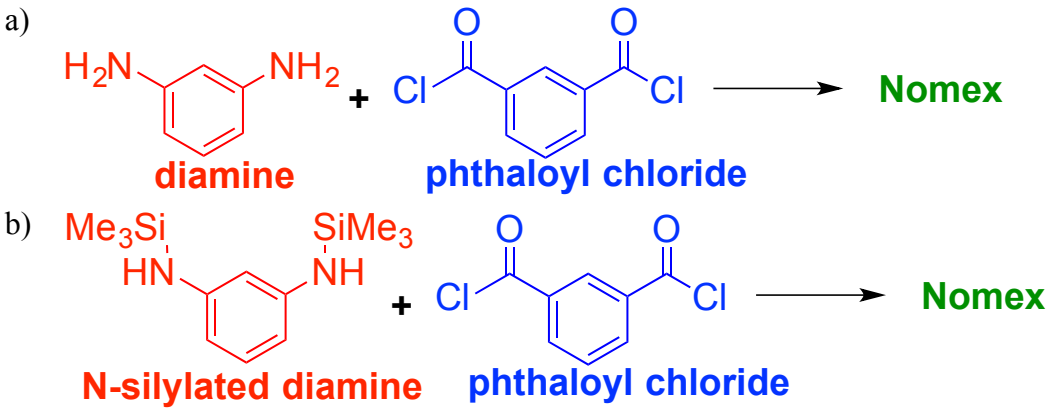

Scheme 2-4. Nomex ® synthesis using (a) DA with PCL, and (b) N-silylated DA with PCL.

Low temperatures solution polymerization with N-silylated DA and PCL resulted with higher inherent viscosity (η_{inh}) than their DA equivalents (Table 2-15).[131-133] Inherent viscosity is a relative measure of the MW of the polymer. Additionally, these reactions proceeded faster. Amide solvents are used for this polymerization at –10 °C. N-silylated PPD-T was synthesized in a solvent mixture comprised of NMP and HPT containing LiCl at –10 °C to –5 °C for 12 h. N-sylilated MPD-I was synthesized in NMP with LiCl at –10 °C to –5 °C for 5 h.

Table 2-15. η_{inh} of synthetic Nomex ®.

Polymer	η_{inh}	
	N-silylation method	Diamine
PPD-T	7.41	3.23
MPD-I	2.45	1.03

Silicon has a strong affinity for oxygen, and the carbocation on the ß-position to the silicon can be stabilized through the silicon σ-π effect in a two-step mechanism (Scheme 2-5).[134-136] The carbonyl oxygen is attracted to the silicon atom on the amine, making it possible for a nucleophilic attack of the nitrogen at the carbonyl carbon. A tetrahedral intermediate is formed. The second step involves the elimination of the chloride ion from the tetrahedral intermediate that is stabilized by the σ-π effect.

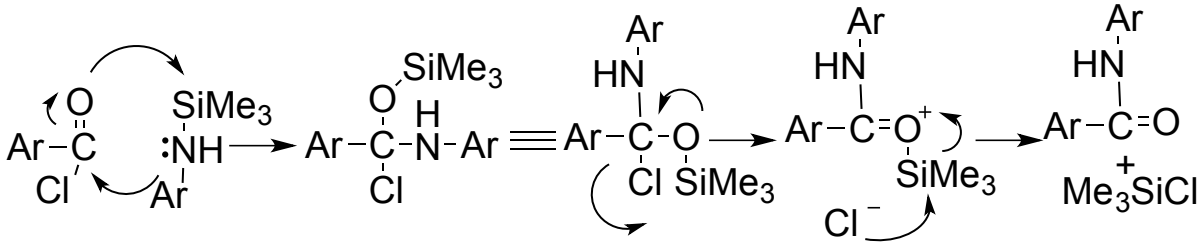

Scheme 2-5. Mechanism for reaction of N-silylated DA and PCL.

As previously mentioned, η_{inh} provides a relative, and simple measure of the MW of these polymers. Inherent viscosity is an approximation of intrinsic viscosity ([η]). Intrinsic

viscosity can be related to molecular weight through the Mark-Houwink (Equation 2-10):[127]

$$[\eta] = kM_w^a \qquad (2-10)$$

where *k* and *a* are constants dependent on the polymer-solvent pair, but are independent of MW. However, the Mark-Houwink equation does not hold true for viscosity-MW relationships at a polyaramid MW > 40,000. Inherent viscosity measurements for PPD-T are typically done with a viscometer in 96-98 % sulfuric acid, and for MPD-I in amide solvents. Gel permeation chromatography (GPC) can also be used to obtain these values. Other, more complex methods for determining MW of a polymer include: light scattering and elemental analysis.

These polyaramids are known to have higher specific strength and modulus than glass and steel due to their low density, and have been used to make products to protect personnel from fire, bullets, and cuts, reduce the weight of aircraft and automobiles, and hold drilling platforms in place.[127] However, they exhibit extremely high transition temperatures, which lie above their decomposition temperatures, and very poor solubility in common organic solvents, making them difficult to process and limiting their applications. PPD-T is even more insoluble than MPD-I. An all *para* - wholly aromatic structure creates a stiff, rod-like macromolecule with high cohesive energy and a high tendency for crystallization due to favorable intramolecular H-bonding and pi-stacking. The tendency for crystallization is so strong, that it is even maintained in the liquid state. MPD-I is not as linear, which causes a reduction in its cohesive energy and crystallization tendency, making it a HPM that is easier to process than PPD-T due to its inherent flexibility from the "kinks" in its structure. However, for the same reason it slightly underperforms PPD-T (Table 2-16).

In view of the remarkable characteristics displayed by polyaramids, research efforts are directed in two areas: (1) reducing the cohesive energy resulting from H-bonding and pi-stacking

Table 2-16.[74] Properties of PPD-T and MPD-I.

Property	PPD-T	MPD-I
Density (g /cm^3)	1.44	1.38
Water uptake (%)	3.9	5.2
Thermal Properties		
T_g (°C)	---	275
T_m (°C)	> 500 d[b]	365 d[b]
T_d (°C, in N_2)	520-540	400-430
Tensile Properties		
Strength (GPa)	2.9-3.0	0.59-0.86
Modulus (GPa)	70-112	7.9-12.1
Elongation (%)	2.4-3.6	20-45
Crystallinity (%)	100	68-95
Flammability (L.O.I.)	29	29

[a] 65 % RH [b] Decomposes (d)

so these materials are easier to process, and soluble in common organic solvents without sacrificing high performance properties, and (2) expanding their high-performance properties to additional applications in new and promising fields, such as: optically active, luminescent, ionic exchange, flame-resistant and fiber-forming materials.

Research on the stereo-isomers of aromatic polyamides has been given little recognition. However, Koning et. al. have looked at *cis/trans* isomers of a non-aromatic polyamides, formed from the reaction of 1,4-cyclohexanedicarboxylic acid, and 1,4-diaminocyclohexane acid (Figure 2-33).[137] It was observed that the *trans* isomer exhibited a more 'stretched' configuration due to its symmetry, and was capable of increasing the T_m, whereas the *cis* isomer did not significantly alter the T_m. Additionally, the intersheet distance of the polyamides increased with increasing *trans* content, and remained the same with increasing *cis* content. These results clearly

demonstrate that the incorporation of the more highly symmetric *trans* isomer into the polyamide back bone gives rise to a unit-cell expansion, resulting from the larger intersheet distance without any effect on the interchain distance. The reason for this occurrence has been attributed to the reduction of rotational ability intrinsic to the *trans* polymer, hampering the formation of intersheet H-bonds. Furthermore, the "kinky" *cis* structure is not incorporated into the crystalline region of the polymer. Conversely, the *trans* structure is present in both the crystalline and amorphous regions. All these effects were seen with aliphatic polyamides and thus do not incorporate additional effects such as pi-stacking that could be present in a polyaramid.

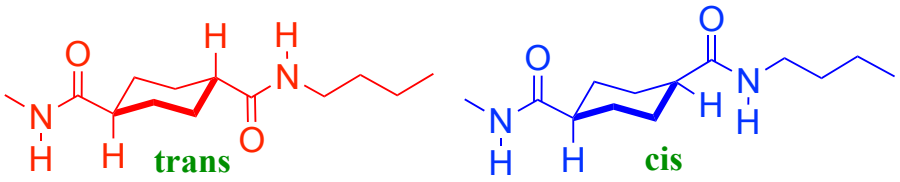

Figure 2-33.[137] Stereoisomers of a polyamide.

An important feature of polyaramids to be considered is that water or polar, protic solvents can diffuse into the amorphous regions and disrupt H-bonding (Figure 2-34). Interchain H-bonds can be replaced by interactions with water, or other polar molecules, thus weakening interchain interactions and allowing freedom of movement about the amide group. This can have a large effect on polymer properties, specifically decreasing T_g.[138]

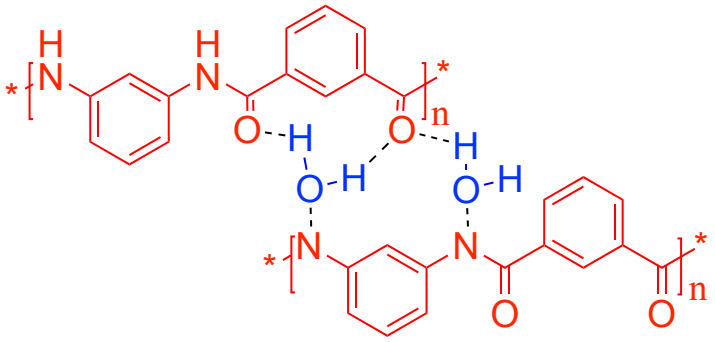

Figure 2-34.[138] Diffusion of water into the chain of a polyaramid.

There have not been any cage-like SQ modified polyaramids of Kevlar ® or Nomex ®. However, there have been reports of cage-like monofunctionalized SQs (SQ F, Figure 2-3) to modify PA6, which is the non-aromatic version of these polymers (Table 2-1).[34] These reports demonstrate that the incorporation of monofunctionalized SQ *F* through blending with PA6 decreases the T_g for injection molded samples. For melt-spun fiber samples, there is an increase in tensile modulus and strength of ca. 50 % for up to a composition of 2.5 % SQ. This value was then decreased at higher compositions of SQ. Additionally; it was revealed in DMA experimenta that above T_g, the rubbery modulus for the blends was significantly higher than neat PA6. Although these studies have demonstrated improved thermomechanical properties for PA6, the SQ itself is not covalently bonded to PA6, which could potentially have a more significant effect on the polymer properties.

2.5.3 Ionic Liquid

An ionic liquid (IL) is defined as a salt with a T_m below 100 °C.[21] They are very attractive materials due to their wide variety of properties: wide liquid range, excellent electrochemical, thermal, and chemical stability, dispersant capabilities, high ionic conductivity, tunable dielectric constants, and biocompatibility. Additionally, they have low vapor pressure and are soluble in a wide variety of common solvents. Furthermore, they can be recycled in liquid-liquid processes, and potentially recovered. These combined properties make ILs part of the "green chemistry" classification. There applications include: replacing volatile organic solvents in an industrial setting for conventional as well as catalytic reactions and separation processes, absorbents in gas separations, CO_2 storage, SO_2 and hydrofluorocarbon absorption,

electrolytes for energy storage devices such as dye sensitized solar cells, electric double-layer capacitors, and fuel cells.[139] Properties of ILs can be enhanced through the incorporation of nanoparticles such as: silica and metal supporting oxides. These nanoparticles will act as IL-supporting substrates and have found applications in catalysis and the development of ion lithium batteries.[140-142]

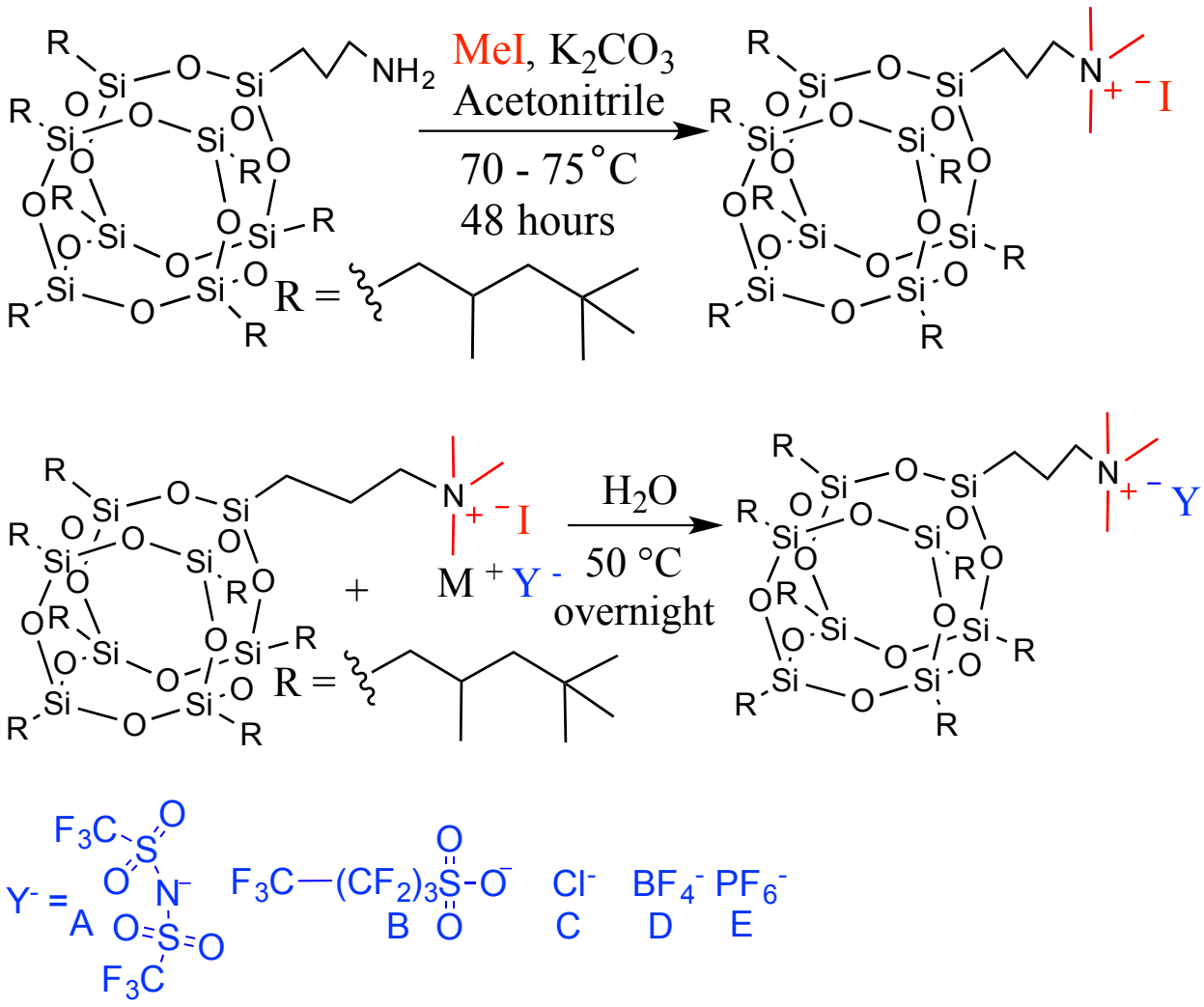

Scheme 2-6. Synthesis of SQ ionic liquids.

More recently, cage-like SQs have been nanoparticles selected for IL-supporting substrates.[21,143-145] Reacting a corner-capped aminopropyl SQ with methyl iodide has successfully produced an IL with I^- as the anion and $-NMe_3^+$ as the cation (Scheme 2-6).[21] Ion exchange then led to additional SQ ILs. All of these ILs had relatively high T_g values, low-polarity, and were amorphous materials when compared with tetraalkylammonium ILs. Additionally, when compared to standard ILs, dielectric constants as well as room-temperature conductivity were found to be much lower. The extraction capability for the sodium salt [H_2TPP^{4-}] from aqueous solutions confirmed that these ILs have cationic surfactant behavior. There was no considerable aggregation in solution with the exception of the iodide and chloride ILs. These studies demonstrate that cage-like SQs have great potential in the field of ILs. No studies on ILs and DDSQs were carried out prior to this dissertation.

REFERENCES

REFERENCES

(1) Yang, B.; Li, M.; Wu, Y.; Wan, X. *Polymers & Polymer Composites* **2013**, *21*, 37.

(2) Wu, S.; Hayakawa, T.; Kikuchi, R.; Grunzinger, S.; Kakimoto, M. *Macromolecules* **2007**, *40*, 5698.

(3) Wu, S.; Hayakawa, T.; Kakimoto, M.; Oikawa, H. *Macromolecules* **2008**, *41*, 3481.

(4) Wu, J.; Mather, P. T. *Polymer Reviews* **2009**, *49*, 25.

(5) Fan, H.; Yang, R. *Industrial & Engineering Chemistry Research* **2013**, *52*, 2493.

(6) Rakesh, S.; Dharan, C. P. S.; Selladurai, M.; Sudha, V.; Sundararajan, P. R.; Sarojadevi, M. *High Performance Polymers* **2013**, *25*, 87.

(7) Vahabi, H.; Ferry, L.; Longuet, C.; Otazaghine, B.; Negrell-Guirao, C.; David, G.; Lopez-Cuesta, J. M. *Materials Chemistry and Physics* **2012**, *136*, 762.

(8) Vahabi, H.; Eterradossi, O.; Ferry, L.; Longuet, C.; Sonnier, R.; Lopez-Cuesta, J. M. *European Polymer Journal* **2013**, *49*, 319.

(9) Li, L.; Li, X.; Yang, R. *Journal of Applied Polymer Science* **2012**, *124*, 3807.

(10) Fox, D. M.; Lee, J.; Zammarano, M.; Katsoulis, D.; Eldred, D. V.; Haverhals, L. M.; Trulove, P. C.; De Long, H. C.; Gilman, J. W. *Carbohydrate Polymers* **2012**, *88*, 847.

(11) Wang, X.; Xuan, S.; Song, L.; Yang, H.; Lu, H.; Hu, Y. *Journal of Macromolecular Science Part B-Physics* **2012**, *51*, 255.

(12) Chrissafis, K.; Bikiaris, D. *Thermochimica Acta* **2011**, *523*, 1.

(13) Ni, Y.; Zheng, S. X. *Chemistry of Materials* **2004**, *16*, 5141.

(14) Gnanasekaran, D.; Reddy, B. S. R. *Polymer Composites* **2012**, *33*, 1197.

(15) Guenthner, A. J.; Lamison, K. R.; Lubin, L. M.; Haddad, T. S.; Mabry, J. M. *Industrial & Engineering Chemistry Research* **2012**, *51*, 12282.

(16) Rizvi, S. B.; Yildirimer, L.; Ghaderi, S.; Ramesh, B.; Seifalian, A. M.; Keshtgar, M. *International journal of nanomedicine* **2012**, *7*, 3915.

(17) Vila Ramirez, N.; Sanchez-Soto, M. *Polymer Composites* **2012**, *33*, 1707.

(18) Blanco, I.; Abate, L.; Bottino, F. A.; Bottino, P. *Polymer Degradation and Stability* **2012**, *97*, 849.

(19) Jin, L.; Ishida, H. *Polymer Composites* **2011**, *32*, 1164.

(20) *Zheng, L.; Waddon, A. J.; Farris, R. J.; Coughlin, E. B. Macromolecules* **2002***,* 35*,* 2375.

(21) Cardiano, P.; Lazzara, G.; Manickam, S.; Mineo, P.; Milioto, S.; Lo Schiavo, S. *European Journal of Inorganic Chemistry* **2012**, 5668.

(22) Geng, Z.; Ba, J.; Zhang, S.; Luan, J.; Jiang, X.; Huo, P.; Wang, G. *Journal of Materials Chemistry* **2012**, *22*, 23534.

(23) Ke, F.; Zhang, C.; Guang, S.; Xu, H. *Journal of Applied Polymer Science* **2013**, *127*, 2628.

(24) Phillips, S. H.; Haddad, T. S.; Tomczak, S. J. *Current Opinion in Solid State & Materials Science* **2004**, *8*, 21.

(25) Seurer, B.; Vij, V.; Haddad, T.; Mabry, J. M.; Lee, A. *Macromolecules* **2010**, *43*, 9337.

(26) Kim, G. M.; Qin, H.; Fang, X.; Sun, F. C.; Mather, P. T. *Journal of Polymer Science Part B-Polymer Physics* **2003**, *41*, 3299.

(27) Kannan, R. Y.; Salacinski, H. J.; Sales, K. M.; Butler, P. E.; Seifalian, A. M. *Cell Biochemistry and Biophysics* **2006**, *45*, 129.

(28) Markovic, E.; Constantopolous, K.; Cordes, D. B.; Lickiss, P. D.; Ward, A. J.; Masters, A. F.; Williams, K. G.; Gido, S. P.; DeArmitt, C.; Iacono, S. T.; Peloquin, A. J.; Hartmann-Thompson, C.; Brandhorst Jr, H. W.; Ghanbari, H.; Marashi, S. M. *Applications of Polyhedral Oligomeric Silsesquioxanes*; Springer: Netherlands, 2011.

(29) Li, G.; Wang, L.; Ni, H.; Pittman, C. U. *Journal of Inorganic and Organometallic Polymers* **2001**, *11*, 123.

(30) Haddad, T. S.; Lichtenhan, J. D. *Macromolecules* **1996**, *29*, 7302.

(31) Lichtenhan, J. D.; Otonari, Y. A.; Carr, M. J. *Macromolecules* **1995**, *28*, 8435.

(32) Mather, P. T.; Jeon, H. G.; Romo-Uribe, A.; Haddad, T. S.; Lichtenhan, J. D. *Macromolecules* **1999**, *32*, 1194.

(33) Tsuchida, A.; Bolln, C.; Sernetz, F. G.; Frey, H.; Mulhaupt, R. *Macromolecules* **1997**, *30*, 2818.

(34) Milliman, H. W.; Ishida, H.; Schiraldi, D. A. *Macromolecules* **2012**, *45*, 4650.

(35) Zeng, K.; Liu, Y.; Zheng, S. *European Polymer Journal* **2008**, *44*, 3946.

(36) Xu, H. Y.; Kuo, S. W.; Lee, J. S.; Chang, F. C. *Polymer* **2002**, *43*, 5117.

(37) Liu, S.; Yi, L.-Z.; Liang, Y.-Z. *Journal of Separation Science* **2008**, *31*, 2113.

(38) Kuo, S.-W.; Chang, F.-C. *Progress in Polymer Science* **2011**, *36*, 1649.

(39) Willard, J. J.; Wondra, R. E. *Textile Research Journal* **1970**, *40*, 203.

(40) McCusker, C.; Carroll, J. B.; Rotello, V. M. *Chemical Communications* **2005**, 996.
(41) Gitli, T.; Silverstein, M. S. *Polymer* **2011**, *52*, 107.

(42) Amir, N.; Levina, A.; Silverstein, M. S. *Journal of Polymer Science Part a-Polymer Chemistry* **2007**, *45*, 4264.

(43) Gurevitch, I.; Silverstein, M. S. *Journal of Polymer Science Part a-Polymer Chemistry* **2010**, *48*, 1516.

(44) Normatov, J.; Silverstein, M. S. *Polymer* **2007**, *48*, 6648.

(45) Normatov, J.; Silverstein, M. S. *Journal of Polymer Science Part a-Polymer Chemistry* **2008**, *46*, 2357.

(46) Normatov, J.; Silverstein, M. S. *Chemistry of Materials* **2008**, *20*, 1571.

(47) Silverstein, M. S.; Shach-Caplan, M.; Khristosov, M.; Harel, T. *Plasma Processes and Polymers* **2007**, *4*, 789.

(48) Wright, M. E.; Schorzman, D. A.; Feher, F. J.; Jin, R. Z. *Chemistry of Materials* **2003**, *15*, 264.

(49) Brunsvold, A. L.; Minton, T. K.; Gouzman, I.; Grossman, E.; Gonzalez, R. *High Performance Polymers* **2004**, *16*, 303.

(50) Minton, T. K.; Wright, M. E.; Tomczak, S. J.; Marquez, S. A.; Shen, L.; Brunsvold, A. L.; Cooper, R.; Zhang, J.; Vij, V.; Guenthner, A. J.; Petteys, B. J. *Acs Applied Materials & Interfaces* **2012**, *4*, 492.

(51) Hoque, M. A.; Kakihana, Y.; Shinke, S.; Kawakami, Y. *Macromolecules* **2009**, *42*, 3309.

(52) Seino, M.; Hayakawa, T.; Ishida, Y.; Kakimoto, M.-a.; Watanabe, K.; Oikawa, H. *Macromolecules* **2006**, *39*, 3473.

(53) Gilman, J. W.; Schlitzer, D. S.; Lichtenhan, J. D. *Journal of Applied Polymer Science* **1996**, *60*, 591.

(54) Lichtenhan, J. D. *Comments on Inorganic Chemistry* **1995**, *17*, 115.

(55) Katoh, T.; Kikukawa, T.; Ito, K.; Yoshida, K.; Yamamoto, Y.; Japan . 2006, p 21pp.

(56) Lichtenhan, J. D.; Vu, N. Q.; Carter, J. A.; Gilman, J. W.; Feher, F. J. *Macromolecules* **1993**, *26*, 2141.

(57) Espinas, J.; Pelletier, J. D. A.; Abou-Hamad, E.; Emsley, L.; Basset, J.-M. *Organometallics* **2012**, *31*, 7610.

(58) Hay, M. T.; Seurer, B.; Holmes, D.; Lee, A. *Macromolecules* **2010**, *43*, 2108.

(59) Aminuzzaman, M.; Watanabe, A.; Miyashita, T. *Journal of Materials Chemistry* **2008**, *18*, 5092.

(60) Goto, Y.; Yoshida, K.; Sawada, H. *Colloid and Polymer Science* **2011**, *289*, 1493.

(61) Kucuk, A. C.; Matsui, J.; Miyashita, T. *Journal of Colloid and Interface Science* **2011**, *355*, 106.

(62) Wei, K.; Wang, L.; Zheng, S. *Polymer Chemistry* **2013**, *4*, 1491.

(63) Wang, L.; Zhang, C.; Zheng, S. *Journal of Materials Chemistry* **2011**, *21*, 19344.

(64) Vij, V.; Haddad, T. S.; Yandek, G. R.; Ramirez, S. M.; Mabry, J. M. *Silicon* **2012**, *4*, 267.

(65) Watanabe, Y.; Sakai, Y.; Shibasaki, Y.; Ando, S.; Ueda, M.; Oishi, Y.; Mori, K. *Macromolecules* **2002**, *35*, 2277.

(66) Maier, G. *Progress in Polymer Science* **2001**, *26*, 3.

(67) Leu, C. M.; Chang, Y. T.; Wei, K. H. *Chemistry of Materials* **2003**, *15*, 3721.

(68) Leu, C. M.; Reddy, G. M.; Wei, K. H.; Shu, C. F. *Chemistry of Materials* **2003**, *15*, 2261.

(69) Leu, C. M.; Chang, Y. T.; Wei, K. H. *Macromolecules* **2003**, *36*, 9122.

(70) Seino, M.; Hayakawa, T.; Ishida, Y.; Kakimoto, M.; Watanabe, K.; Oikawa, H. *Macromolecules* **2006**, *39*, 3473.

(71) Mitsuishi, M.; Zhao, F.; Kim, Y.; Watanabe, A.; Miyashita, T. *Chemistry of Materials* **2008**, *20*, 4310.

(72) Lee, W.; Ni, S.; Deng, J.; Kim, B.-S.; Satija, S. K.; Mather, P. T.; Esker, A. R. *Macromolecules* **2007**, *40*, 682.

(73) Gunawidjaja, R.; Huang, F.; Gumenna, M.; Klimenko, N.; Nunnery, G. A.; Shevchenko, V.; Tannenbaum, R.; Tsukruk, V. V. *Langmuir* **2009**, *25*, 1196.

(74) Garcia, J. M.; Garcia, F. C.; Serna, F.; de la Pena, J. L. *Progress in Polymer Science* **2010**, *35*, 623.

(75) Li, G.; Wang, Z. *Macromolecules* **2013**, *46*, 3058.

(76) Slegt, M.; Overkleeft, H. S.; Lodder, G. *European Journal of Organic Chemistry* **2007**, 5364.

(77) Wang, L.; Du, W.; Wu, Y.; Xu, R.; Yu, D. *Journal of Applied Polymer Science* **2012**, *126*, 150.

(78) Stock, A. *Berichte Der Deutschen Chemischen Gesellschaft* **1916**, *49*, 108.

(79) Baudrillard, V.; Davoust, D.; Ple, G. *Magnetic Resonance in Chemistry* **1994**, *32*, 40.

(80) Holmes, D.; Johnson, K. *Determining C-H Connectivity: gHMQC and gHMBC;* http://www2.chemistry.msu.edu/facilities/nmr/handouts/gHMQC.pdf, **2010**.

(81) Holmes, D.; Johnson, K. *The Gradient-Selected COSY (gCOSY) Experiment;* http://www2.chemistry.msu.edu/facilities/nmr/handouts/gCOSY.pdf **2011**.

(82) Raya, J.; Hirschinger, J.; Ovarlez, S.; Giulieri, F.; Chaze, A.-M.; Delamare, F. *Physical Chemistry Chemical Physics* **2010**, *12*, 14508.

(83) Liepinsh, E.; Sekacis, I.; Lukevics, E. *Magnetic Resonance in Chemistry* **1985**, *23*, 10.

(84) Myasnikov, S. K.; Uteshinsky, A. D.; Kulov, N. N. *Theoretical Foundations of Chemical Engineering* **2009**, *43*, 227.

(85) Tadie, M.; Bahadur, I.; Reddy, P.; Ngema, P. T.; Naidoo, P.; Deenadayalu, N.; Ramjugernath, D. *Journal of Chemical Thermodynamics* **2013**, *57*, 485.

(86) Wang, T.-C.; Li, Y.-J.; Chen, Y.-P. *Journal of Chemical and Engineering Data* **2012**, *57*, 3519.

(87) Tam Le, M.; Lorenz, H.; Seidel-Morgenstern, A. *Chemical Engineering & Technology* **2012**, *35*, 1003.

(88) Ji, H.-Z.; Meng, X.-C.; Zhao, H.-K. *Journal of Chemical and Engineering Data* **2010**, *55*, 2590.

(89) Lohmann, J.; Ropke, T.; Gmehling, J. *Journal of Chemical and Engineering Data* **1998**, *43*, 856.

(90) Prausnitz, J. M.; Lichtenthaler, R. N.; Azevedo, E. G. d. *Molecular thermodynamics of fluid-phase equilibria*; 3rd ed.; Prentice Hall PTR: Upper Saddle River, N.J., 1999.

(91) Gmehling, J. G.; Anderson, T. F.; Prausnitz, J. M. *Industrial & Engineering Chemistry Fundamentals* **1978**, *17*, 269.

(92) Elliott, J. R.; Lira, C. T. *Introductory chemical engineering thermodynamics*; 2nd ed.; Prentice Hall: Upper Saddle River, NJ, 2012.
(93) Renon, H.; Prausnit.Jm *Industrial & Engineering Chemistry Process Design and Development* **1969**, *8*, 413.

(94) Gavezzotti, A. *Journal of the Chemical Society-Perkin Transactions 2* **1995**, 1399.

(95) Pinal, R. *Organic & Biomolecular Chemistry* **2004**, *2*, 2692.

(96) Plass, K. E.; Engle, K. M.; Matzger, A. J. *Journal of the American Chemical Society* **2007**, *129*, 15211.

(97) Slovokhotov, Y. L.; Neretin, I. S.; Howard, J. A. K. *New Journal of Chemistry* **2004**, *28*, 967.

(98) Lloyd, M. A.; Patterson, G. E.; Simpson, G. H.; Duncan, L. L.; King, D. P.; Fu, Y.; Patrick, B. O.; Parkin, S.; Brock, C. P. *Acta Crystallographica Section B-Structural Science* **2007**, *63*, 433.

(99) Sysoev, S. V.; Cheremisina, T. N.; Zelenina, L. N.; Tkachev, S. V.; Zherikova, K. V.; Morozova, N. B.; Kuratieva, N. V. *Journal of Thermal Analysis and Calorimetry* **2010**, *101*, 41.

(100) Slovokhotov, Y. L.; Batsanov, A. S.; Howard, J. A. K. *Structural Chemistry* **2007**, *18*, 477.

(101) Aoki, K.; Nakagawa, M.; Ichimura, K. *Journal of the American Chemical Society* **2000**, *122*, 10997.

(102) Patra, A.; Richert, C. *Journal of the American Chemical Society* **2009**, *131*, 12671.

(103) Aakeroy, C. B.; Forbes, S.; Desper, J. *Journal of the American Chemical Society* **2009**, *131*, 17048.

(104) Simperler, A.; Watt, S. W.; Bonnet, P. A.; Jones, W.; Motherwell, W. D. S. *Crystengcomm* **2006**, *8*, 589.

(105) Kuduva, S. S.; Sarma, J.; Katz, A. K.; Carrell, H. L.; Desiraju, G. R. *Journal of Physical Organic Chemistry* **2000**, *13*, 719.

(106) Plato, C.; Glasgow, A. R. *Analytical Chemistry* **1969**, *41*, 330.

(107) Yamashita, H.; Hirakura, Y.; Yuda, M.; Teramura, T.; Terada, K. *Pharmaceutical Research* **2013**, *30*, 70.

(108) He, B.; Martin, V.; Setterwall, F. *Fluid Phase Equilibria* **2003**, *212*, 97.

(109) Lane, G. A. *Solar heat storage : latent heat materials*; CRC Press: Boca Baton, Fla., 1983.

(110) Walas, S. M. *Phase equilibria in chemical engineering*; Butterworth: Boston, 1985.

(111) Jones, W.; Motherwell, S.; Trask, A. V. *Mrs Bulletin* **2006**, *31*, 875.

(112) Stahly, G. P. *Crystal Growth & Design* **2007**, *7*, 1007.

(113) Bhogala, B. R.; Nangia, A. *New Journal of Chemistry* **2008**, *32*, 800.

(114) Yoshimoto, N.; Nakamura, T.; Suzuki, M.; Sato, K. *Journal of Physical Chemistry* **1991**, *95*, 3384.

(115) Wei, D.; Jin, K. *Journal of Chemical Thermodynamics* **2009**, *41*, 145.

(116) Wei, D.; Zhang, X.; Li, H. *Journal of Chemical Thermodynamics* **2013**, *60*, 94.

(117) Coutinho, J. A. P. *Fluid Phase Equilibria* **1999**, *158*, 447.

(118) Thompson, C. M.; Hergenrother, P. M. *Macromolecules* **2002**, *35*, 5835.

(119) Simone, C. D.; Scola, D. A. *Macromolecules* **2003**, *36*, 6780.

(120) Hergenrother, P. M.; Connell, J. W.; Smith, J. G. *Polymer* **2000**, *41*, 5073.

(121) Smith, J. G.; Connell, J. W.; Hergenrother, P. M. *Journal of Composite Materials* **2000**, *34*, 614.

(122) Connell, J. W.; Smith, J. G.; Hergenrother, P. M.; Rommel, M. L. *High Performance Polymers* **2000**, *12*, 323.

(123) Smith, J. G.; Connell, J. W. *High Performance Polymers* **2000**, *12*, 213.

(124) Jensen, B. J.; Bryant, R. G.; Smith, J. G.; Hergenrother, P. M. *Journal of Adhesion* **1995**, *54*, 57.

(125) Chen, J.; Zuo, H.; Fan, L.; Yang, S. *High Performance Polymers* **2009**, *21*, 187.

(126) Zuo, H. J.; Chen, J. S.; Yang, H. X.; Hu, A. J.; Fan, L.; Yang, S. Y. *Journal of Applied Polymer Science* **2008**, *107*, 755.

(127) J., G. In *Encyclopedia of Polymer Science and Technology*; John Wiley & Sons: New York, 2005; Vol. 3, p 558.

(128) J., P. In *Encyclopedia of Polymer Science and Engineering*; John Wiley & Sons: New York, 1988; Vol. 11, p 381.

(129) Fedorov, A. A.; Savinov, V. M.; Sokolov, L. B. *Polymer Science U.S.S.R.* **1970**, *12*, 2475.

(130) Chaudhuri, A. K.; Min, B. Y.; Pearce, E. M. *Journal of Polymer Science: Polymer Chemistry Edition* **1980**, *18*, 2949.

(131) Imai, Y.; Oishi, Y. *Progress in Polymer Science* **1989**, *14*, 173.

(132) Oishi, Y.; Kakimoto, M.; Imai, Y. *Macromolecules* **1987**, *20*, 703.

(133) Oishi, Y.; Kakimoto, M. A.; Imai, Y. *Macromolecules* **1988**, *21*, 547.

(134) Cai, H.; Yu, J.; Qiu, Z. *Polymer Engineering & Science* **2012**, *52*, 233.

(135) Arai, F.; Takeshita, H.; Dobashi, M.; Takenaka, K.; Miya, M.; Shiomi, T. *Polymer* **2012**, *53*, 851.

(136) Scott, R. L. *Journal of Chemical Physics* **1949**, *17*, 268.

(137) Vanhaecht, B.; Willem, R.; Biesemans, M.; Goderis, B.; Basiura, M.; Magusin, P.; Dolbnya, I.; Koning, C. *Macromolecules* **2004**, *37*, 421.

(138) Murthy, N. S. *Journal of Polymer Science Part B-Polymer Physics* **2006**, *44*, 1763.

(139) Armand, M.; Endres, F.; MacFarlane, D. R.; Ohno, H.; Scrosati, B. *Nature Materials* **2009**, *8*, 621.

(140) Lu, Y.; Moganty, S. S.; Schaefer, J. L.; Archer, L. A. *Journal of Materials Chemistry* **2012**, *22*, 4066.

(141) Lu, W.; Goering, A.; Qu, L.; Dai, L. *Physical Chemistry Chemical Physics* **2012**, *14*, 12099.

(142) Moganty, S. S.; Jayaprakash, N.; Nugent, J. L.; Shen, J.; Archer, L. A. *Angewandte Chemie-International Edition* **2010**, *49*, 9158.

(143) Tanaka, K.; Ishiguro, F.; Chujo, Y. *Polymer Journal* **2011**, *43*, 708.

(144) Tanaka, K.; Chujo, Y. *Journal of Materials Chemistry* **2012**, *22*, 1733.

(145) Colovic, M.; Jerman, I.; Gaberscek, M.; Orel, B. *Solar Energy Materials and Solar Cells* **2011**, *95*, 3472.

CHAPTER 3

SYNTHESIS OF MONOMERS

Keywords

double decker silsesquioxane, NMR, ^{1}H; ^{29}Si NMR, cis/trans isomers

3. Synthesis of Monomers

3.1 Introduction

As previously mentioned in the background section, a recently developed class of nano-structured silsesquioxanes provides a unique opportunity to investigate and characterize the influence of *cis* and *trans* configurations on the physical and chemical properties of inorganic-organic hybrid materials (Figure 3-1). The *cis* and *trans* descriptors characterize the orientation of the *X* and *R* moieties with respect to the Si-O core of the silsesquioxane. This class of

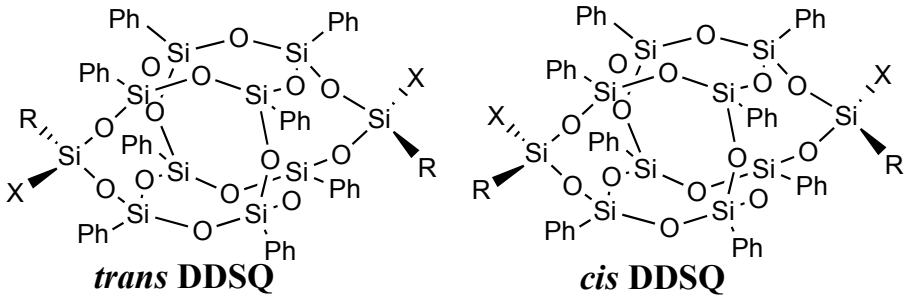

Figure 3-1. *Trans* (left) and *cis* (right) isomers of DDSQ(X)(R).

silsesquioxanes are formally known as double decker silsesquioxanes (DDSQ) because they are comprised of two "decks" of silsesquioxanes stacked on top of one another forming a cage-like structure.[1] Prior to the advent of DDSQ, the majority of cage-like silsesquioxanes did not incorporate *cis* and *trans* isomers.[2-5] Of the few cage-like silsesquioxanes that did incorporate geometric isomers, none have been synthesized in large quantities.[6,7] Cage-like silsesquioxanes have demonstrated superior properties over their organic counterparts in areas such as: thermal and mechanical properties,[8-11] solubility,[12-14] flame retardance,[15-23] oxidative resistance,[24-27] and dielectric properties.[28-30] For this dissertation, four different DDSQ molecules were synthesized (Figure 3-2). The R-moiety was varied from methyl to cyclohexyl while the X-

moiety was meta-amninophenyl. Additionally, the X-moiety was changed from meta-aminophenyl to para-aminophenyl while the R-moiety was methyl.

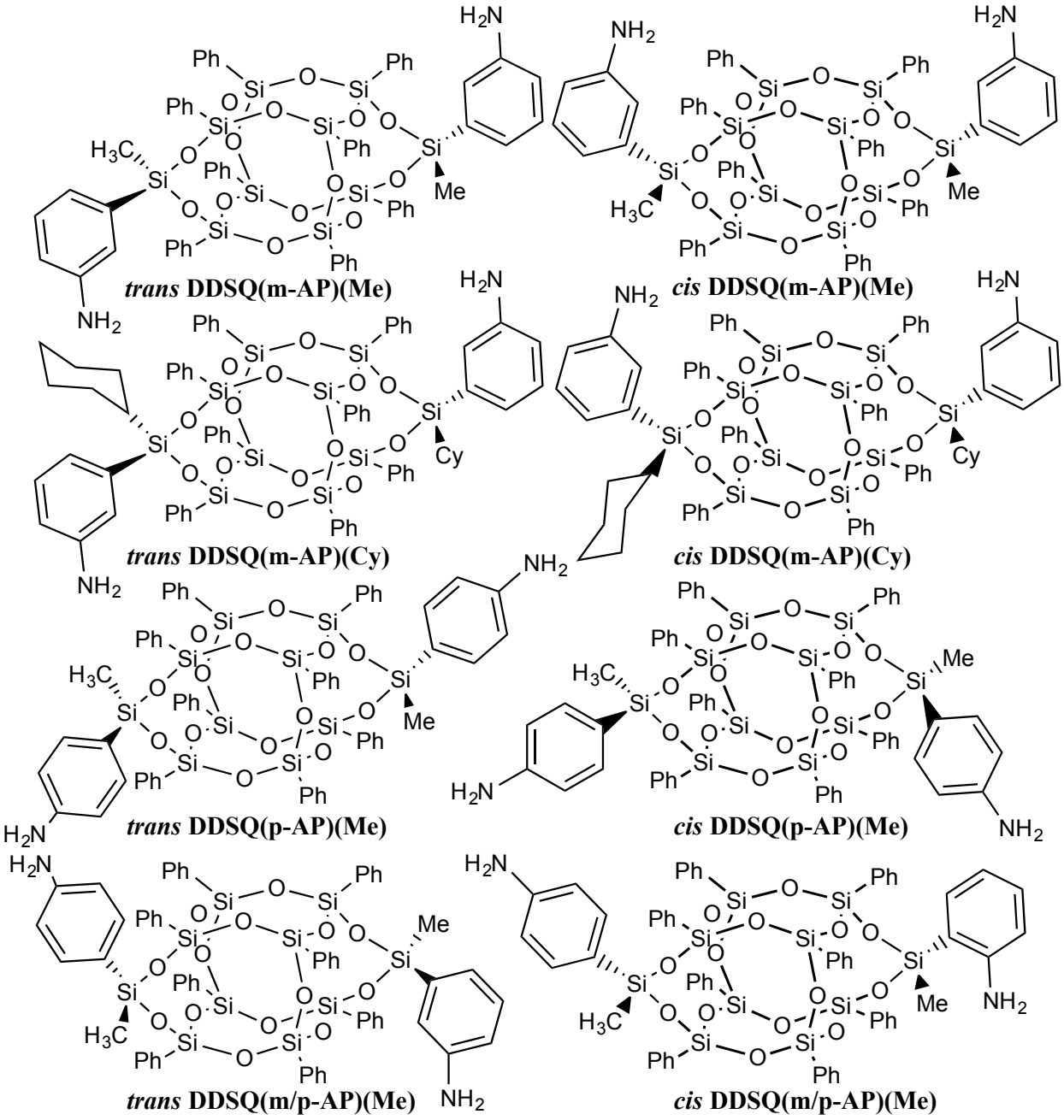

Figure 3-2. *Cis* and *trans* isomers of compounds **3a-d.**

The four structures studied in this work and their notation is described in this section. The naming scheme for these DDSQ will be abbreviated as DDSQ(X)(R), where X is the X-moiety,

and R is the R-moiety (Figure 3-1). The first set of *cis* and *trans* isomers, [(meta-aminophenyl) methylsilyl]-bridged-(phenyl)$_8$-double-decker silsesquioxane, will be designated as DDSQ(m-AP)(Me), and will be represented with shorthand notation-**3a**. The second set of isomers [(meta-aminophenyl)cyclohexylsilyl]-bridged-(phenyl)$_8$-double-decker silsesquioxane, will be designated DDSQ(m-AP)(Cy) and represented by shorthand notation-**3b**. The third set of isomers [(para-aminophenyl)methylsilyl]-bridged-(phenyl)$_8$-double-decker silsesquioxane, will be designated by DDSQ(p-AP)(Me) and represented by shorthand notation-**3c**, and [(meta/para-aminophenyl)methylsilyl]-bridged-(phenyl)$_8$-double-decker silsesquioxane, will be designated by DDSQ(m/p-AP)(Me) and represented by shorthand notation-**3d.** Compounds **3a** and **3b** are both meta- with respect to the aminophenyl (X) moiety, but differ at the organic (R) moiety (Figure 3-2). Compound **3a** has a methyl moiety, whereas **3b** has a cyclohexyl moiety. Compound **3c** is para- with respect to the aminophenyl group and has a methyl moiety. Compound **3d** incorporates once side that is meta- and one side that is para- with respect to the aminophenyl group and has a methyl moiety.

3.2 Solvents and Reagents

Tricycle[7.3.3(3,7)]octasiloxane-5,14,17-tetraol-1,3,5,7,9,11, 14,17-octaphenyl (Ph_8tetrasilanol-POSS) was obtained from Hybrid Plastics (Hattiesburg, MS). Tetrahydrofuran (THF), hexanes, diethyl ether, magnesium turnings, triethylamine, trichloromethyl silane, trichlorocyclohexylsilane, 3-[bis(trimethylsilyl)amino]phenyl-magnesium chloride, and 4-[bis(trimethylsilyl)amino]phenyl(bromo)magnesium were obtained from Sigma-Aldrich. The solvents were distilled under nitrogen and degassed using Freeze-Pump-Thaw methods.

3.3 NMR spectroscopy

Compounds **3a-c** were measured at 25 ºC on a Varian UNITY-Inova 600 spectrometer equipped with a 5 mm Pulsed-Field-Gradient (PFG) switchable broadband probe and operating at 599.80 MHz (^{1}H) and 119.16 MHz (^{29}Si). ^{1}H NMR data were acquired using a recycle delay of 20 s and 32 scans to ensure accurate integration. The pulse angle was set to 45°. The ^{1}H-chemical shifts were referenced to that of residual protonated solvent in $CDCl_3$ (7.24 ppm). $^{29}Si\{^{1}H\}$ NMR data were acquired using a recycle delay of 12 s with inverse-gated decoupling. The pulse angle was set to 90°. $^{29}Si\{^{1}H\}$ spectra were referenced against the lock solvent using vendor supplied lock referencing. $^{13}C\{^{1}H\}$ NMR data were acquired using a recycle delay of 1 s and 256 scans. The pulse angle was set to 45°.

3.4 Synthesis

All compounds, **3a-d**, were synthesized by capping DDSQ tetrasilanol with dichlorosilanes (Scheme 3-1).[31,32] The synthetic procedure generated a mixture of *cis* and *trans* isomers (Figure 3-2).

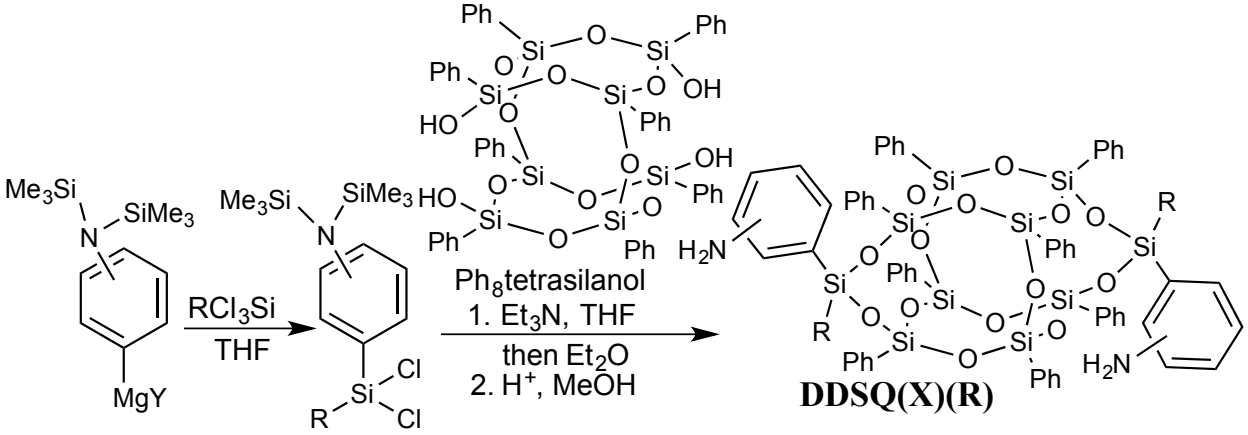

Scheme 3-1. Synthesis of DDSQ(AP)(R); X = Cl/Br, R = Me/Cy.

3.4.1 Compound 3a

Under a nitrogen atmosphere in a drybox, a solution of 1 M 3-[bis(trimethylsilyl)amino] phenyl(chloro)magnesium (60 mL, 60 mmol) was added dropwise via an addition funnel to a stirred solution of trichloromethyl silane (11.077 g, 112 mmol) and THF (20 mL). The solution was stirred for 20 h at 25 °C and then purified by fractional distillation[i] to obtain (*N*-trimethylsilyl)$_2$-aniline-3-(dichloromethylsilane) (18.66 g, 53.24 mmol, 88 % yield) as a colorless liquid. $^{29}Si\{^1H\}$ NMR, δ: 18.40 (1 Si), 5.22 (2 Si). $^{13}C\{^1H\}$ NMR, δ: 148.43, 134.74, 133.82, 133.62, 130.35, 128.8, 128.58, 128.16, 123.73, 5.71, 2.27. ^1H NMR δ: 7.48 (1 H, multiplet), 7.35 (1 H, multiplet), 7.30 (1 H, multiplet), 7.12 (1 H multiplet), 1.06 (3 H, CH_3, singlet), 0.14 (18 H, TMS, singlet) (Figure 3-3).

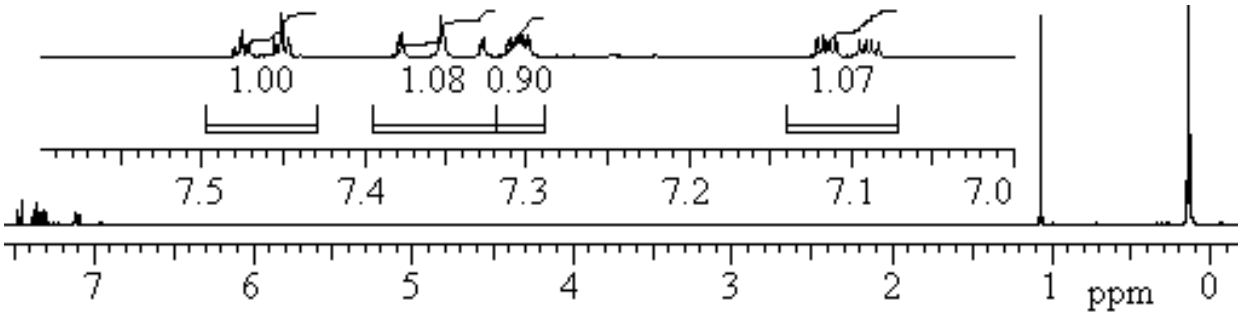

Figure 3-3. ^1H NMR spectrum of (*N*-trimethylsilyl)$_2$-aniline-3-(dichloromethylsilane).

A solution of (N-trimethylsilyl)$_2$-aniline-3-(dichloromethylsilane) (3.03 g, 8.64 mmol) and triethylamine (2.01 g, 19.90 mmol) in THF (10 mL) was added dropwise via an addition funnel into a stirred solution of Ph_8tetrasilanol-POSS (4.50 g, 4.21 mmol) at 25 °C THF (40 mL). After 30 minutes, the $HNEt_3Cl$ precipitate was separated by filtration, and the solvent was removed from the filtrate under vacuum. To the resultant residue diethyl ether (2 mL) was added followed by acidified methanol, which gave a white suspension that was stirred at 25 °C for 20 h.

The heterogeneous mixture was filtered, and the retentate was dried under nitrogen to yield **3a**, (5.379 g, 4.03 mmol, 96 % yield). $^{29}Si\{^{1}H\}$ NMR, δ: -30.6 (4 Si), -78.4 (8 Si), -79.4 (2 Si), -79.6 (4 Si), -79.8 (2 Si). $^{13}C\{^{1}H\}$ NMR, δ: 145.99, 137.24, 134.27, 134.15, 132.03, 131.05, 130.87, 130.50, 130.43, 130.34, 128.96, 127.91, 127.81, 127.72, 127.62, 123.70, 119.92, 116.81, -0.40. ^{1}H NMR δ: 7.54-6.92 (40 H, overlapping multiplets), 6.92 (4 H, multiplet), 6.67 (4 H, multiplet) 3.16 (4 H, NH_2, broad singlet), 0.51 (6H, CH_3, 2 overlapping singlets)[ii] (Figure 3-4).

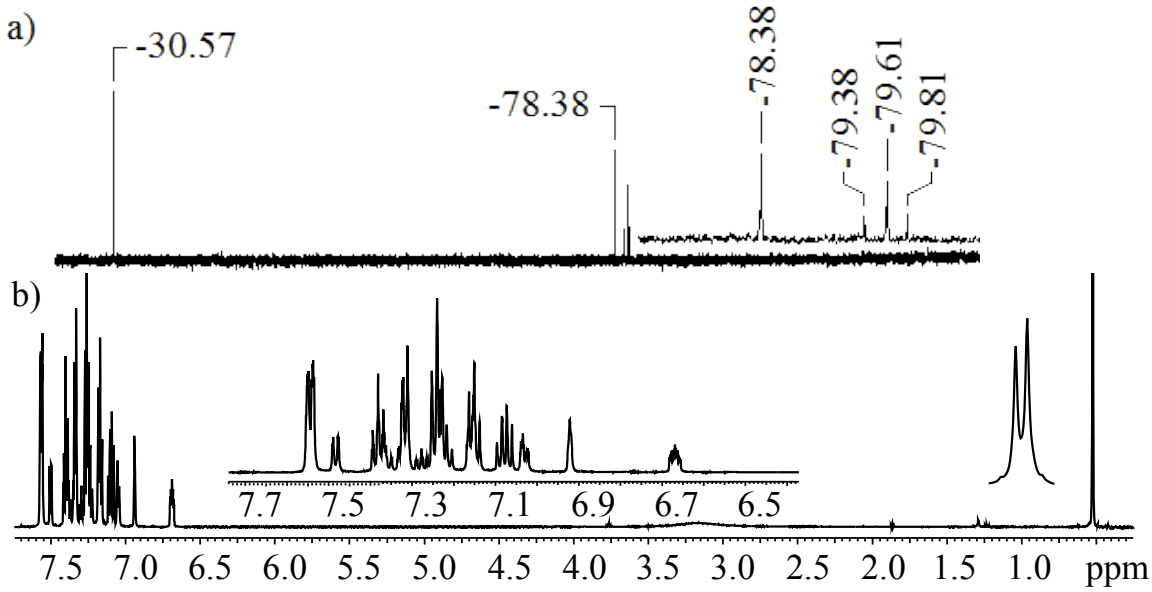

Figure 3-4. NMR spectra of compound **3a** (a) ^{29}Si and (b) ^{1}H.

3.4.2 Compound 3b

Under a nitrogen atmosphere in a drybox, a solution of 1 M 3-[bis(trimethylsilyl) amino]phenyl(chloro)magnesium (16.99 mL, 16.99 mmol) was added dropwise via an addition funnel to a stirred solution of cyclohexyl trichlorosilane (3.69 g, 16.99 mmol) and THF (5 mL). The solution was stirred for 20 h at 25 °C and then purified by Kugelrohr distillation[i] to obtain (*N*-trimethylsilyl)$_2$-aniline-3-(cyclohexyl dichlorosilane) (12.64 g, 53.24 mmol, 74 % yield) as a

colorless liquid. $^{29}Si\{^{1}H\}$ NMR, δ: 18.45 (1 Si), 5.12 (2 Si). $^{13}C\{^{1}H\}$ NMR, δ: 148.17, 135.55, 133.40, 131.77, 130.32, 129.04, 128.68, 128.53, 123.64, 30.72, 27.29, 26.45, 26.02, 2.20. ^{1}H NMR δ: 7.41 (1 H, multiplet), 7.30 (1 H, multiplet), 7.23 (1 H, multiplet), 7.04 (1 H multiplet), 1.78, 1.71, 1.29 (11 H, C_6H_{11}, multiplets), 0.08 (18 H, TMS, singlet) (Figure 3-5).

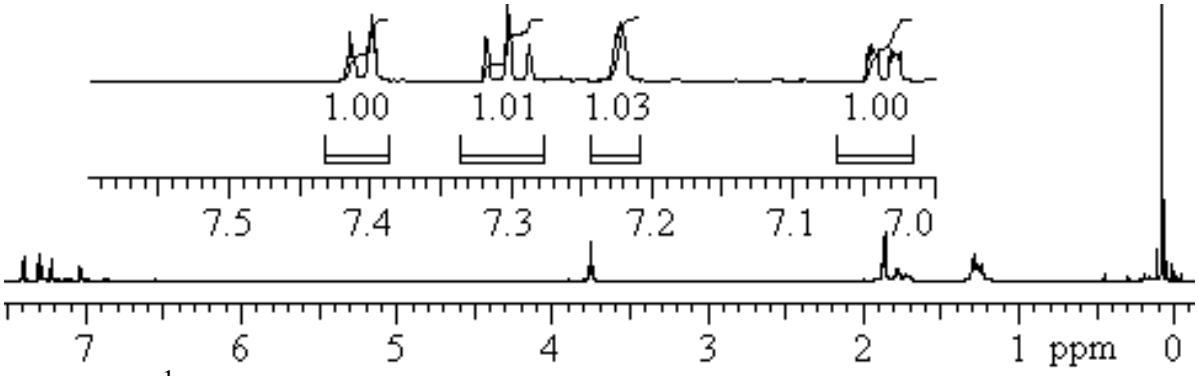

Figure 3-5. ^{1}H NMR spectrum of (*N*-trimethylsilyl)$_2$-aniline-3-(cyclohexyl dichlorosilane).

A solution of (N-trimethylsilyl)$_2$-aniline-3-(dichloromethylsilane) (1.00 g, 2.39 mmol) and triethylamine (0.48 g, 4.73 mmol) in THF (5 mL) was added dropwise via an addition funnel into a stirred solution of Ph_8tetrasilanol-POSS (1.26 g, 1.18 mmol) at 25 °C THF (5 mL). After 30 minutes, the $HNEt_3Cl$ precipitate was separated by filtration, and the solvent was removed from the filtrate under vacuum. To the resultant residue diethyl ether (2 mL) was added followed by acidified methanol, which gave a white suspension that was stirred at 25 °C for 20 h. The heterogeneous mixture was filtered, and the retentate was dried under nitrogen to yield **3b**, (1.19 g, 0.81 mmol, 69 % yield). $^{29}Si\{^{1}H\}$ NMR, δ: -34.1 (4 Si), -78.5 (8 Si), -79.3 (2 Si), -79.5 (4 Si), -79.7 (2 Si). $^{13}C\{^{1}H\}$ NMR, δ: 145.82, 135.62, 134.26, 134.23, 132.24, 131.10, 130.86, 130.71, 130.43, 130.32, 128.81, 127.89, 127.76, 127.63, 127.49, 124.43, 120.72, 116.75, 27.64, 26.81, 26.43, 26.22, 2.15, 1.49. ^{1}H NMR δ: 7.57-6.97 (40 H, overlapping multiplets), 6.83 (4 H,

multiplet), 6.67 (4 H, multiplet) 3.24 (4 H, NH_2, broad singlet), 1.79, 1.58, 1.19, 1.08, 1.03 (11 H, C_6H_{11}, multiplets) (Figure 3-6).

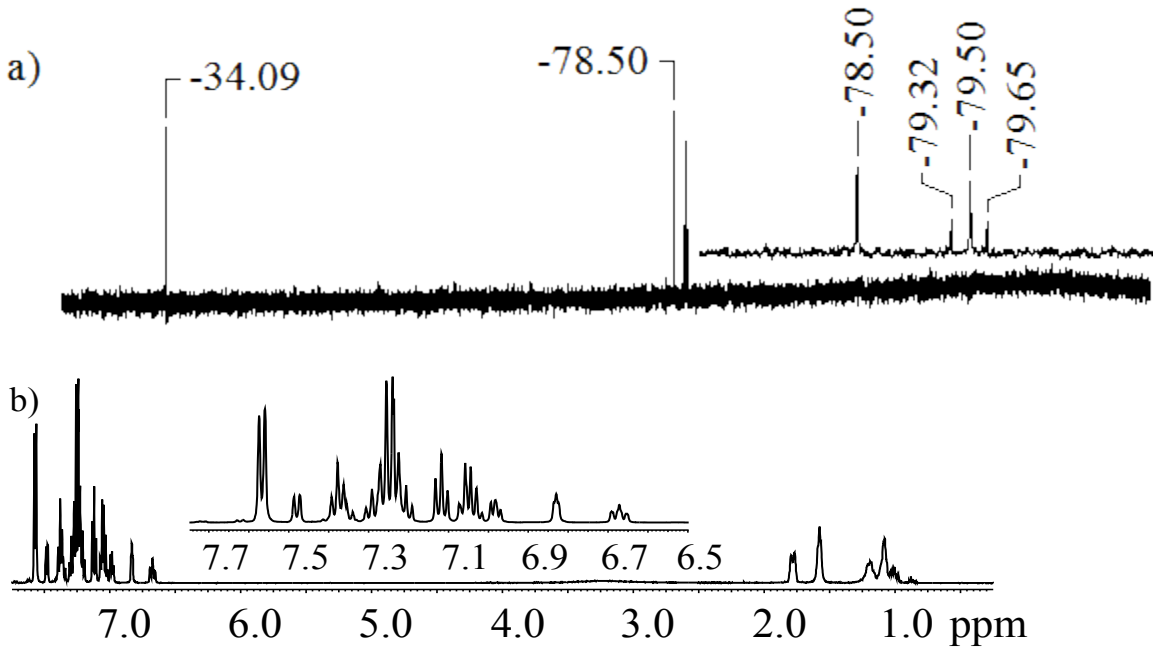

Figure 3-6. NMR spectra of compound **3b** (a) ^{29}Si and (b) ^{1}H.

Two impurities were found and removed through solvent washing. Toluene was added to dry **3b** until most solid was dissolved. The remaining precipitate was mostly impurity and was separated by filtration. Toluene was removed from the filtrate under vacuum. Diethyl ether was then added to the resultant residue, which gave a white suspension that was separated by filtration and the rententate was dried under Nitrogen to yield pure **3b**. It was later determined the product could also be purified by column chromatography.

3.4.3 Compound 3c

Compound **3c** was synthesized based on the same described method, except the Grignard was synthesized and not purchased (Scheme 2). Briefly, under a nitrogen atmosphere in a drybox, a solution of 4-bromo-N,N-bis(trimethylsilyl)aniline (9.48 g, 30.0 mmol) was added

dropwise via an addition funnel into a stirred solution of magnesium turnings (0.91 g, 37.4 mmol) and THF (25 mL). The solution was stirred for 20 h and then used crude in the following reaction. $^{29}Si\{^{1}H\}$ NMR, δ: 12.20 (2 Si).

Crude 4-[bis(trimethylsilyl)amino]phenyl(bromo)magnesium (30.0 mmol) was added dropwise via an addition funnel into a stirred solution of trichloromethyl silane (5.431 g, 36.3 mmol) and THF (10 mL). The solution was stirred for 20 h and then purified by fractional distillation[i] to obtain (*N*-trimethylsilyl)$_2$-aniline-4-(dichloromethylsilane) (9.02 g, 25.7 mmol, 95 % yield) as a colorless liquid. $^{29}Si\{^{1}H\}$ NMR, δ: 18.92 (1 Si), 5.18 (2 Si). $^{13}C\{^{1}H\}$ NMR, δ: 152.31, 133.72 130.11, 127.78, 5.95, 2.32. ^{1}H NMR δ: 7.60 (2 H, multiplet), 7.01 (2 H, multiplet), 1.03 (11 H, CH_3, singlet), 0.10 (18 H, TMS, singlet) (Figure 3-7).

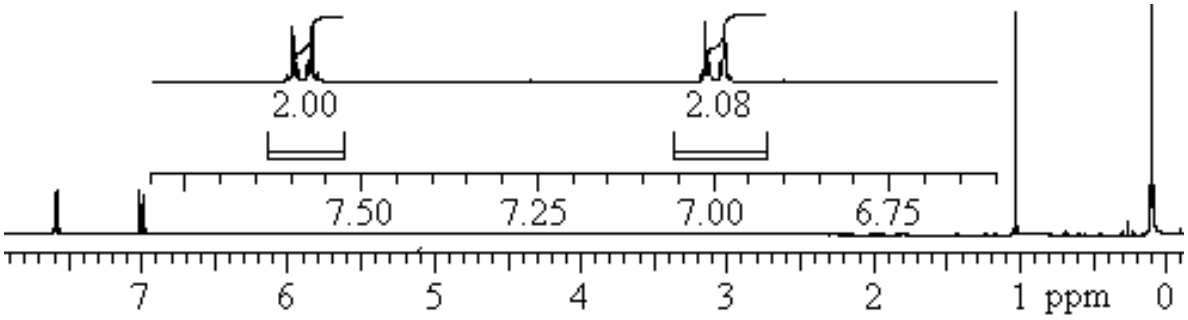

Figure 3-7. ^{1}H NMR spectrum of (*N*-trimethylsilyl)$_2$-aniline-4-(cyclohecyl dichlorosilane).

A solution of (N-trimethylsilyl)$_2$-aniline-4-(dichloromethylsilane) (2.95 g, 8.42 mmol) and triethylamine (1.86 g, 18.4 mmol) in THF (10 mL) was added dropwise via an addition funnel into a stirred solution of Ph$_8$tetrasilanol-POSS (4.46 g, 4.17 mmol) in THF (40 mL). The reaction mixture became cloudy after the addition of a few drops of the dichloromethylsilane/ triethylamine solution, indicating formation of insoluble $HNEt_3Cl$ salt.

After 30 min, the $HNEt_3Cl$ was separated by filtration, and the solvent was removed from the filtrate under vacuum. To the resultant residue diethyl ether (2 mL) was added followed by acidified methanol, which gave a white suspension that was stirred at 25 °C for 20 h. The heterogenous mixture was filtered, and the retentate was dried under nitrogen to yield **3c**, (4.69 g, 3.51 mmol, 84 % yield). $^{29}Si\{^{1}H\}$ NMR, δ: -29.7 (4 Si), -78.2 (8 Si), -79.1 (2 Si), -79.3 (4 Si), -79.5 (2 Si). $^{13}C\{^{1}H\}$ NMR, δ: 148.27, 135.13, 134.39, 134.35, 134.30, 134.22, 132.29, 131.40, 131.19, 130.98, 130.52, 130.47, 130.38, 130.24, 127.93, 127.88, 127.69, 127.52, 124.64, 114.56, -0.10. ^{1}H NMR δ: 7.55-7.10 (44 H, overlapping multiplets), 6.53 (4 H, multiplet), 3.69 (4H, NH_2, broad singlet), 0.51 (6H, CH_3, 2 overlapping singlets)[ii] (Figure 3-8).

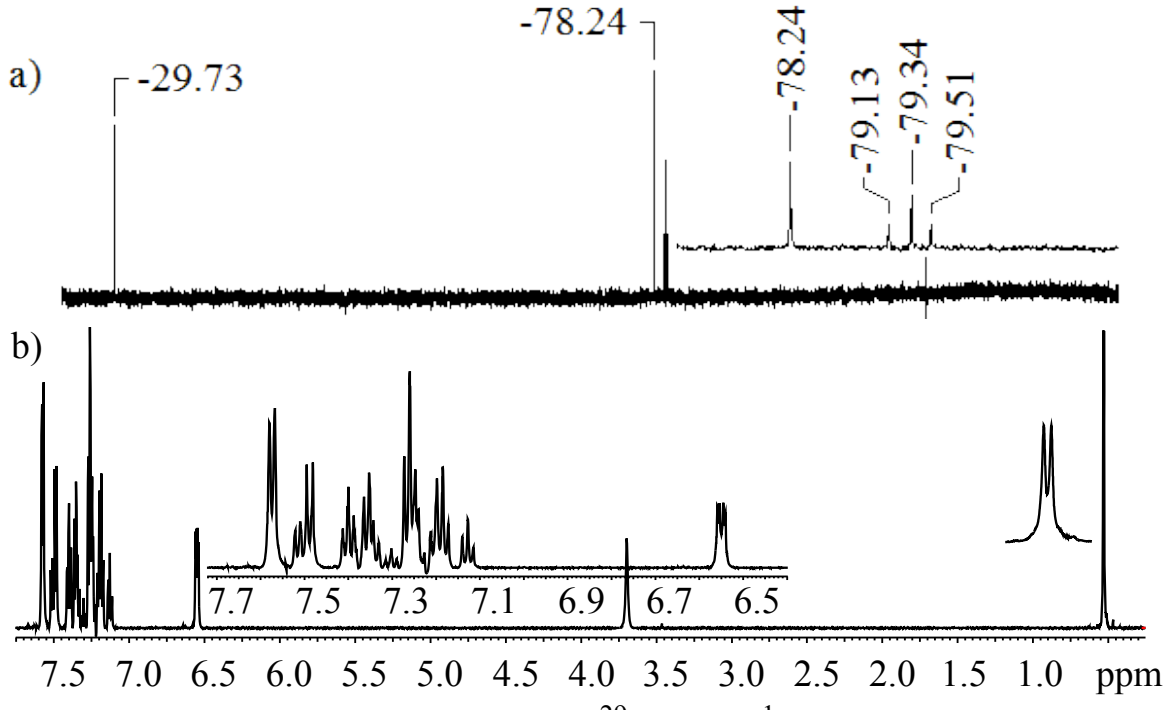

Figure 3-8. NMR spectra of compound **3c** (a) ^{29}Si and (b) ^{1}H.

3.4.4 Compound 3d (mixture of 3a and 3c)

Compound **3d**, was comprised of an AP moiety with a combination of meta- and para-isomers (Figure 3-2). However, the synthetic procedure is anticipated to form 25 % compound **3a**, 25 % compound **3c**, and 50 % compound **3d**. A solution of (N-trimethylsilyl)$_2$-aniline-3-(dichloromethylsilane) (0.679 g, 1.94 mmol), (N-trimethylsilyl)$_2$-aniline-4-(dichloromethyl silane) (0.679 g, 1.94 mmol), and triethylamine (0.792 g, 7.82 mmol) in THF (10 mL) was added dropwise via an addition funnel into a stirred solution of Ph$_8$tetrasilanol-POSS (2.05 g, 1.92 mmol) at 25 °C THF (40 mL). After 30 minutes, the $HNEt_3Cl$ precipitate was separated by filtration, and the solvent was removed from the filtrate under vacuum. To the resultant residue diethyl ether (2 mL) was added followed by acidified methanol, which gave a white suspension that was stirred at 25 °C for 20 h. The heterogeneous mixture was filtered, and the retentate was dried under nitrogen to yield compound **3d**, (2.348 g, 1.75 mmol, 92% yield). $^{29}Si\{^1H\}$ NMR, δ: -29.96 (1 Si), -29.99 (1 Si), -30.59 (1 Si), -30.61 (1 Si), -78.38 (4 Si), -78.49 (4 Si), -79.39 (2 Si), -79.59 (2 Si), -79.61 (2 Si), -79.79 (2 Si). $^{13}C\{^1H\}$ NMR, δ: 1438.19, 145.94, 137.27, 135.08, 134.30, 134.28, 134.16, 132.25, 132.20, 132.11, 132.06, 131.30, 131.24, 131.17, 131.15, 130.94, 130.47, 130.41, 1130.32, 130.29, 128.96, 127.89, 127.85, 122.83, 127.80, 127.71, 127.70, 127.61, 127.52, 127.43, 124.68, 124.65, 123.76, 119.98, 116.83, 114.52, -0.37. ^1H NMR δ: 6.91 (1 H, multiplets), 6.94 (2 H, multiplet), 6.68 (2 H, multiplet), 6.55 (4 H, multiplet), 3.45 (4 H, NH_2, broad singlet), 0.51 (6 H, CH_3, 6 overlapping singlets)[iii] (Figure 3-9).

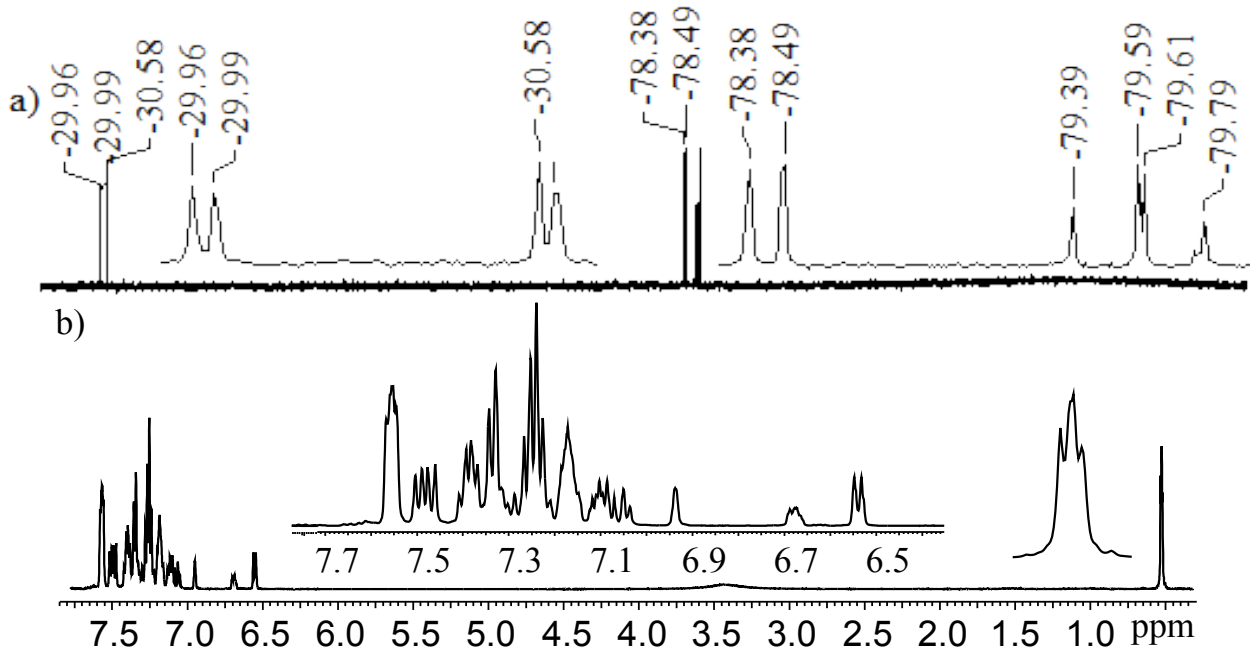

Figure 3-9. NMR spectra of compound **3d** (a) ^{29}Si and (b) ^{1}H.

3.5 Yield analysis of synthetic procedures

All experiments for compounds **3a-c** were performed multiple times, and the results analyzed based upon yields (Table 3-1). "Lowest" and "highest" refer to the lowest and highest yield reported of all experiments for that reaction/compound. Reaction one refers to the dichlorosilane product, **2**, and reaction two refers to the final product, **3** (Scheme 3-1). Only experiments that were performed more than twice have a reported "average" yield. For reaction one, all compounds had yields within a similar range. Overall, for reaction one, compounds **3a** and **c** had higher yields than compound **3b**. The scale of the reaction did not appear to have an affect on the yield. There were several more experiments associated with reaction two for all compounds. Compounds **3a** and **c** had much higher average yields (88 ± 9 and 83 ± 15, respectively) over four experiments than compound **3b** (43 ± 11) did over 10 experiments. Again, the scale of the reaction did not appear to have an affect on the yield.

Table 3-1. Yield analysis of the products of the reactions involved for compounds **3a-c**.

Reaction 1:	Dichlorosilane	Product mass (g)	Yield %	
3a	lowest	16.68	77	
	highest	6.60	94	
	average	--	--	
3b	lowest	1.09	69*	
	highest	5.29	74+	
	average	--	--	
3c	lowest	12.8	47	
	highest	9.00	81	
	average	--	81 ± 15	5 experiments
Reaction 2:	DDSQ(AP)(R)	Product mass	Yield %	Overall yield %
3a	lowest	4.76	84	65
	highest	5.38	96	90
	average	--	88 ± 9	4 experiments
3b	lowest	0.057	29	20
	highest	1.19	69	51
	average	--	43 ± 11	10 experiments
3c	lowest	4.69	84	51
	highest	9.80	88	84
	average	--	83 ± 15	4 experiments

* Contained unreacted starting material. + Kugelrohr significantly improved purity.

3.6 Concluding remarks on synthesis

In this chapter, compounds **3a-d** were successfully synthesized. A yield analysis was prepared for all experiments that were performed more than once, and high yields were acheived for all compounds except **3b**. For additional information on synthesis including a deprotection analysis, please see appendix A.

NOTES

NOTES

(i) The first fraction had slight impurities and was discarded. All remaining material was pure product.

(ii) One singlet represents the *cis* isomer protons (CH_3, 3H), and the other represents the *trans* isomer protons (CH_3, 3H).

(iii) There is one singlet representative of the methyl protons (CH_3) for each of the following geometries: *cis* meta, *trans* meta, *cis* para, *trans* para, and the reamining two singlets are representative of the *cis* and *trans* isomers of the structure that has 1 meta-aminophenyl and 1 para-aminophenyl on a single DDSQ.

REFERENCES

REFERENCES

(1) Takashi, K.; Takashi, K.; Masaya, I.; Kazuhiro, Y.; Yasuhiro, Y. Japan, 2006.

(2) Li, G. Z.; Wang, L. C.; Ni, H. L.; Pittman, C. U. *Journal of Inorganic and Organometallic Polymers* **2001**, *11*, 123.

(3) Phillips, S. H.; Haddad, T. S.; Tomczak, S. J. *Current Opinion in Solid State & Materials Science* **2004**, *8*, 21.

(4) Joshi, M.; Butola, B. S. *Journal of Macromolecular Science-Polymer Reviews* **2004**, *C44*, 389.

(5) Kannan, R.; Salacinski, H.; Butler, P.; Seifalian, A. *Accounts of Chemical Research* **2005**, *38*, 879.

(6) Lichtenhan, J. D.; Vu, N. Q.; Gilman, J. W.; Feher, F. J. United States, 1995; Vol. 5,412,053.

(7) Lichtenhan, J. D.; Vu, N. Q.; Carter, J. A.; Gilman, J. W.; Feher, F. J. *Macromolecules* **1993**, *26*, 2141.

(8) Yang, B.; Li, M.; Wu, Y.; Wan, X. *Polymers & Polymer Composites* **2013**, *21*, 37.

(9) Wu, S.; Hayakawa, T.; Kikuchi, R.; Grunzinger, S.; Kakimoto, M. *Macromolecules* **2007**, *40*, 5698.

(10) Wu, S.; Hayakawa, T.; Kakimoto, M.; Oikawa, H. *Macromolecules* **2008**, *41*, 3481.

(11) Wu, J.; Mather, P. T. *Polymer Reviews* **2009**, *49*, 25.

(12) Gnanasekaran, D.; Reddy, B. S. R. *Polymer Composites* **2012**, *33*, 1197.

(13) Guenthner, A. J.; Lamison, K. R.; Lubin, L. M.; Haddad, T. S.; Mabry, J. M. *Industrial & Engineering Chemistry Research* **2012**, *51*, 12282.

(14) Rizvi, S. B.; Yildirimer, L.; Ghaderi, S.; Ramesh, B.; Seifalian, A. M.; Keshtgar, M. *International journal of nanomedicine* **2012**, *7*, 3915.

(15) Fan, H.; Yang, R. *Industrial & Engineering Chemistry Research* **2013**, *52*, 2493.

(16) Rakesh, S.; Dharan, C. P. S.; Selladurai, M.; Sudha, V.; Sundararajan, P. R.; Sarojadevi, M. *High Performance Polymers* **2013**, *25*, 87.

(17) Vahabi, H.; Ferry, L.; Longuet, C.; Otazaghine, B.; Negrell-Guirao, C.; David, G.; Lopez-Cuesta, J. M. *Materials Chemistry and Physics* **2012**, *136*, 762.

(18) Vahabi, H.; Eterradossi, O.; Ferry, L.; Longuet, C.; Sonnier, R.; Lopez-Cuesta, J. M. *European Polymer Journal* **2013**, *49*, 319.

(19) Li, L.; Li, X.; Yang, R. *Journal of Applied Polymer Science* **2012**, *124*, 3807.

(20) Fox, D. M.; Lee, J.; Zammarano, M.; Katsoulis, D.; Eldred, D. V.; Haverhals, L. M.; Trulove, P. C.; De Long, H. C.; Gilman, J. W. *Carbohydrate Polymers* **2012**, *88*, 847.

(21) Wang, X.; Xuan, S.; Song, L.; Yang, H.; Lu, H.; Hu, Y. *Journal of Macromolecular Science Part B-Physics* **2012**, *51*, 255.

(22) Chrissafis, K.; Bikiaris, D. *Thermochimica Acta* **2011**, *523*, 1.

(23) Ni, Y.; Zheng, S. X. *Chemistry of Materials* **2004**, *16*, 5141.

(24) Vila Ramirez, N.; Sanchez-Soto, M. *Polymer Composites* **2012**, *33*, 1707.

(25) Blanco, I.; Abate, L.; Bottino, F. A.; Bottino, P. *Polymer Degradation and Stability* **2012**, *97*, 849.

(26) Jin, L.; Ishida, H. *Polymer Composites* **2011**, *32*, 1164.

(27) Zheng, L.; Waddon, A. J.; Farris, R. J.; Coughlin, E. B. *Macromolecules* **2002**, *35*, 2375.

(28) Cardiano, P.; Lazzara, G.; Manickam, S.; Mineo, P.; Milioto, S.; Lo Schiavo, S. *European Journal of Inorganic Chemistry* **2012**, 5668.

(29) Geng, Z.; Ba, J.; Zhang, S.; Luan, J.; Jiang, X.; Huo, P.; Wang, G. *Journal of Materials Chemistry* **2012**, *22*, 23534.

(30) Ke, F.; Zhang, C.; Guang, S.; Xu, H. *Journal of Applied Polymer Science* **2013**, *127*, 2628.

(31) Seurer, B.; Vij, V.; Haddad, T.; Mabry, J. M.; Lee, A. *Macromolecules* **2010**, *43*, 9337.

(32) Vij, V.; Haddad, T. S.; Yandek, G. R.; Ramirez, S. M.; Mabry, J. M. *Silicon* **2012**, *4*, 267.

CHAPTER 4*

IDENTIFICATION AND QUANTIFICATION OF *cis* AND *trans* **3a-c** of USING ^{1}H-^{29}Si gHMBC NMR

Keywords

NMR; ^{1}H; ^{29}Si; 2D NMR; ^{1}H–^{29}Si HMBC; double decker silsesquioxanes; cis/trans isomers

* This chapter has already been published with the following citation: Schoen, B. W.; Holmes, D.; Lee, A. *Magnetic Resonance in Chemistry* **2013**, *51*, 490.

4. Identification and quantification of *cis* and *trans* 3a-c using ^{1}H-^{29}Si gHMBC NMR

4. 1 Introduction

In this chapter, the ^{1}H NMR spectra of *cis* and *trans* isomers of compounds **3a-c** (Figure 4-1) are assigned and their ratios quantified. In order to unambiguously assign the proton

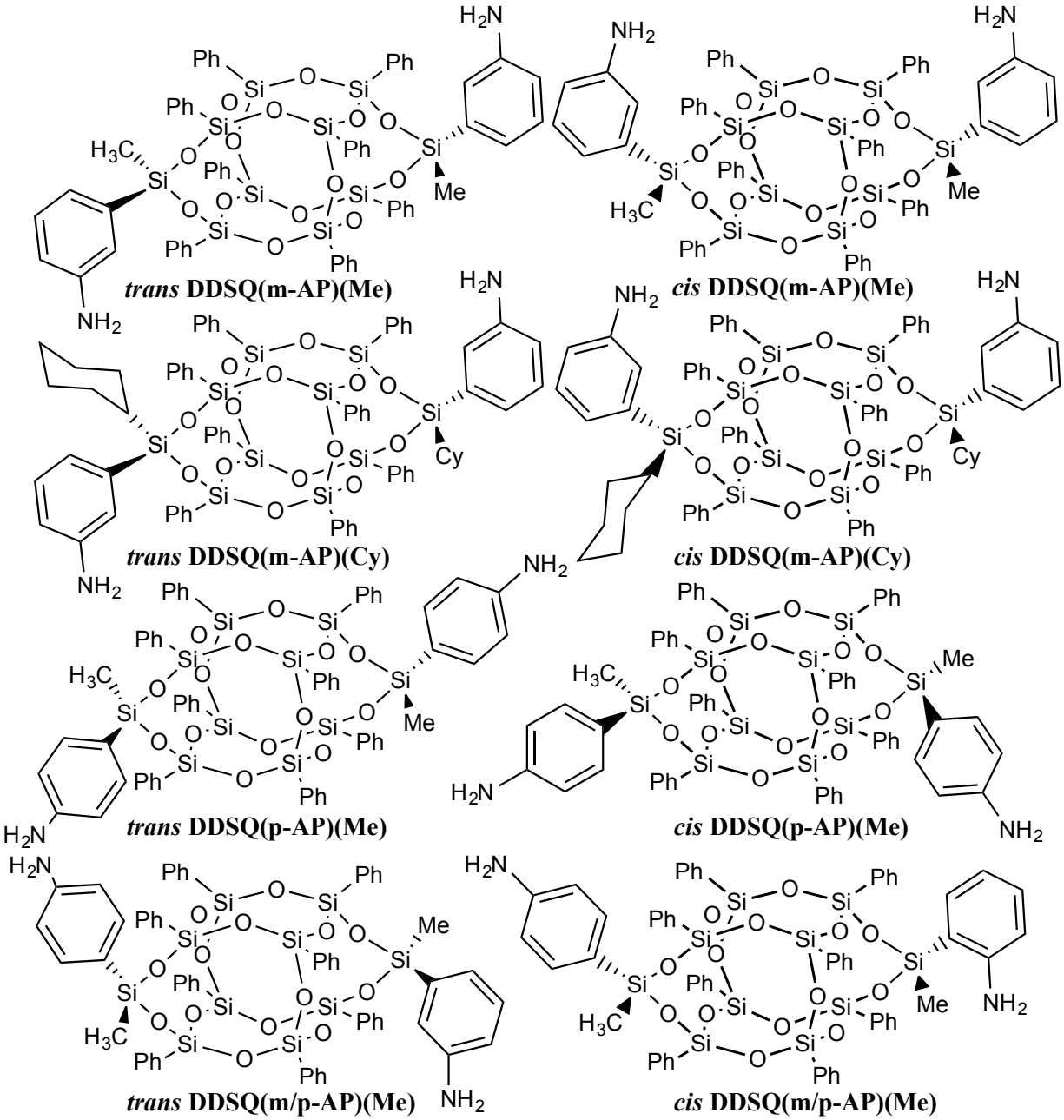

Figure 4-1. *Cis* and *trans* isomers of (a) **3a**, (b) **3b,** (c) **3c**; AP = aminophenyl.

resonances and use them for quantitation, two-dimensional (2D) NMR techniques was necessary. Specifically, proton correlations to the silicon nuclei of the silsesquioxane core not only facilitates ^{1}H spectral assignment but also confirms previous ^{29}Si assignments for these DDSQ.

4.2 Spectroscopic characterization methods

Compounds **3a-c** were measured at 25 ºC on a Varian UNITY-Inova 600 spectrometer equipped with a 5 mm Pulsed-Field-Gradient (PFG) switchable broadband probe and operating at 599.80 MHz (^{1}H) and 119.16 MHz (^{29}Si). One-dimensional (1D) ^{1}H NMR data were acquired using a recycle delay of 20 s and 32 scans to ensure accurate integration. The pulse angle was set to 45°. The ^{1}H-chemical shifts were referenced to that of residual protonated solvent in $CDCl_3$ (7.24 ppm). 1D $^{29}Si\{^{1}H\}$ NMR data were acquired using a recycle delay of 12 s with inverse-gated decoupling. The pulse angle was set to 90°. $^{29}Si\{^{1}H\}$ spectra were referenced against the lock solvent using vendor supplied lock referencing. All two-dimensional (2D) NMR spectra were obtained using gradient pulses on a 5 mm PFG switchable broadband probe without sample spinning. Phase-sensitive spectra were acquired using the hyper-complex States method. Threefold linear prediction was applied to the *F*1 dimension as implemented by standard Varian software. ^{1}H-^{29}Si-gHMBC (gradient enhanced Heteronuclear Multi-Bond Correlation) spectra were acquired with spectral widths of 6600 Hz and 14370 Hz for *F*2 and *F*1, respectively.[1] The pre-acquisition delay was set to 1.0 s, and 400 increments with 8 transients per increment containing 1069 data points were acquired. The three-bond J-filter was set to 7 Hz (Varian parameter; Jnxh = 7). Unshifted sine-bell windows, which were matched to the acquisition time, were used for processing both dimensions. Zero filling to 4096 data points was applied to *F*1

prior to 2D Fourier transformation. ^{1}H-^{1}H-gCOSY (gradient enhanced COrrelation SpectroscopY) spectra were obtained using a spectral width of 8000 Hz in both dimensions. The pre-acquisition delay was set to 1.0 s and 128 increments with 4 transients of 1152 data points were acquired. Both F2 and F1 were multiplied by unshifted sine bell weighting functions that were matched to the acquisition or evolution time. Prior to 2D Fourier transformation, F2 and F1 were zero filled to 2048 and 1024 data points, respectively.

4.3 Identification and quantification analysis

The isomeric mixture of each compound was assessed by ^{29}Si and ^{1}H NMR, and diagnostic chemical shifts for each isomer were observed in the spectra.[2] The isomeric mixture of **3a** shows the expected ^{29}Si resonances at δ -30.6, -78.4, -79.4, -79.6, -79.8 in a ratio of 2:4:1:2:1 (Figure 4-2a). *Trans* **3a** shows characteristic ^{29}Si resonances at δ -30.6, -78.4, -79.6 in the ratio of 2:4:4 (Figure 4-2b) and *cis* **3a** has ^{29}Si resonances at δ -30.6, -78.4, -79.4, and -79.8 in a ratio of 2:4:2:2 (Figure 4-2c).[2] The ^{29}Si resonance at δ -30.6 has been assigned to the D-group silicon atoms (Si-3), silicon atoms bonded to 2 oxygen atoms (Figure 4-1).[3] The ^{29}Si resonance at δ -78.4 has been assigned to the T-group silicon atoms, silicon atoms bonded to 3 oxygen atoms, nearest to the D-group silicon atoms (Si-2). ^{29}Si resonances at δ -79.4, -79.6, and -79.8 have been assigned to the internal T-group silicon atoms; Si-1cR, Si-1t, Si-1cL, respectively. Each Si-1t has the same chemical environment with proximity to one methyl and one aminophenyl group giving rise to a single silicon resonance. In contrast, Si-1cR atoms are only proximal to the methyl group and Si-1cL to the aminophenyl group thereby leading to two

resonances. The ^{29}Si resonances for **3b** and **3c** are nearly identical; δ -34.1, -78.5, -79.32, -79.5, -79.7 (Figure 4-2d), and δ -29.7, -78.2, -79.1, -79.3, -79.5 in the ratio of 2:4:1:2:1 (Figure 4-2e), respectively.

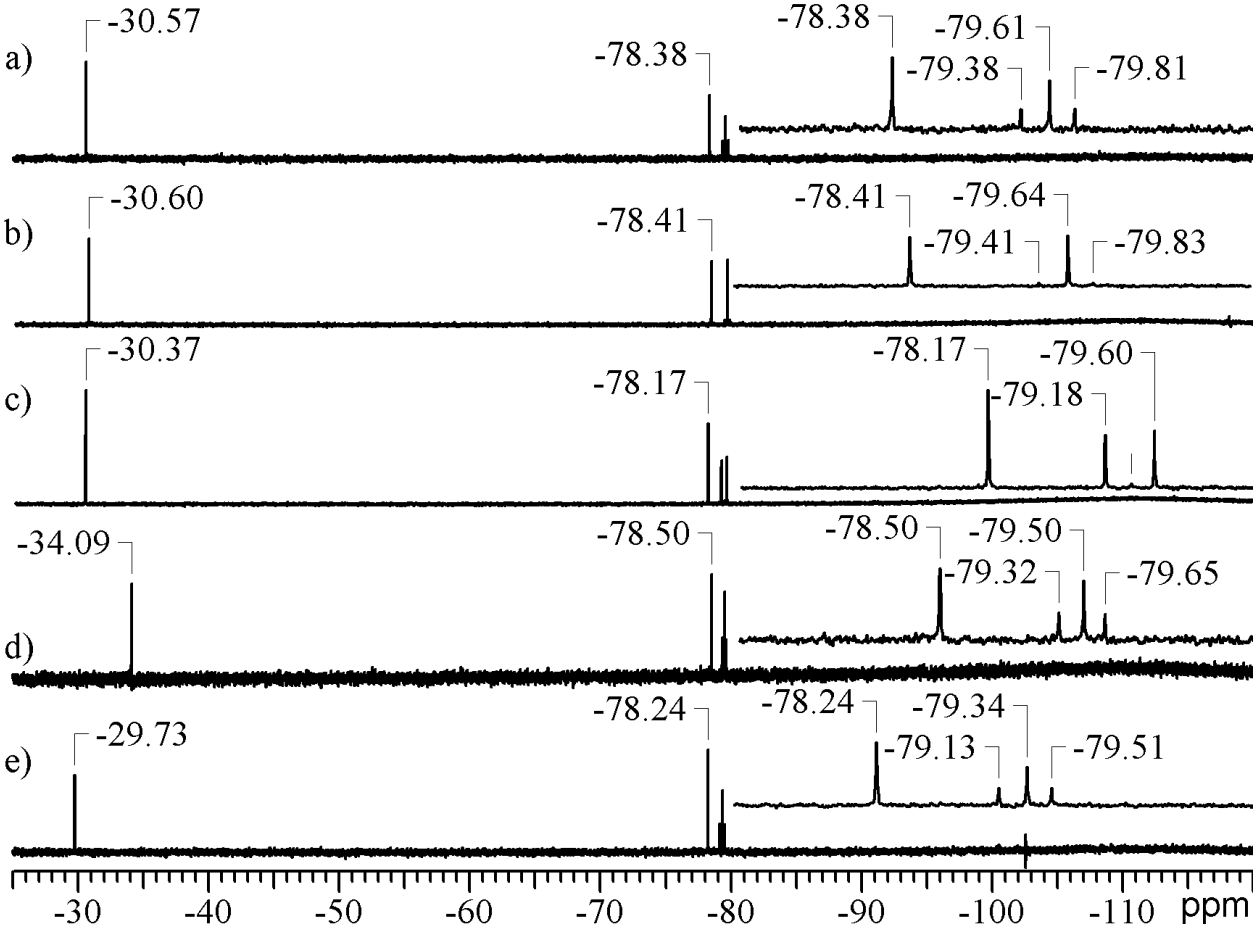

Figure 4-2. ^{29}Si NMR spectra of (a) *cis/trans* 3a, (b) majority *trans* 3a, (c) majority *cis* 3a, (d) *cis/trans* 3b, and (e) *cis/trans* 3c.

The ^{1}H NMR spectra for these DDSQ derivatives reveal that the proton resonances in the phenyl region (6.5 – 8 ppm) are the best candidates for the quantitation of isomeric ratios (Figure 4-3). Proton signals belonging to the R-substituents (Me or Cy) proved to be ambiguous when attempting to decipher between *cis* and *trans* isomers. First, the proton signals belonging to the cyclohexyl groups are broad, significantly overlapped, and have complicated coupling patterns

for *cis* and *trans* isomers. The proton signals belonging to the methyl groups of each isomer are broad singlets and overlap, making it difficult to integrate the individual peaks in this region. Secondly, the ^{29}Si signals associated with both organic R-groups (Me and Cy), as evidenced by

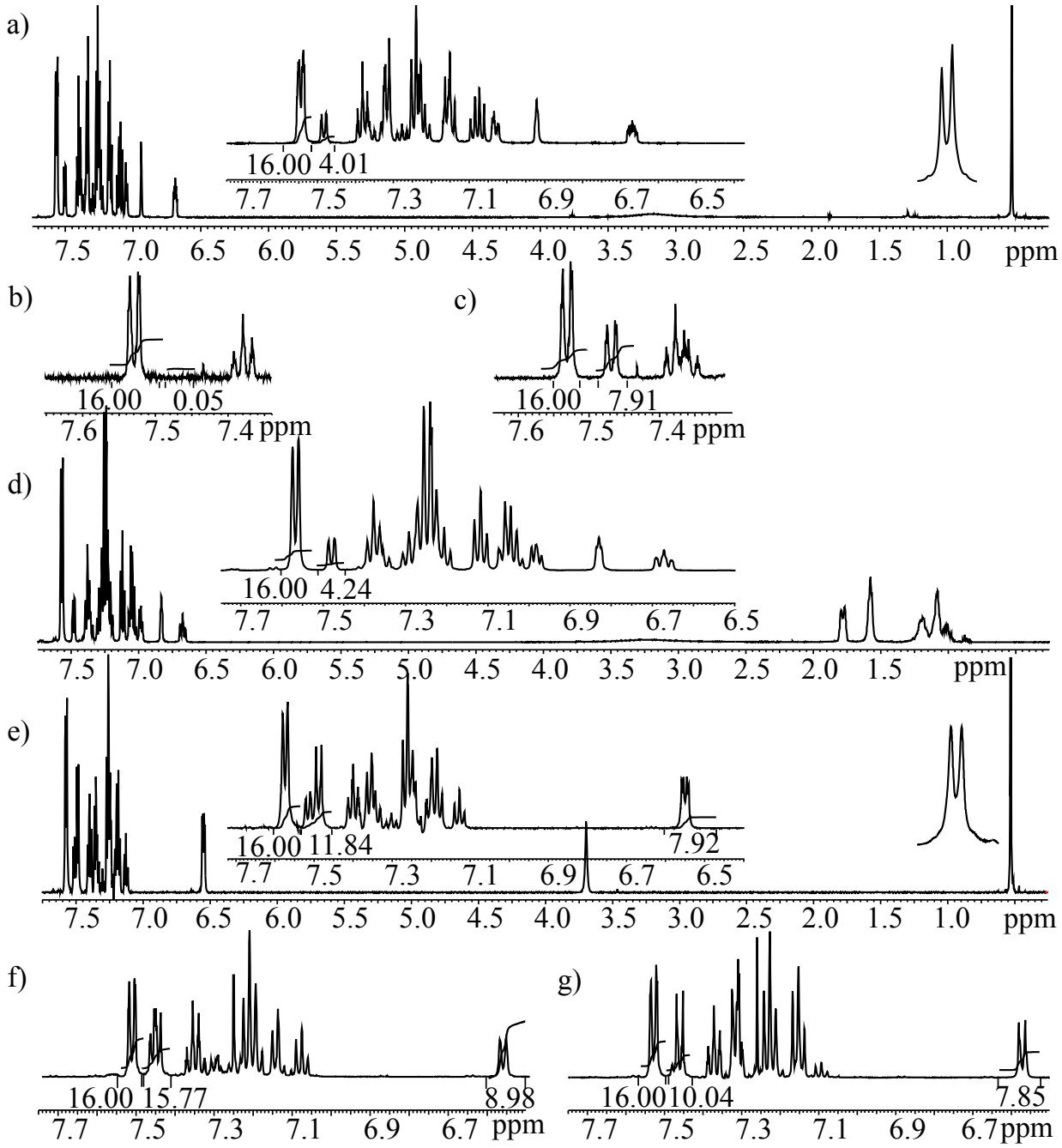

Figure 4-3. ^{1}H NMR spectrum of (a) *cis/trans* **3a**, (b) majority *trans* **3a**, (c) majority *cis* **3a**, (d) *cis/trans* **3b**, (e) *cis/trans* **3c**, (f) majority *trans* **3c**, (g) majority *cis* **3c**.

$^{1}H - ^{29}Si$ gHMBC cross-peaks, are isochronous for *cis* and *trans* isomers. This makes it impossible to use the previously established ^{29}Si shift assignments to determine the *cis* and *trans* proton signals in these regions, even if the signals were deconvoluted.

4.3.1 Compound 3a

The proton resonance at δ_H 7.54 was assigned to H-2a and H-2a′ (m, 16 H) based on the gHMBC three-bond correlation with the ^{29}Si single resonance at δ_{Si} -78.4 (Si-2), which is isochronous for both *cis* and *trans* isomers (Figure 4-4a). Whereas the *trans* isomer exhibits a single resonance for Si-1t (δ_{Si} -79.6), the *cis* isomer, due to its asymmetry, has two pairs of Si-1 atoms, labeled Si-1cL (left) and Si-1cR (right), (δ_{Si} -79.4 and -79.8) in a ratio of 2:2. The proton multiplet at δ_H 7.48 was assigned to H-1acR and H-1acR′ (*cis*, m, 4 H) as evidenced by the gHMBC correlation with the two Si-1cR atoms (δ_{Si} -79.8). The proton multiplet at δ_H 7.16 was also assigned to H-1acL and H-1acL′ (*cis*, m, 4 H) based on the gHMBC correlation with the two Si-1cL atoms (δ_{Si} -79.4). For the *trans* isomers, the proton multiplet at δ_H 7.32 was assigned to H-1at and H-1at′ (*trans*, m, 8 H), which is confirmed by the gHMBC correlation with the Si-1t atoms (δ_{Si} -79.6). Both the *cis* and *trans* isomers show isochronous resonances at δ_H 6.92 and 7.03 and were assigned to H-3a and H-3e (m, 4 H and m, 4 *H*) based on the gHMBC correlation with the four Si-3 atoms (δ_{Si} -30.5). Analysis of the ^{1}H-^{1}H gCOSY spectrum revealed that proton signals at δ_H 6.67 and 7.08 show correlations with δ_H 6.92 and 7.03 thereby establishing their assignment as H-3b and H-3d. Proton multiplets assigned to H-1acL and H-1acL′ (δ_H

7.16) and H-1at and H-1at′ (δ_H 7.32) exhibit too much overlap for accurate quantification. Thus, the proton resonances assigned to H-1acR and H-1acR′ (δ_H 7.48) and H-2a and H-2a′ (δ_H 7.54) are the best candidates for quantification. An equivalent ratio of the *cis* to *trans* isomers would, therefore, be represented by a ratio of 1:4 for these resonances. The remaining protons were identified by ^{1}H-^{1}H gCOSY cross-peaks and coupling patterns (Table 4-1).

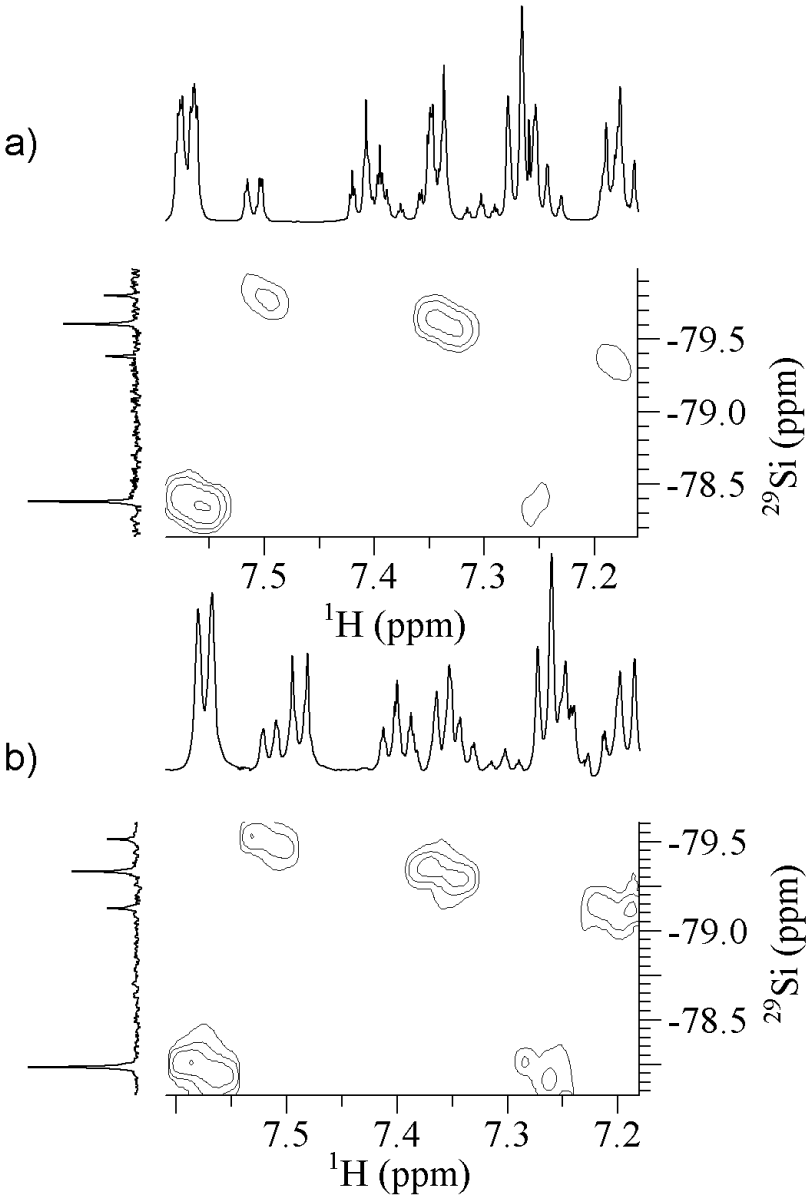

Figure 4-4. ^{1}H-^{29}Si gHMBC connectivity of (a) *cis/trans* **3a** and (b) *cis/trans* **3c.**

Table 4-1. ^{29}Si and ^{1}H resonances of *cis/trans* **3a**.

Atom	^{1}H (mult.)	^{29}Si (mult.)
1 (Si)	---	-79.4(2 Si)*, -79.6(4 Si)†, -79.8(2 Si)*
1-(C_6H_5)	---	---
-a,a′ (CH)	7.16(m, 4H)*, 7.32(m, 8H)†,7.48(m, 4H)*	---
-b,b′ (CH)	7.31(m, 4H)*, 7.15(m, 8H)†, 7.23(m, 4H)*	---
-c (CH)	7.39(m, 4H)§, 7.38(m, 4H)§,	---
2 (Si)	---	-78.4 (8 Si)$^{\#}$
2-(C_6H_5)	---	---
-a,a′ (CH)	7.54(m, 16H)$^{\#}$	---
-b,b′ (CH)	7.24(m, 16H)$^{\#}$	---
-c (CH)	7.39(m, 4H)§, 7.38(m, 4H)§,	---
3 (Si)	---	-30.6 (4 Si)$^{\#}$
3-(CH_3)	0.51 (s, 12H)§	---
3-(C_6H_6N)	---	---
-a (CH)	6.92 (m, 4H)	---
-b (NH_2)	3.16 (s, 8H)$^{\#}$	---
-c (CH)	6.67 (m, 4H)$^{\#}$	---
-d (CH)	7.08 (m, 4H)$^{\#}$	---
-e (CH)	7.03 (m, 4H)$^{\#}$	---

† = trans, * = cis, § = cannot distinguish between cis/trans, # = isochronous cis/trans

4.3.2 Compound 3b

The ^{1}H and ^{29}Si NMR spectra of **3b** shows an analogus coupling pattern to that of **3a** with only a slight variation of chemical shifts. Additionally, the 2D ^{1}H – ^{29}Si gHMBC is analogous to that of **3a** (Figure 4-3d).

4.3.3 Compound 3c

Similar to compounds **3a** and **3b,** the proton resonance at δ_H 7.55 was assigned to H-2a and H-2a′ (m, 16 H) based on the correlation with the ^{29}Si single resonance at δ_{Si} -78.2 (Si-2),

isochronous for both *cis* and *trans* isomers (Figure 4-4b). The proton multiplet at δ_H 7.50 was assigned to H-1acR and H-1acR´ (*cis*, m, 4 H) as evidenced by the gHMBC correlation with the Si-1cR atoms (δ_{Si} -79.5). The proton multiplet at δ_H 7.19 was also assigned to H-1acL and H-1acL´ (*cis*, m, 4 H) based on the gHMBC correlation with the other two Si-1cL atoms (δ_{Si} -79.1). For the *trans* isomers, the proton multiplet at δ_H 7.33 was assigned to H-1at and H-1at´ (*trans*, m, 8 H) based on the gHMBC correlation with the Si-1t atoms (δ_{Si} -79.3). The proton multiplet at δ_H 6.53 (8H) was assigned to H-3a and H-3a´ as evidenced by the gHMBC correlation with the four Si-3 atoms, and is isochronous for *cis* and *trans* isomers. The assignment of H-3a and H-3a´ is unique to the para-structure (**3c**). All 8 H-3 protons that demonstrate a three-bond gHMBC correlation with the Si-3 atoms of **3c** (H-3a and H-3a´), are represented by a single multiplet. The same 8 H-3 protons of the meta-species (**3a** and **3b**), are represented by two multiplets (H-3a, 4H and H-3e, 4H), due to the asymmetry inherent to the meta-structure. Analysis of the ^{1}H-^{1}H gCOSY spectrum reveals that proton signal at δ_H 6.53 shows correlations with δ_H 7.47 (H-3b and H-3b´; isochronous for *cis* and *trans*, m ,8H). However, also contrary to the ^{1}H NMR spectra of the meta-species, the proton multiplet assigned to H-3b and H-3b´ (δ_H 7.47) overlaps the proton multiplet assigned to H-1acR and H-1acR´ (δ_H 7.50), which was used for quantification of the isomeric ratio of the previous two compounds. Similar to compounds **3a** and **3b**, the proton multiplets assigned to H-1acL and H-1acL´ (δ_H 7.19) and H-1act and H-1act´ (δ_H 7.33) exhibit too much overlap for accurate quantification, and to a much larger extent than the overlap

of proton multiplets assigned to H-3b and H-3b′ (δ_H 7.47) and H-1acR and H-1acR′ (δ_H 7.50) (Figure 4-3). Thus, the proton resonances assigned to H-2a and H-2a′ (δ_H 7.55) and H-1acR and H-1acR′ (δ_H 7.50), combined with H-3b and H-3b′ isomers is represented by the proton signals at δ_H 7.50 and 7.47 integrating to 12 H and the proton signal at δ_H 7.55 integrating to 16 H, a ratio of 3:4. As the ratio of these signals increase, the ratio of isomers in the sample becomes majority *cis* **3c** (Figure 4-3e-g). A ratio of 1:2 would signify an isolated *trans* **3c**. The remaining protons were identified by ^{1}H-^{1}H gCOSY cross-peaks and coupling patterns (Table 4-2).

Table 4-2. ^{29}Si and ^{1}H resonances of *cis/trans* **3c**.

Atom	^{1}H (mult.)	^{29}Si (mult.)
1 (Si)	---	-79.1(2 Si)*, -79.3(4 Si)†, -79.5(2 Si)*
1-(C_6H_5)	---	---
-a,a′ (CH)	7.19(m, 4H)*, 7.33(m, 8H)†, 7.50(m, 4H)*	---
-b,b′ (CH)	7.32(m, 4H)*, 7.18(m, 8H)†, 7.20(m, 4H)*	---
-c (CH)	7.39(m, 4H)§, 7.38(m, 4H)§,	---
2 (Si)	---	-78.2 (8 Si)$^\#$
2-(C_6H_5)	---	---
-a,a′ (CH)	7.55(m, 16H)$^\#$	---
-b,b′ (CH)	7.23(m, 16H)$^\#$	---
-c (CH)	7.39(m, 4H)§, 7.38(m, 4H)§,	---
3 (Si)	---	-29.7 (4 Si)$^\#$
3-(CH_3)	0.51 (s, 12H)§	---
3-(C_6H_6N)	---	---
-a,a′ (CH)	6.53 (m, 8H)$^\#$	---
-b,b′ (CH)	7.47 (m, 8H)$^\#$	---
-c (NH_2)	3.69 (s, 8H)$^\#$	---

† = *trans*, * = *cis*, § = cannot distinguish between *cis/trans*, # = isochronous *cis/trans*

With the established ^{1}H NMR chemical shift assignments, integration was possible and samples containing *cis* and *trans* isomers could be quantified (Table 4-3). All quantitative ^{1}H were run with a sufficient recycle delay to allow for complete relaxation as determined by T_1 analysis. ^{29}Si NMR experiments were run with an empirically determined recycle delay of 12 seconds even though the T_1's ranged from 50 to 55 seconds.[i] Determining the percentage of *cis* isomer present in samples of material **3c** was complicated by signal overlap around δ_H 7.50-7.47.[ii] For this system it was necessary to subtract the integrated value of the protons at δ_H 6.60 (H-3b and H-3b´**of** *cis*-**3c**) from that of δ_H 7.50-7.47 in order to determine the percentage of *cis* isomer.

Table 4-3. Integrated values of ^{1}H NMR spectra from various mixtures of **3**.

compound	δ_1	δ_2	ratio	% *cis*
3a	0.05	16	0.0031	< 1
	4.08	16	0.26	51
	7.91	16	0.49	99
3b	4.24	16	0.27	53
3c	12.35	16	0.77	50
	10.04	16	0.63	27
	15.77	16	0.99	85

Integrals are taken at the following δ and can be seen in Figure 3:
3a: δ_1 = 7.48 ppm, δ_2 = 7.54 ppm; **3b**: δ_1 = 7.48 ppm, δ_1 = 7.57;
3c: δ_1 = 7.50 + 7.47 ppm, δ_2 = 7.55 ppm

For comparative purposes, the percentage of the *cis* isomer in various samples of **3a** was also determined using ^{29}Si NMR spectra and compared with their ^{1}H NMR counterparts (Table 4-4). Analysis times for ^{29}Si NMR spectra varied from 10 minutes to 12 hours, while all ^{1}H NMR spectra were acquired in 13 minutes. Increasing the time of acquisition for the proton experiment

did not lead to an appreciable change in calculated ratios. Contrariwise, as the length of analysis time for ^{29}Si NMR spectra was extended, the percentage of *cis* isomer determined approached the percentages determined using the ^{1}H NMR spectra. No improvement was seen when extending ^{29}Si experiments past 4 hours. The limiting factor was the poorer signal-to-noise (S/N) in the ^{29}Si NMR spectra. This not only made it more difficult to determine the limits of integration on ^{29}Si NMR spectra as compared to that of the ^{1}H NMR spectra but also increased the uncertainty in the former (Figure 4-2). Even after 12 hours, the S/N of the ^{29}Si NMR spectrum was not comparable to its ^{1}H NMR spectrum (Table 4-4), which was run for 13 minutes. For example, at 12 hours, the S/N of the smallest signal integrated was 19:1 and the S/N

Table 4-4. Integrated values of ^{1}H NMR spectra vs. ^{29}Si NMR spectra from **3a** mixtures.

Exp #	nucleus	time	ratio	% cis	S/N range (low-high)
1	^{29}Si	10 min.	0.43	43	6-15
	^{1}H	13 min.	0.26	51	57-183
2	^{29}Si	30 min.	0.43	43	11-28
	^{1}H	13 min.	0.25	49	52-201
3	^{29}Si	2 hr.	0.48	48	12-23^{+}
	^{1}H	13 min.	0.25	51	33-90
4	^{29}Si	4 hr.	0.97	97	2-34*
	^{1}H	13 min.	0.49	99	91-149
5	^{29}Si	12 hr.	0.37	37	19-64
	^{1}H	13 min.	0.2	39	49-239

^{29}Si: δ_1 = -79.4 ppm, δ_2 = -79.6 ppm, & δ_3 = - 79.8 ppm

+ effect of concentration *lower peak is low quantity *trans* S/N = range of signal to noise

of the largest integrated signal was 64:1 (exp 5-^{29}Si). The lowest and highest S/N for the ^{1}H NMR spectrum of the same material was 49:1 and 239:1, respectively (exp 5-^{1}H). For mixtures

containing predominately one isomer, it becomes increasingly more difficult to accurately determine isomeric purity. As an example, after 4 hours, the ^{29}Si NMR spectrum of a sample that is majority *cis* isomer had a S/N for the *trans* isomer signal of 2:1 while the S/N of the *cis* isomer signal was 34:1 (exp 4-^{29}Si). The signal representing the *trans* isomer could potentially be mistaken for, or hidden under, noise had the analysis time been shortened, the purity of the *cis* isomer increased, or the concentration of the sample decreased. All ^{29}Si samples had to be heavily concentrated, approximately 50 mg in 0.6 mL of solution, whereas the ^{1}H NMR spectra could be obtained with a concentration of < 5 mg in 0.6 mL of solution. Overall, more accurate data was acquired with ^{1}H NMR using less material and shorter analysis time.

4.4 Concluding remarks on spectroscopy

In this study, ^{1}H – ^{29}Si gHMBC and ^{1}H – ^{1}H gCOSY were used to assign the chemical shifts of the protons for the *cis* and *trans* isomers of **3a-c** as well as to verify the chemical shifts of ^{29}Si- NMR. Once the proton chemical shifts of these compounds were identified, a routine access methodology to determine the *cis* and *trans* isomeric ratio was developed. The method described herein offers a more accurate quantification of the isomeric ratio in a shorter analysis time using standard NMR equipment with less material required per sample when compared to utilizing ^{29}Si NMR spectroscopy. With the ability to identify the isomeric ratios, attempts to isolate the individual isomers can be made, and the influence of stereo-configurations on the physical and chemical properties of these hybrid nanostructuered chemicals can be studied and utilized.

NOTES

NOTES

(i) A comparison of ^{29}Si NMR data collected with a 300 second delay, which would be appropriate for quantitative work, and with a 12 second delay yielded integration ratios within experimental error. Experiments run with the 12 second delay gave improved Signal-to-Noise per unit time and were, thus, preferred. For additional information on the T_1 analysis, please see appendix B.

(ii) A europium shift reagent also provides a solution to this problem. For more information, please see appendix B.

REFERENCES

REFERENCES

(1) Hurd, R.E.; *Journal of Magnetic Resonance* **1990**, 87, 422.

(2) Seurer, B.; Vij, V.; Haddad, T.; Mabry, J. M.; Lee, A. *Macromolecules* **2010**, *43*, 9337.

(3) Stock, A. *Berichte Der Deutschen Chemischen Gesellschaft* **1916**, *49*, 108.

CHAPTER 5*

CHRACTERIZATION OF SOLUBILITY BEHAVIOR OF *cis* AND *trans* ISOMERS IN NANO-STRUCTURED DOUBLE DECKER SILSESQUIOXANES

Keywords

double decker silsesquioxane, fractional crystallization, solubility, solid-liquid equilibria, NRTL model, isomer separation, cis/trans isomers

* This chapter has been submitted for publication under the following citation: Schoen, B. W.; Lira, C. T.; Lee, A. *Fluid Phase Equilibria* **2013**, *submitted July 8, 2013*.

5. Characterization of the solubility behavior of *cis* and *trans* isomers in nano-structured double decker silsequioxanes

5.1 Introduction

DDSQ with various reactive chemical moieties have been prepared and their *cis* and *trans* isomers partially isolated.[1,2] With the ability described in the previous chapter to identify *cis* and *trans* isomers using ^{1}H NMR, a ratio of *cis* and *trans* isomers of **3a-c** can now be accurately quantified.[3] This allows for verification of purity and the development of a model representing the quantitative measurements and parameters needed for fractional crystallization of these isomers. Furthermore, it provides an opportunity to understand how these configurations influence the structure-property relationship of these DDSQs.

Fractional crystallization provides a platform for larger quantities of material to be separated into fewer fractions as compared to other methods such as chromatography.[4-6] Furthermore, fractional crystallization provides a much lower energy demand as opposed to an energy-intensive thermal separation method such as distillation. Hence, it is accepted as an appropriate economic approach for an industrial scale.[7] A fractional crystallization method involving the variation in solvent polarity was used to separate the *cis* and *trans* isomers of compounds **3a-c** and is described in this chapter. For the precipitates, molar ratios of the individual isomers were obtained using ^{1}H NMR data.[3] Experimental solubility results were modeled using the NRTL activity coefficient method. Activity coefficients, thermodynamic properties, and structural characteristics all contributed to the solubility model for the solution of mixed isomers. In this chapter, solubility, separation, and chemical properties were studied for isomers of compounds **3a-c**.

5.2 Materials and Methods

5.2.1. Solvents and Reagents

Triethylamines were obtained from JT Baker® Chemicals (Pleasant Prairie, WI) when used for column chromatography. Dichloromethane was obtained from Macrom^{TM} Chemicals Products (Nashville, TN). SiliaFlash ® P60 Silica gel was purchased from Silicycle Ultra Pure Silica Gels (Quebec City, Quebec, Canada). Silica gel 60 F_{254}, (0.2 mm thick, Sigma Aldrich) pre-coated plastic plates were used for thin layer chromatography (TLC).

5.2.2. Isomer separation

A fractional crystallization method was used to separate the *cis* and *trans* isomers. Each structure, **3a-c**, was studied individually. Solvent polarity was varied by changing the ratio of solvent (THF) to anti-solvent (hexanes) using the procedure outlined in Figure 5-1. Purity of the individual isomers was confirmed using ^{1}H-NMR, and DSC data. A typical example of the separation procedure for compounds **3a-c** follows: solid DDSQ for one of the variants **3a-c** (varying between 0.1 – 1.1 g, 0.077 – 0.81 mmole) was placed in a round bottom flask. The ratio of isomers in the initial sample varied. Minimal THF was added to the flask, at 25 ºC, until the solid completely dissolved. Hexanes were added dropwise until a white suspension persisted. The precipitate (designated ppt1) was isolated by filtration and dried under a stream of nitrogen. The first precipitate, ppt1, was usually predominantly the *trans* isomer, since it is less soluble. Depending on the initial *cis*:*trans* ratio and the solvent ratio, some *cis* isomer can be present. Within this filtrate, the *trans* was at the solubility limit, however the *cis* was not always at the solubility limit. The filtrate solvent mix of THF and hexanes was removed under vacuum, leaving a solid cake (designated ppt2). For collection of this precipitate, hexanes were added to

create a pourable suspension. The solids (ppt2) were collected by filtration and dried under a stream of nitrogen. In general, the average recovery of total material in all experiments was greater than 90 % for all three compounds. By a material balance, the quantities of DDSQ and solvent in the supernatant of the first precipitation were the compositions used in solubility modeling. Cases where the *cis* isomer was below the solubility limit are noted below.

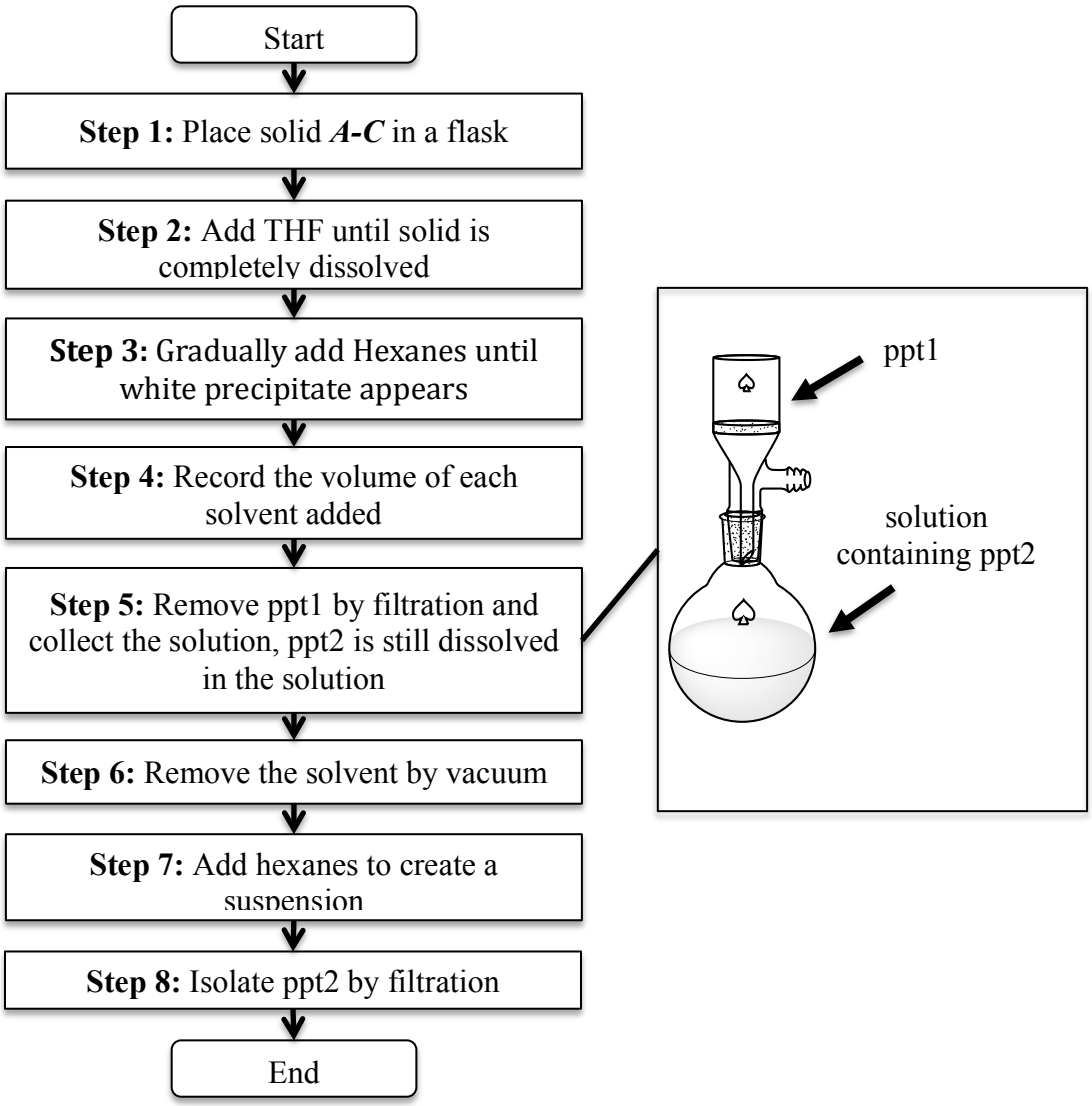

Figure 5-1. Flow chart describing the fractional crystallization/isomer separation procedure of *trans* and *cis* isomers of compounds **3a**, **3b**, and **3c**.

5.2.3 Chromatographic Purification

Thermal properties for pure isomers of **3a-c** were important in modeling the saturation curves. In order to obtain accurate values, the highest purity feasible of each isomer was desired. The *trans* isomer solid can be isolated easily by selectively precipitating *trans* while maintaining a solution undersaturated in *cis*. However, the *cis* isomer is more difficult to isolate at high purity by precipitation. Hence, chromatography columns were utilized to further purify the *cis* isomers from selected ppt2 solids (mixture with high *cis* fraction). Flash silica gel chromatography was performed using siliaflash ® P60 silica gel with a particle size of 0.043-0.063 mm (230-400 mesh) at room temperature. The column had a length of 203 mm and a diameter of 31.8 mm. The column was packed according to methods described by Still et. al.[8] To prevent loss of the stationary phase through the bottom, the column was plugged with cotton. Silica gel was packed approximately three quarters of the total length of the column. A thin layer of sand (approximately 6.35 mm) was positioned above and below the silica gel in order to provide an even base for the stationary phase, and prevent concentration and streaking of the bands as they came off the column and were collected. Solid DDSQ (0.2 – 1.0 g) was dissolved in minimal dichloromethane and loaded on the top of the column bed. The mobile phase was 1% triethylamine in dichloromethane. Silica gel 60 F_{254}, (0.2 mm thick) pre-coated plastic plates were used for TLC. A small spot of each column fraction was applied to a TLC plate, approximately 1.5 cm from the bottom edge. A small amount of dichloromethane was placed in a glass beaker to a depth of less than 1 cm. The TLC plates were place in the beaker so that the spots do not touch the dichloromethane, and the beaker was closed with a lid. Dichloromethane moved up each plate by capillary action, carrying the sample. The TLC plates were removed

before the dichloromethane reached the top of the plates, and spots were visualized by viewing them under short-wave range ultraviolet light.

5.2.4 NMR spectroscopy

Compounds **3a-c** were measured at 25 ºC on a Varian UNITY-Inova 600 spectrometer equipped with a 5 mm Pulsed-Field-Gradient (PFG) switchable broadband probe and operating at 599.80 MHz (^{1}H). ^{1}H NMR data were acquired using a recycle delay of at least 20 s and 32 scans to ensure accurate integration. The ^{1}H-chemical shifts were referenced to that of residual protonated solvent in $CDCl_3$ (7.24 ppm).

5.2.5 Differential scanning calorimetry

Melting behavior was studied using a TA Instrument Q2000 equipped with a mechanical cooling system under a nitrogen atmosphere. Samples were placed in a Q-zero^{TM} aluminum pan and sealed with a lid to evaluate the *cis* and *trans* isomers. Samples were first equilibrated at 40°C for 1 min and subsequently heated to 350 °C with a constant heating rate of 10 °C/min.

5.2.6 Modeling

Solubility was modeled by the Schröder-van Laar equation (Equation 5-1):[9,10]

$$\ln(x_i\gamma_i) = \frac{-\Delta H_m}{RT}\left[1 - \frac{T}{T_m}\right] \qquad (5-1)$$

where x is the mole fraction of isomer (i) that remains in saturated solution at a given temperature (T = *room temperature*), based on its melting transition (T_m), and heat of fusion (ΔH_m), and R is the ideal gas constant. The activity coefficient (γ) quantifies deviations from an

ideal solution. An ideal solution is a solution formed with no accompanying energy or volume change on mixing and no excess entropy; the intermolecular attractive/repulsive forces (or intermolecular interactions) between the various pair types are all similar, and $\gamma = 1$.

For a given temperature, the solution of Equation 5-1 (RHS) is a constant and depends only on the T_m and ΔH_m of the pure substance. The left hand side (LHS) of Equation 5-1 is associated with the mole fraction of the substance soluble in the given solvent system and its activity coefficient. For $\gamma = 1.00$, or ideal solubility, the solubility of the substance in the solvent depends only on the experimental temperature. When $\gamma < 1.00$, the substance becomes more soluble in that solvent than ideal solubility (a favorable interaction) and when $\gamma > 1.00$, the substance is less soluble in that solvent than the ideal solubility (an unfavorable interaction).[11]

In order to develop a comprehensive model for the separation procedure, the solubility/fractional crystallization data of the quaternary system, *cis* + *trans* + THF + hexanes (c + t + T + H), were included in the parameter fitting. It is recognized that the structures of compounds **3a-c** are so large in comparison to the solvent molecules. Therefore, it is expected that this solution is non-ideal. The activity coefficient model used to fit the experimental data was a simplified version of the non-random two liquid model (NRTL, Equation 5-2):[12]

$$\ln\gamma_i = \frac{\sum_j x_j \tau_{ji} G_{ji}}{\sum_k x_k G_{ki}} + \sum_j \frac{x_j G_{ij}}{\sum_k x_k G_{kj}} \left[\tau_{ij} - \frac{\sum_m x_m \tau_{mj} G_{mj}}{\sum_k x_k G_{kj}} \right] \qquad (5-2)$$

$$G_{ij} = \exp\left(-\alpha_{ij}\tau_{ij}\right); \quad \tau_{ij} = a_{ij} + \frac{b_{ij}}{T}; \quad \tau_{ii} = 0; \quad G_{ii} = 1;$$

where γ is the activity coefficient of solute (i), x represents the mole fraction of each of the remaining constituents in this quaternary system, τ_{ij} is an intermediate parameter representing the

binary interaction parameters a_{ij} and b_{ij}, and α_{ij} represents the non-randomness parameter. For the THF + hexane binary pair, a full set of parameters are available from Aspen Plus® ver 7.3.[13] For the limited data collected in this work at a single temperature, the number of parameters will be reduced by equating the *ij* interactions for some pairs and by setting some parameters to zero.

For each of the three DDSQ structures, since *cis* and *trans* isomers possess the same functional groups, the binary energy interaction parameters for *cis* to *trans* are assumed to be the same as *cis* to *cis*, and *trans* to *trans*, and thus $\tau_{ct} = \tau_{tc} = 0$. For the same reason, the *cis* to hexanes interaction is assumed to be the same as the *trans* to hexanes interaction, and the *cis* to THF interaction is assumed to be the same as *trans* to THF. These assumptions resulted in the simplifications, $a_{cis,\mathrm{H}} = a_{trans,\mathrm{H}}$ and $a_{cis,\mathrm{T}} = a_{trans,\mathrm{T}}$. These parameters will thus be abbreviated $a_{DDSQ,\mathrm{H}}$ and $a_{DDSQ,\mathrm{T}}$ without distinction of the *cis* and *trans* isomers. It was further assumed that the non randomness parameter, α, for DDSQ to THF interactions and DDSQ to hexanes are equal to zero. These simplifications reduce the binary NRTL equation to the two suffix (one parameter) Margules equation (Equation 5-3):[11]

$$ln\gamma_1 = x_2^2[\tau_{12} + \tau_{21}] \equiv ln\gamma_1 = x_2^2[2\tau_{12}];\ \ ln\gamma_2 \equiv x_1^2[2\tau_{12}] \quad (5-3)$$

This equation is shown as a binary in order to help the reader understand how the binary contribution to the multi-component model simplifies with these assumptions.

5.3 Results and Discussion

5.3.1 Separation of cis and trans 3a-c

Sections 3.3.1.1 – 3.3.1.3 describe the recoveries and purities of the samples. Within each section, the discussion starts with conditions providing the highest purity of the *cis* and *trans*

Table 5-1.[i] Isomers were obtained from fractional crystallization/solubility experiments; ppt1 (step 5, Figure 3-1), and ppt 2 (step 8, Figure 3-1). Their purity was determined by ^{1}H NMR spectroscopy, experimental data was determined from material recovered in step 8 (ppt2) of Figure 3-1 for compounds (a) **3a**, (b) **3b**, and (c) **3c**.

Compound	Exp.	SM[a]	ppt1 (% *trans*)	ppt2 (% *cis*)	x_H:x_T[c]	x_{cis}	x_{trans}
3a	1	1:1	84	90	0.137	1.35E-02	1.50E-03
	2	1:1	90	95	0.616	3.47E-03	1.96E-04
	3	1:1	58	86	1.361	5.32E-04	8.49E-05
	4	1:1	59	92	1.155	7.75E-04	6.45E-05
	5	1:1	96	99	0.899	4.29E-03	4.33E-05
	6[b]	1:1	85	77	0.286	6.03E-03[b]	1.84E-03
	7[b]	1:1	93	83	0.362	3.97E-03[b]	8.07E-04
	8[b]	4:6	95	75	0.342	3.06E-03[b]	1.04E-03
	9[b]	2:8	97	31	0.123	1.45E-03[b]	3.27E-03
	10[b]	2:8	96	60	0.347	1.54E-03[b]	1.02E-03
	11[b]	1:9	99	16	0.240	2.52E-04[b]	1.37E-03
	12[b]	2:8	91	93	0.521	3.35E-03[b]	2.35E-04
	13	8:2	35	86	0.205	2.60E-02	4.29E-03
	14	9:1	20	91	0.539	6.98E-03	6.90E-04
	15	9:1	12	89	0.411	1.61E-02	1.92E-03
	16	9:1	15	85	0.240	2.55E-02	4.50E-03
	17	9:1	7	85	0.308	1.46E-02	2.59E-03
	18	8:2	33	84	0.220	2.64E-02	4.92E-03
3b	1	7:3	36	84	0.88	8.22E-04	1.61E-04
	2	8:2	31	86	0.994	8.68E-04	1.37E-04
	3	8:2	15	91	0.616	1.79E-03	1.74E-04
	4	6:4	29	73	0.37	2.51E-03	9.46E-04
	5	8:2	20	85	0.264	5.45E-03	9.90E-04
3c	1	6:4	71	99	0.880	5.91E-03	8.34E-05
	2	6:4	68	95	0.513	7.85E-03	4.46E-04
	3	6:4	78	96	0.616	5.74E-03	2.68E-04
	4[b]	6:4	82	87	1.174	7.45E-04[b]	1.09E-04
	5[b]	6:4	88	86	1.115	8.21E-04[b]	1.34E-04
	6[b]	3:7	92	71	0.689	2.59E-04[b]	1.03E-04
	7[b]	3:7	92	63	0.603	2.75E-04[b]	1.59E-04
	8[b]	3:7	93	39	0.123	4.86E-04[b]	7.47E-04
	9[b]	9:1	8	87	1.400	1.52E-03[b]	2.27E-04
	10	9:1	3	88	1.155	4.52E-03	5.99E-04
	11	9:1	7	92	1.369	1.42E-03	1.30E-04
	12	9:1	32	97	0.822	4.63E-03	1.61E-04

[a] starting material in a ratio of *cis:trans*, [b] undersaturated *cis* isomer, [c] hexanes to tetrahydrofuran molar ratio

fractions. Table 5-1 provides a summary of the composition of each precipitate and solubility of each isomer that will be discussed in sections 3.3.1.1-3.3.1.3. The *trans* isomer was often predominant in ppt1 while the *cis* isomer was predominant in ppt2 samples with exceptions discussed below. Solubilities were determined based on composition data from the solid obtained in Step 8 of Figure 5-1. The mole fractions were determined by using the material balance on the total mass of each solvent and the mass of DDSQ with ^{1}H NMR analysis. Samples that were fully saturated with both isomers were evaluated for the quantity of each isomer that remains in solution (ppt2) as the solvent is varied from polar (THF-rich) to nonpolar (hexane-rich) (Figures 4-6). As the solution became hexane-rich, less of each isomer remained in solution. The *cis* isomer predominated throughout the range of solvents used.

5.3.1.1. Compound 3a

From the 18 experiments summarized in Table 5-1, the highest purity of *trans* (ppt1) was obtained in experiment 11, when 0.447 g **3a** (3.34e-4 moles) were placed in an anti-solvent to solvent molar ratio of 5:10 (9:13 v/v) to yield 0.369 g (2.76e-4 moles, > 99 % *trans*). The highest purity of *cis* was obtained in ppt2 of experiment 5, when 0.710 g **3a** (5.31e-4 moles) were placed in a 9:10 mixture of anti-solvent to solvent ratio by mole (7:4, v/v) to yield 0.327 g (2.45e-4 moles, > 99 % *cis*). Generally, the average recovery of total material in all experiments was 92 ± 9 %.

3a -Experiments that comprised a starting material (SM) of approximately 1:1 *cis/trans* ratio and a supernatant fully saturated with both isomers displayed a high *trans* purity in **3a** -ppt1 and a high *cis* purity in **3a**-ppt2, according to ^{1}H NMR results (experiments1-5). Those comprised of a supernatant fully saturated with *trans* isomers and an undersaturated *cis* isomer

displayed high *trans* purity in **3a**-ppt1 and a lower *cis* purity in **3a**-ppt2 (experiments 6-8). Additional separations were then carried out using the products from the first 8 experiments as the SM (9-21). Experiments using the first ppt1 (with a higher *trans* ratio) as a SM mostly displayed a supernatant fully saturated for the conditions tested with *trans* isomers, *cis* isomers were undersaturated, and displayed a high *trans* purity in ppt1 and a much lower *cis* purity in ppt2 (experiments 9-12). An attempt was then made to obtain the highest purity *cis* isomer with experiments comprised of a SM with a higher *cis* ratio (experiments 13-18). These experiments

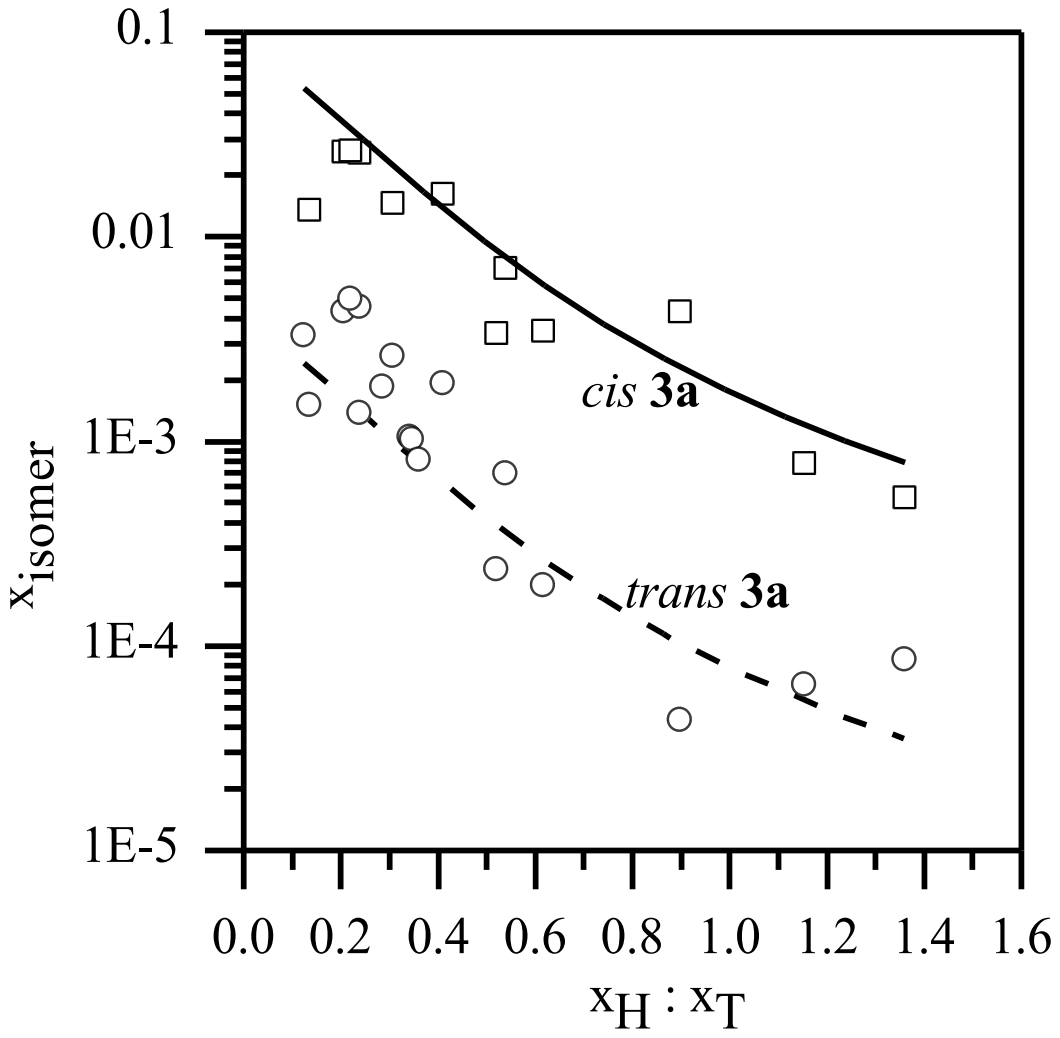

Figure 5-2. Experimental, circle (○) = *cis*, square (□) = *trans*, and modeled, solid line (—) = *cis*, dashed line (---) = *trans*, solubility limits in a hexanes to THF (X_H : X_T) solvent solution for isomers of compound **3a**.

contained a supernatant fully saturated with both isomers, and displayed a low *trans* purity in **3a**-ppt1 and a high *cis* purity in **3a**-ppt2. The ratio of isomers in the SM did not have an effect on the solubility of the isomers. For all experiments that were comprised of a supernatant fully saturated with *cis* isomer, the average percentage of *cis* isomer in **3a**-ppt2 was 90 ± 4.6 % (Figure 5-2).

5.3.1.2. Compound 3b

Experimental purities are summarized in Table 5-1. The highest purity of the *trans* (**3b**-ppt1) was obtained in experiment 1, when 0.328 g (2.22e-4 moles) were placed in a 6:7 mixture of anti-solvent and solvent by mole (3:2 v/v) to yield 0.257 g (1.75e-4 moles, 36 % *trans*). The highest purity of the *cis* (**3b**-ppt2) was obtained in experiment 3, when 0.270 g **3b** (1.82 e-4 moles) were placed in an anti-solvent to solvent molar ratio of 1:1 (1:1, v/v) to yield 0.058 g (3.91e-5 moles, 91 % *cis*). Generally, the average recovery of total material in all experiments was 94 ± 3 %.

The SM of all **3b** experiments was majority *cis* isomer due to a more complicated synthetic procedure, which provided not only a lower reaction yield, but also additional by-products and required further purification. One of the by-products had a similar solubility to the *trans* isomer, and in order to purify **3b**, some *trans* isomer was lost with by-product. However, since fraction ppt2 (majority *cis* isomer) is the principal solid, and the experimental data from compound **3a** demonstrated that the ratio of isomers in the SM did not have any effect on the solubility of the isomers, having all SM for experiments **3b** comprised of majority *cis* isomer helped ensure that the *cis* isomer was not undersaturated. It was determined that these experiments contained a supernatant fully saturated with both isomers, and displayed a low *trans* purity in ppt1 and a high *cis* purity in ppt2. The average percentage of *cis* isomer in ppt2 was 84 ± 7.0 % (Figure 5-3).

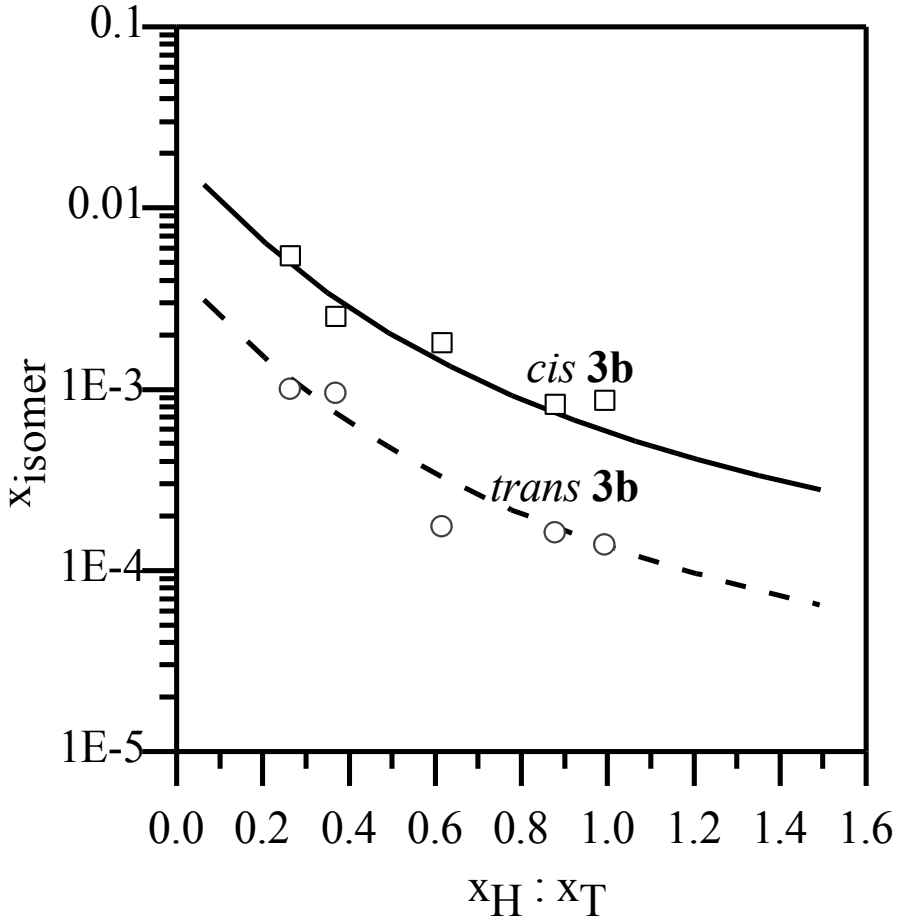

Figure 5-3. Experimental, circle (○) = *cis*, square (□) = *trans*, and modeled, solid line (—) = *cis*, dashed line (---) = *trans*, solubility limits in a hexanes to THF ($X_H : X_T$) solvent solution for isomers of compound **3b**.

5.3.1.3. Compound 3c

Experimental are summarized in Table 5-1. The highest purity of the *trans* (ppt1) was obtained in Experiment 8, when 0.322 g **3c** (3.34e-4 moles) were placed in a 7.5:5.5 mixture of anti-solvent and solvent by mole (9:4 v/v) to yield 0.0273 g (2.04e-5 moles, > 99 % *trans*). The highest purity *cis* fraction (ppt2) was obtained in Experiment 1, when 0.331 g **3c** (2.48e-4 moles) were placed in a 7.5:8.5 mixture of anti-solvent and solvent by mole (1:0.7 v/v) to yield 0.131 g (9.79e-5 moles, > 99 % *cis*). Generally, the average recovery of total material in all experiments was 96 ± 5 %.

As with **3a**, experiments using a starting material (SM) of approximately 6:4 *cis/trans* ratio and a supernatant fully saturated with both isomers displayed a moderately high *trans* purity in ppt1 and a high *cis* purity in ppt2, according to ^{1}H NMR results (experiments1-3). Additional separations were then carried out using the products from the first 5 experiments as the SM (experiments 6-12). Experiments that comprised a SM with a higher *trans* content mostly displayed a supernatant fully saturated for the conditions tested with *trans* isomers, *cis* isomers were undersaturated, and displayed a high *trans* purity in ppt1 and a much lower *cis* purity in

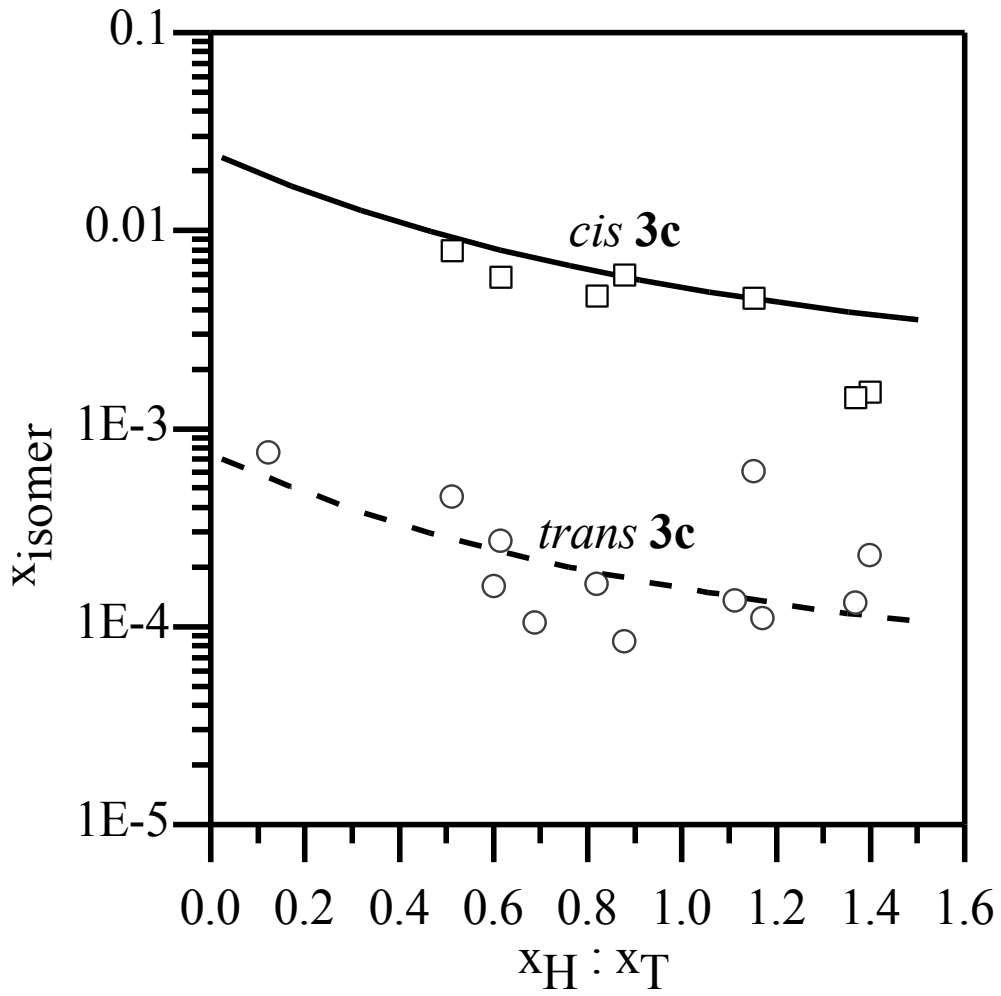

Figure 5-4. Experimental, circle (○) = *cis*, square (□) = *trans*, and modeled, solid line (—) = *cis*, dashed line (---) = *trans*, solubility limits in a hexanes to THF (X_H : X_T) solvent solution for isomers of compound **3c**.

ppt2 (experiments 6-8). An attempt was then made to obtain the highest purity *cis* isomer with experiments comprised of a SM with a higher *cis* ratio (experiments 9-12). These experiments contained a supernatant fully saturated with both isomers, and displayed a low *trans* purity in ppt1 and a high *cis* purity in ppt2. Similarly to the meta-species **3a**, it was demonstrated that the ratio of isomers in the SM did not have an effect on the solubility of the isomers for the para-species. For all experiments that were comprised of a supernatant fully saturated with *cis* isomer, the average percentage of *cis* isomer in ppt2 was 93 ± 4.6 %.

5.3.2 Chromatography Results

Chromatography columns were used to obtain the highest purity of each isomer.[ii] There were up to 60 fractions (5 – 10 mL each) from one chromatography column. TLC plates and ^{1}H NMR spectra were used to identify the pure fractions. The *trans* isomer eluted before the *cis* isomer for all materials. There was sufficient separation in the order of elution to achieve complete separation of the two isomers.

5.3.3 DSC Results

Pure component properties (T_m and ΔH_m) were determined from DSC heating traces for compounds **3a**, **3b**, and **3c**. Results are summarized in Table 5-2 and were used to fit the

Table 5-2. Melting temperature (T_m) and the heat of fusion (ΔH_m) for compounds **3a-c** as determined by differential scanning Calorimetry, from T = 40 °C –350 °C with a heating rate of 10 °C/min.

Compound	**3a**-cis	**3a**-trans	**3b**-*cis*	**3b**-*trans*	**3c**-*cis*	**3c**-*trans*
T_m (°C)	289.5	312.0	265.9	270.0	272.6	309.3
ΔH_m	42	56	39	46	38	58

sharp endothermic peak was observed, which is representative of a melting transition. The onset of melting (T_m) is calculated by extrapolating the slope from the peak width at half height to the baseline and the total heat of fusion (ΔH_m) is the total area of the melting endotherm.

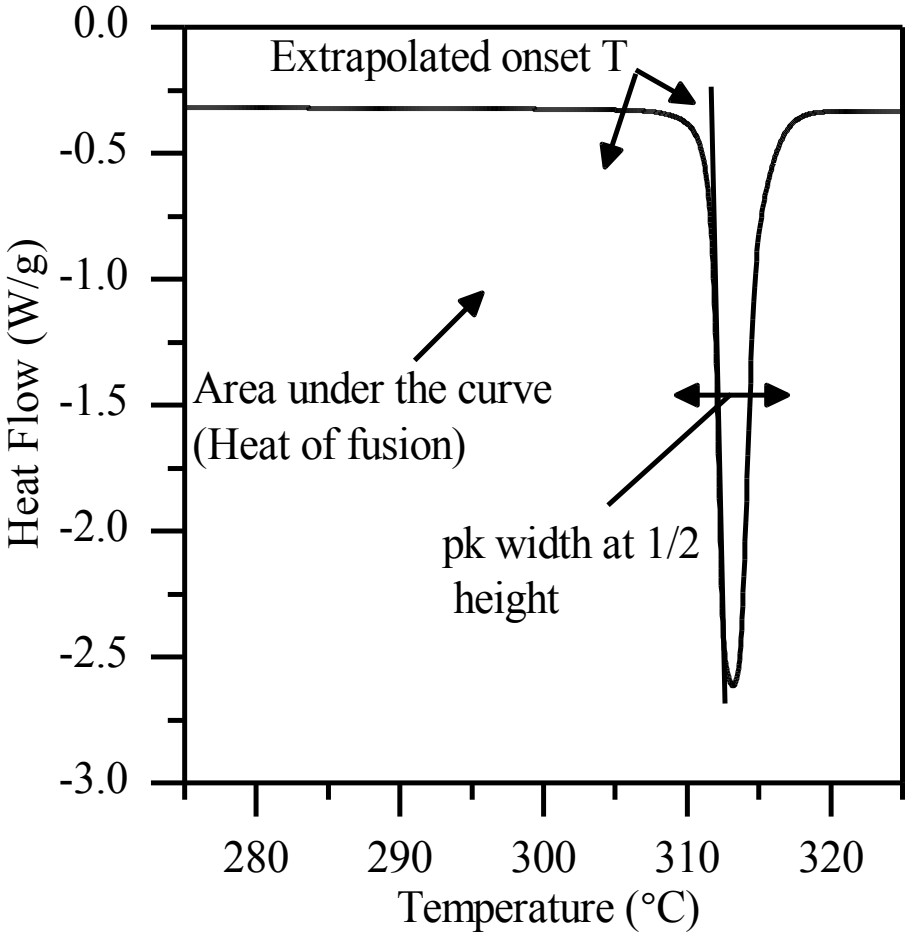

Figure 5-5. Example of a melting endotherm (*trans* 3a) showing the melting temperature and heat of fusion as determined by differential scanning Calorimetry, from T = 40 °C –350 °C with a heating rate of 10 °C/min.

5.3.4 Results of Model Fitting

Binary parameters for *THF* + *hexanes* were taken from the VLE regression sets in Aspen Plus® ver. 7.3 ($a_{H,T} = a_{T,H} = 0$, $b_{H,T} = -15.0959$ K, $b_{T,H} = 233.6258$ K and $\alpha_{T,H} = 0.3$).[13] Only the binary a_{ij} for *cis/trans* + *hexanes* and *cis/trans* + *THF* ($a_{DDSQ,H}$ and $a_{DDSQ,T}$) were

adjusted while x_i values were fitted along the saturation curves. Since all data were collected at room temperature only, the temperature dependence is ignored; thus $b_{DDSQ,H} = b_{DDSQ,T} = 0$. For the interaction between DDSQ and each solvent $\tau_{DDSQ,H} = a_{DDSQ,H}$ and $\tau_{DDSQ,T} = a_{DDSQ,T}$. Therefore, a negative value of a_{ij} will provide a negative value of τ_{ij} and $\gamma < 1.00$. A positive value of a_{ij} will provide a positive value of τ_{ij} and $\gamma > 1.00$. As the magnitude of a_{ij} increases, the solution becomes less ideal. For large negative values of a_{ij}, the material is more soluble than in an ideal solution; for large positive values the solution is an anti-solvent, and the material is less soluble than in an ideal solution. The model results are compared to experimental results in Figure 5-2 through Figure 5-4 and compared between compounds **3a-c** in Figure 5-6.

The scatter seen in Figure 5-2 through Figure 5-4 can be attributed to the experimental uncertainties due to the small sample sizes used. The relative uncertainty that provides the most error (according to differential error analysis) is from the solid composition obtained by ^{1}H NMR (Table 5-1). The experimental measurements in Table 5-1 lie within the computed confidence intervals of +/- 5%. For example, the point in Figure 5-2 with a solid $x_H : x_T$ ratio of 0.899 has a 500% relative error (% RE), determined by the error in the composition of the *trans* isomer (Table 5-3). The RE is very high for this data point because 99% of the 326 mg sample is the *cis* isomer. Therefore, the mass of the *trans* isomer is only 3.3 mg, or 1 % of the sample, which is below is threshold of detection for ^{1}H NMR. The +/- 5% confidence interval, as discussed previously is applied to the entire sample mass, yielding a confidence interval of approximately +/- 16 mg, which is 5 times larger than mass of the *trans* isomer. Clearly, as the

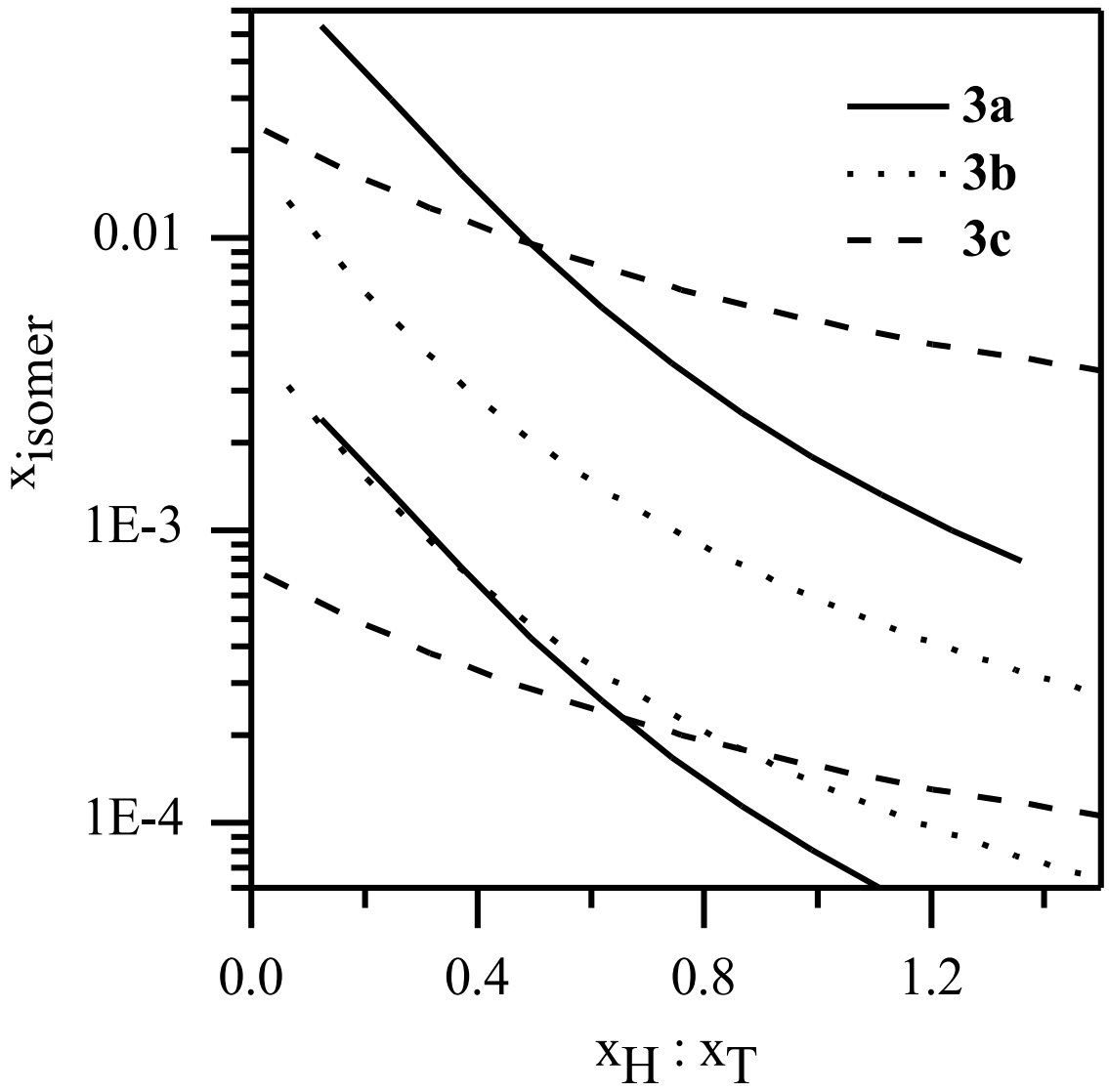

Figure 5-6. Modeled solubility limits in a hexanes to THF ($X_H : X_T$) solvent solution for the *cis* and *trans* isomers of compounds **3a**, **3b**, and **3c**. The three upper curves represent *cis* and the lower three curves represent *trans*.

mass of a component decreases, the relative uncertainty for that component increases significantly which explains the larger scatter in the experimental *trans* data points. Another feasible cause for error is experimental masses and volumes of all four components, which provide a % RE of < 10 for the *trans* isomer and < 1 for the *cis* isomer. Additional causes for error in the experimental values and the model may be attributed to: room temperature and filtration methods, which are more ambiguous to estimate. When the model was adjusted to

account for the % RE in x_i, activity coefficients and binary interaction parameters were minimally affected.

Table 5-3. % Relative error (% RE) determined by a +/- 5% confidence interval in ^{1}H NMR measurements.

Compound	x_H:x_T [a]	% RE_{cis}	% RE_{trans}	Compound	x_H:x_T [a]	% RE_{cis}	% RE_{trans}
3a	0.123	16	7	**3b**	0.264	5	83
	0.137	6	50		0.370	7	18
	0.205	6	35		0.616	5	56
	0.220	6	32		0.880	5	59
	0.240	6	33		0.994	6	37
	0.240	32	6	**3c**	0.123	8	13
	0.286	7	21		0.513	5	93
	0.308	6	33		0.603	8	14
	0.342	7	20		0.616	5	112
	0.347	8	13		0.689	7	18
	0.362	6	30		0.822	5	148
	0.411	6	47		0.880	5	359
	0.521	5	76		1.115	6	36
	0.539	5	56		1.155	6	43
	0.616	5	93		1.174	6	39
	0.899	5	500		1.369	5	60
	1.155	5	65		1.400	6	39
	1.361	6	36				

[a] hexanes to tetrahydrofuran molar ratio

Activity coefficients as a function of the mole fraction of solvent, THF or hexanes, for all three DDSQ compounds investigated are presented in Figure 5-7. Adjustable parameters representing the interaction between DDSQ compounds to solvent ($a_{DDSQ,T}$ and $a_{DDSQ,H}$) are summarized in Table 5-4. For compounds **3a-c** the solubility in 100 % THF (left side of Figure 5-6), is higher than the ideal value (Table 5-5). From the model the $\ln(\gamma_{solute\text{-}solvent}) < 0$ and the $\ln(\gamma_{solute\text{-}anti\text{-}solvent}) > 0$, which confirms that the THF is a good solvent and hexanes are an

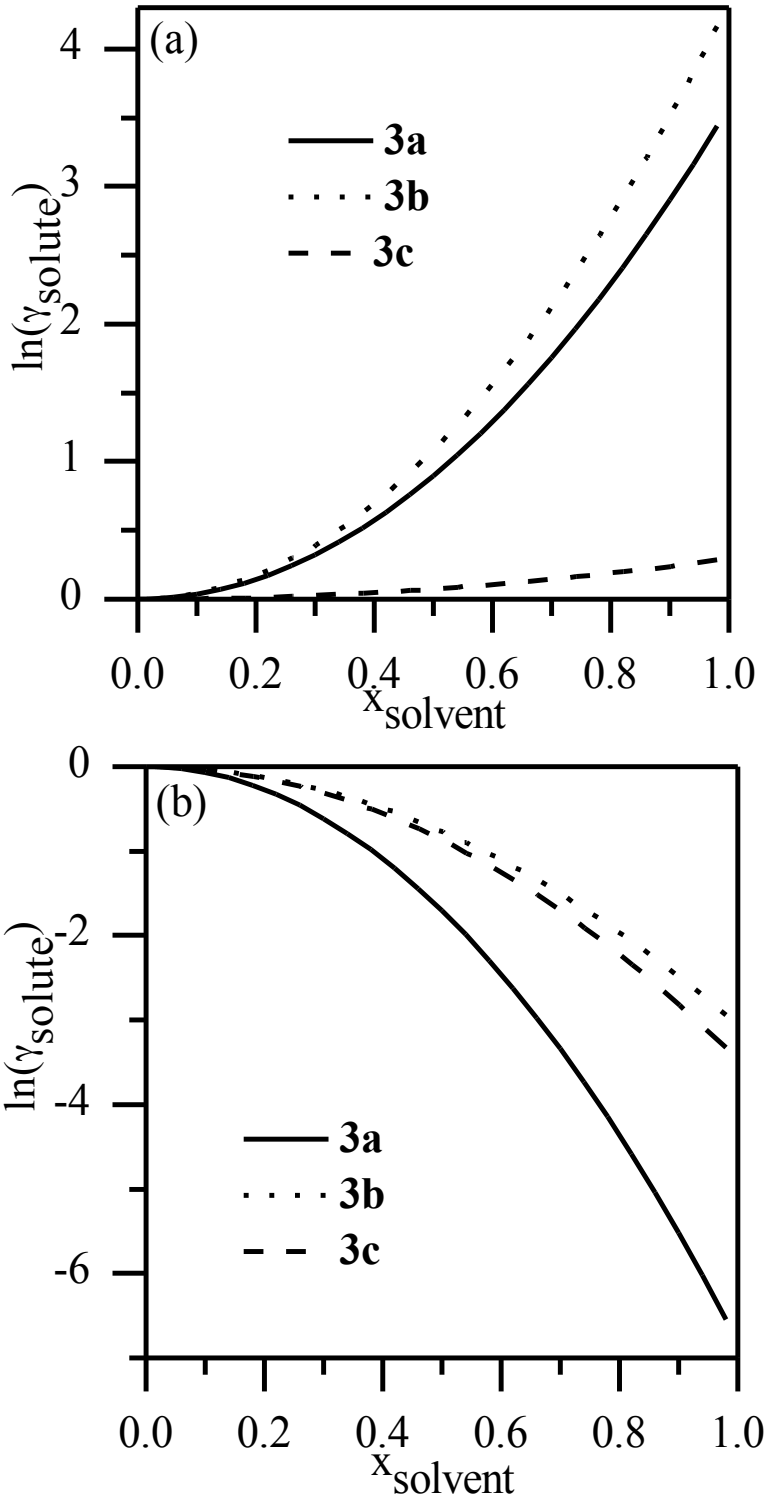

Figure 5-7. Activity coefficients of the solute vs. the mole fraction of (a) anti-solvent (hexanes) and (b) solvent (THF), when each compound is considered a binary. When the natural logarithm of the activity coefficient is larger than zero, the interaction is between DDSQ and hexanes. When the natural logarithm of the activity coefficient is below zero, the interaction is between DDSQ and THF.

Table 5-4. Binary interaction coefficients for **3a**, **3b**, and **3c**.

Compound	$a_{DDSQ,H}$	$a_{DDSQ,T}$
3a	1.7904	-3.4085
3b	2.1676	-1.5328
3c	0.1474	-1.7338

anti-solvent for these three DDSQ compounds. The γ_{solute} is highly non-ideal for all conditions tested, since $x_{solvent}$ is very close to 1.00 and the saturated solutions are close to infinite dilution for DDSQ. The relation between the activity coefficients and the binary interaction parameters are most obvious in Equation 5-3 for a binary, recalling that $\tau_{ij} = a_{ij}$, and $\ln \gamma_i^{\infty} = 2a_{ij}$.

Table 5-5. Result of Schröder-van Laar equation (RHS) at room temperature and the corresponding solubility limits based on ideal solution assumptions (γ = 1.00) for compounds **3a**, **3b**, and **3c**.

Compound	RHS	x_{ideal} [a]
3a-cis	-7.97	3.47E-04
3a-trans	-11.08	1.54E-05
3b-cis	-7.03	8.83E-04
3b-trans	-8.37	2.32E-04
3c-cis	-6.96	9.54E-04
3c-trans	-11.42	1.10E-05

[a] x_{ideal}: (γ= 1.00)

The magnitude of the binary interaction parameter of DDSQ and THF ($a_{DDSQ,T}$) combined with the RHS of the Schröder-van Laar equation (Equation 5-1) can be used to explain the overall solubility of compounds **3a-c**. For all three compounds investigated, the solubility of the *cis* species is always higher than the *trans* species in a solvent with a fixed ratio of THF to hexanes. Experimental saturation curves for both the *cis* and *trans* species in a THF/hexanes mixture, as shown in Figure 5-2 through Figure 5-4, appear to exhibit the same slope. This

observation validated the assumption that the interaction parameters between each isomer and solvent is the same, $a_{DDSQ,T} = a_{DDSQ,H}$. However, the magnitude of the separation between the *cis* and *trans* saturation curves for each compound (Figure 5-6) varies and is dependent on the physical melting characteristics, which is given by the ratio of the ideal solubility for the two isomers (Table 5-5). Isomers of compound **3c** exhibited the largest magnitude of separation in their saturation curves (Figure 5-6). *Cis* isomers of compound **3c** were 33 times more soluble than their *trans* isomers, a partitioning threshold of 33:1. The separation of the saturation curves of the isomers of compound **3a** was slightly closer; *cis* isomers were 22 times more soluble than *trans* isomers. Isomers of compound **3b** exhibited the smallest magnitude of separation in their saturation curves; *cis* isomers were only 3.5 times more soluble than *trans* isomers. Isomers of **3c** exhibit the largest difference in T_m and ΔH_m, and the isomers of **3b** exhibit the smallest difference, which is consistent with this solubility data.[14,15]

The *cis* isomers, which are the more soluble species, of compounds **3b** and **3c** approached the same solubility in THF (left side of Figure 6). This is because they have very similar values for their binary interaction parameter between DDSQ and THF, $a_{3b,T}$ = -1.5328 and $a_{3c,T}$ = -1.7338, and similar T_m and ΔH_m values (RHS ≅ -7). *Cis* **3a** possesses a higher solubility in THF than the other two compounds because its value of $a_{3a,T}$ is most negative (- 3.4085) and the T_m and ΔH_m values (RHS ≅ -8) are larger than the other compounds. The slopes of the saturation curves in Figure 6 are very different for *cis* **3b** and **3c**, which results from their binary interaction coefficients with the anti-solvent (hexanes), $a_{3b,H}$ = 2.1676 and $a_{3c,H}$ = 0.1474. The magnitude of $a_{DDSQ,H}$ provides information on how quickly the solubility will decrease as hexanes are

added to THF. Since, $a_{3c,H}$ is so close to zero, the interaction of *cis* **3c** and hexanes is nearly ideal. Therefore, the solubility of *cis* **3c** with the addition of hexanes will not decrease as rapidly as the other compounds and the lower solubility is largely due to dilution of the stronger THF solvent. The slope of the saturation curve of *cis* **3a** is similar to that of *cis* **3b** because they have similar values for their interaction with hexanes, $a_{3a,H}$ = 1.7904.

The t*rans* isomers, which are the less soluble species, of compounds **3a** and **3c** have similar values for T_m and ΔH_m (RHS ≅ -11), =but since $a_{3a,T}$ (-3.4085) has a larger magnitude than $a_{3c,T}$ (-1.7338), *trans* **3a** is more soluble in THF than *trans* **3c**. Additionally, *trans* **3a** and *trans* **3b** have different T_m and ΔH_m values (RHS ≅ -11 and -8, respectively) and different values for $a_{DDSQ,T}$ (-3.4085 and -1.5328, respectively), but coincidentally have similar solubilities in THF. This further confirms that the Schröder-van Laar equation *and* binary interaction coefficients are *both* necessary when determining solubility.

5.4 Concluding remarks on isomer separations

Cis and *trans* isomers of a series of DDSQ(X)(R) were successfully separated using a fractional crystallization method. The Schröder-van Laar equation (Equation 1), and the NRTL model (Equation 2) were used to fit the experimental data. The model was simplified to reduce the number of adjustable parameters. The NRTL model parameters are consistent with the solubility trends, suggesting they have physical meaning. In this paper, the solubility of the *cis* and *trans* isomers were represented using the same binary interaction coefficients for DDSQ + solvent and DDSQ + anti-solvent for each isomer. The two isomers of each compound do not interact differently with a given solvent even though they have different solubilities. The

difference in solubility of the *cis* and *trans* isomers is due to the pure component properties (RHS), not the DDSQ + solvent and DDSQ + anti-solvent interactions. Between the different compounds, the differences in solubility are due to *both* the Schröder-van Laar equation *and* binary interaction coefficients.

Overall it was determined that changing the R-group from a methyl to a bulkier cyclohexyl moiety, **3a** to **3b**, decreases the solubility of the compound and also decreases the partitioning threshold between the *cis* and *trans* isomers. The difference in T_m and ΔH_m were consistent with the change in the isomeric partitioning threshold of these compounds. Additionally the solubility of the meta-structures, compounds **3a** and **3b**, decrease at similar rates with increasing content of hexanes, which was verified by the interaction parameters with hexanes. Changing the *X*-group from meta- to para-, **3a** to **3c**, leads to an increase in the partitioning threshold, and a decrease in the rate of solubility. Overall, the models show that assumptions were valid over the range of experiments, and the determined saturation curves can be used for the separation of the *cis* and *trans* isomers of compounds **3a-c**.

NOTES

NOTES

(i) A total mass balance of each isomer was performed to verify solubility data and can be seen in appendix C.

(ii) The retardation factors (R_F) are reported in appendix C.

REFERENCES

REFERENCES

(1) Hoque, M. A.; Kakihana, Y.; Shinke, S.; Kawakami, Y. *Macromolecules* **2009**, *42*, 3309.

(2) Seurer, B.; Vij, V.; Haddad, T.; Mabry, J. M.; Lee, A. *Macromolecules* **2010**, *43*, 9337.

(3) Schoen, B. W.; Holmes, D.; Lee, A. *Magnetic Resonance in Chemistry* **2013**, *51*, 490.

(4) Myasnikov, S. K.; Uteshinsky, A. D.; Kulov, N. N. *Theoretical Foundations of Chemical Engineering* **2009**, *43*, 227.

(5) Tadie, M.; Bahadur, I.; Reddy, P.; Ngema, P. T.; Naidoo, P.; Deenadayalu, N.; Ramjugernath, D. *Journal of Chemical Thermodynamics* **2013**, *57*, 485.

(6) Wang, T.-C.; Li, Y.-J.; Chen, Y.-P. *Journal of Chemical and Engineering Data* **2012**, *57*, 3519.

(7) Tam Le, M.; Lorenz, H.; Seidel-Morgenstern, A. *Chemical Engineering & Technology* **2012**, *35*, 1003.

(8) Still, W. C.; Kahn, M.; Mitra, A. *Journal of Organic Chemistry* **1978**, *43*, 2923.

(9) Prausnitz, J. M.; Lichtenthaler, R. N.; Azevedo, E. G. d. *Molecular thermodynamics of fluid-phase equilibria*; 3rd ed.; Prentice Hall PTR: Upper Saddle River, N.J., 1999.

(10) Gmehling, J. G.; Anderson, T. F.; Prausnitz, J. M. *Industrial & Engineering Chemistry Fundamentals* **1978**, *17*, 269.

(11) Elliott, J. R.; Lira, C. T. *Introductory chemical engineering thermodynamics*; 2nd ed.; Prentice Hall: Upper Saddle River, NJ, 2012.

(12) Renon, H.; Prausnit.Jm *Industrial & Engineering Chemistry Process Design and Development* **1969**, *8*, 413.

(13) In *Aspen Physical Property System. Physical Property Methods and Model* Burlington: 2010.

(16) Pinal, R. *Organic & Biomolecular Chemistry* **2004**, *2*, 2692.

(17) Gavezzotti, A. *Journal of the Chemical Society-Perkin Transactions 2* **1995**, 1399.

CHAPTER 6

PHASE BEHAVIOR FOR *cis* AND *trans* ISOMERS OF THREE AMINOPHENYL DOUBLE DECKER SILSESQUIOXANES

Keywords

double decker silsesquioxane, solid-liquid equilibria, NRTL model, eutectic, isomorphous

cis/trans isomers

6. Phase behavior for *cis* and *trans* isomers of three aminophenyl double decker silsesquioxanes

6.1 Introduction

Configurational modifications, such as varying the structural conformation of a small organic molecule, tend to have large effects on thermodynamic, physical, and structural properties.[1] Para-di-substituted benzenes typically have a higher symmetry than meta-di-substituted benzenes. Thus, para-di-substituted benzenes can more easily pack in a crystal lattice, forming more stable and higher melting crystals.[1-4] Similarly, *trans* isomers generally exhibit a higher order of symmetry over their *cis* counterparts; which also provides them with higher melting temperatures.[4-6] Other modifications, such as changing a ligand from methyl to cyclohexyl can affect symmetry, molecular packing, and melting temperature.[1,7] The addition of the cyclohexyl moiety provides increased surface area and intermolecular interactions, which increase the melting temperature.[8,9] Moreover, the way molecules pack, their packing density, and affinity for hydrogen bonding in the crystal lattice can also affect the melting temperature.[7,10] Furthermore, the melting point of a pure substance can be altered when "guest" molecules substitute or diffuse into the crystal and distort the lattice of a "host" molecule.[11] "Guest" molecules can be a geometrical isomer of the material being studied. Lattice defects and solid solutions result in lower melting temperature, but are not necessary for melting depression, which can occur in mixtures where the solid and liquid compositions differ. Binary mixtures that exhibit this type of phenomena can be classified as a general eutectic, congruent eutectic, or incongruent eutectic. Eutectic systems have two solid phases in equilibrium with the liquid phase

at the melting temperature.[12] A congruent melting system displays a liquid and solid phase with identical compositions at the equilibrium melting temperature.[13] Incongruent melting systems display a peritectic, or an incongruent melting point, where the composition of the solid and the liquid states are not equivalent at the equilibrium melting temperature.[13,14] Both congruent and incongruent eutectic-type binary mixtures occur in systems with co-crystals. Co-crystal formation has been seen to improve physiochemical properties such as solubility, mechanical properties, and bioavailability.[15] If the "guest" molecule is of a similar size and shape to the "host" molecule, the lattice may not be distorted and the melting temperature will gradually decrease with increasing content of the lower melting material. Binary mixtures that exhibit this type of phenomena can be classified as an isomorphous, solid-state solution.[15] An isomorphous melting system displays complete miscibility of both the liquid and solid phases.[13]

These thermodynamic, physical, and structural behavios for different configurations of small organic molecules have been well established and can be easily predicted. However, the same behaviors are much more complex for larger molecules, especially for compounds containing a large inorganic portion. Understanding these behaviors for different configurations of aminophenyl DDSQ allows for the selection of a structure with the desired melting, crystalline, and solubility features that would be necessary to isolate a novel material. Melting characteristics of compounds **3a-c** were determined using differential scanning calorimetry, and structural characteristics were examined through single crystal x-ray diffraction studies. Solubility characteristics were previously determined and were reported in the previous chapter.[16] Thermal behavior of binary mixtures was studied from samples with various ratios of

cis and *trans* isomers, which were prepared from chromatography columns. Isomer ratios were quantified according to ^{1}H NMR spectroscopy.[17] Phase diagrams of binary mixtures were modeled using the Schröder-van Laar equation and activity coefficients and binary interaction parameters were determined with the non-random two liquid (NRTL) model. These calculated parameters allowed for the concise description of a solid-liquid equilibrium phase diagram for each compound, which can be used to select an isomer, or ratio of isomers, necessary for reaction conditions, and/or desired characteristics for a novel engineering design. The three structures studied in this chapter will be discussed in a different order than previously. Compound **3a**, where R = methyl, and X = para- aminophenyl will be discussed first, followed by compound **3b**, where R = methyl, and X = meta- aminophenyl, and finally compound **3c**, where R = cyclohexyl, and X = meta- aminophenyl will be discussed last.

6.2 Materials and Methods

6.2.1 Solvents and Reagents

Tetrahydrofuran (THF), hexanes, benzene, methylene chloride, toluene, and triethylamine were obtained from Sigma-Aldrich and used as received. SiliaFlash ® P60 Silica gel was purchased from Silicycle Ultra Pure Silica Gels (Quebec City, Quebec, Canada). Silica gel 60 F_{254}, (0.2 mm thick, Sigma Aldrich) pre-coated plastic plates were used for thin layer chromatography (TLC).

6.2.2 Cis/trans isomers sample preparation

Samples containing isolated *cis* and *trans* isomers as well as mixtures with different ratios of *cis* to *trans* isomers were obtained using column chromatography using the same chromatography procedure in chapter 5. Individual fractions were analyzed for ratios of *cis* to

trans isomers. There were up to 30 eluent fractions (5 – 10 mL each) from one chromatography column. The *trans* isomer eluted before the *cis* isomer for all compounds, with sufficient separation in the order of elution to allow for complete isolation.[16] Several eluent fractions between the pure isomer fractions were collected to obtain binary mixtures of different *cis:trans* ratios. A specific example of the preparation for binary mixtures of compound **3c** follows (Table 6-1). The relative fraction of *trans* isomers for each eluent fraction was determined by ^{1}H NMR analysis. Fractions collected before eluent 17 contained isolated *trans* **3b**. Fractions collected after eluent 21 contained isolated cis **3b**. Additional ratios were obtained through the mixing of pure isomers in desired ratios and results were verified with ^{1}H NMR analysis.

Table 6-1. Composition, in % *trans* isomer, of the eluent fraction obtained in column chromatography for compound **3c**.

Fraction	% *trans*
17	78
18	52
19	33
20	18
21	14

6.2.3 Characterization

6.2.3.1 NMR spectroscopy

^{1}H NMR was used to quantify the ratios of the *cis* to *trans* isomers in the binary mixtures from previously determined methods.[17] Compounds were measured at 25 ºC on a Varian UNITY-Inova 600 spectrometer equipped with a 5 mm Pulsed-Field-Gradient (PFG) switchable

broadband probe and operating at 599.80 MHz (^{1}H). ^{1}H NMR data were acquired using a recycle delay of at least 20 s and 32 scans to ensure accurate integration. The ^{1}H-chemical shifts were referenced to that of residual protonated solvent in $CDCl_3$ (7.24 ppm).

4.2.3.2 Differential scanning calorimetry

Melting and solidification behavior were studied using a TA Instrument Q2000 equipped with a mechanical cooling system under a nitrogen atmosphere. Samples were placed in a Q-zero^{TM} aluminum pan and sealed with a lid. Samples were equilibrated at 40 °C for 1 min and then heated to 350 °C with a constant heating rate of 10 °C/min. After which, samples were held at 350 °C for 1 minute and cooled to 40 °C with a constant cooling rate of 5 °C/min. A second heating cycle rate of 10 °C/min was imposed on selected samples.

6.2.3.3 Single crystal X-ray diffraction

Crystals were grown from various solvent solutions for isolated pure isomers (Table 6-2) and were mounted on a Nylon Loop using very small amount of paratone oil. Data were collected using a Bruker CCD (charge coupled device) based diffractometer equipped with an Oxford Cryostream low-temperature apparatus operating at 173 K. Data were measured using omega and phi scans of 0.5° per frame for 30s. The total number of images was based on results from the program COSMO[19] where redundancy was expected to be 4.0 and completeness of 100% out to 0.83 Å. Cell parameters were retrieved using APEX II software[20] and refined using SAINT on all observed reflections. Data reduction was performed using the SAINT software[21] which corrects for Lp. Scaling and absorption corrections were applied using SADABS[22] multi-

scan technique, supplied by George Sheldrick.[22] The structures are solved by the direct method using the SHELXS-97 program and refined by least squares method on F^2, SHELXL- 97, which are incorporated in SHELXTL-PC V 6.10.[23] All non-hydrogen atoms are refined anisotropically. Hydrogens were calculated by geometrical methods and refined as a riding model. The crystal used for the diffraction study showed no decomposition during data collection. All drawings are done at 50% ellipsoids.

Table 6-2. Solvents used for crystallization of compounds **3a**, **3b**, and **3c**.

Solvent [a]	Compound(s)Benzene
Benzene	*cis*-**3c** and **3a**, *trans*-**3a** and *trans*-**3b** [b]
Methylene chloride	*trans*-**3c**
Toluene	*trans*-***3b*** [c]

[a] All solvents were layered with hexanes, [b] Polymorph B and C, [c] Polymorph A.

6.3 Results

Sections 4.3.1 – 4.3.5 describe the results of thermal experiments, structural investigations, and data analysis. All thermal data were taken from the first heating cycle (melting) and first cooling cycle (solidification) unless otherwise noted. Section 4.3.1 begins with melting and solidification behavior of isolated *cis* and *trans* isomers. Section 4.3.2 provides results of single crystal XRD. Section 4.3.3 shows results of melting behavior for *cis/trans* binary mixtures. Melting behavior was analyzed according to solid-liquid equilibria equations that allowed for the concise representation of phase diagrams, which are presented in section 4.3.4. Finally, section 4.3.5 shows results of the solidification behavior of *cis/trans* binary

mixtures, which could not be analyzed according to solid-liquid equilibria equations due to the large undercoolings exhibited by all compounds.

6.3.1 Thermal behavior of isolated cis and trans isomers

Melting and solidification behavior of the purest *cis* and *trans* isomers were evaluated using TA Universal Analysis software,[24] and results were summarized in Table 6-3. Melting data was acquired from the first heating of all isomers (Figure 6-1). All *trans* isomers exhibited a higher melting temperature (T_m) than their *cis* counterparts. Solidification behavior was investigated using the first cooling cycle of the DSC trace (Figure 6-2). All *trans* isomers and *cis*

Table 6-3. Melting temperature and the heat of fusion for compounds **3a-c** as determined by differential scanning Calorimetry, from T = 40 °C –350 °C with a heating rate of 10 °C/min.

Compound	T_m (°C)	ΔH_m (kJ/mol)	ΔS_m (J/mol·K)	T_c (°C)	ΔH_c (kJ/mol)	ΔL (°C)
3c-*trans*	310.6	55	94.2	266.1	53	44.5
3c-*cis*	275.7	38	69.2	131.0	32	144.7
3a-*trans*	312.0	56	95.7	284.4	55	27.6
3a-*cis*	291.8	42	74.3	--[a]	--[a]	--[a]
3b-*trans*	270.0	46	84.7	202.0	45	68.0
3b-*cis*	265.9	39	72.3	200.8	42	65.1

[a] **3a**-*cis* did not exhibit T_c, but did exhibit a T_g and then a T_r during the 2nd heating, where T_g = 54 °C, T_r = 91 °C, ΔHr = 22 kJ/mol, and ΔS_r = 60.4E-2 J/mol·K.

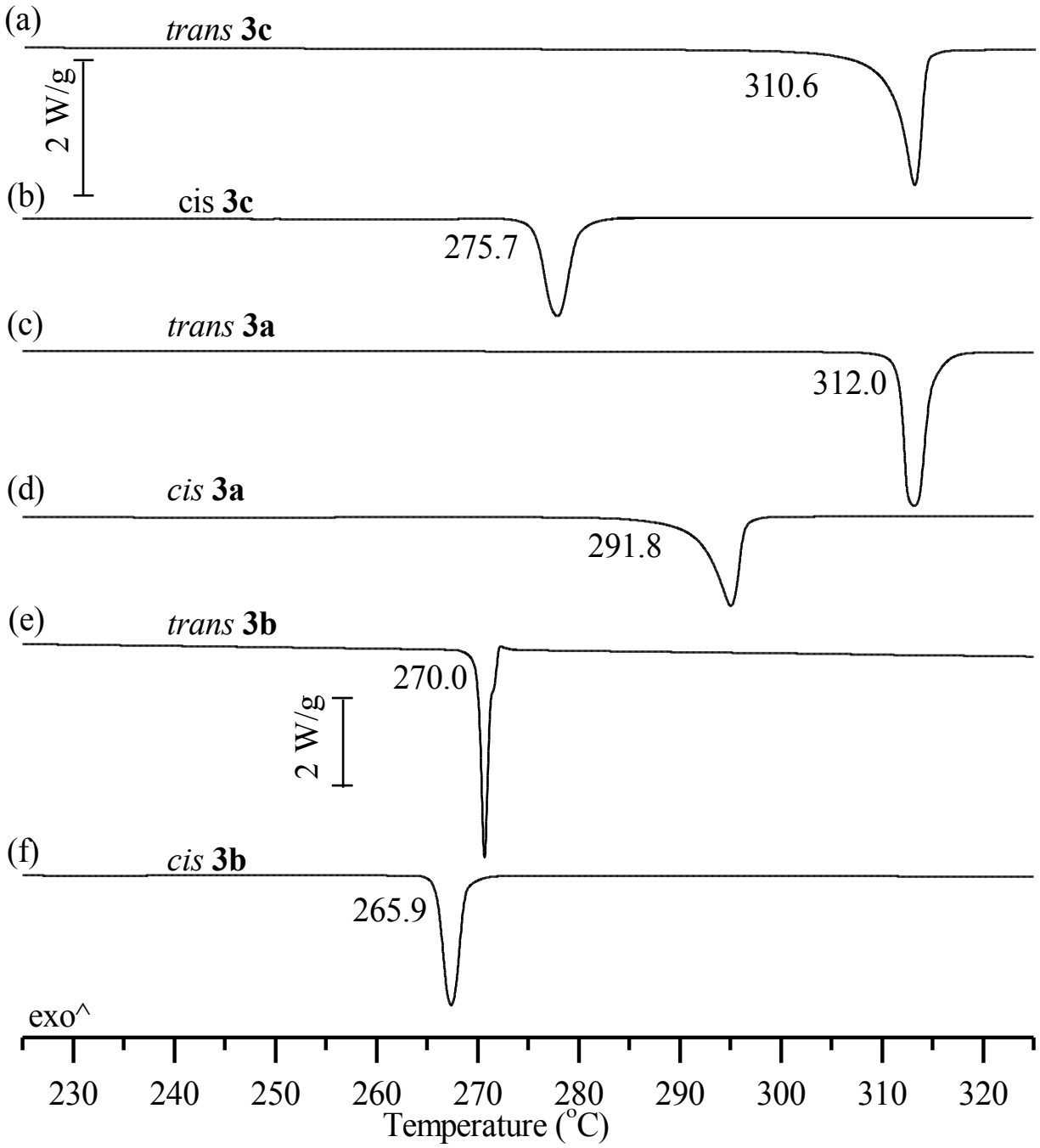

Figure 6-1. Melting endotherms of *trans* and *cis* isomers for compounds **3a-c**; from T = 225 °C –325 °C with a heating rate of 10 °C/min. All isomers have the same scale bar as (a) unless otherwise noted.

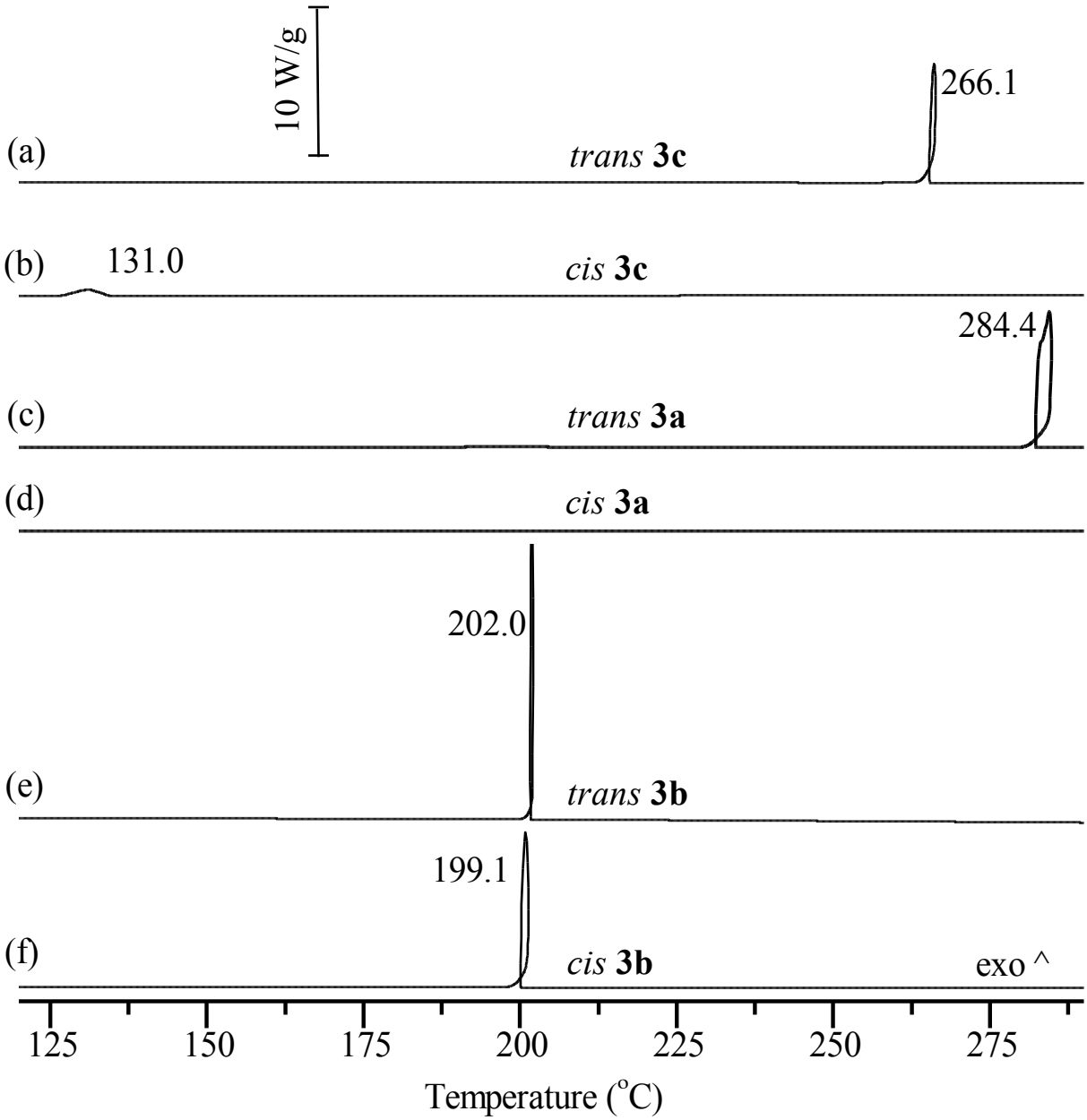

Figure 6-2. Cooling exotherms of *trans* and *cis* isomers for compounds **3a-c**; from T = 120 °C – 290 °C with a cooling rate of 5 °C/min. All isomers have the same scale bar as (a).

3b exhibited a rapid, complete crystallization upon cooling, where the endset temperature is equivalent to the supercool point. *Cis* **3c** also exhibited crystallization upon cooling, but the process was much slower as indicated with a broad exothermic peak. *Cis* **3a** did not exhibit crystallization upon cooling, even when the cooling rate was reduced from 5 °C/min to 1 °C/min. Therefore, a second heating was performed to investigate its crystallization behavior. The trace showed a step-like glass transition followed by an exothermic peak representing a cold crystallization transition (Figure 6-3).

6.3.2 Structural results

To confirm structural arrangement and assist in explaining melting and solidification behavior, single crystal structures were obtained using XRD. Persistent crystallization attempts resulted in several polymorphs for compounds **3a-c**. All crystal data displayed good quality, all R1's < 0.085, and data completeness to ~ 25 ° > 99.3 % (Table D-I, appendix D). All crystal structures obtained are shown in appendix D.

6.3.2.1 Compound 3c

One distinct crystal structure for *trans* **3c** was determined (Figure D-2, appendix D). It was observed as a needle-like structure from a layered mixture of methylene chloride and hexanes, and crystallized in the monoclinic space group P2(1)/n with a packing density (ρ) of 1.39 Mg/m^3. For *cis* **3c**, one distinct crystal structure was also determined (Figure D-2, appendix D). It was observed as a flat sheet from a layered mixture of benzene and hexanes, and crystallized in the triclinic space group P-1 as a twinned structure with $\rho = 1.366$ Mg/m^3.

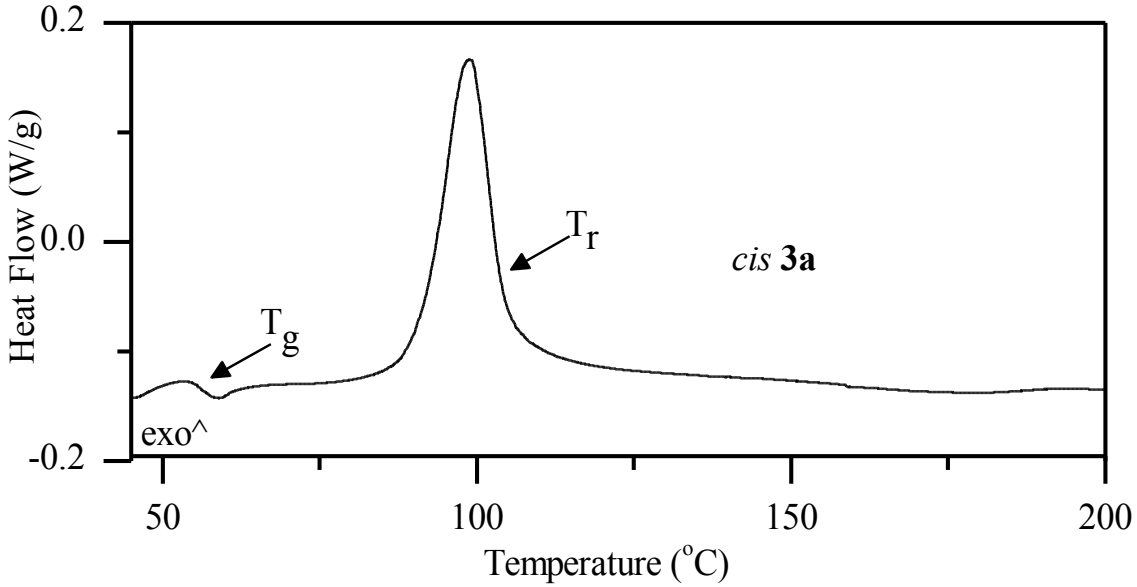

Figure 6-3. Second heating of *cis* **3a**, which demonstrates a glass transition (T_g), and a recrystallization (T_r); from T = 45 °C –200 °C with a heating rate of 10 °C/min.

6.3.2.2 Compound 3a

Two distinct crystal structures for *trans* **3a** (polymorph A and B) were determined (Figure D-3, appendix D). Polymorph A was observed as a solid block, whereas polymorph B was observed as a long needle-like structure from a layered mixture of benzene and hexanes and both crystallized in the triclinic space group P-1 with ρ = 1.397 and 1.399 Mg/m^3, respectively. One distinct crystal structure for *cis* **3a** was determined (Figure D-3, appendix D). It was also observed as a solid block from a layered mixture of benzene and hexanes and crystallized in the monoclinic space group C 2 / c with ρ = 1.365 Mg/m^3. The aminophenyl groups of two adjacent *cis* **3a** molecules were connected via hydrogen bonding within the crystal packing structure (Figure 6-4). There is no hydrogen bonding within the crystal packing structure of either *trans* polymorph.

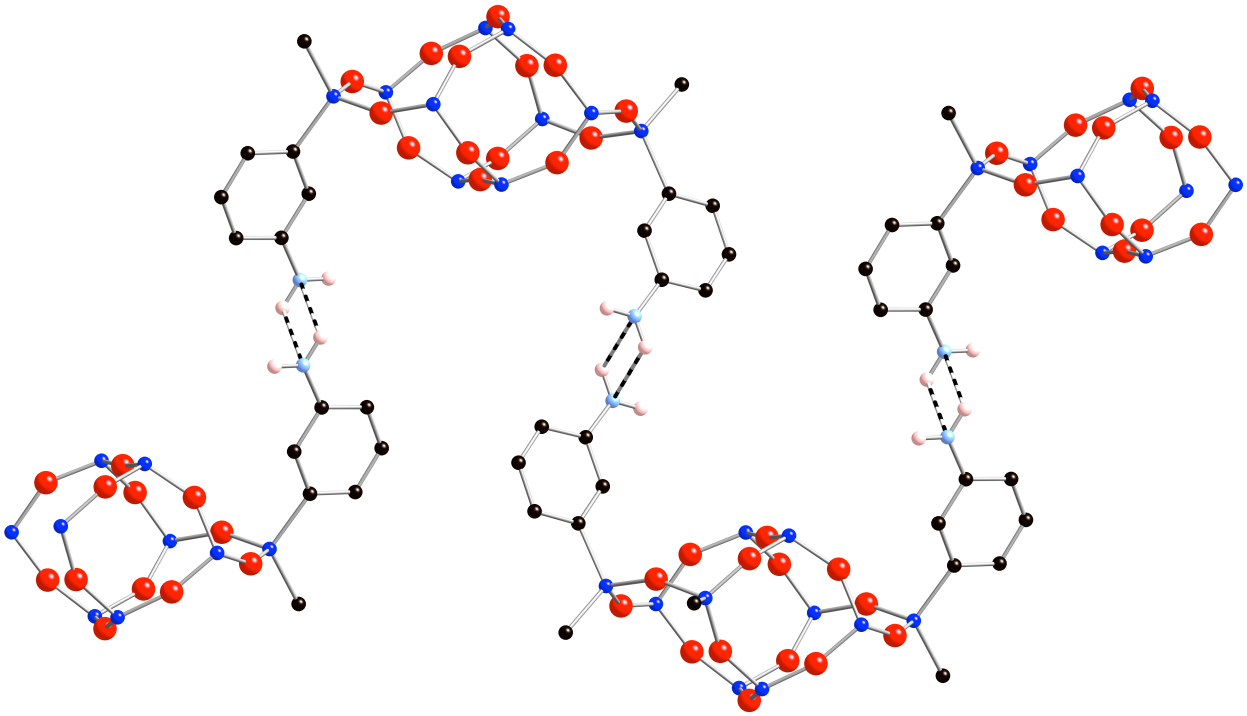

Figure 6-4. Hydrogen bonding (dotted line) in the crystal lattice of *cis* **3a**; red = O, blue = Si, black = C, light blue = N, and pink = H. Phenyl moieties and other H's not shown for simplicity.

6.3.2.3 Compound 3b

Three distinct crystal structures for *trans* **3b** (polymorph A, B, and C) were determined (Figure D-4, appendix D). Polymorph A, B and C were all observed as a solid blocks from a layered mixture of toluene and hexanes (A) and benzene and hexanes (B and C). Polymorph A crystallized in the monoclinic space group P 2(1) / c, while both polymorphs B and C crystallized in the triclinic space group P-1. The ρ for polymorphs A-C were 1.35, 1.349, and 1.33 Mg/m^3, respectively. Both triclinic polymorphs contain disorder in the unit cell, whereas polymorph A does not. Exhaustive attempts were made to crystallize *cis* **3b** in a large variety of solvents, but were unsuccessful. Diffraction patterns did not result far passed 2 θ.

6.3.2.4 Structural symmetry

After attaining the crystal structures, point group symmetry was examined. All *trans* isomers exhibit C_i symmetry and all *cis* isomers exhibit C_2 symmetry as determined by Platon ©.[24] This gives all six isomers 2 irreducible representations.

6.3.3 Melting behavior of binary cis/trans mixtures

Melting behavior was investigated for samples with systematically varying *cis* to *trans* ratios. For compounds **3c** and **3a**, as the content of *trans* isomer in the sample increased from 100 % *cis*, the onset of melting generally decreased, and the melting endotherm became broader until the eutectic composition. After the eutectic composition, the onset of melting began to increase and the melting endotherm again became broader until the sample approached 100 % *trans* isomer. For compound **3b**, the onset of melting constantly increased from $x_{trans} = 0$ to $x_{trans} = 1$ and the width of the melting endotherm remained narrow and constant.

6.3.3.1 Data analysis

In order to describe the melting behavior of binary *cis/trans* mixtures, the DSC data was analyzed with solid-liquid equilibrium equations. For systems that are immiscible in the solid state and miscible in the liquid state, the melting behavior can be analyzed according to the Schröder-van Laar equation (Equation 6-1):[14]

$$ln(x_i\gamma_i) = \frac{-\Delta H_{mi}}{RT}\left[1 - \frac{T}{T_{mi}}\right] \qquad (6-1)$$

where x_i is the mole fractions of isomer (i) that is in the liquid phase, T_{mi} is the melting temperature of the pure isomer (i) and ΔH_{mi} is the heat of fusion of the melting transition, T is

the altered melting temperature of the binary sample, and R is the universal gas constant. The activity coefficient (γ) quantifies deviations from the ideal behavior in the mixture for isomer (i).[25] The activity coefficient model used to fit the experimental data was the non-random two liquid model (NRTL, Equation 6-2):[26]

$$\ln\gamma_i = x_i^2\left[\left(\frac{G_{ji}}{x_i + x_j G_{ji}}\right)^2 + \left(\tau_{ij} - \frac{\tau_{ij}G_{ij}}{\left(x_j + x_i G_{ji}\right)^2}\right)\right] \qquad (6-2)$$

$$G_{ij} = \exp\left(-\alpha_{ij}\tau_{ij}\right); \qquad \tau_{ij} = a_{ij} + \frac{b_{ij}}{T}$$

where i and j are *trans* and *cis* isomers, respectively, γ is the activity coefficient, x is the mole fraction, τ_{ij} is an intermediate parameter representing the binary interaction parameters a_{ij} and b_{ij}, and α_{ij} represents the non-randomness parameter. It was assumed that the non randomness parameter, α, for *trans* to *cis* interactions and cis to *trans* interactions are equivalent and equal to 0.3, which is within the suggested range (0.2 – 0.47).[26]

A system that is completely miscible in both solid and liquid states, a correction to the Schröder-van Laar equation, must be made (Equation 6-3):

$$ln\frac{x_{iL}\gamma_{iL}}{x_{iS}\gamma_{iS}} = \frac{-\Delta H_{mi}}{RT}\left[1 - \frac{T}{T_{mi}}\right] \qquad (6-3)$$

where x_{iS} and γ_{iS}, and x_{iL} and γ_{iL} are the mole fractions and activity coefficient of isomer (i) that are in the solid state and liquid state, respectively.

6.3.4 Determination of the solid + liquid phase diagrams of cis/trans binary mixtures

Sections 4.3.5.1-4.3.5.4 show the results generated from the solid-liquid equilibrium data analysis for the melting behavior of binary *cis/trans* mixtures. Sections 4.3.5.1-4.3.5.2 show phase diagrams for the melting behavior of compounds **3c** and **3a**. Both were of the incongruent-eutectic type. Section 4.3.5.3 shows the binary interaction parameters and activity coefficients that resulted from these analyses. Finally, Section 4.3.5.4 shows the isomorphous phase diagram of compound **3b**.

6.3.4.1 Phase diagram of binary cis/trans mixtures for compound 3c

The phase diagram of compound **3c** is of an incongruent type that has a eutectic point at approximately T_E = 256.5 °C and x_{trans} = 0.33 and a meta-stable eutectic point at approximately $T_{m\text{-}E}$ = 247.0 °C and x_{trans} = 0.40 (Figure 6-5). When viewing the DSC trace of the eutectic composition, one sharp melting endotherm appears, which is similar to that of the pure isomers (Figure 6-6). Above the eutectic composition, where x_{trans} = 0.50, three melting endotherms are observed. When this mixture is heated, all of the *cis* isomer and part of the *trans* isomer in the mixture melt at the meta-stable eutectic temperature ($T_{m\text{-}E}$), and cocrystal behavior is formed. Subsequently, the cocrystal will melt and the *trans* isomer will recrystallize at the incongruent melting temperature, or peritectic point (T_P), until a liquid of composition P is reached. After which, the *trans* isomer will melt gradually at a temperature above T_P. As seen in Figure 6-6, this is represented by a clear endothermic peak associated with the $T_{m\text{-}E}$, which is followed by an exothermic peak associated with cocrystal formation. Then, another endothermic peak is observed associated with cocrystal melting, which is followed by another exothermic peak that is

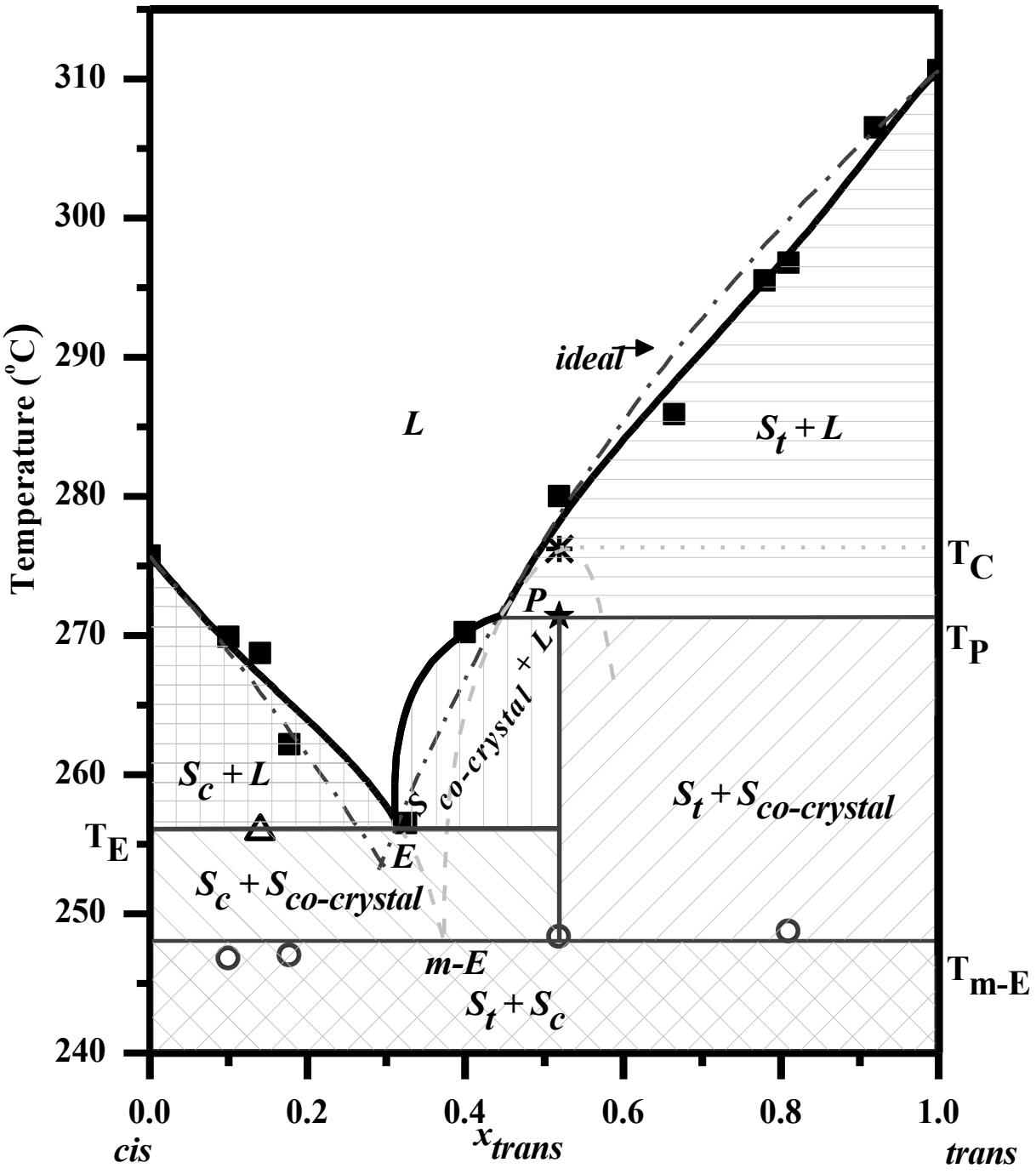

Figure 6-5. Solid-liquid equilibrium phase diagram for binary mixtures of *cis/trans* isomers for compound **3c**, plotted as melting temperature (T_m) as a function of *trans* mole fraction (x_{trans}); square (■) = experimental T_m measured with DSC apparatus, star (★) = experimental T_p, starburst (✳) = experimental T_c, triangle (△) = experimental T_E, circle (○) = experimental $T_{m\text{-}E}$, solid line (—) = calculated T_m from NRTL model (equation 6-2), and dash dot (- · - · -) = ideal T_m, from Schröder-van Laar equation (equation 6-1) where $\gamma = 1.00$.

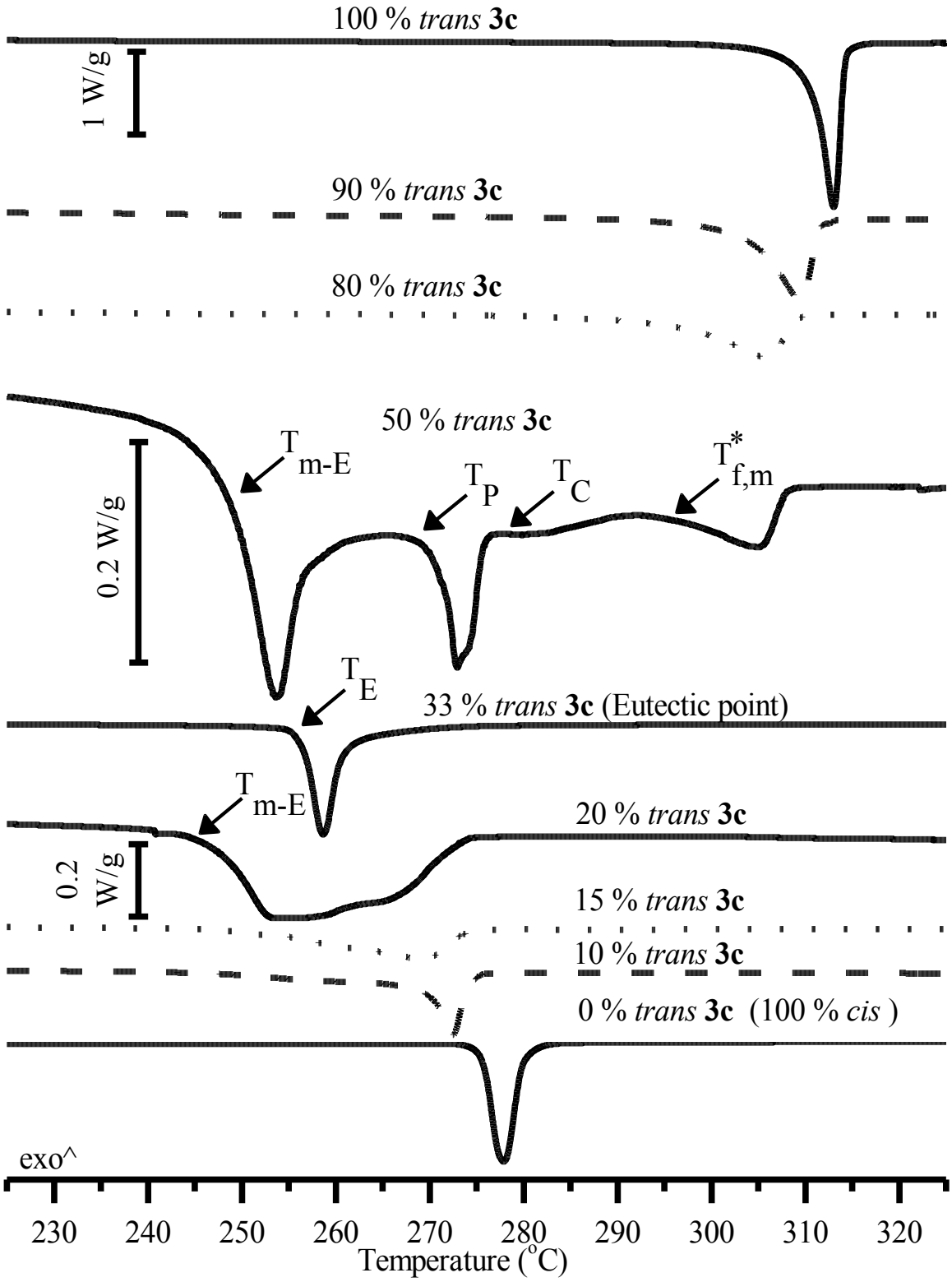

Figure 6-6. Melting behavior of binary *cis/trans* mixtures for compound **3c**; T = 225 °C –325 °C with a heating rate of 10 °C/min. All thermal traces have the same scale bar as 100 % *trans* unless otherwise noted. * $T_{f,m}$ is the final melting of 50 % *trans* **3c**.

associated with recrystallization of the *trans* isomer at T_P. Finally, a third, more broad endothermic deflection is observed, which is associated with the complete melting of the *trans* isomer. Below the eutectic point, where $x_{trans} = 0.20$, the melting endotherm appears to be very broad, and is representative of two overlapping melting endotherms, $T_{m\text{-}E}$ and $T_{m\text{-}0.20}$.

6.3.4.2 Phase diagram of binary cis/trans mixtures for compound 3a

The phase diagram of compound **3a** is also of an incongruent type that has a eutectic point at approximately $T_E = 260$ °C and $x_{trans} = 0.25$ and a meta-stable eutectic point at approximately $T_{m\text{-}E} = 252$ °C and $x_{trans} = 0.33$ (Figure 6-7). Similarly to compound ***A***, when viewing the DSC trace of the eutectic composition, one sharp melting endotherm appears (Figure 6-8). Above the eutectic composition, where $x_{trans} = 0.35$, multiple melting endotherms are observed. As seen in Figure 6-8, two broad endothermic transitions are associated with this composition. The first transition is clearly representative of the T_E and the second represents the T_m. The endotherm representing the $T_{m\text{-}E}$ is not distinctly observed because it is overlapped by the T_E endotherm. However, the existence of a $T_{m\text{-}E}$ is evidenced by a descent in the baseline that occurs earlier than the T_E endotherm. The peritectic temperature was found at approximately $T_P = 268$ °C. This was evidenced by the DSC traces of samples that were $x_{trans} = 0.60$ and 0.80, since there was a clear endothermic transition before the T_m. For other samples that were above the eutectic composition, the T_P endotherm was overlapped by the $T_{m\text{-}E}$ and T_m endotherms. Similar to

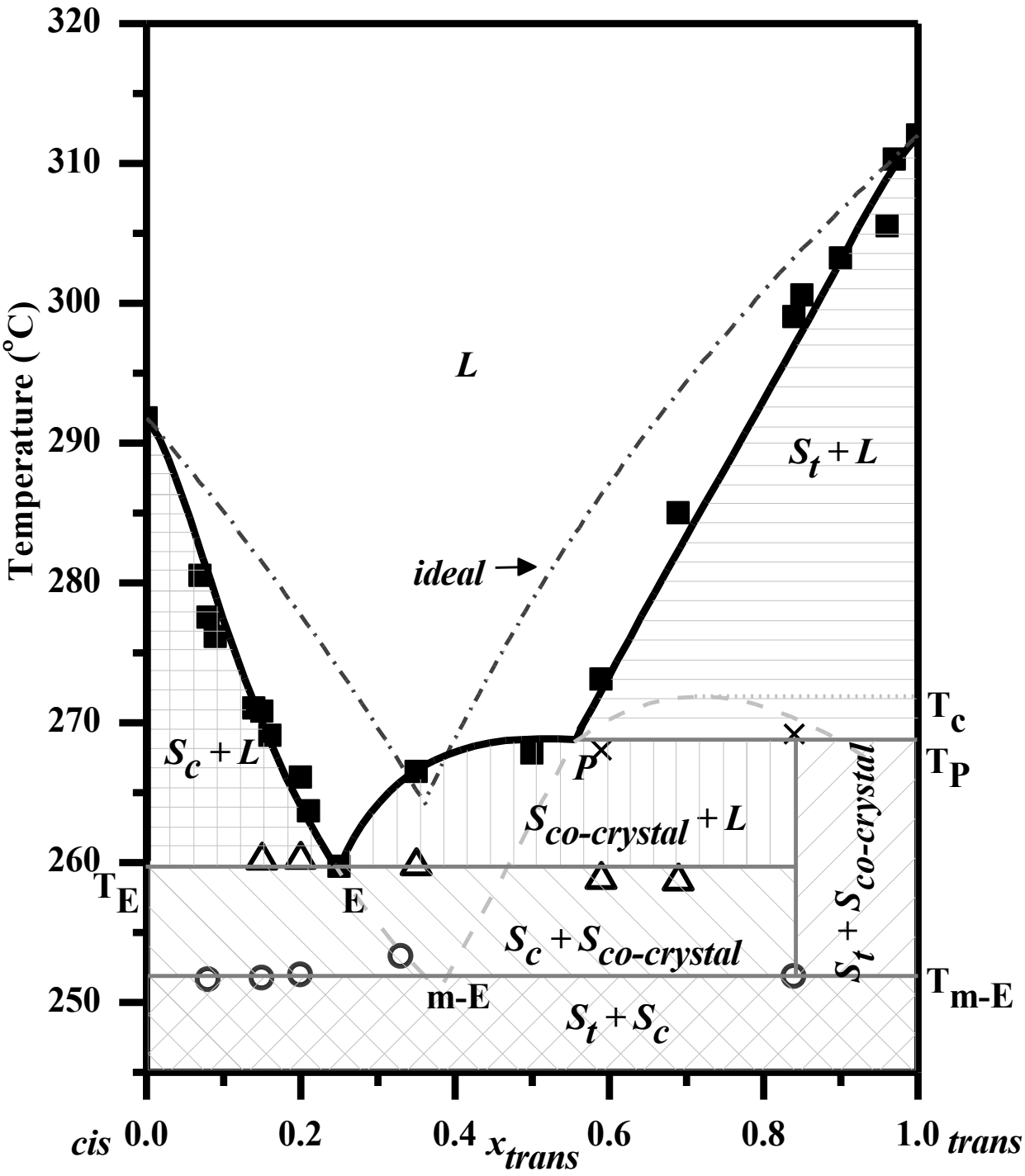

Figure 6-7. Solid-liquid equilibrium phase diagram for binary mixtures of *cis/trans* isomers for compound **3a**, plotted as melting temperature (T_m) as a function of *trans* mole fraction (x_{trans}); square (■) = experimental T_m measured with DSC apparatus, ex (x) = experimental T_p, triangle (△) = experimental T_E, circle (○) = experimental $T_{m\text{-}E}$, solid line (—) = calculated T_m from NRTL model (equation 6-2), and dash dot (-·-·-) = ideal T_m, from Schröder-van Laar equation (equation 6-1) where $\gamma = 1.00$.

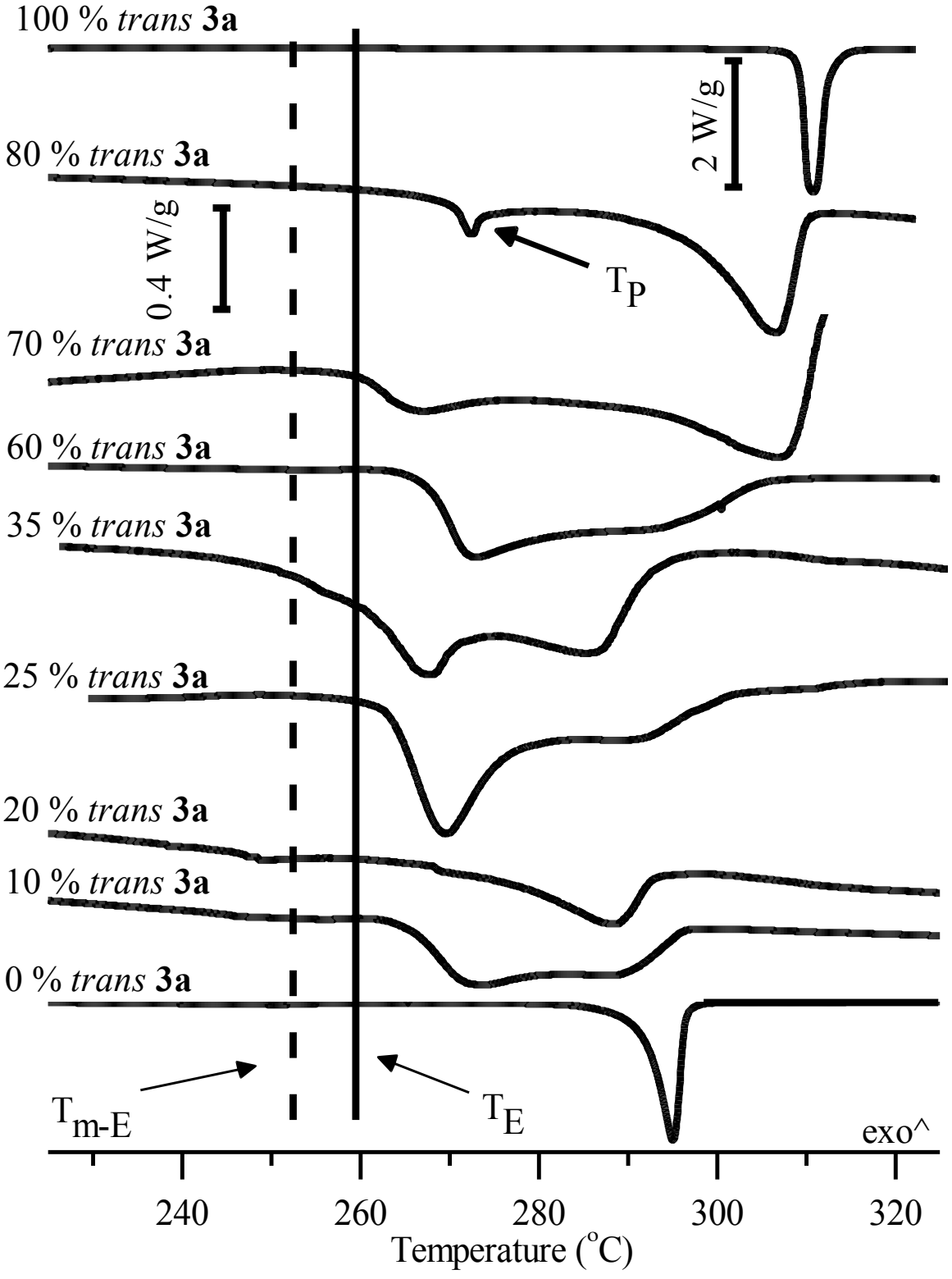

Figure 6-8. Melting behavior of binary *cis/trans* mixtures for compound **3a**; T = 225 °C –325 °C with a heating rate of 10 °C/min. All thermal traces have the same scale bar as 80 % *trans* unless otherwise noted.

compound **3c**, the melting endotherm becomes broader below the eutectic point until it approaches 0 % *trans* (100 % *cis*).

6.3.4.3 Calculated binary interaction parameters of eutectic-type model fitting

Binary interaction parameters between *trans* and *cis* isomers, a_{tc} and b_{tc}, and between *cis* and *trans* isomers, a_{ct} and b_{ct}, were adjusted while fitting x_i values along the solid-liquid curves on the phase diagrams and are summarized in Table 6-4. For compound **3c**, the experimental

Table 6-4. Binary interaction parameters of compounds **3c** and **3a**.

Compound	a_{tc}	a_{ct}	b_{tc}	b_{ct}
3c	19.68	-53.85	-11272.78	30229.48
3a	-21.60	-42.80	10291.98	23535.62

values on the left hand side of the phase diagram (Figure 6-5) are near ideal values, and the right hand side is slightly below ideal values. For compound **3a**, the experimental values on both sides of the diagram (Figure 6-7) are largely below ideality. The determined parameters provided theoretical models for binary melting behavior that fit experimental data and experimental activity coefficients well (Figure 6-9).

6.3.4.4 Phase diagram of binary cis/trans mixtures for compound 3b

Unlike the other compounds, the phase diagram of compound **3b** is of an isomorphous (homogeneous solid solution) type. There is complete miscibility of both the liquid and solid states. Applying the pure component properties of *cis/trans* **3b** to the modified Schröder-van Laar equation (equation 6-3), and assuming both the liquid and solid phases are ideal, provides calculated solidus and liquidus values (Figure 6-10). Experimental liquidus values are very close

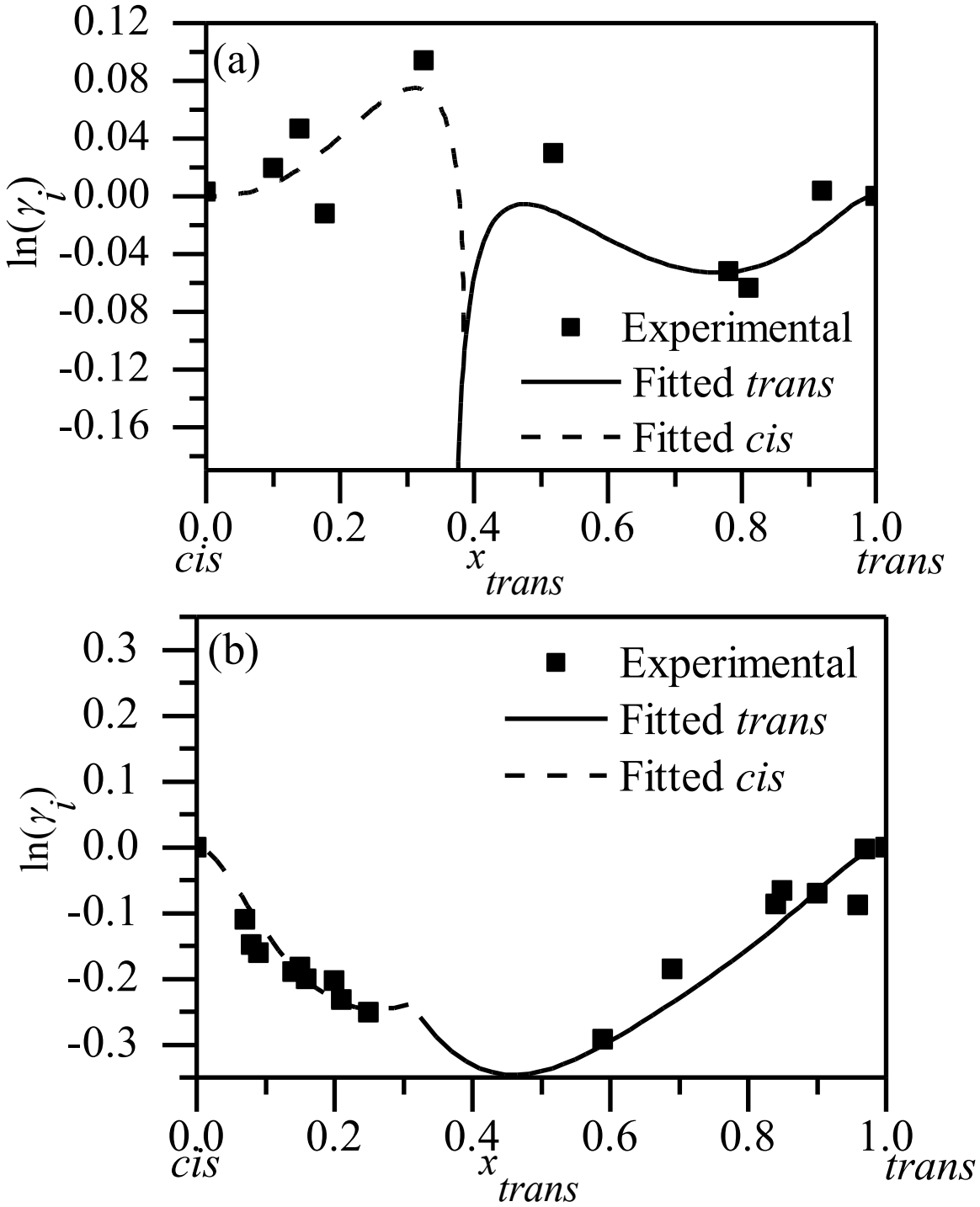

Figure 6-9. Activity coefficients (γ) of isomer (*i*) vs. the mole fraction of (x_{trans}) for compounds (a) **3c** and (b) **3a**; left hand side *i* = *cis* isomers, and right hand side, *i* = *trans* isomer; square (■) = experimental x_i, and solid line (—) = calculated x_i.

to ideal calculations (Table 6-5). Additionally, the two phase region is very small; solidus and liquidus values are within 0.2 °C. The DSC trace of a solid solution is represented by a single, narrow endothermic melting transition upon heating for all binary mixtures (Figure 6-11).

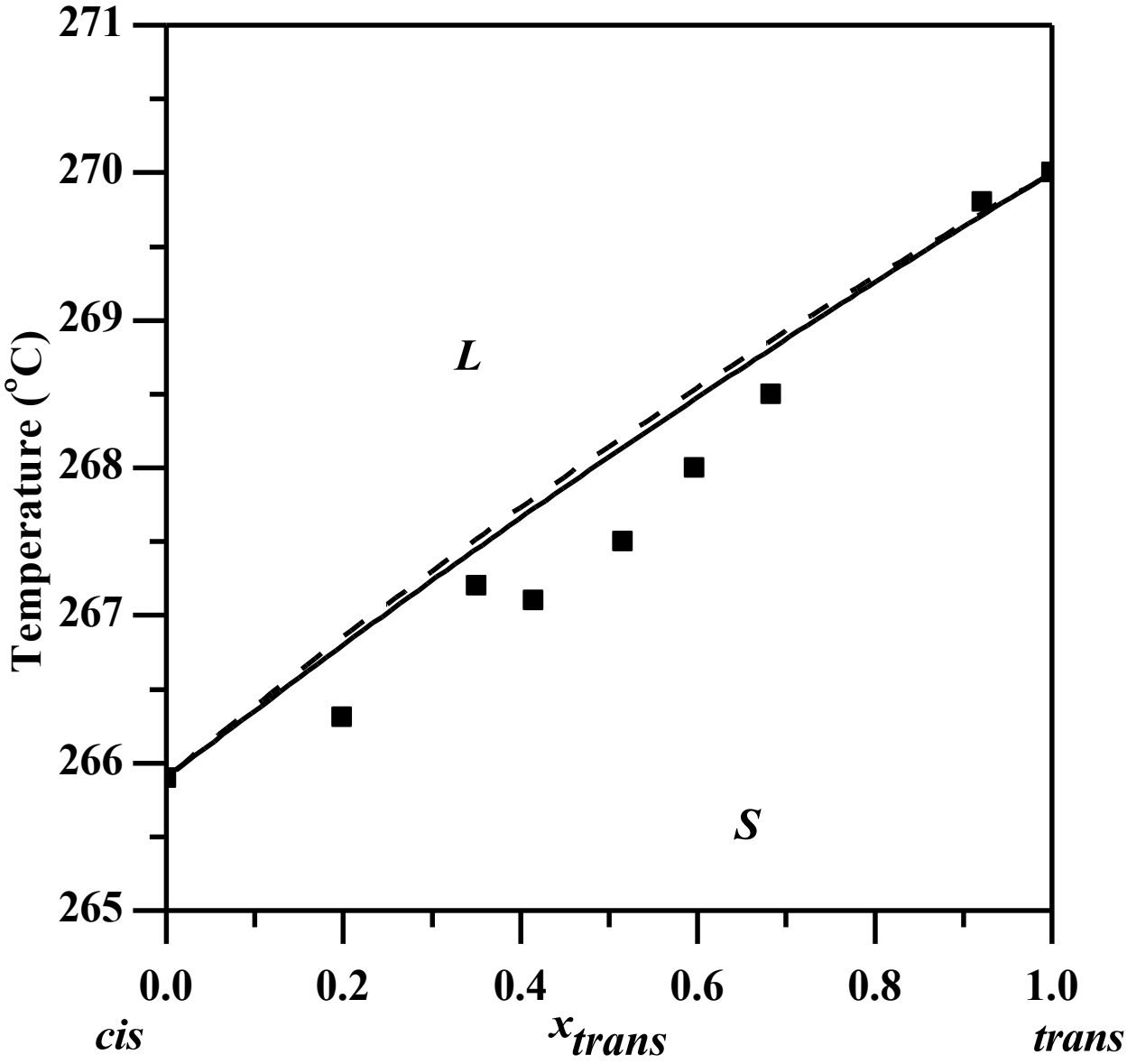

Figure 6-10. Solid-liquid equilibrium phase diagram for binary mixtures of *cis/trans* isomers for compound **3b**, plotted as melting temperature (T_m) as a function of *trans* mole fraction (x_{trans}); square (■) = experimental T_m measured with DSC apparatus, solid line (—) = liquidus line, dashed line (---) = solidis line. Solidus and liquidus lines are determined from an ideal solution to the Schröder-van Laar equation for an isomorphous solution (Equation 6-3) with an ideal approximation, where $\gamma = 1.00$.

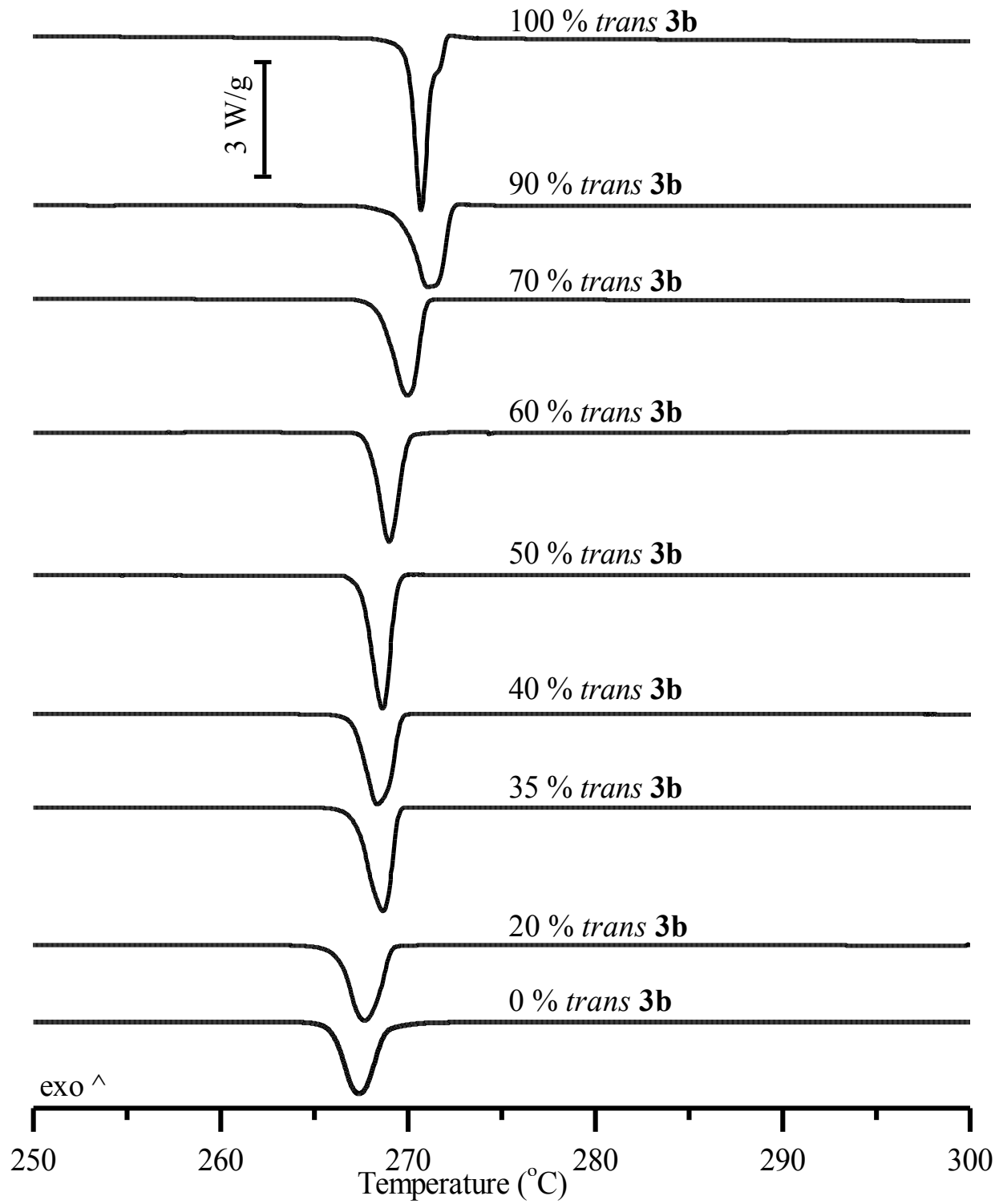

Figure 6-11. Melting behavior of binary *cis/trans* mixtures for compound **3b**; T = 250 °C –300 °C with a heating rate of 10 °C/min. All thermal traces have the same scale bar as 100 % *trans* unless otherwise noted.

Table 6-5. Experimental melting temperatures ($T_{experimental}$) determined from DSC apparatus vs. calculated melting temperatures ($T_{calculated}$) determined from an ideal solution to the Schröder-van Laar equation for an isomorphous solution (equation 6-3) with an ideal approximation, where $\gamma = 1.00$of compound **3b**.

x_{trans}	$T_{experimental}$ (°C)	$T_{calculated}$ (°C)
1.00	270.0	270.0
0.92	269.8	269.7
0.68	268.5	268.8
0.60	268.0	268.5
0.52	267.5	268.1
0.42	267.1	267.7
0.35	267.2	267.4
0.20	266.3	266.8
0.00	265.9	265.9

6.3.5 Solidification behavior

Solidification behavior for samples of *trans* **3a-c** with increasing quantities of *cis* **3a-c** was also investigated. The onset of solidification of compound **3c** generally decreased from $x_{trans} = 1$ to $x_{trans} = 0$ (Figure 6-12). For compound **3a**, the onset of solidification decreased with increasing content of *cis* isomer until the eutectic composition where this transition was no longer visible. For samples of **3a** that did not exhibit solidification upon cooling, a glass transition and recrystallization was visible during the second heating and both increased with increasing content of *cis* isomer. The onset of solidification for compound **3b** was more complicated. It generally increased as it moved towards a less pure composition, and was largest at $x_{trans} = 0.50$.

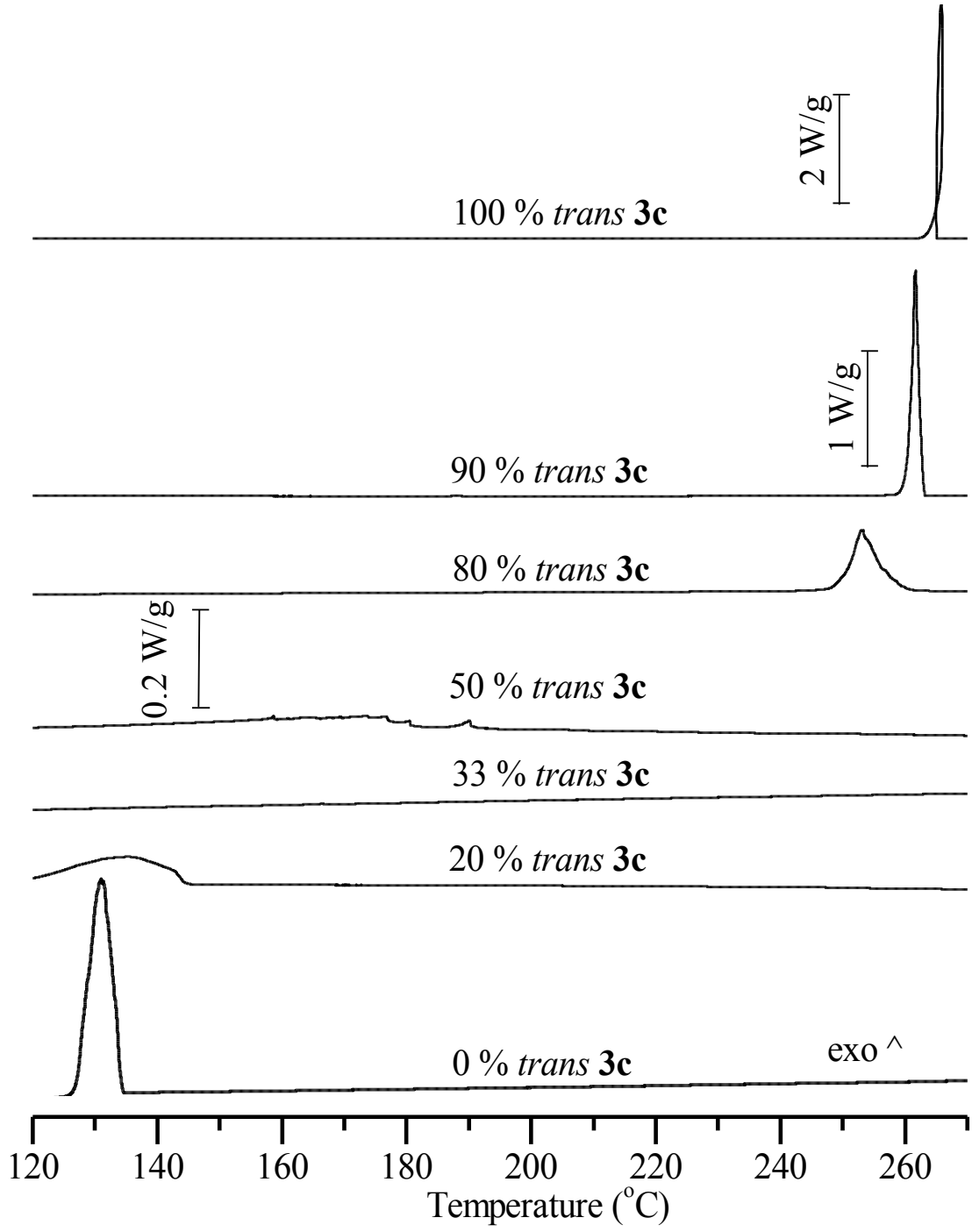

Figure 6-12. Solidification behavior of binary *cis/trans* mixtures for compound **3c**; T = 270 °C – 120 °C with a cooling rate of 5 °C/min. All cooling traces have the same scale bar as the trace immediately above it unless otherwise noted.

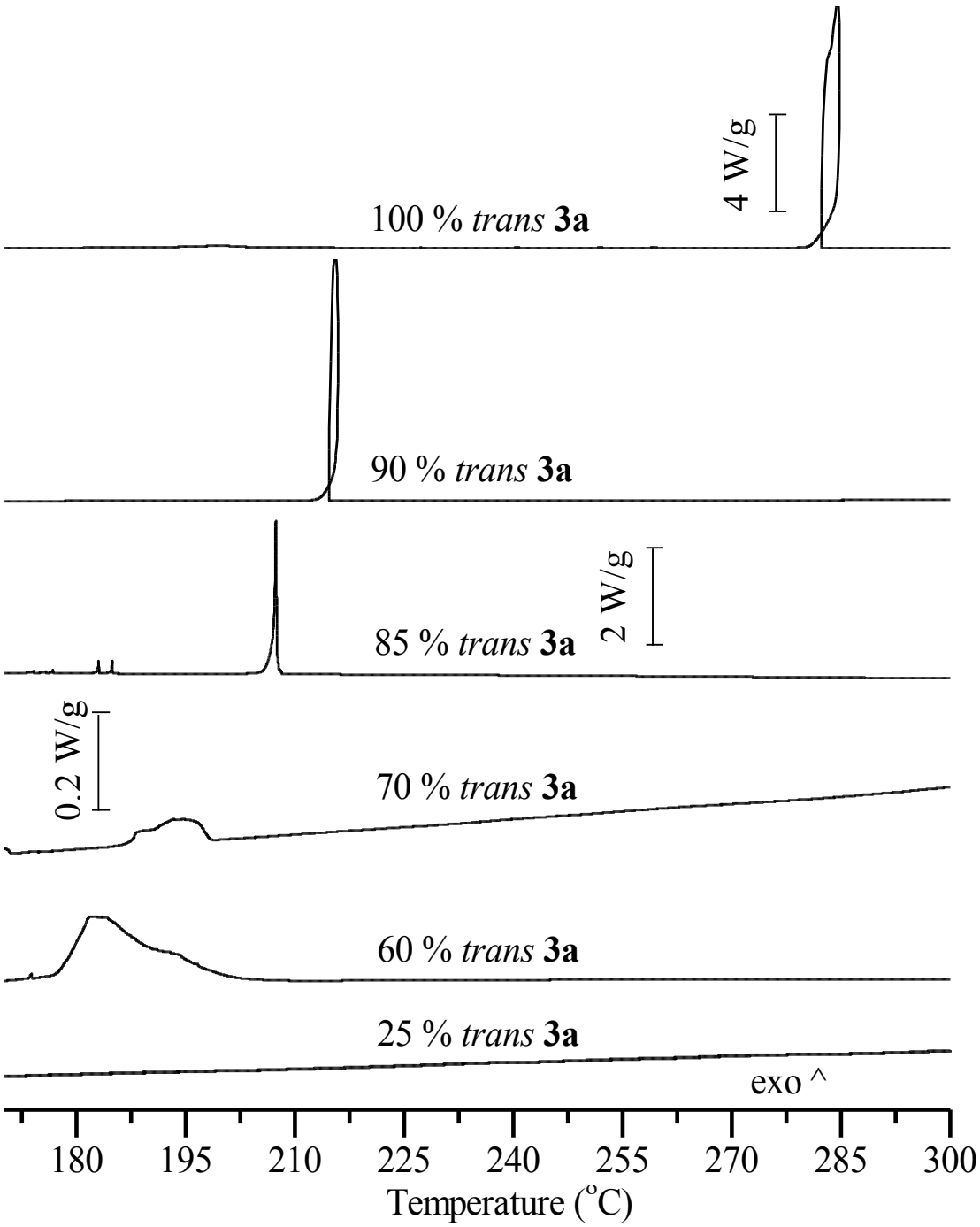

Figure 6-13. Solidification behavior of binary *cis/trans* mixtures for compound **3a**; T = 300 °C – 170 °C with a cooling rate of 5 °C/min. All cooling traces have the same scale bar as the trace immediately above it unless otherwise noted.

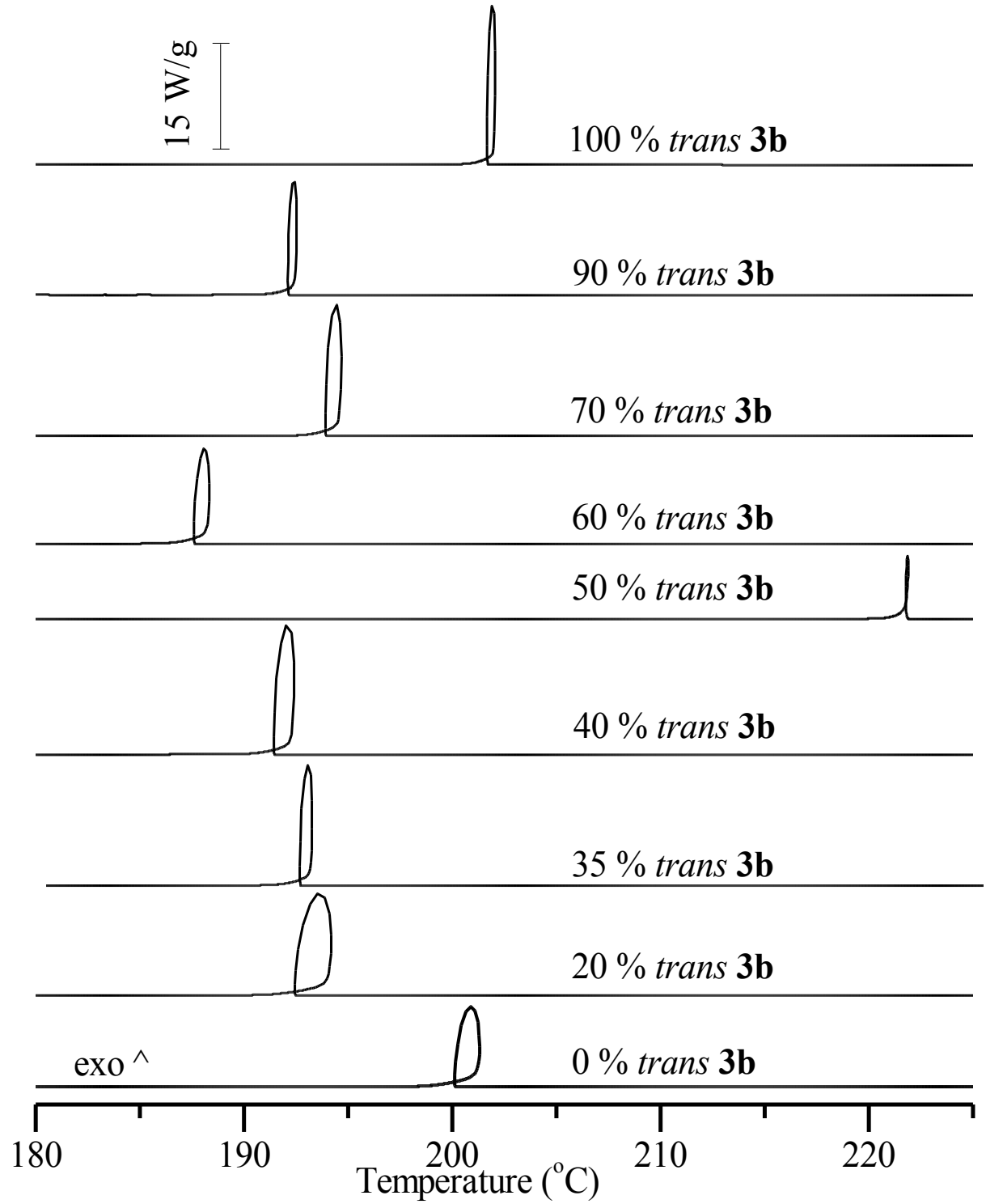

Figure 6-14. Solidification behavior of binary *cis/trans* mixtures for compound **3b**; T = 230 °C – 180 °C with a cooling rate of 5 °C/min. All cooling traces have the same scale bar as 100 % *trans*.

6.4 Discussion

The discussion is split into several sections that generally mirror the results sections. Section 4.4.1 discusses trends observed in the melting behavior of the pure isomers, and is followed by the solidification behavior of the pure isomers in section 4.4.2. Structural information such as packing density and hydrogen bonding within the crystal lattice were also discussed in these two sections to provide rationale of experimental observations. Additional structural information and observed polymorphs were discussed further in section 4.4.3, and moleulcar symmetry in section 4.4.4. Section 4.4.5 discusses the phase diagrams that resulted from the data analysis for the melting behavior of the binary *cis/trans* isomer mixtures. Finally, section 4.4.6 discusses the solidification behavior of the binary *cis/trans* isomer mixtures.

6.4.1 Melting Behavior

Melting behavior of the pure isomers is divided into several smaller discussion sections so that trends can be more easily observed and discussed (4.4.1.1-4.4.1.3). *Trans* vs. *cis* isomers are generally compared in section 4.4.1.1. Then, the melting behavior of the analogous para- and meta-aminophenyl DDSQ (compounds **3c** and **3a**, R = Me) is compared in section 4.4.1.2. Finally, the melting behavior of the meta-structures where R = Me (compound **3a**) and where R = Cy (compound **3b**) is also compared.

6.4.1.1 Trans vs. cis isomers

The *trans* isomers of all three compounds exhibited a higher T_m than their *cis* counterparts (Table 6-3). A general rule of thumb is that structures that exhibit a higher T_m are less soluble, at a given temperature, and have higher lattice energies.[1] Lattice energy is a quantitative measure of the internal cohesion in the crystal structure, and depends on the

intermolecular forces.[3] It can be determined experimentally by measuring the total ΔH_m, or the thermal energy necessary for these molecules to overcome intermolecular forces and fully melt. It was previously known that all three *trans* isomers were less soluble[16] and, as seen in Table 6-3, the *trans* isomers had a larger ΔH_m as a result of their higher packing densities. *Trans* **3c** had a packing density of 1.39 Mg/m^3, and for *cis* **3c** ρ = 1.366 Mg/m^3. Compound **3a** had very similar packing densities for *trans* and *cis*, ρ = 1.399 and 1.365 Mg/m^3, respectively. For compound **3b**, *trans* had a ρ of 1.35 Mg/m^3 and it was anticipated that this is higher than *cis* **3b**. A higher density increases intermolecular forces between molecules, thus illustrating why all three *trans* isomers exhibited a higher ΔH_m and T_m than their *cis* counterparts.[1,8]

6.4.1.2 Para vs. meta

Trans **3c** and **3a** exhibited a similar T_m (**3c** = 310.6 and **3a** = 312.0 °C), suggesting that there are minimal differences in lattice energy, which was demonstrated by similar ΔH_m (**3c** = 55 and **3a** = 56 kJ/mol) and ρ (**3c** = 1.39 and **3a** = 1.399 Mg/m^3). Conversely, the T_m of *cis* **3c** **(**275.4 °C**)** and ***B*** (291.8 °C) was approximately a 16 °C difference. However, both exhibited a similar ΔH_m (**3c** = 38 and **3a** = 42 kJ/mol) and ρ (**3c** = 1.366 and **3a** = 1.365 Mg/m^3), suggesting other factors contributed to their difference in T_m. It was apparent from the crystal structures that *cis* **3a** exhibited intermolecular hydrogen bonding (Figure 6-4), while *cis* **3c** does not. Hydrogen bonding increases intermolecular interactions and requires more thermal energy to melt.[27-29] To verify this, the entropy of fusion, $\Delta S_m = \Delta H_m/T_m$, which normalizes ΔH_m with

respect to T_m and is a measure of the disorder of the system, was determined.[25] For *cis* **3a**, ΔS_m = 74.3 J/mol·K which is larger than *cis* **3c** (ΔS_m = 69.2 J/mol·K). More disorder throughout the melt transition confirms that it takes more energy to melt the ordered crystal lattice.

6.4.1.3 Methyl vs. cyclohexyl

Changing the moiety from methyl to cyclohexyl had the largest effect on the melting behavior. *Trans* and *cis* **3b** exhibited approximately a 42 and 26 °C decrease in T_m, as compared to compound **3a**, respectively. More bulky substituents can in fact decrease the T_m in a set of closely related substances by disrupting the lattice packing.[30] Two approaches were used to verify this fact: (1) a direct ρ determination using single crystal XRD data, and (2) ΔS_m. With single crystal XRD studies, it was determined that the ρ for *trans* **3b** was 1.35 Mg/m^3, which was 0.04 Mg/m^3 less than *trans* **3b**. Additionally, the ΔS_m of *trans* and *cis* **3b** (*trans* = 84.7 J/mol·K and *cis* = 72.3 J/mol·K) were smaller than the ΔS_m of *trans* and *cis* **3a** (*trans* = 95.7 J/mol·K and *cis* = 74.3 J/mol·K). Thus, the isomers of compound **3a** originally had a more ordered and dense crystal lattice, which explained the determined trend in the melting data.

6.4.2 Solidification behavior

Solidification behavior of the pure isomers is also divided into several smaller discussion sections so that trends can be more easily observed and discussed (4.4.2.1 and 4.4.2.2). *Trans* isomers are compared in section 4.4.2.1, and *cis* isomers are compared in section 4.4.2.2. Except for compound *cis*-**B**, all pure isomers investigated exhibited a complete recrystallization upon

cooling from the liquid state and the values for the heat of crystallization are nearly equal to the heat of melting during heating.

6.4.2.1 Trans isomers

During cooloing, *trans* **3c** and **3a** exhibited a sharp exothermic crystallization transition peak where the endset point was nearly equivalent to the supercool point. This suggested that the crystallization process was rapid and dominated by the nucleation process. To examine the effect of *para* vs *meta* on the energy barrier associated in forming stable nuclei for crystallization, the degree of undercooling ($\Delta L = T_c - T_m$), was evaluated.[59,60] It was found that the value of ΔL for t*rans* **3c** was much larger than *trans* **3a**, (45.0 °C vs. 27.6 °C). Since the melting temperature for both was nearly identical, this result can only be used to explain the multiple polymorphs, or multiple stable configurations, observed for *trans* **3a**. The multiple configurations allowed for crystalline *trans* **3a** to require less of a driving force to form stable nuclei. Once a particular crystalline configuration is formed the others will quickly follow due to the increase in the change of surface free energy.

Although similar *trans* **3a**, the *trans* **3b** isomers also exhibited multiple stable configurations (polymorphs A-C), the value of ΔL for *trans* **3b** was about 68.0 °C which was 40 °C larger than *trans* **3a**. This result suggested that the bulky cyclohexyl moiety of *trans* **3b** effectively inhibited the molecular rotation needed to form equilibrium crystalline solids.[33]

6.4.2.2 Cis isomers

Cis **3c** also exhibited a crystallization transition upon cooling. However, its exothermic crystallization peak was much broader, and the degree of undercooling was quite large (~ 145 °C) as compared to *trans* **3c**. This is indicative of a crystallization process dominated by a

diffusional crystal growth process that is kinetically controlled rather than thermodynamically controlled. Therefore, *cis* **3c** crystals take longer to grow than the other isomers. Furthermore, ΔH_c indicates that *cis* **3c** does not fully crystallize upon cooling, $\Delta H_c / \Delta H_m = 84$ %, while ΔH_c for all other isomers is greater than 96 %. This behavior suggests that the configuration necessary for *cis* **3c** to crystallize upon cooling is more difficult to attain than the other isomers, and the cooling rate may need to be slower.

Cis **3a** did not exhibit crystallization upon cooling at a cooling rate of 5 ^{o}C/min from its liquid state. However, *cis* **3a** did exhibit a glass transition ($T_g = 56.0$ °C) followed by a cold crystallization ($T_r = 90.8$ °C) during a second heating. Therefore, slower cooling rates were investigated to determine if this was a kinetic effect. Lowering the cooling rate to 1 °C/min and holding it isothermally at anticipated crystallization temperatures still did not allow it to crystallize upon cooling. This was attributed to the hydrogen bonding in the crystal lattice. During cooling, it becomes difficult for *cis* **3a** to arrange in the orientation necessary for intermolecular hydrogen bonding.[62] Thus, energy was needed for the recrystallization process to occur, which was provided through heating. The crystallinity associated with T_r is 63 % ($\Delta H_r / \Delta H_m = 0.63$), which was much lower crystallinity than the other isomers, and indicative of semi-crystalline behavior.

Cis **3b** exhibited a crystallization transition upon cooling most similar to the *trans* isomers, it also had an endset point nearly equivalent to the supercool point, and $\Delta L = 65.1$ °C. Surprisingly, this was approximately 3 °C smaller than *trans* **3b**. Since both isomers have a bulky cyclohexyl moiety, it was anticipated this was a result of the number of stable configurations, with *cis* **3b** having more than *trans* **3b**, and thus able to form stable nuclei faster.

6.4.3 Crystal structures

Polymorphs were only found for *trans* **3a** and **3b**, and the different polymorphs did not affect packing density. It was anticipated that *trans* **3b** has more polymorphs than *trans* **3a** due to the additional stable confirmations from the bulky cyclohexyl moiety inhibiting rotation. It was also anticipated that *trans* **3a** has more polymorphs than *trans* **3c**, but for different reasons. There are two locations meta- to the D-Si atom bonded to the aminophenyl moiety. Since the meta- moiety can freely rotate, it can be crystallized in either of these two positions. Conversely, there is only one location para- to the D-Si atom. Furthermore, when attempting to grow single crystals, *trans* **3c** proved much more difficult. Exhaustive attempts in numerous solvent solutions provided only one structure that was not co-crystallized with solvent. On the other hand, two polymorphs of *trans* **3a** were simultaneously crystallized in the first solvent system attempted.

Cis **3c** did not exhibit polymorphs, and was the only crystal with a twinned structure. The key to attaining *cis* **3c** was purity. Samples that were of high purity (> 95 %) failed to form single crystals in a large variety of solvents. Successful crystals were grown only after *cis* **3b** was placed in a liquid chromatography column and further purified (> 99 %). It is unlikely that there are any polymorphs for *cis* **3a** due to the hydrogen bonding potential of the aminophenyl groups in the determined crystal structure. The distance between these hydrogen atoms and the intermolecular nitrogen atoms was 2.582 (Å) of *cis* **3a**. Of all the other structures, polymorph A of *trans* **3a** was the only one that had a similar conformation to *cis* **3a**, where the intermolecular aminophenyl groups are pointed towards one another. However, the distance between theses hydrogen atoms and the intermolecular nitrogen atom was 2.69 (Å), which was too large for hydrogen bonding. Failed crystallization attempts showed that *cis* **3b** was polycrystalline, and the

bulky cyclohexyl group suggested that it was possible that there are multiple stable conformations, thus it was anticipated that *cis* **3b** has a lot of polymorphs.

6.4.4 Same molecular symmetry, different molecular structures

For a small molecule, para- and *trans* are typically more symmetric than meta- and *cis* and therefore, generally they will exhibit will generally, they will exhibit a more dense packing arrangement.[1,3] As was previously mentioned, all *trans* isomers exhibited C_i symmetry and all *cis* isomers exhibited C_2 symmetry, giving all isomers 2 irreducible representations within the molecule itself. Therefore, one isomer was not more symmetric than the other. Thus, the fact that the *trans* isomers exhibited a higher packing density is unique, and can only be attributed to desired arrangements of the molecules within the unit cells. Furthermore, since all isomers have the same molecular symmetry, it was proposed that the *cis* and *trans* isomers could be mixed without completely destroying the crystalline order.

6.4.5 Melting behavior for Incongruent-type phase diagrams (compounds 3c and 3a)

For the phase diagrams of compounds **3c** (Figure 6-5) and **3a** (Figure 6-7) the melting point was depressed from the pure material and the melting endotherms became broader until the eutectic composition was reached. The left hand side of both phase diagrams is indicative of the melting point depression of the gradual addition of *trans* isomer to pure *cis* isomer. Whereas the right hand side of both diagrams shows the melting point depression upon the gradual addition of *cis* isomer to pure *trans* isomer. The melting point depression for compound **3a** was more rapid and further from ideal than compound **3c** on both sides of the phase diagram. Since hydrogen bonding is necessary in the crystal lattice in order to form stable crystallites for *cis* **3a**, it is speculated that the melting point will depress more rapidly for this compound.

6.4.6 Melting behavior for isomorphous solid solution-type phase diagram (compound 3b)

Melting points can be altered when a "guest" molecule is able to substitute into the crystal lattice of a "host" molecule. If the "guest" molecule is very similar in size and dimensions to the "host" molecular, the mixture exhibits solid solubilities at all compositions because the lattice is not distorted. The melting point decreases with increasing content of the lower melting molecule, or increases with increasing content of the higher melting material. This type of phenomena is consistent with an isomorphous solid solution melting system, such as the phase diagram of compound **3b** (Figure 6-10), where the melting point decreased linearly from x_{trans} = 1 (T_m = 270.0 °C) to x_{trans} = 0 (T_m = 265.9 °C). Melting point behavior was modeled using the Schröder-van Laar equation for all compounds.

From the solid-liquid equilibria results, it was apparent that the experimental liquidus values were very close to ideal calculations for compound 3b (

Table 6-5). Additionally, the solidus and liquidus values were very similar, within 0.2 °C, suggesting that the two-phase region hardly exists (Figure 6-10). This was verified by DSC traces for binary mixtures of compound **3b** (Figure 6-11). Typically, as the composition moved further from a pure component, the endotherm became broader. The broadness is indicative of the distance between the solidus and liquidus curves, the more broad, the larger the distance. Thus, the fact that experimental melting endotherms of all compositions of compound **3b** were narrow, suggesting that the ideal calculation of the solidus curve was accurate.

In order for a system to be isomorphous, both components must solidify in the same crystal system with similar lattice dimensions and related chemical constitution.[13] Ideal behavior of an isomorphous system is achieved when the lattice dimensions of both components match and the compounds are chemically similar. Additionally, the "guest" molecule cannot interrupt

the attractive-repulsive forces within the crystal lattice of the "host" component. Positive deviations from ideality would result from disruption and negative deviations from excess attractive forces. Since, it was determined that compound **3b** was an ideal, isomorphous solution, it supported the hypothesis that the crystal structures of *cis/trans* **3b** are similar. Additionally it was anticipated that *trans* **3b** acts as nucleation sites for the *cis* isomer.

6.4.7 Solidification of binary cis/trans mixtures

Compounds **3a-c** exhibited a large degree of undercooling, or supersaturation when they were cooled. Supersaturation occurs when there is more solute than is permitted by stable thermodynamic equilibrium.[13] For compound **3c**, as the composition moved further from a pure isomer, the transition became broader and the undercooling increased until it reached the eutectic composition where there was no solidification observed (Figure 6-12). Additionally, when the eutectic composition was heated a second time, there was no melting endotherm observed. The solidification of compound **3c** was generally linear, unlike the melting transition, which exhibited an incongruent eutectic. The undercooling followed the same linear trend (Figure 6-15). Compound **3a** followed a similar trend; however, after it approached the eutectic composition there was no solidification observed for the remaining compositions.

Compound **3b** was the only structure that continued to exhibit a supercool point equivalent to the onset point of solidification throughout the whole range of compositions, suggesting that even as a mixture, the material is highly crystalline. The undercooling generally increased as it moved towards a less pure composition (Figure 6-15). However, at $x_{trans} = 0.50$, the solidification and undercooling had the smallest value.

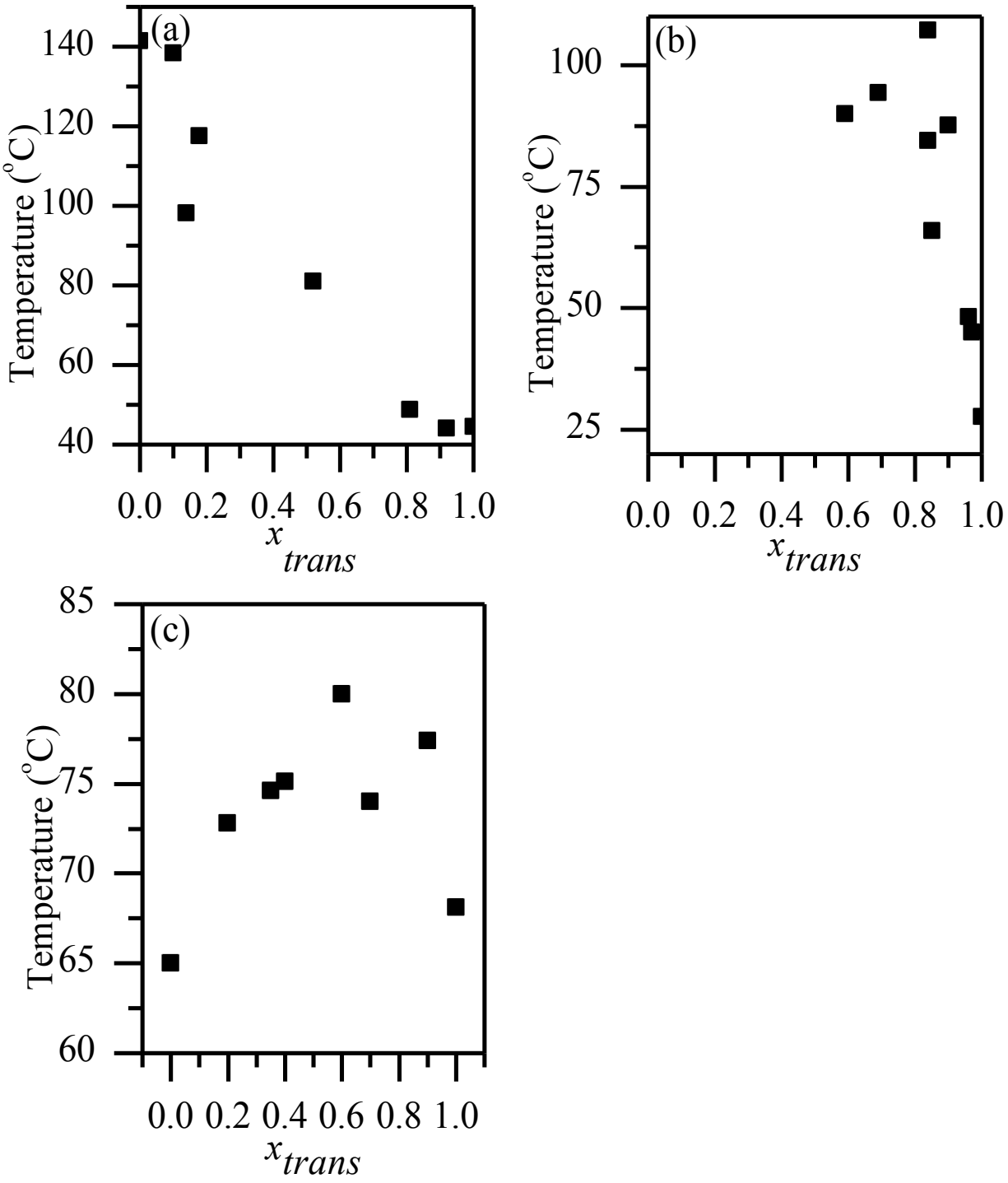

Figure 6-15. Undercooling (T_m-T_c) of binary *cis/trans* mixtures vs. x_{trans} for compounds (a) **3c** (b) **3a**, and (c) **3b**.

6.5 Concluding remarks on solid-liquid thermal equilibria

Solid-liquid equilibrium phase diagrams based on the thermal behavior for binary mixtures of *cis* and *trans* isomers for a series of DDSQ(X)(R) were successfully determined. The Schröder-van Laar equation (Equation 6-1), and the NRTL model (Equation 6-2) were used to fit the experimental data. Compounds **3c** and **3a** both exhibited incongruent melting, while compound **3b** was an ideal isomorphous solution. Changing the X-moiety from para- to meta-aminophenyl shifted the solid-liquid equilibrium further from ideal values and increased activity coefficients. Changing the R-moiety from methyl to cyclohexyl created an isomorphous system, which was anticipated to result from cyclohexyl being more similar to the phenyl moieties. Additionally, it was anticipated that both isomers have similar, multiple stable configurations and thus can form solid solutions easily when one acts as a nucleation site for the other.

Single crystal XRD was used to explain the thermal behavior. All isomers exhibited the same 2 irreproducible representations according to point group symmetry. Thus, *trans* was not more symmetric than *cis*, but still melted at a higher temperature for all compounds, which could only be attributed to the desired arrangements of the molecules within the unit cell that increased the packing density; increasing the ΔH_m and T_m. Similarly, para was not more symmetric than meta, and the fact that *cis* **3a** (meta) had a higher T_m than *cis* **3c** (para) was a result of its intermolecular hydrogen bonding potential within the unit cell. Although cyclohexyl (compound **3b**) increased the surface area of the DDSQ, it actually melted at a lower temperature than the analogous methyl DDSQ (compound **3a**). This was attributed to the bulkiness of the cyclohexyl moiety disrupting the crystal packing. Exhaustive crystallization attempts were made to crystallize *cis* **3b**, but without any success. However, *cis* **3b** demonstrated a large affinity towards crystallization upon cooling in the DSC, which was attributed to *trans* **3b** acting as

nucleation sites for the *cis* isomer. This was entirely possible due to the fact that compound **3b** was an ideal isomorphous solid solution with very similar solidus and liquidus curves, which suggested that the crystal structures of its isomers are nearly identical. Overall, the determined phase diagrams could be used to select an isomer, or ratio of isomers necessary for reaction conditions, and/or desired characteristics for a novel engineering design.

REFERENCES

REFERENCES

(1) Pinal, R. *Organic & Biomolecular Chemistry* **2004**, *2*, 2692.

(2) Plass, K. E.; Engle, K. M.; Matzger, A. J. *Journal of the American Chemical Society* **2007**, *129*, 15211.

(3) Gavezzotti, A. *Journal of the Chemical Society-Perkin Transactions 2* **1995**, 1399.

(4) Slovokhotov, Y. L.; Neretin, I. S.; Howard, J. A. K. *New Journal of Chemistry* **2004**, *28*, 967.

(5) Lloyd, M. A.; Patterson, G. E.; Simpson, G. H.; Duncan, L. L.; King, D. P.; Fu, Y.; Patrick, B. O.; Parkin, S.; Brock, C. P. *Acta Crystallographica Section B-Structural Science* **2007**, *63*, 433.

(6) Sysoev, S. V.; Cheremisina, T. N.; Zelenina, L. N.; Tkachev, S. V.; Zherikova, K. V.; Morozova, N. B.; Kuratieva, N. V. *Journal of Thermal Analysis and Calorimetry* **2010**, *101*, 41.

(7) Aoki, K.; Nakagawa, M.; Ichimura, K. *Journal of the American Chemical Society* **2000**, *122*, 10997.

(8) Bansal, R. K. *A Textbook of Organic Chemistry*; 5th ed.; New Age International: New Delhi, India, 2007.

(9) Gilbert, A. S. *Thermochimica Acta* **1999**, *339*, 131.

(10) Aakeroy, C. B.; Forbes, S.; Desper, J. *Journal of the American Chemical Society* **2009**, *131*, 17048.

(11) Plato, C.; Glasgow, A. R. *Analytical Chemistry* **1969**, *41*, 330.

(12) He, B.; Martin, V.; Setterwall, F. *Fluid Phase Equilibria* **2003**, *212*, 97.

(13) Lane, G. A. *Solar heat storage : latent heat materials*; CRC Press: Boca Baton, Fla., 1983.

(14) Walas, S. M. *Phase equilibria in chemical engineering*; Butterworth: Boston, 1985.

(15) Yamashita, H.; Hirakura, Y.; Yuda, M.; Teramura, T.; Terada, K. *Pharmaceutical Research* **2013**, *30*, 70.

(16) Schoen, B. W.; Lira, C. T.; Lee, A. *Fluid Phase Equilibria* **2013**, *submitted July 8, 2013*.

(17) Schoen, B. W.; Holmes, D.; Lee, A. *Magnetic Resonance in Chemistry* **2013**, *51*, 490.

(18) Still, W. C.; Kahn, M.; Mitra, A. *Journal of Organic Chemistry* **1978**, *43*, 2923.

(19) *Software for the CCD Detector Systems for Determining Data Collection Parameters*; 1.61 ed.; Systems, B. A. X.-r., Ed. Madison, Wisconsin, 2009, *Software for the CCD Detector Systems for Determining Data Collection Parameters*.

(20) 2010.11-3 ed.; Systems, B. A. X.-r., Ed. Madison, Wisconsin, 2010, Software *for the CCD Detector System*.

(21) *Software for the Integration of CCD Detector System*; 7.68A ed. Madison, Wisconsin, 2010, Software *for the Integration of CCD Detector System*.

(22) Blessing, R. *Acta Crystallographica Section A* **1995**, *51*, 33.

(23) Sheldrick, G. *Acta Crystallographica Section A* **2008**, *64*, 112.

(24) TA Instruments Universal Analysis 2000, TA instruments Inc. version 4.5A Build 4.5.0.5, Waters LLC, **2000**.

(25) Spek, A. L. *Acta Crystallographica Section D-Biological Crystallography* **2009**, *65*, 148.

(26) Elliott, J. R.; Lira, C. T. *Introductory chemical engineering thermodynamics*; 2nd ed.; Prentice Hall: Upper Saddle River, NJ, 2012.

(27) Prausnitz, J. M.; Lichtenthaler, R. N.; Azevedo, E. G. d. *Molecular thermodynamics of fluid-phase equilibria*; 3rd ed.; Prentice Hall PTR: Upper Saddle River, N.J., 1999.

(28) Kaiser, T. E.; Stepanenko, V.; Wuerthner, F. *Journal of the American Chemical Society* **2009**, *131*, 6719.

(29) Kuduva, S. S.; Sarma, J.; Katz, A. K.; Carrell, H. L.; Desiraju, G. R. *Journal of Physical Organic Chemistry* **2000**, *13*, 719.

(30) Manin, A. N.; Voronin, A. P.; Perlovich, G. L. *Thermochimica Acta* **2013**, *551*, 57.

(31) Slovokhotov, Y. L.; Batsanov, A. S.; Howard, J. A. K. *Structural Chemistry* **2007**, *18*, 477.

(32) Baird, J. A.; Van Eerdenbrugh, B.; Taylor, L. S. *Journal of Pharmaceutical Sciences* **2010**, *99*, 3787.

(33) Wunderlich, B.; Springer,: Berlin, 2005, p xvi.

(34) Karis, T. E.; Kim, S. J.; Gendler, P. L.; Cheng, Y. Y. *Journal of Non-Crystalline Solids* **1995**, *191*, 293.

(35) Zhou, J.; Kye, Y.; Harbison, G. *Journal of the American Chemical Society* **2004**, *126*, 8392.

(36) Ahn, H. W.; Clarson, S. J. *Journal of Inorganic and Organometallic Polymers* **2001**, *11*, 203.

CHAPTER 7

APPLICATIONS

Keywords

polyimide, thermoset, polyamide, Nomex, ionic liquid

7. Applications

7.1 Polyimide thermoset

7.1.1 Introduction

Polyimides exhibit high viscosity, which requires high pressure to be used in order to process and fabricate the structural composites and adhesive joints. Additionally, since the solid to liquid phase transition is so close to the curing reaction, the processing window of polyimide thermosetting materials is quite small. Furthermore, the characteristics of current polyimide thermosetting material are polydispersed since the MW of the oligomers themselves are polydispersed. Therefore, research on polyimides has been directed towards decreasing the viscosity and increasing the processing window without sacrificing HPM characteristics. It was anticipated that using DDSQ as a backbone for these polyimide thermosetting materials would allow these objectives to be reached, while providing monodispersed characteristics. Since an amorphous material provides a lower viscosity than a crystalline one, only compounds **3a**, **3c**, and **3d** were used for this application.

7.1.2 Solvents and reagents

Tetrahydrofuran (THF) and toluene were obtained from Sigma-Aldrich and distilled under nitrogen. Phenylethynylphthalic anhydride (PEPA) was obtained from Chriskev Company.

7.1.3 Nuclear magnetic resonance

Compounds were measured at 25 ºC on a Varian UNITY-Inova 600 spectrometer equipped with a 5 mm Pulsed-Field-Gradient (PFG) switchable broadband probe and operating at 599.80 MHz (^{1}H). ^{1}H NMR data were acquired using a recycle delay of at least 20 s and 32

scans to ensure accurate integration. The ^{1}H-chemical shifts were referenced to that of residual protonated solvent in $CDCl_3$ (7.24 ppm). ^{29}Si NMR data were acquired using a recycle delay of 12 s with inverse-gated decoupling. The pulse angle was set to 90°. ^{29}Si spectra were referenced against the lock solvent using vendor supplied lock referencing. ^{13}C NMR data were acquired using a recycle delay of 1 s and 256 scans.

7.1.4 Synthesis

Scheme 7-1 shows the synthesis of *cis* and *trans* [(meta-phenylethynylphthalimide) methylsilyl]-bridged-(phenyl)$_8$-double-decker silsesquioxane, DDSQ(m-PEPI)(Me)-**5a**, [(para-phenylethynylphthalimide)methylsilyl]-bridged-(phenyl)$_8$-double-decker silsesquioxane,

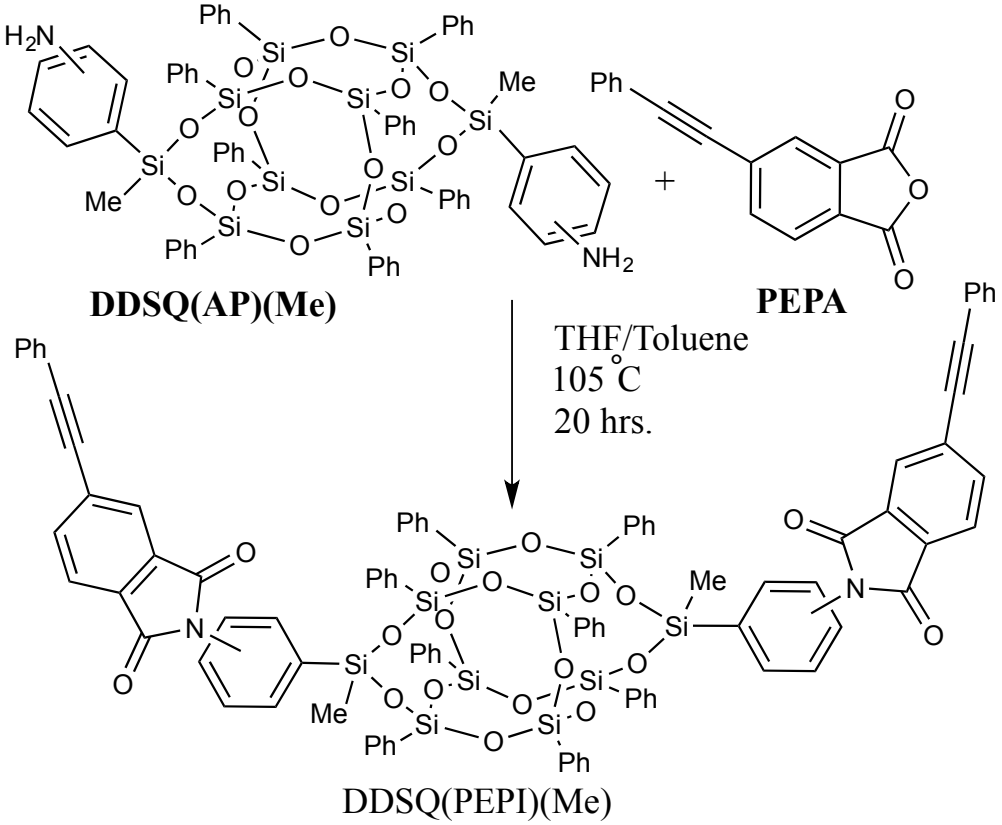

Scheme 7-1. Synthesis of compound **5**.

DDSQ(p-PEPI)(Me)-**5c**, and [(meta/para- phenylethynylphthalimide)methylsilyl]-bridged-(phenyl)$_8$-double-decker silsesquioxane, DDSQ(p-PEPI)(Me)-**5d**, through the reaction of DDSQ(AP)(Me), compound **3**, with phenylethynyl phthalic anhydride (Figure 7-1).[1,2]

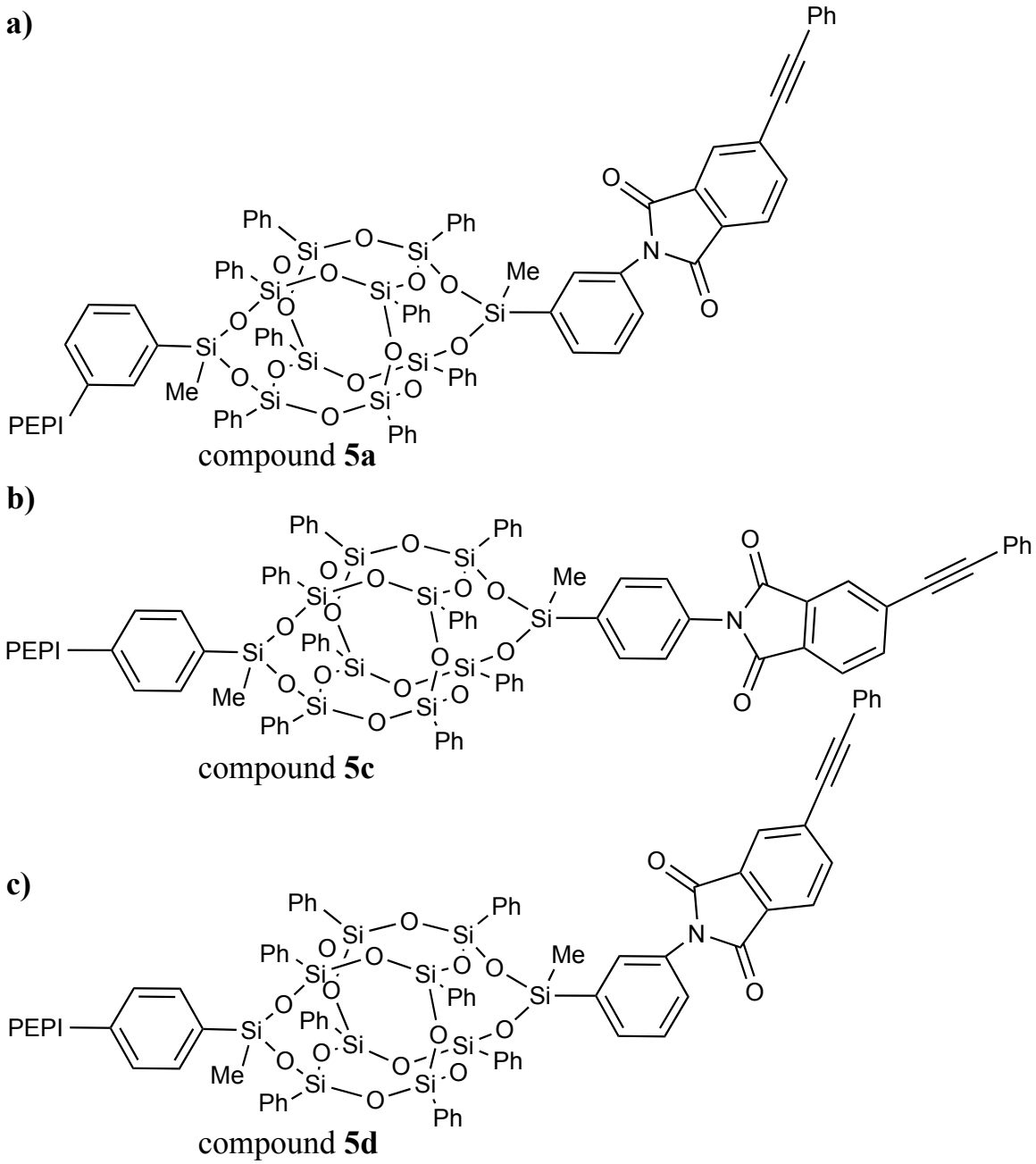

Figure 7-1. Compounds (a) **5a**- all meta, (b) **5c**- all para, (c) **5d**$^{\mathbf{i}}$- one side meta and one side para. All compounds also have *cis* and *trans* isomers about the SQ cage with respect to the D-Silicon, as seen in the previous chapters for compounds **3a**, **3b**, and **3d**.

7.1.4.1 Compound 5a

Under a nitrogen atmosphere, a well-stirred solution of **3a** (5.35 g, 4.00 mmol) and PEPA (2.18 g, 8.80 mmol) in anhydrous THF (70 mL) and toluene (70 mL) was stirred at room temperature (25 °C) for 1 h. The solution was heated to 60 °C for 2 h and refluxed at 115 °C for 20 h. Solvent was removed under vacuum and subsequently washed and precipitated with methanol. The product was filtered and dried in a vacuum oven at 125 °C for 24 h (6.52 g, 3.63 mmole, 91% yield). NMR resonances (ppm) follow. ^{29}Si NMR, δ: -31.5, -77.9, -79.1, -79.2, -79.3. ^{13}C NMR, δ: 166.6, 166.5, 137.7 137.6, 137.2, 134.1, 133.3, 132.2, 132.0, 131.6, 131.4, 131.3, 131.0, 130.7, 130.5, 130.4, 130.0, 129.4, 128.8, 128.7, 128.2, 128.0, 127.9, 127.7, 127.6, 126.55, 123.8, 122.14, 94.2, 87.9, -0.3. ^{1}H NMR, δ: 8.10-7.11 (64 H, overlapping multiplets), 0.66 and 0.65 (6 H, overlapping singlets)[ii] (Figure 7-2).

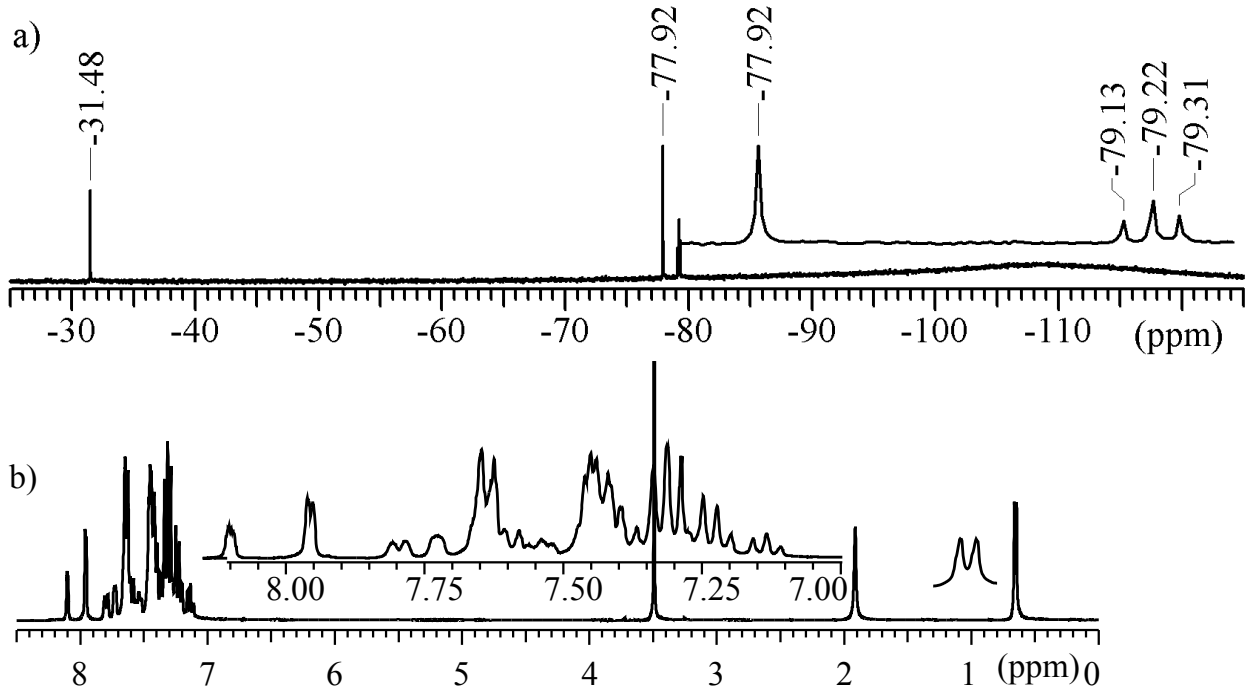

Figure 7-2. NMR spectra of compound **5a** (a) ^{29}Si and (b) ^{1}H, the resonances at δ_H 3.5 and 1.9 ppm are residual methanol.

7.1.4.2 Compound 5c

Under a nitrogen atmosphere, a well-stirred solution of **3c** (8.00 g, 5.99 mmol) and PEPA (3.04 g, 12.23 mmol) in anhydrous THF (65 mL) and toluene (78 mL) was stirred at room temperature (25 °C) for 1 h. The solution was heated to 60 °C for 2 h and refluxed at 115 °C for 20 h. Solvent was removed under vacuum and subsequently washed and precipitated with methanol. The product was filtered and dried in a vacuum oven at 125 °C for 24 h (10.12 g, 5.63 mmole, 94% yield). NMR resonances (ppm) follow. ^{29}Si NMR, δ: -31.3, -78.1, -79.0, -79.2, -79.4. ^{13}C NMR, δ: 166.6, 166.5, 137.3 136.4, 134.4, 134.2, 134.1, 133.3, 132.2, 132.0, 131.8, 130.8, 130.6, 130.5, 130.2, 129.4, 128.7, 128.0, 127.9, 127.8, 127.7, 126.7, 125.7, 123.9, 122.2, 94.4, 87.9, -0.3. ^{1}H NMR, δ: 8.14-7.16 (64 H, overlapping multiplets), 0.63 and 0.62 (6 H, overlapping singlets)[ii] (Figure 7-3).

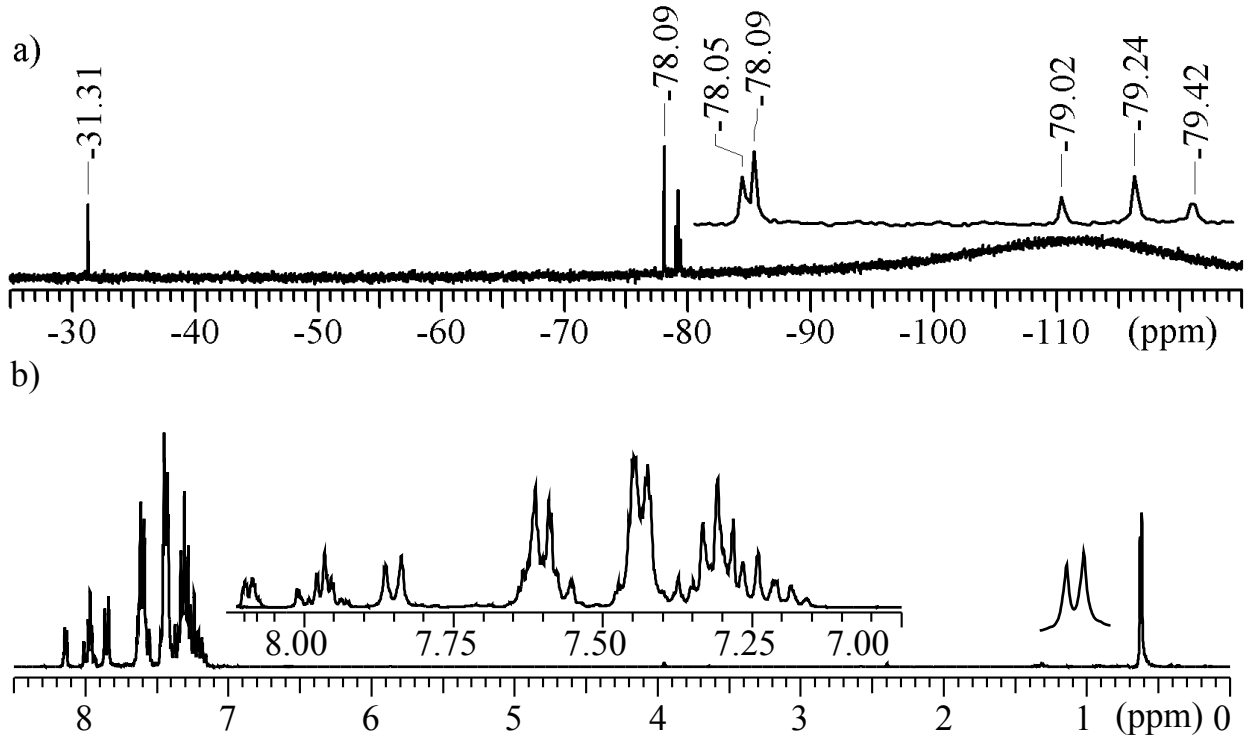

Figure 7-3. NMR spectra of compound **5c** (a) ^{29}Si and (b) ^{1}H.

7.1.4.3 Compound 5d[j]

Under a nitrogen atmosphere, a well-stirred solution of Ph_8bisaniline-POSS (0.997 g, 0.744 mmol) and PEPA (0.744 g, 2.97 mmol) in anhydrous THF (8 mL) and toluene (8 mL) was stirred at room temperature (25 °C) for 1 hour. The solution was heated to 60 °C for 2 h and refluxed at 115 °C for 20 h. Solvent was removed under vacuum and subsequently washed and precipitated with methanol. The product was filtered and dried in a vacuum oven at 125 °C for 24 h (1.12 g, 0.623 mmole, 84% yield). Due to complications with the synthetic procedure (Appendix V), additional excess PEPA was used for the synthesis of compound **5d**. Unreacted PEPA was removed using silica gel chromatography columns (dichloromethane : hexane = 7 : 3), NMR resonances (ppm) follow. ^{29}Si NMR, δ: -31.1, -31.3, -77.7 (2 overlapping singlets), -78.87, -78.93, -78.98, -79.02, -79.04, -79.07, -79.14, -79.17, -79.19. ^{13}C NMR, δ: 166.4, 138.7, 137.2, 137.1, 134.3, 134.1, 133.2, 132.0, 131.7, 131.4, 131.0, 130.5, 129.7, 129.3, 128.6, 127.9,

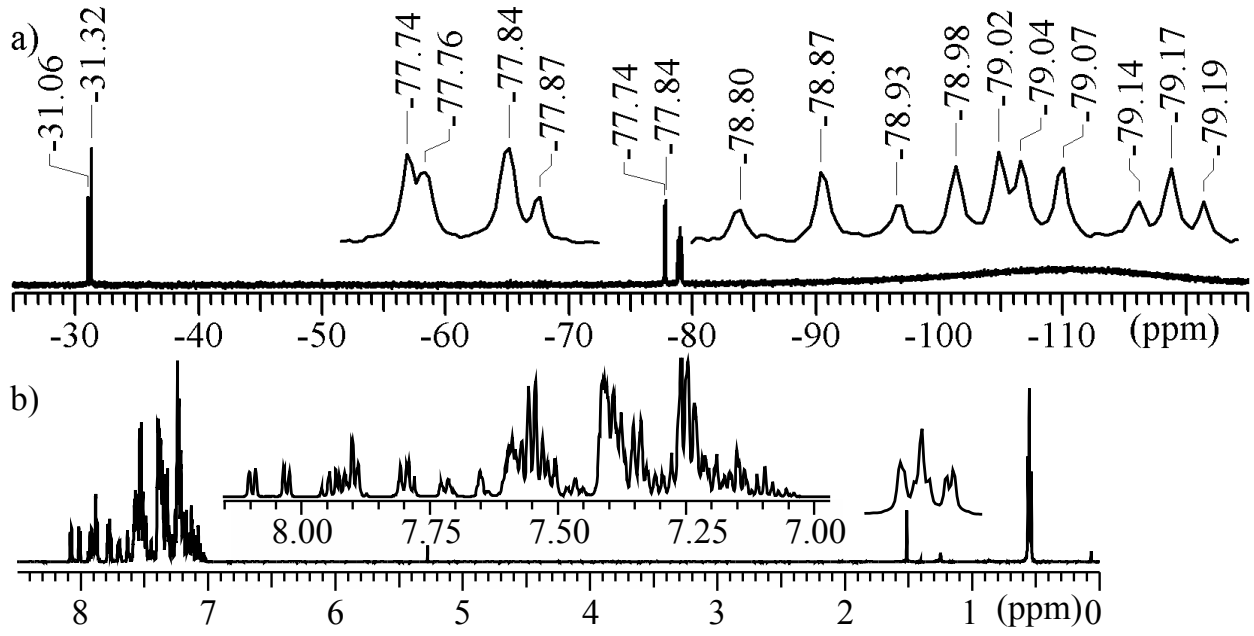

Figure 7-4. NMR spectra of compound **5d** (a) ^{29}Si and (b) ^{1}H.

127.8, 127.7, 127.6, 127.5, 126.6, 126.5, 125.6, 123.8, 122.1, 94.3, 94.2, 87.9, 87.8, -0.3. ^{1}H NMR, δ: 8.08-7.03 (64 H, overlapping multiplets), 0.56, 0.55, and 0.54 (6 H, 6 overlapping singlets)[iii] (Figure 7-4).

7.1.5 Thermal behavior

Melting behavior was studied using a Mettler Tolido DSC-1 equipped with a mechanical cooling system under a nitrogen atmosphere. Samples were placed in a Q-zero^{TM} aluminum pan and sealed with a punctured lid to evaluate solid to liquid transitions and the curing polymerization reaction. Samples were first equilibrated at 25°C for 1 min and subsequently heated to 500 °C with a constant heating rate of 10 °C/min.

7.1.6 Viscosity measurements

Viscosity measurements were conducted on a TA Instruments AR 2000, equipped with an environmental control system. Steady-state shear viscosity (10 s^{-1}) as a function of temperature was measured using an 8 mm diameter parallel plate fixture with a 0.4 mm gap. For handling purposes, sample powders (approximately 70 mg) were prepared through press-molding at room temperature. The fixture was equilibrated to the initial temperature (170 °C) for 30 min, and the sample was then placed between the gap. The temperature was then increased at a constant heating rate until the final temperature (250 °C) was reached. Steady-state viscosity as a function of shear rate was also measured at 170 °C, 200 °C, and 250 °C, from a shear rate of 1 s^{-1} through 100 s^{-1}.

7.1.7 Results and discussion

7.1.7.1 Thermal analysis

Differential scanning Calorimetry (DSC) was used to evaluate the glass (T_g) and melting transitions (T_m and ΔH_m) of the uncured oligomers and the subsequent curing reaction (T_{RXN} and ΔH_{RXN}). Results are summarized in Table 7-1, and DSC curves are shown in Figure 7-5.

Table 7-1. DSC data for polyimide thermosets.

Compound	T_g (°C)	T_m (°C)	ΔH_m (kJ/mole)	T_{RXN} (°C)	ΔH_{RXN} (kJ/mole)
5a	--	127.1	9	326.3	256
5c	--	256.7	13	337.4	206
trans **5c**	--	302.5	59	343.6	226
cis **5c**	123.4	186.8	19	327.6	221
5d	106.4	--	--	332.2	287

Compounds **5a** and **5c** showed several transitions before the curing reaction, which were anticipated to be from the incomplete mixing of the isomers (Figure 7-5a,b). In order to determine if this were true, *trans* and *cis* oligomers of **5c** also evaluated. The DSC curve of *trans* **5c** showed a sharper melting transition (T_m = 302.5 °C) and a smoother baseline (Figure 7-5c) than the mixed isomer of **5c** (Figure 7-5d). The second T_m shown in the mixture of isomers of **5c** (Figure 7-5b) was at approximately 256.7 °C, which is likely representative of the *trans* **5c** melting transition. It is depressed from its pure value as a result of the incorporation of the *cis* isomers. Similarly, the T_g and the first T_m (Figure 7-5b) are representative of the *cis* isomers in **5c** (Figure 7-5d), which were also depressed as a result of the incorporation of the *trans* isomer. It is not surprising that the *cis* isomer exhibited a larger depression in the T_g and the first T_m

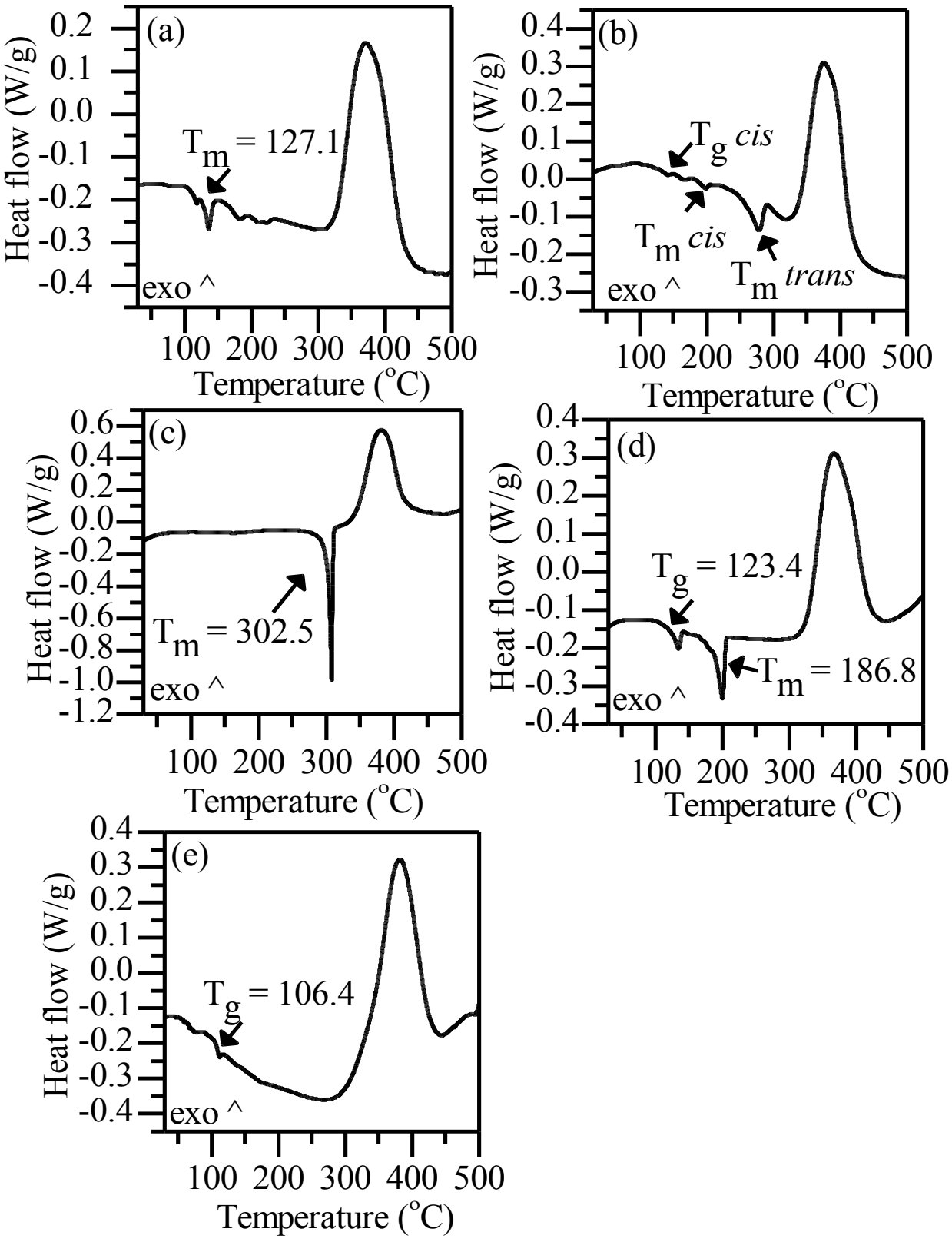

Figure 7-5. DSC curves of (a) **5a**, (b) **5c**, (c) *trans* **5c**, (d) *cis* **5c**, and (d) **5d**, from 30 to 500 °C with a constant heating rate of 10 °C / min.

since a similar trend was observed in the melting data for binary *cis/trans* mixtures of compound **3** (Chapter 6). This data demonstrates that compounds **5a** and **5c** are semi-crystalline. Compound **5d** is the only oligomer that is completely amorphous, and its T_g is lower than other phenyl ethynyl end-capped oligomers.[3] Using a melting point apparatus, it was determined that at this T_g, compound **5d** completely undergoes a solid-liquid transition.

The cure reaction occurred at approximately 330 °C for all compounds. The largest difference between the solid to liquid transition and the curing reaction was for compound **5d**. Compound **5d** also had the largest heat of reaction (ΔH_{RXN} = 287 kJ/mole). It was anticipated that this was a result of the degree of crosslinking. The curing reaction occurred considerably lower (326 – 344 °C) than the onset of degradation for all compounds (475 °C).

7.1.7.2 Viscosity

Eliminating crystallinity and the processing window of the oligomer are the principal motifs for this application, and compound **5d** had the most desirable combination of the two. It was fully amorphous and exhibited the largest processing window, completely melting below 170 °C which has been attributed to the inherent asymmetry of the molecule. Thus, only the viscosity of compound **5d** was studied. Steady state shear viscosity was measured from 170 °C through 250 °C for compound **5d**. Results were evaluated using TA Rheology advantage data analysis.[4] Two different batches were compared to test for consistency of the synthesis and characteristics (Figure 7-6). Results indicated that there is consistency in the two different

batches, which is an indication that the oligomer properties are mono-dispersed. Additionally, the viscosity continuously decreased with increasing temperature throughout the temperatures

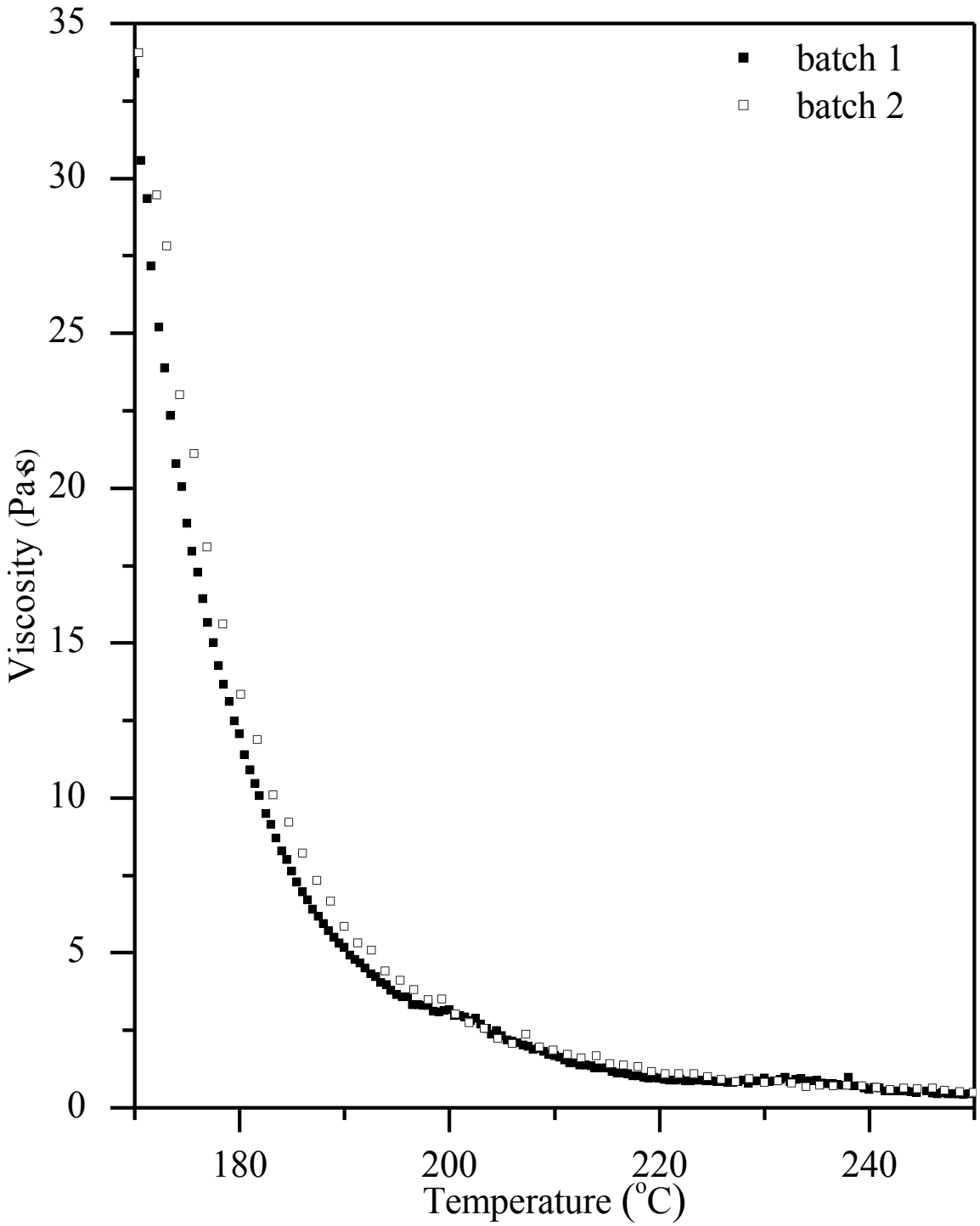

Figure 7-6. Complex viscosity of two batches of compound **5d**; filled square (■) = batch 1, and unfilled square ( ) = batch 2.

range chosen. Compared to literature values,[3,5,6] the viscosity of compound **5d** was much lower throughout the range of temperatures observed (Table 7-2).

Table 7-2. Complex viscosity for compound **5d**.

	Complex viscosity (Pa·s) at the following T (°C)				
Compound	170	200	230	250	Mmv (Pa s, °C)
Batch 1	33.37	3.16	0.94	0.47	0.42 at 249
Batch 2	34.04	3.03	0.80	0.49	0.49 at 250
PI-A (G:A)[a,6]	--	--	--	0.58	0.25 at 288
PI-A (G:B)[a,5]	--	--	--	1.0	0.27 at 299
PI-A (3G:A)[a,6]	--	--	--	0.61	0.28 308
PETI-3K[3]	--	--	--	--	9 at 353

[a] Background information (p. 48)

7.1.8 Concluding remarks on polyimide thermosets

A series of phenylethynyl-encapped oligomides were prepared from compounds **3a**, **3c**, **3d**, and PEPA. The incorporation of the silsesquioxane cage decreased the glass transition temperature, while maintaining high thermomechanical features of the oligoimide, which provided a larger processing window. According to DSC investigations, all oligomers exhibited an irreversible cross-linking reaction above 320 °C to form a polyimide thermoset. DSC studies were also used to study the existence of specific thermal features, such as a crystalline melting and glass transition of the resulting oilgoimides. Results showed that both compounds **5a** and **5c** with mixtures of *cis/trans* exhibited a glass transition and broad endothermic crystalline melting transitions, whereas isolated *cis* and *trans* isomers exhibited sharper endothermic melting transitions. Thus, suggesting that mixtures of isomers were more amorphous than isolated isomers. Compound **5d** did not exhibit any form of an endothermic crystalline melting transition, which suggested that it was wholly amorphous. Additionally, compound **5d** exhibited the lowest

T_g and solid to liquid transition, it was completely liquidus below 170 °C. Thus, it appears that the assymetric mixture of stereo- (*cis* and *trans*) and regio- (para- and meta-) isomers eliminates crystallinity and increases the processing window. Steady state shear viscosity of compound **5d** was also investigated. It was determined that the viscosity continuously decreases with increasing temperature throughout the temperatures range chosen and is lower than literature values. Additionally, two batches of compound **5d** were examined, with similar findings, suggesting that these oligomers and their properties are monodispersed. Therefore compound **5d** is a viable alternative for this class of polyimide thermosetting materials.

7.2 Polyaramid thermoplastics

7.2.1 Introduction

In light of the remarkable characteristics displayed by polyaramids, research efforts are directed in two areas: (1) reducing the cohesive energy resulting from H-bonding and pi-stacking so these materials are easier to process, and soluble in common organic solvents without sacrificing high performance properties, and (2) expanding their high-performance properties to additional applications in new and promising fields, such as: optically active, luminescent, ionicexchange, flame-resistant and fiber-forming materials. Prior to this dissertation, studies have demonstrated that SQ based polyamides improve thermomechanical properties for PA6. However, no studies have used an SQ cage-like structure that is covalently bonded to a polyamide backbone, which could potentially have a more significant effect on the polymer properties. This section investigates the synthesis of DDSQ-based Nomex and the affect that the cage has on the melting and degradation characteristics of these polymers. Various mass fractions of compound **3a** and MPDA are reacted with ICL to determine if the amount of DDSQ in the backbone affects the MW of the polymer. It was proposed that the bulky Si-O core would reduce the cohesive energy without sacrificing the thermomechanical properties of neat Nomex.

7.2.2 Solvents and reagents

Trimehtylchlorosilane, triethyl amines, toluene, m-phenylene diamine, and isophthloyl chloride were purchased from Sigma Aldrich. Solvents were distilled under nitrogen. Lithium chloride was purchased from Jade Scientific (Canton, Michigan) and used without further purification. Dry n-methylpyrrollidine was purchased from Alfa Aesar (Ward Hill, Massachussettes) and used without further purification.

7.2.3 Nuclear magnetic resonance

Compounds were measured at 25 ºC on a Varian UNITY-Inova 600 spectrometer equipped with a 5 mm Pulsed-Field-Gradient (PFG) switchable broadband probe and operating at 599.80 MHz (^{1}H). ^{1}H NMR data were acquired using a recycle delay of at least 20 s and 32 scans to ensure accurate integration. The ^{1}H-chemical shifts were referenced to that of residual protonated solvent in $CDCl_3$ (7.24 ppm).

7.2.4 Synthesis

DDSQ-based Nomex was synthesized from compound **3a**, N-silylated m-phenylene diamine (MPDA), and isophthloyl chloride (ICL) (Scheme 7-2).[7] MPDA was silylated prior to polymerization.

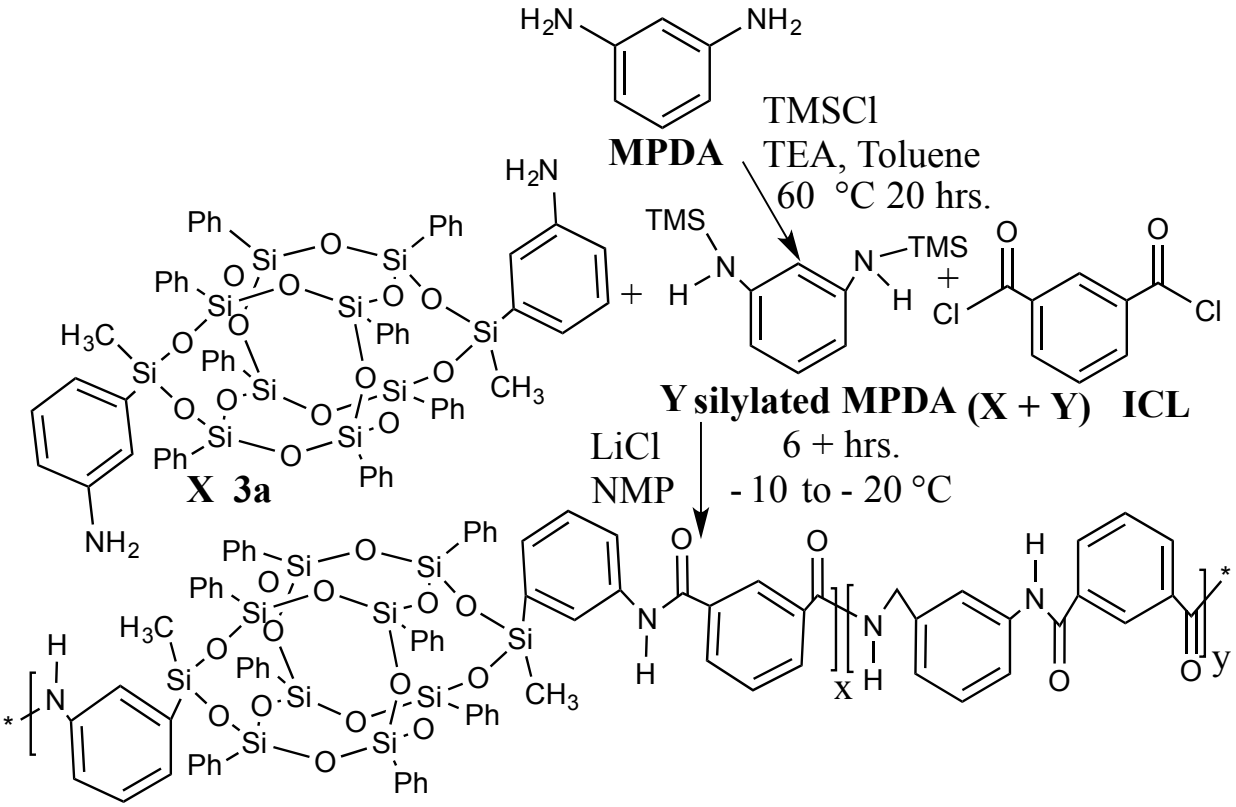

Scheme 7-2. DDSQ-based Nomex scheme.

7.2.4.1 Silylated MPDA

Under a nitrogen atmosphere, TMSCl was added dropwise to a stirring solution of solid MPDA (30.0 g, 277 mmole), triethylamines (72.3 g, 665 mmole), and Toluene (300 mL). The solution turned yellow almost immediately. It was then heated to 60 °C. After 20 h, the solution became a viscous liquid. Solvent was removed under vacuum and the product was purified by fractional distillation to yield a colorless, viscuous liquid (60.93 g, 243 mmole). ^{1}H NMR δ: 6.94 (1 H, multiplet), 6.12-5.96 (3 H, overlapping multiplets), 6.51 (2 H, NH_2, broad singlet), 0.25, 0.24, 0.14, 0.05 (18 H, singlets) (Figure 7-7).

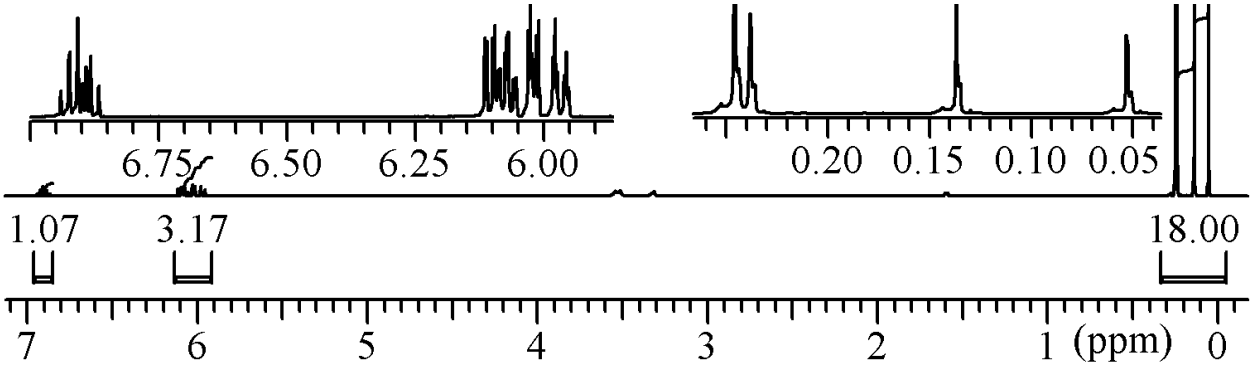

Figure 7-7. ^{1}H NMR spectrum of silylated MPDA.

7.2.4.2 DDSQ-like Polyaramide

All polyaramids were prepared according to the following general procedure. The value of X and Y was varied (Table 7-3). Under a nitrogen atmosphere, a solution of ICL (X + Y mmole) and NMP was added dropwise to a stirred solution of **3a** (X mmole), silylated MPDA (Y mmole), LiCl (5 wt %), and N-methyl pyrrolidone (NMP) (ca. 0.5 mmole (X+Y)/mL),[2] at -10 °C to -20 °C. After 5 h, the solution became viscous and was precipitated into cold Methanol to form a white solid. The product was isolated by filtration and dried under vacuum. A total of 17

polymers were synthesized according to this procedure. Nomex (0 mole % DDSQ) was synthesized as a model polymer for these studies (P-1 - P-5).

Table 7-3. Polymer experiments.

Exp #	Mass % DDSQ	Mole % DDSQ[a]	Product mass (g)	Yield %
P-1	0	0	0.198	84
P-2	0	0	1.32[b]	--
P-3	0	0	0.538	90
P-4	0	0	0.579	98
P-5	0	0	0.718	100
P-6	1.1	0.2	--	--
P-7	1.1	0.2	0.710	76
P-8	5.3	1	--	--
P-9	5.3	1	0.501	78
P-10	10.2	2	0.550	83
P-11	14.5	3	--	--
P-12	14.5	3	0.535	78
P-13	22.3	5	--	--
P-14	22.3	5	--	--
P-15	22.3	5	0.580	
P-16	78.3	50	0.051	43
P-17	100	100	0.051	63

[a] Mole % of total amines used: X/(X+Y). [b] Not fully dry. -- not calculated.

Three additional polymers (Table 7-4) were synthesized in order to achieve the highest MW feasible. All were comprised of 1.1 mass % DDSQ (0.2 mole %). Under a nitrogen atmosphere, a solution of ICL (0.609 g, 2.99 mmole) and NMP was added dropwise to a stirred solution of silylated MPDA (0.631 g, 2.99 mmole), LiCl (0.318 g, 5.14 mmole), and NMP (5 mL), at -10 °C to -20 °C. After (1 – 4.5 h), a solution of **3a** (0.008 g, 0.006 mmole) and NMP (0.013 mL) was added to the reaction and allowed to stir. Subsequently, a solution of ICL

Table 7-4. Additional polymer reactions.

Exp #	Mole % DDSQ	Mass % DDSQ	time added [a]	Product (g)	Yield
P-18	1.1	0.2	1	0.733^	102 [b]
P-19	1.1	0.2	3	0.765^	107 [b]
P-20	1.1	0.2	4.5	0.705	98

[a] Time DDSQ added [b] May not be fully dry

(0.0001 g, 0.005 mmole) and NMP was added dropwise to the reaction. After 5 additional h, the solution became viscous and was precipitated into cold methanol to form a white solid. The product was isolated by filtration and dried under vacuum.

According to ^{1}H NMR spectra, the resonance at approximately δ 3.5 (NH) in the silylated MPDA product (Figure 7-7) shifted upfield to approximately δ 10.5 (NH) after polymerization (Figure 7-8). The figure demonstrates that there are two distinct resonances in this region for the co-polymers (Figure 7-8b). One is associated with the amine in Nomex (Figure 7-8a) and the other is associated with the amine on the DDSQ (Figure 7-8c).

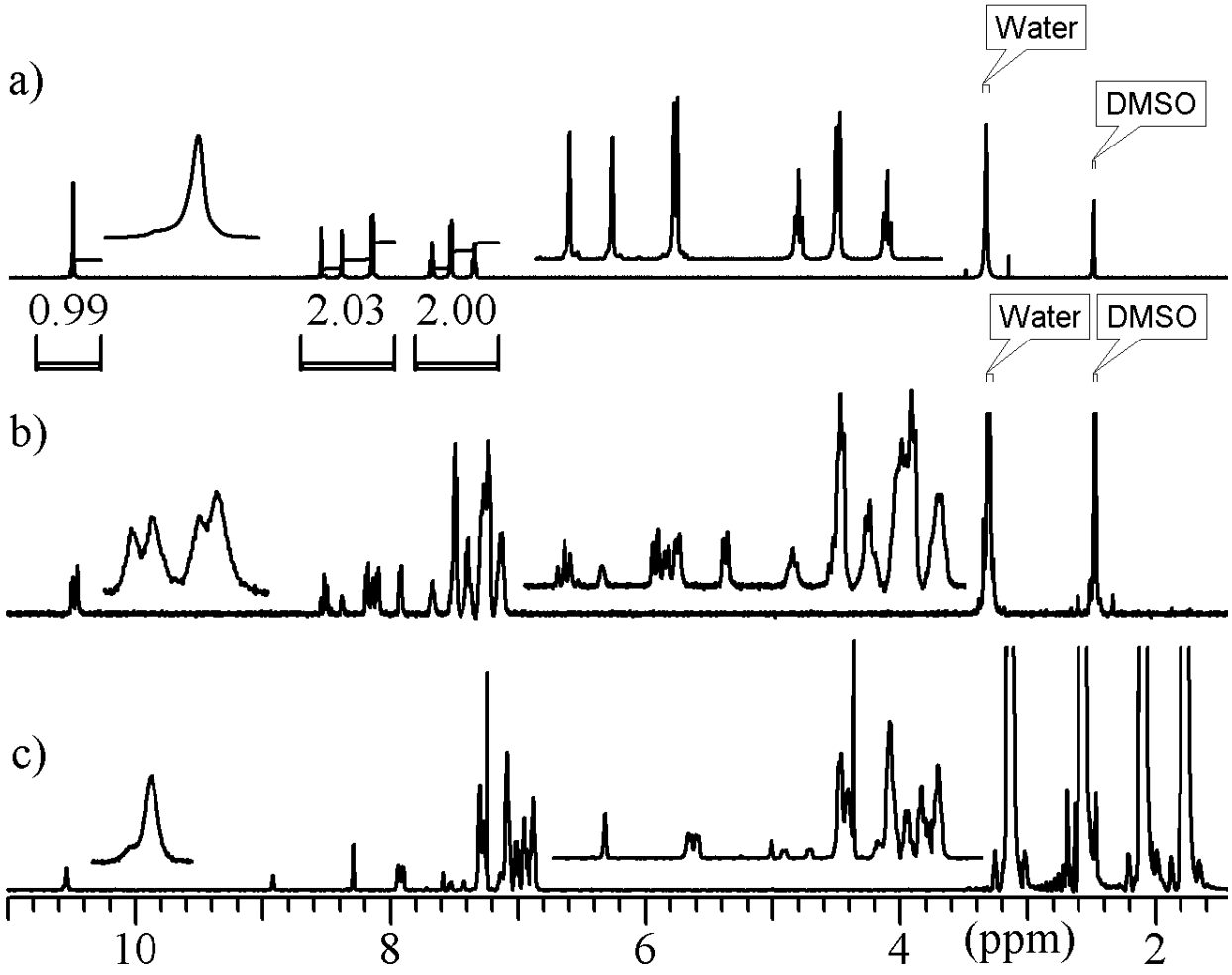

Figure 7-8. ^{1}H NMR spectra of (a) 0 mole % DDSQ (Nomex), (b) 50 mole % DDSQ, and (c) 100 mole % DDSQ.

7.2.5 Molecular weight

Molecular weight of the polymers was determined using two different methods. First, gel permeation chromatography (GPC) was used for the polymers that were soluble in DMF. Second, the polymers that were not soluble in DMF were measured relative to the same polymer/solvent pair using viscometer measurements.

7.2.5.1 Gel permeation chromatography

For polymers that were soluble in DMF, GPC could be used in order to determine the number average MW (M_n) was attainable using GPC analysis. The M_n can be defined by the following formula (Equation 7-1):

$$M_n = \frac{\sum_{i=1}^{\infty} N_i M_i}{\sum_{i=1}^{\infty} N_i} \qquad (5-1)$$

where N_i M_i is the total weight of polymers and N_i is the total number of polymers. Typical M_n for Nomex polymers is in the range of 10-30 x 10^3 g/mol. This would provide approximately 42 – 126 units of *y* per polymer chain (Scheme 7-2). The PDI for these polymers is typically near 2.0 for polymers with a lower M_n and 3 for polymers with an M_n > 35 x 10^3 g/mol.

Table 7-5. Mn for select polymers that are soluble in DMF.

Exp #	Mass % DDSQ	M_n (10^3 g/mol)	units	PDI
P-2	0	93900	394	3.8
P-3	0	109388	459	1.66
P-6	1.1	58250	231	2.5
P-8	5.3	68036	224	2.17
P-16	78.3	11547	14	2.0
P-17	100	11000	8	2.1

It appears that P-2, 3, 6, and 8 are all high MW polyaramids according to their M_n, PDI and number of units per polymer chain. Conversely, P-16 and P-17 appear to be oligomers. Furthermore, it was determined that P-16 and 17 are soluble in THF, whereas all other polymers were not. This confirms that P-16 and 17 are low molecular weight polymers, or oligomers. It is anticipated that the remaining polymers that were not soluble in DMF have a higher MW, since increasing MW of Nomex polymers has been seen to exhibit decreased solubility.[8]

7.2.5.2 Viscosity measurements

Viscosity was used as a relative measure of the MW of the polymers, since according to the Mark-Houwink equation it is proportional to MW (Equation 7-2):

$$[\eta] = KM^{\alpha} \qquad (7-2)$$

where [η] is intrinsic viscosity, M is molecular weight, and K and α are constants that are unique to the specific polymer and solvent pair. Since K and α are unknown for these polymer and solvent pairs, [η] alone was used as a relative measure of the molecular weight of the polymers.

To measure the intrinsic viscosity experimentally, first the specific viscosity reduced by the concentration (η_{sp} / c) of the solution is extrapolated to zero. A simple linear extrapolation of the Huggins equation is a common method for determining the intrinsic viscosity (Equation 7-3):

$$\frac{\eta_{sp}}{c} = [\eta] + k'[\eta]^2 c \qquad (7-3)$$

where c is concentration and k′ is a constant that depends on the specific polymer, solvent, and temperature of the solution, but is independent of MW.

Alternatively, extrapolating inherent viscosity (η_{inh}) to zero can also provide a measurement of the intrinsic viscosity (Equation 7-4):

$$\eta_{inh} = [\eta] + k''[\eta]^2 c \qquad (7-4)$$

where k′′ is a constant dependent on the polymer, solvent, and temperature of the given system.

The inherent viscosity (η_{inh}) and specific viscosity (η_{sp}) can be determined by comparing the time (t) that it takes the polymer solution to flow through the capillary to the flow time of the pure solvent (t_0) (Equation 7-5).

$$\eta_{sp} = \frac{t - t_0}{t_0}, \eta_{inh} = ln\left(\frac{\eta_r}{c}\right), \eta_r = \frac{t}{t_0} \qquad (7-5)$$

Since viscosity can only be measured relative to the same polymer, polymers comprised of the same mass % DDSQ were compared (Figure 7-9). At 1.1 mass %, it was important to see if the time that the DDSQ was added had an affect on the MW of the polymer. It does not appear that the time of addition largely affects the MW of the polymer with the exception of P-20. For P-20, DDSQ was added to the reaction solution 4.5 h after the polymerization began. When all the components were added simultaneously, the polymerization takes approximately 5 h

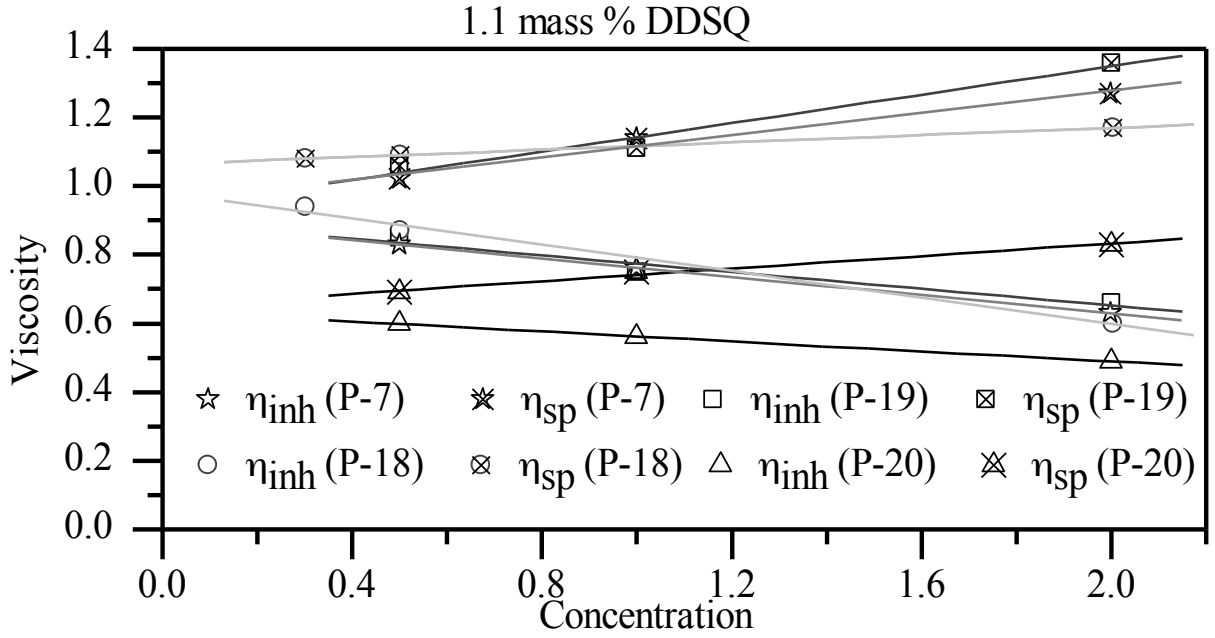

Figure 7-9. Extrapolation to intrinsic viscosity for 1.1 mass % DDSQ.

Therefore, when DDSQ was added for P-20, the polymerization may have been complete. Both intrinsic viscosity and specific viscosity were linearly extrapolated to zero, from three different concentrations in NMP, in order to determine an accurate value of the intrinsic viscosity, and both constants, k′ and k′′. The y-intercept represents intrinsic viscosity, and the constants k′ and k′′ were determined from equations 7-2 and 7-3. Intrinsic viscosity, and values for the constants of several of the polymers were evaluated (Table 7-6). Once k′ and k′′ are determined, the intrinsic viscosity of the same polymer, solvent pair can be determined from one concentration.

Table 7-6. Intrinsic viscosity measurements of selected polymers in NMP.

Polymer	Mass % DDSQ	[η] (dl/g)	k′	k′′
P-4	0	0.69	0.34	0.58
P-5	0	0.59	0.25	0.42
P-7	1.1	0.92	0.18	0.34
P-18	1.1	1.0	0.046	0.24
P-19	1.1	0.92	0.23	0.39
P-20	1.1	0.64	0.21	0.38
P-9	5.3	0.83	0.42	0.43
P-10	10.2	1.2	0.17	0.31
P-12	14.5	0.65	0.14	0.34
P-15	22.3	0.64	0.28	0.44

7.2.6 Degradation analysis

Degradation characteristics of the polymers were determined using thermal gravimetric analysis under a nitrogen atmosphere. Samples were equilibrated at 50 °C and then heated to 500 °C with a heating rate of 10 °C/min. All polymers appear to have an onset of degradation (T_d) over 400 °C (Table) which is typical of Nomex polymers (400-430 °C for neat Nomex).[8] It appears that as the mass % of DDSQ is increased, then T_d also appears to increase. Adding the DDSQ to neat Nomex at a later time during the reaction did not appear to have any affect on T_d.

Features of degradation were also evaluated by observing the % weight loss vs. the temperature and the derivative of the % weight lost and the temperature (Figure 7-10). Even

Table 7-7. Onset of degradation (T_d) of Nomex polymers.

Exp #	Mole % DDSQ	T_d (°C)
P-1	0.0	395
P-2	0.0	408
P-4	0.0	402
P-3	0.0	411
P-5	0.0	408
P-7	1.1	400
P-6	1.1	406
P-8	5.3	406
P-9	5.3	404
P-10	10.2	405
P-12	14.5	403
P-15	22.0	401
P-16	50.0	423
P-17	100.0	444
P-18	1.1 (1 h)	405
P-19	1.1 (3 h)	407
P-20	1.1 (4.5 h)	406

though P-2 and P-3 may only be oligomers according to their M_n, they actually exhibit a much higher T_d than the other polymers. There appear to be two characteristics to the degradation curves, which are emphasized when viewing the derivative of the % weight loss vs. the temperature (Figure 7-10b). For P-18 (0 mass % DDSQ), the % weight loss exhibits a rapid onset at approximately 400 °C and then a maximum at approximately 425 °C. The % weight loss then becomes more gradual until approximately 475 °C where the % weight loss becomes more rapid again, but not as rapid as the initial weight loss. As the mass % DDSQ is increased in the polymer, the initial weight loss is not as rapid, and the first maximum is much lower. At 78.3 mass % DDSQ, the second maximum is higher than the first. At 100 mass % DDSQ, there first

and second maximum appear to have converged. These features demonstrate that the addition of DDSQ increased the degradation properties of neat Nomex.

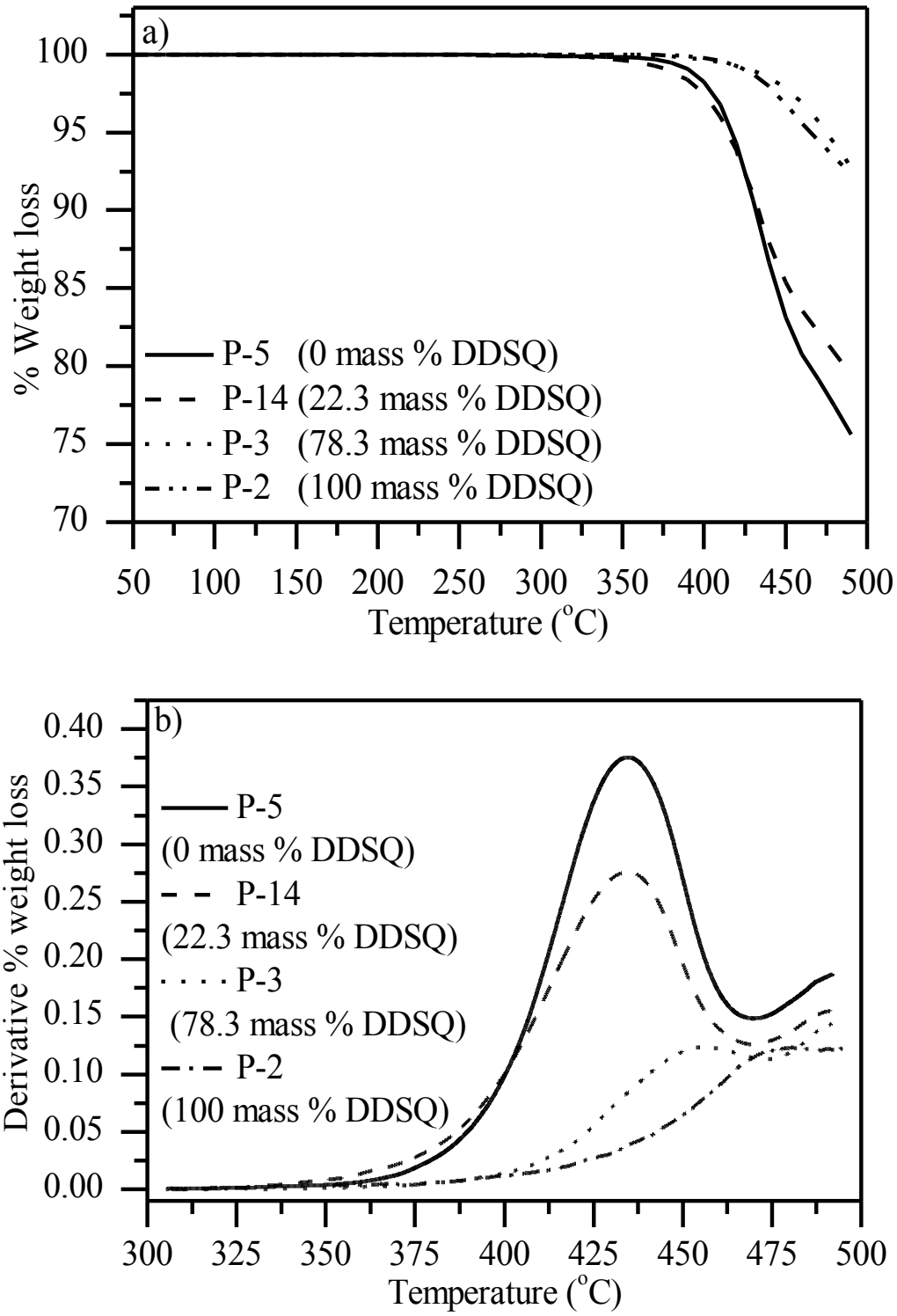

Figure 7-10. TGA analysis of select polymers, (a) degradation (b) derivative of the degradation.

7.2.7 Glass transition and melting temperatures

Differential scanning Calorimetry (DSC) was used to determine he glass transition (T_g) and the melting transition (T_m and ΔH_m) of the polymers. According to the literature, neat Nomex generally has a T_g of approximately 275 °C, and a T_m that is very close to its degradation temperature. From these studies, it appears that as the mass % of DDSQ is increased, then the onset of degradation is decreased. Additionally, the melting transition is decreased and the heat of fusion associated with the melting transition is also decreased.

Table 7-8. T_g and T_m of selected Nomex polymers.

Exp #	Mass % DDSQ	T_g onset	T_m onset	ΔH_m (J/g)
P-3	0	261	411	70
P-4	0	266	408	47
P-5	0	263	404	30
P-7	1.1	268	407	66
P-9	5.3	263	405	16
P-10	10.15	252	404	15
P-12	14.5	256	406	31
P-15	22.26	243	401	11
P-18	1.1	243	408	35
P-19	1.1	265	410	73
P-20	1.1	262	407	19

7.2.8 Films

Films were made for some of the polymers. Films were made using three different methods: (1) slow evaporation, (2) vacuum oven, and (3) UV lamp. For method 1, P-4 (0 mass % DDSQ) was dissolved in a minimal amount of NMP, and added to a glass, evaporating dish. Solvent was allowed to evaporate, and a white solid appeared (Figure 7-11a). The films were not transparent. For method 2, polymer was dissolved in minimal NMP, and the solution dripped onto glass slides. The slides were placed in a vacuum oven at 80 °C for two hours. Some of the

films were transparent (Figure 7-11b). However, the thickness of the films was not well controlled, and therefore the transparency of the films varied. For method 3, from left to right, P-12 (14.5 mass % DDSQ), two slides of P-15 (22.3 mass % DDSQ), and P-4 and P-5 (0 mass % DDSQ) were dissolved in minimal NMP and then placed on aluminum foil. The thickness of the films were controlled to 100 μm and left under a UV lamp for 20 h. These films were all transparent.

a)

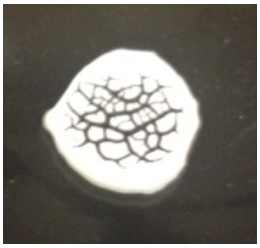

b)

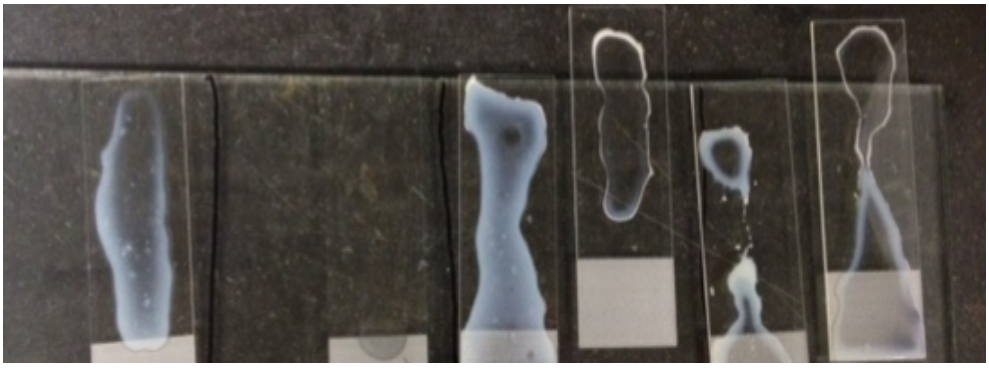

c)

Figure 7-11. Films made from select polymers (a) slow evaporation, (b) vacuum oven, and (c) UV lamp.

7.2.9 Concluding remarks on DDSQ-based Nomex

DDSQ-based Nomex was synthesized and inherent viscosity was determined. From the inherent viscosity studies, it appears that the polymers have high MW, but further analyses such as determining the MW using a high temperature GPC with NMP need to be carried out. Polymers were also characterized according to their characteristics. These features demonstrate that the addition of DDSQ increased the degradation properties of neat Nomex. Additionally, the melting transition decreased and the heat of fusion associated with the melting transition is also decreased. Films could be made with these polymers. Once accurate MW are determined, mechanical testing can be carried out to determine if these properties are improved from the DDSQ macromer.

7.3 Ionic Liquid

7.3.1 Introduction

Properties of ionic liquids (ILs) can be enhanced through the incorporation of nanoparticles such as silica and metal supporting oxides. Cage-like, monofunctionalized silsesquioxanes have been used as IL-supporting substrates with the intention of applying them as electrolytes in fuel cells.[9] These silsesquioxane-based ILs have demonstrated improved thermal properties such as decreasing the melting temperature of ionic salts such that they become ILs.[10] Furthermore, they improved the thermal stability of salts that had intrinsically low decomposition temperatures. To date, no difunctionalized ionic liquids have been synthesized, which would provide a new series of IL-based materials that have the added feature of geometrical isomers.

7.3.2 Solvents and reagents

Tetrahydrofuran (THF) and iodomethane were purchased from Sigma-Aldrich. Iodomethane was filtered through silica gel prior to use. SiliaFlash ® P60 Silica gel was purchased from Silicycle Ultra Pure Silica Gels (Quebec City, Quebec, Canada). Potassium carbonate was purchased from Spectrum (Canton, Michigan) and used as received. Solvents used for liquid chromatography-mass spectroscopy were aqueous ammonium acetate and acetonitrile, obtained as HPLC-grade from Sigma Aldrich and used as received.

7.3.3 Synthesis of ionic liquid (6a)

DDSQ Ionic liquid (**6a**) was synthesized according to Scheme 7-3. Under a nitrogen atmosphere, iodomethane (0.568 g, 4 mmole) was added dropwise to a stirring solution of

compound **3a** (0.334 g, 0.25 mmole), potassium carbonate (0.276 g, 2 mmole), and THF (11 mL) at room temperature (25 °C). After two weeks, a white precipitate occurred, which was removed by filtration and the supernatant was dried under vacuum. The supernatant solid was then extracted with acetonitrile and water to isolate the product. Acetonitrile was removed under vacuum and the product was dried under nitrogen. ^{1}H NMR, δ: 8.04-7.01 (40 H, overlapping multiplets), 3.30 (18 H, N-$(CH_3)_3$, multiplet), 0.55 (6 H, Si-CH_3, multiplet) (Figure 7-12a). When not enough MeI is used, then the ionic nature does not fully form (Figure 7-13). ^{1}H NMR, δ: 8.15-6.73 (40 H, overlapping multiplets), 3.35 (18 H, N-$(CH_3)_3$, multiplet), 2.63 (12 H, N-$(CH_3)_3$, multiplet), 0.57 (6 H, CH_3, multiplet), 0.47 (6 H, CH_3, multiplet) (Figure 7-12b).

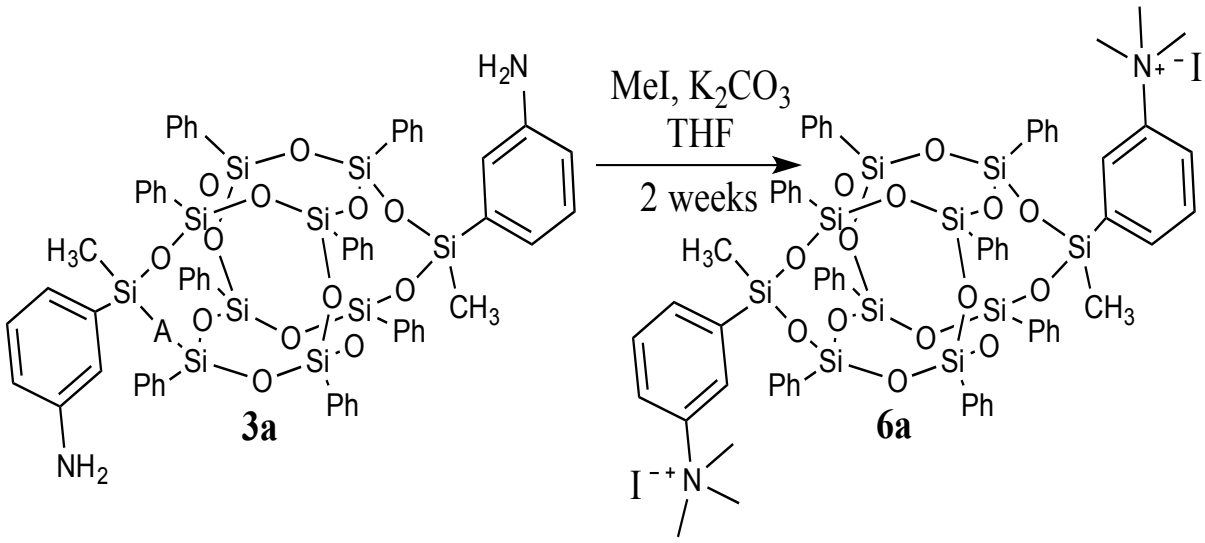

Scheme 7-3. Synthesis of IL, **6a**.

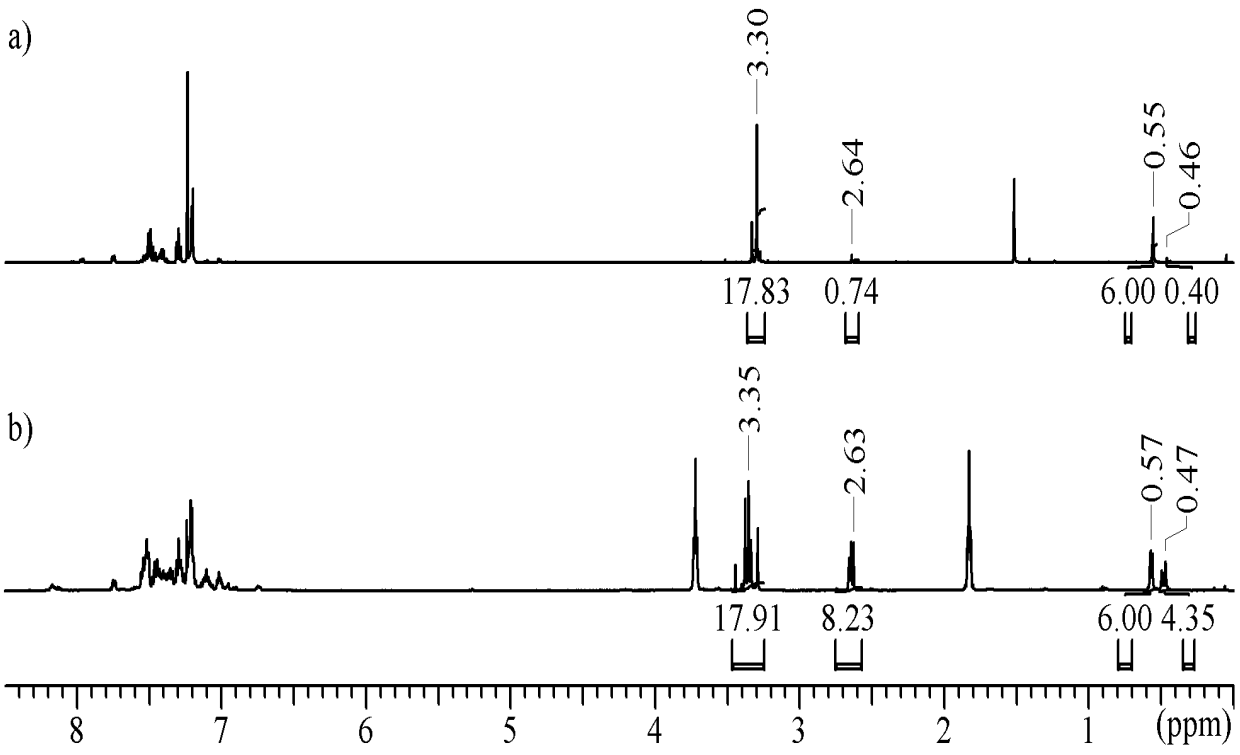

Figure 7-12. ^{1}H NMR of (a) **6a** and (b) **7a**; resonances at 3.72 and 1.83 ppm are residual THF.

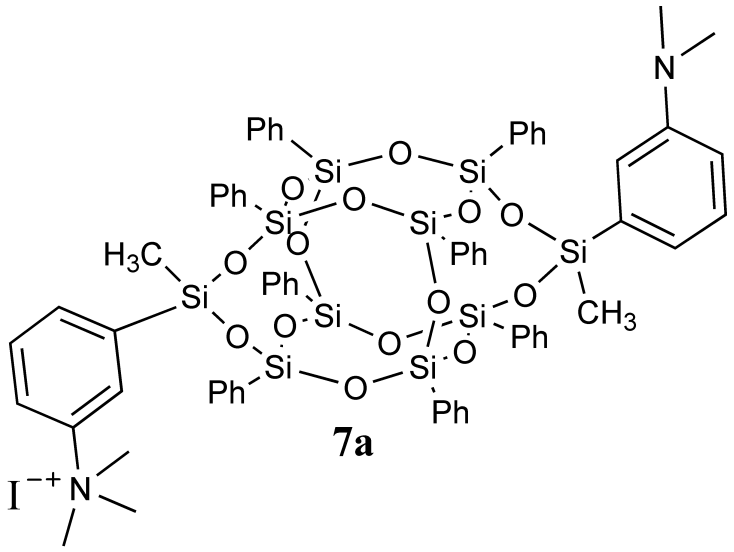

Figure 7-13. Product without enough MeI.

7.3.4 Mass spectroscopy

In order to confirm that the structures were accurate, the samples were analyzed using mass spectroscopy. Mass spectrometry analyses were conducted using a Waters Xevo G2-S QToF (Waters, USA) mass spectrometer equipped with Acquity UPLC chromatography system. All mass spectrometric analyses and data processing were accomplished using MassLynx v. 4.1 software.[11]

Flow injection analysis without chromatography using electrospray in positive ionization mode was performed to acquire high-resolution mass spectra of compound **6a**. Dominant ions are shown at m/z 1336.17, which is consistent with the expected protonated molecular ions, ($[M+H^+]$). Protonated molecular ions are expected since the sample was analyzed under positive ionization conditions. These m/z ions are singly charged**,** and so the m/z value is consistent with the molecular mass, as the value of z (number of charges) equals 1. Other ions are also seen at lower intensities (m/z 668.59). The fact that the ^{13}C ions (669.09, 669.59, ...) for this ion are 0.5 Da higher on the m/z scale than the ^{12}C ions is an indication that z = 2, and hence the sample ions are doubly charged. So, this compound is generating both singly ($[M+H]^+$) and doubly ($[M+2H]^{2+}$) charged ions upon electrospray ionization in positive mode.

7.3.5 Concluding remarks on DDSQ-derived ionic liquids

Difunctionalized (doubly charged) ILs based on DDSQ-were successfully synthesized and characterized. Single ionized DDSQ resulted when not enough MeI was added to the reaction. ^1H NMR spectra and mass spectroscopy results indicate the desired product was produced and there is minimal byproduct without purification. These DDSQ will benefit from

conductivity studies for the potential use as electrolytes in fuel cells. The added feature of the geometrical isomers could potentially provide these DDSQ with distinct characteristics as IL materials that can be used in specific applications.

NOTES

NOTES

(i) Like compound **3d**, compound **5d** is actually a mixture of the following compounds: 25 % **5a**, 25 % **5c**, 50 % **5d** as a result of the statistics of the synthetic procedure for compound **3d** that is highlighted in chapter 3.

(ii) One singlet represents the *cis* isomer protons (CH_3, 3H), and the other represents the *trans* isomer protons (CH_3, 3H).

(iii) There is one singlet representative of the methyl protons (CH_3) for each of the following geometries: *cis* meta, *trans* meta, *cis* para, *trans* para, and the reamining two singlets are representative of the *cis* and *trans* isomers of the structure that has 1 meta-aminophenyl and 1 para-aminophenyl on a single DDSQ.

REFERENCES

REFERENCES

(1) Seurer, B.; Vij, V.; Haddad, T.; Mabry, J. M.; Lee, A. *Macromolecules* **2010**, *43*, 9337.

(2) Vij, V.; Haddad, T. S.; Yandek, G. R.; Ramirez, S. M.; Mabry, J. M. *Silicon* **2012**, *4*, 267.

(3) Simone, C. D.; Scola, D. A. *Macromolecules* **2003**, *36*, 6780.

(4) TA Rheology advantage data analysis version 5.8.0; Waters LLC: New Castle, Delaware, 2002.

(5) Chen, J.; Zuo, H.; Fan, L.; Yang, S. *High Performance Polymers* **2009**, *21*, 187.

(6) Zuo, H. J.; Chen, J. S.; Yang, H. X.; Hu, A. J.; Fan, L.; Yang, S. Y. *Journal of Applied Polymer Science* **2008**, *107*, 755.

(7) Oishi, Y.; Kakimoto, M. A.; Imai, Y. *Macromolecules* **1988**, *21*, 547.

(8) Garcia, J. M.; Garcia, F. C.; Serna, F.; de la Pena, J. L. *Progress in Polymer Science* **2010**, *35*, 623.

(9) Cardiano, P.; Lazzara, G.; Manickam, S.; Mineo, P.; Milioto, S.; Lo Schiavo, S. *European Journal of Inorganic Chemistry* **2012**, 5668.

(10) Jeon, J.-H.; Tanaka, K.; Chujo, Y. *Rsc Advances* **2013**, *3*, 2422.

(11) MassLynx version 4.1; Waters LLC: New Castle, Delaware, 2012.

APPENDICES

APPENDIX A.

SYNTHESIS OF MONOMERS

This appendix addresses the following key features that were not covered in chapter 3: (1) deprotection analysis and (2) additional features and further remarks on synthesis.

A. Synthesis of Monomers

A.1 Deprotection analysis

Acidified methanol with diethyl ether was used for the deprotection of the silylated amines (Scheme A-1). A general rule of thumb when considering the compatibility of an acid or base with the silsesquioxane cage is: anything that can etch glass can also break down the cage.

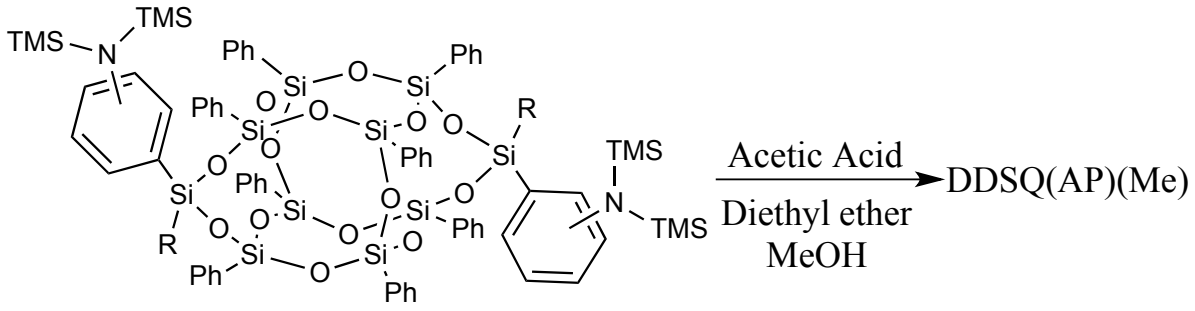

Scheme A-1. Deprotection of aminophenyl groups.

Thus, a weak acid (acetic acid) was chosen for the deprotection. Since too much acetic acid may also break down the cage, different solvent qualities and acid concentrations were evaluated to determine the best combination for deprotection (Table A-1). The aminophenyl moiety was completely deprotected for all conditions tested. The concentrations of acetic acid (HoAc) and DDSQ vs. the % yield were evaluated for optimal conditions of deprotection (Figure A-1a,b).

Table A-1. Deprotection analysis.

	X_{DDSQ}	X_{AA}	X_{DEE}*	X_{MeOH}	conc. AA	conc. DDSQ	% yeild
	2.08E-03	4.91E-04	9.62E-03	9.88E-01	7.20E-04	5.43E-02	94
	2.10E-03	5.01E-04	9.62E-03	9.88E-01	7.34E-04	5.49E-02	94
	1.86E-03	8.24E-04	1.91E-02	9.78E-01	1.19E-03	4.80E-02	85
	2.11E-03	4.91E-04	9.62E-03	9.88E-01	7.20E-04	5.51E-02	84
	1.66E-03	7.19E-04	1.40E-02	9.84E-01	1.05E-03	6.54E-02	81
	1.79E-03	6.47E-04	1.28E-02	9.85E-01	9.43E-04	7.07E-02	80
	1.86E-03	6.59E-04	1.91E-02	9.78E-01	9.52E-04	4.79E-02	75
Avg.	1.92E-03 ± 1.75E-04	6.19E-04 ± 1.30E-04	1.34E-02 ± 4.23E-03	9.84E-01 ± 4.24E-03	9.01E-04 ± 1.84E-04	5.66E-02 ± 8.53E-03	85 ± 7

* DEE: diethyl ether

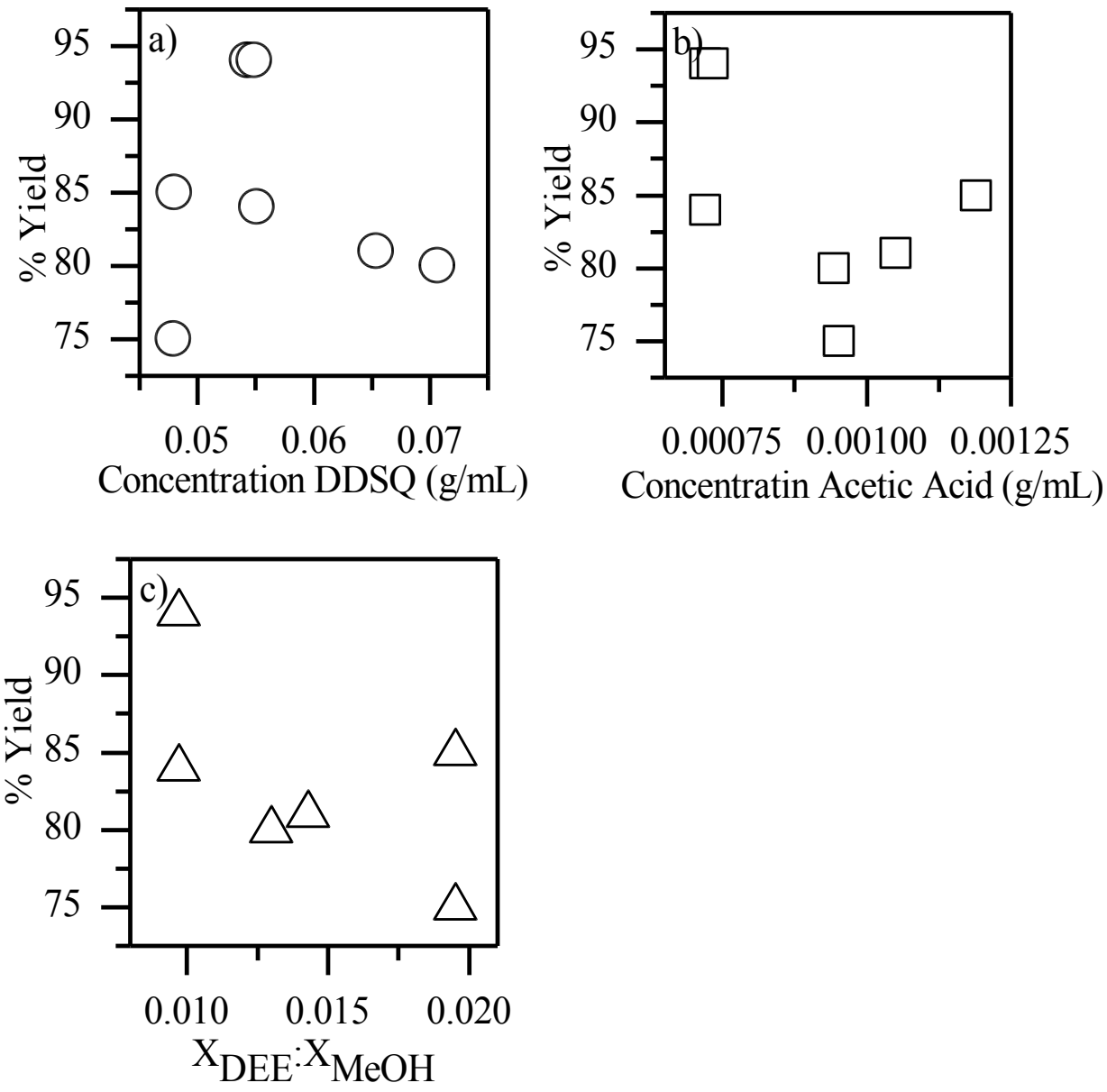

Figure A-1. Deprotection analysis, while investigating the concentrations of (a) DDSQ and (b) acetic acid, and (c) the ratio of X_{DEE} : X_{MeOH} vs. % yield.

Generally, as the concentration of AA and DDSQ is increased, the % yield is decreased. This was expected since too much AA could potentially break down the silsesquioxane cage. Additionally, the ratio of the mole fraction of diethyl ether and methanol vs. % yield were also investigated (Figure A-1c). In general, as this ratio increases the % yield decreases. Solid DDSQ is slightly soluble in diethyl ether and not soluble in methanol. Thus, it would be expected that as

the solubility of the DDSQ is increased (a larger ratio) the silsesquioxane cage has more opportunity to interact with the AA. However, it is difficult to formulate an explicit conclusion since there are multiple changing variables, and only one or two are considered in each graphical analysis (Figure A-1). Furthermore, the scatter in the plots may also be caused by experimental error such as: measurement of masses and solvent volume, the exact value of the room temperature, filtration methods, and flask transfer. Determining an exact trend in the data would require additional experimentation where one variable would be adjusted while all others were held constant. However, after this analysis was completed, over 20 deprotection experiments were successful when the average conditions were applied and resulted within the range of the average % yield. Therefore, the average conditions are sufficient for deprotection of the aminophenyl group.

A.2 Additional features and further remarks on synthesis

The synthetic procedures for compounds **3a** and **c** are well established[1,2] and provide high yields. However, the synthetic procedure for compound **3b** provides low yields and additional experimentation was performed in order to determine how to improve the yield. Additionally, the synthetic procedure for compound **3d** has only been attempted two times with varying yield results. For compound **3b**, the boiling point of the trichlorocyclohexylsilane (90 °C / 10 mmHg) was much higher than methyltrichlorosilane (66 °C / 760 mmHg), which made excess trichlorocyclohexylsilane more difficult to remove. However, this matter was easily resolved by using stoichiometric equivalents of trichlorocyclohexylsilane and 3-[bis(trimethylsilyl)amino] phenyl-magnesium chloride. Additionally, the boiling point of the dichlorocyclohexylsilane product (> 135 °C) was much higher than the methyldichlorosilane product (≈ 75-95 °C).[i] Such a high boiling point required the flask to be heated at temperatures

above 200 °C, which was difficult with standard oil baths. Additionally, any unreacted trichlorocyclohexylsilane was difficult to separate. Therefore, Kugelrohr distillation was used, which improved the yield and the purity.

The synthetic procedure for the reaction between dichlorocyclohexylsilane and Ph_8tetrasilanol had the lowest yield. Several parameters were varied in an attempt to improve the yield (Table A-2). Changing the solvent from THF to toluene actually decreased the yield to approximately 5 %. Using additional triethylamines also decreased the yield to approximately 20 %. Increasing the reaction time, increased the less soluble impurity, or the impurity that was removed by washing with toluene (Figure A-2).[ii] The more soluble impurity was removed by washing with diethyl ether. Refluxing the reaction at 105 °C increased the mass of the product, and deprotected the amines, which provided one less step during the work-up procedure.

Table A-2. Parameters varied in an attempt to improve the yield of the dichlorocyclohexylsilane to Ph_8tetrasilanol coupling reaction (Compound **3b**).

Parameter varied	Notes
THF to toluene	Decreased yield to 5 %
Doubled triethylamines	Decreased yield to 20 %
Increasing reaction time	Increased less soluble impurity
Refluxing at T = 105 °C	Deprotected amines and increased less soluble impurity

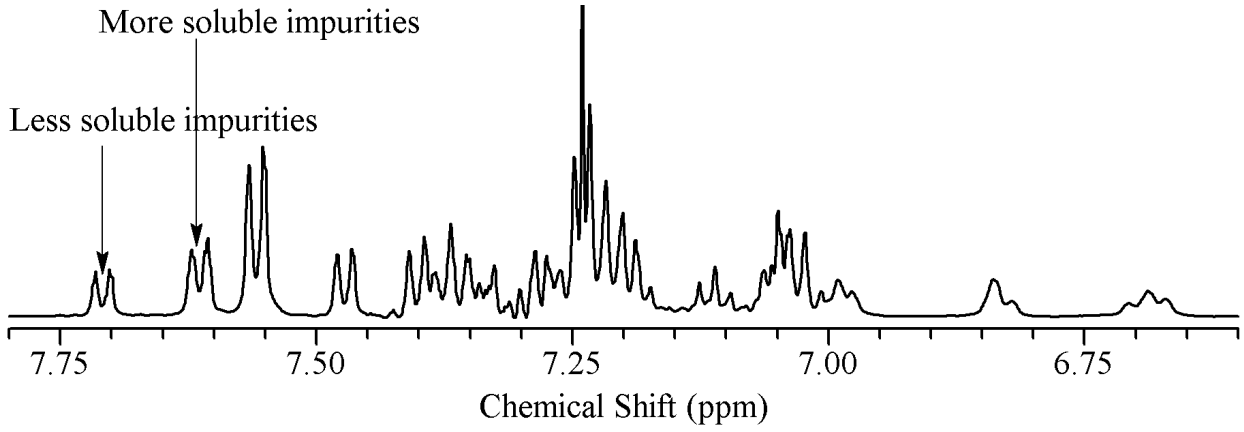

Figure A-2. Compound **3b** impurities.

However, since the less soluble impurity was also increased, it was difficult to tell whether the increase in the mass was an increase in yield or an increase in impurities. It was also difficult to tell if the increase in the less soluble impurity was a result of the increased reaction time, or the heat of the reflux. Thus with the increased impurity, refluxing was not a viable method for synthesis.

It was also found that the yield of compound **3b** might not actually be as low as reported, and the product is actually stuck in solution. During experimentation, it was recognized that the product was very difficult to precipitate from solution. For several of the products, solvent washing was attempted. Toluene and other higher boiling solvents were added to the solution, and then removed by vaccum. Afterwards the product was precipitated and isolated by filtration. The filtrate solvent was then removed by vaccum until a viscous slurry remained. This slurry was precipitated in anti-solvent and more product was recovered and isolated by filtration. For some experiments, repeating this procedure with the new filtrate solvent again yielded additional product. Furthermore, leaving the filtrate solvent for several days to weeks and then attempting to precipitate also yielded additional product. Thus, a better method to precipitate the product must be devised and it also must be determined if the product is low yielding or stuck in solution.

The synthetic scheme for compound **3d** was attempted three times. The first time it was very low yielding (≈ 50 %) and had similar impurities to compound **3b**. The second time the addition of the dichlorosilane was slower, the yield was improved to 92 % and there were fewer impurities.[iii] The third time, the yield was again approximately 50 % initially, but more product was recovered with solvent washing. Additionally, the remaining filtrate solvent after solvent washing shows product in the ^{1}H NMR spectrum. However, this solution has been saved because

attempts to recover this product have so far been unsuccessful. Again, a better method to precipitate the products, specifically compounds **3b** and **d**, needs to be devised.

NOTES

NOTES

(i) This is not measured at a certain pressure, but is based on the Schenck line and vaccuum pump conditions. The reported values are according to the set-up used in this laboratory, but are reported for future work.

(ii) Refer to chapter 3 for information on the solvent washing.

(iii) Is is of interest to try this method with compound **3b**.

REFERENCES

REFERENCES

(1) Seurer, B.; Vij, V.; Haddad, T.; Mabry, J. M.; Lee, A. *Macromolecules* **2010**, *43*, 9337.

(2) Vij, V.; Haddad, T. S.; Yandek, G. R.; Ramirez, S. M.; Mabry, J. M. *Silicon* **2012**, *4*, 267.

APPENDIX B.

SPECTROSCOPY

This appendix addresses the following key features that were not covered in chapter 4:

(1) chemical shift reagents, (2) T1 analysis, (3) isolating protected amines, (4) analyzing NMR spectra of compound **3d**, and (5) quantifying **3d** using Liquid-chromatography/mass spectroscopy (LC/MS).

B. Spectroscopy

B.1 Chemical shift reagents

For integration purposes, it was of interest to resolve the overlapping proton multiplets (δ_H 7.47: H-3b and H-3b´ and δ_H 7.50: H-1acR and H-1acR´) of compound **3c** using tris(6,6,7,7,8,8,8-heptafluoro-2,2-dimethyl-3,5-octanedionate)europium (III) hydrate, or $Eu(FOD)_3$, as a shift reagent (Figure B-1). $Eu(FOD)_3$ complexes with basic electrons, such as the aminophenyl group, and shifts associated resonances to a lower field with a small amount of line broadening (Figure B-2). Accordingly, protons nearest the aminophenyl group (H-3 protons)

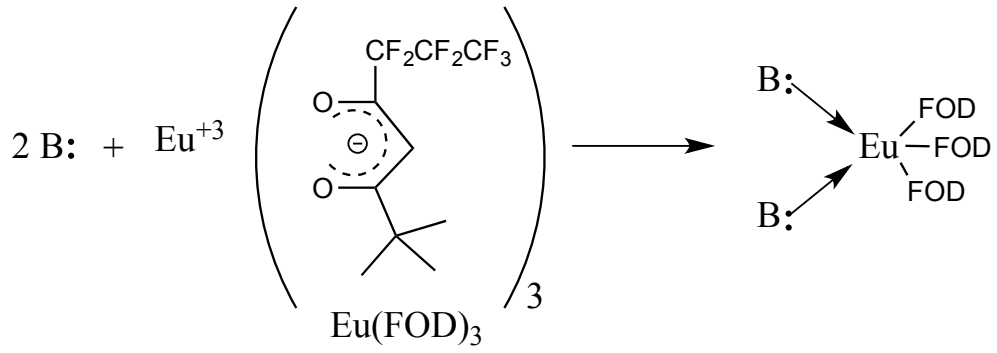

Figure B-1. Europium complex, where B: is the aminophenyl group.

were the most affected. As the content of $Eu(FOD)_3$ was increased, the proton multiplet that was originally at δ_H 7.47 gradually shifted to downfield, while the proton multiplet originally at δ_H 7.50 remained virtually unaffected. When the ratio of **3c** to $Eu(FOD)_3$ was 4:1 (Figure B-2c), the proton multiplet that was originally at δ_H 7.47 no longer exhibited overlap with other resonances. Multiplets that were originally at δ_H 7.55 and 7.50 could then be used for quantification, similar to the quantification methods for compounds **3a** and **b**. However, the proton multiplet that was originally at δ_H 6.53 (H-3a and H-3a´) was also shifted downfield. Initially, this resonance

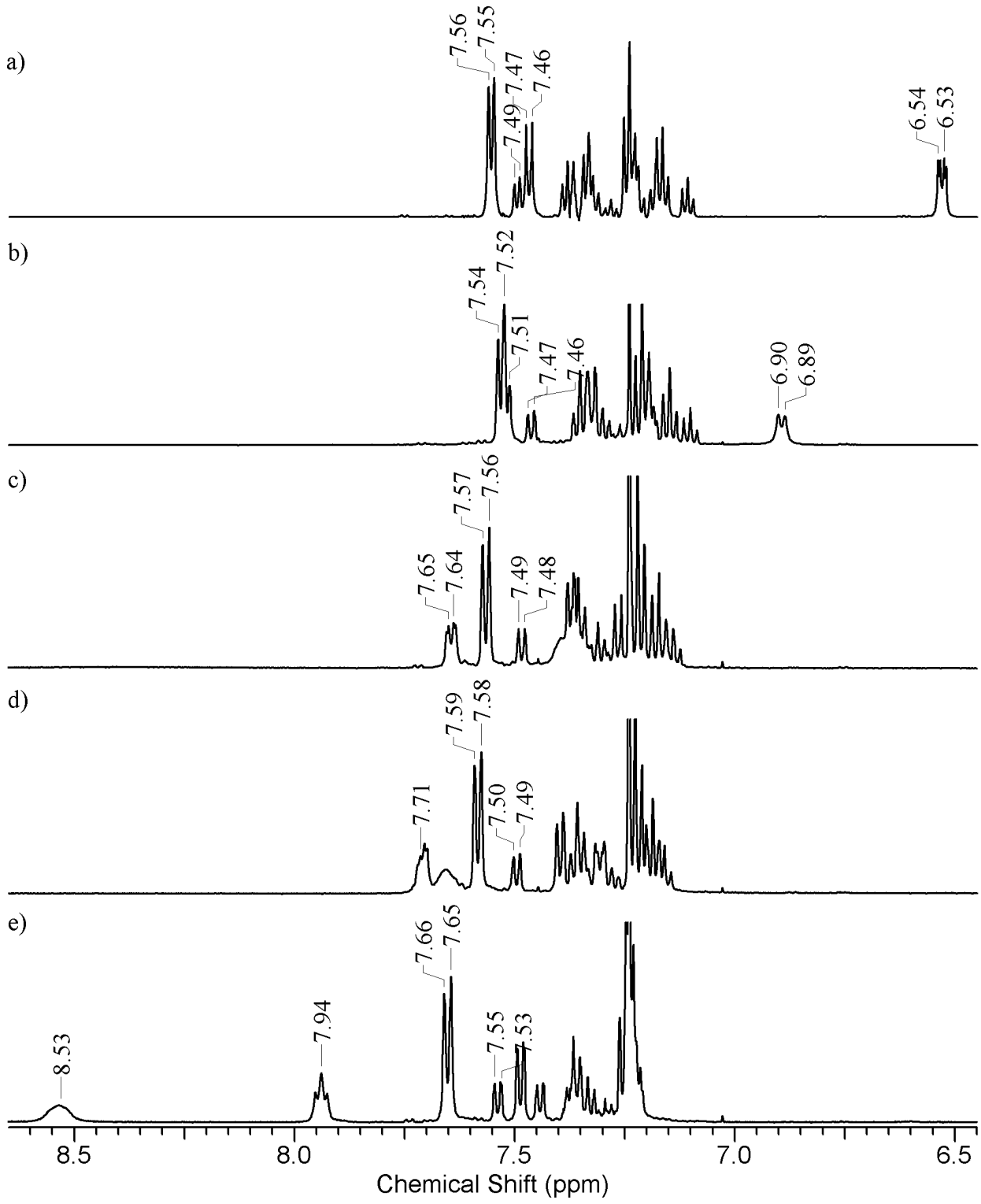

Figure B-2. ^{1}H NMR spectra of increasing content of europium; reported as Compound **3c** : $Eu(FOD)_3$; (a) 1 : 0, (b) 10 : 1, (c) 4 : 1, (d) 2 : 1, (b) 1 : 1.

exhibited no signal overlap. Yet, with increasing content of $Eu(FOD)_3$, it exhibited signal overlap that, again, complicated the capability of determining the percentage of *cis* isomer present in samples of **3c**. When the ratio of **3c** to $Eu(FOD)_3$ was 4:1 (Figure B-2c), it exhibited signal overlap between δ_H 7.35 and 7.45, and when the ratio of **3c** to $Eu(FOD)_3$ was 2:1 (Figure B-2d), it exhibited signal overlap between 7.59 and 7.71. Between these ratios, this resonance will exhibit overlap with multiplets used for quantification. However, when the ratio of **3c** to $Eu(FOD)_3$ was 1:1 (Figure B-2e), it no longer exhibited overlap and shifted downfield to δ_H 8.53. Therefore, the best ratios of **3c** to $Eu(FOD)_3$ for quantification purposes are 4:1 and 1:1. If the content of $Eu(FOD)_3$ is increased past a 1:1 ratio, quantification may still be possible, but line broadening must be considered. Line broadening increases with increasing content of $Eu(FOD)_3$.

B.2 T_1 analysis

A T_1 analysis for both the ^{29}Si and ^{1}H atoms was performed on compound **3a**. It is anticipated that all other compounds have similar T_1 values. Actual T_1 values for ^{29}Si NMR spectra can be seen in Table B-1. The indexes of interest are 3-5. Actual T_1 values for ^{1}H NMR

Table B-1. ^{29}Si T_1 analysis; peaks can be seen in FigureII-3a.

Peak	Frequency (ppm)	T_1	Error
1	-30.6	17.14	0.1597
2	-78.4	59.81	0.932
3	-79.4	50.14	2.469
4	-79.6	54.93	1.273
5	-79.8	54.24	1.931

Table B-2. ^{1}H T_1 analysis; peaks can be seen in FigureII-3b.

Peak	Frequency (ppm)	T_1	Error
1	8.0286	2.401	0.01836
2	8.01453	2.444	0.009801
3	7.95594	2.328	0.05108
4	7.94188	2.358	0.04495
5	7.85516	3.515	0.05858
6	7.83992	3.314	0.06761
7	7.82469	3.26	0.03582
8	7.81766	3.172	0.06714
9	7.80242	3.202	0.115
10	7.78133	3.343	0.1491
11	7.76609	3.117	0.03866
12	7.76375	3.02	0.05968
13	7.75672	2.491	0.03449
14	7.74266	2.533	0.04013
15	7.72859	3.083	0.1194
16	7.71336	3.696	0.1343
17	7.70984	3.914	0.1323
18	7.69695	7.818	0.1534
19	7.68875	7.784	0.6443
20	7.68641	6.681	0.8989
21	7.68055	1.766	0.08184
22	7.66648	2.074	0.01171
23	7.65125	2.125	0.01925
24	7.63836	2.027	0.03045
25	7.62312	2.012	0.09292
26	7.57273	2.062	0.02297
27	7.57039	2.063	0.02349
28	7.5575	2.042	0.01133
29	7.54344	2.024	0.02645
30	7.49187	1.924	0.03527
31	7.48484	2.134	0.08385
32	7.47781	1.925	0.01734
33	7.46492	1.966	0.01806
34	7.44968	1.997	0.02583
35	7.40984	2.204	0.02388
36	7.40046	2.228	0.04198
37	7.39461	2.24	0.02957
38	7.27859	2.583	0.03189
39	6.99616	2.508	0.05217
40	6.98913	2.551	0.04157
41	6.98093	2.545	0.04397

spectra can be seen in Table B-2. The relaxation delay for the 1H NMR spectra used for quantification was 32 seconds. Therefore, all the T1 values were met. 29Si and 1H NMR spectra are shown again, below (Figure B-3).

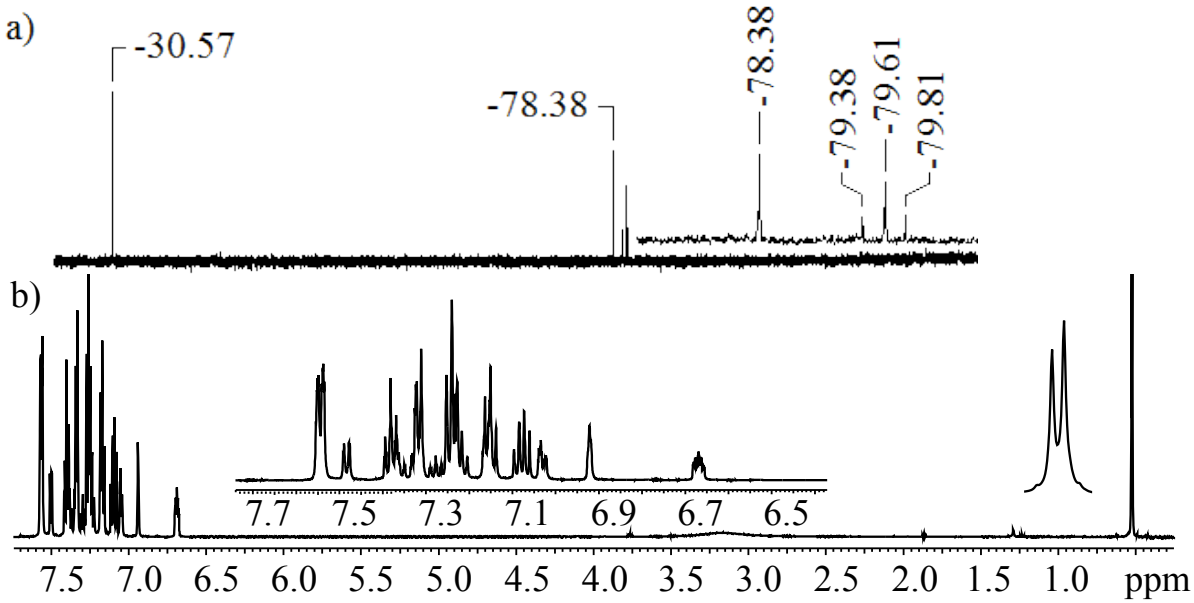

Figure B-3. Spectra of compound **3a** (a) ^{29}Si NMR spectrum and (b) ^{1}H NMR spectrum.

B.3 Isolating protected amines

The N-silylated amines are less reactive than the deprotected aminophenyl group. Therefore, it was of interest to isolate the silylated amines prior to deprotection and determine if the ^{1}H NMR spectrum could be evaluated to the same degree as the deprotected amines. However, this was not possible since the line broadening of the N-silylated amines in the ^{1}H NMR spectrum was too wide (Figure B-4a). Additionally, the resonances representing *cis* and *trans* isomers were no longer distinct in the ^{29}Si NMR spectrum (Figure B-4b).

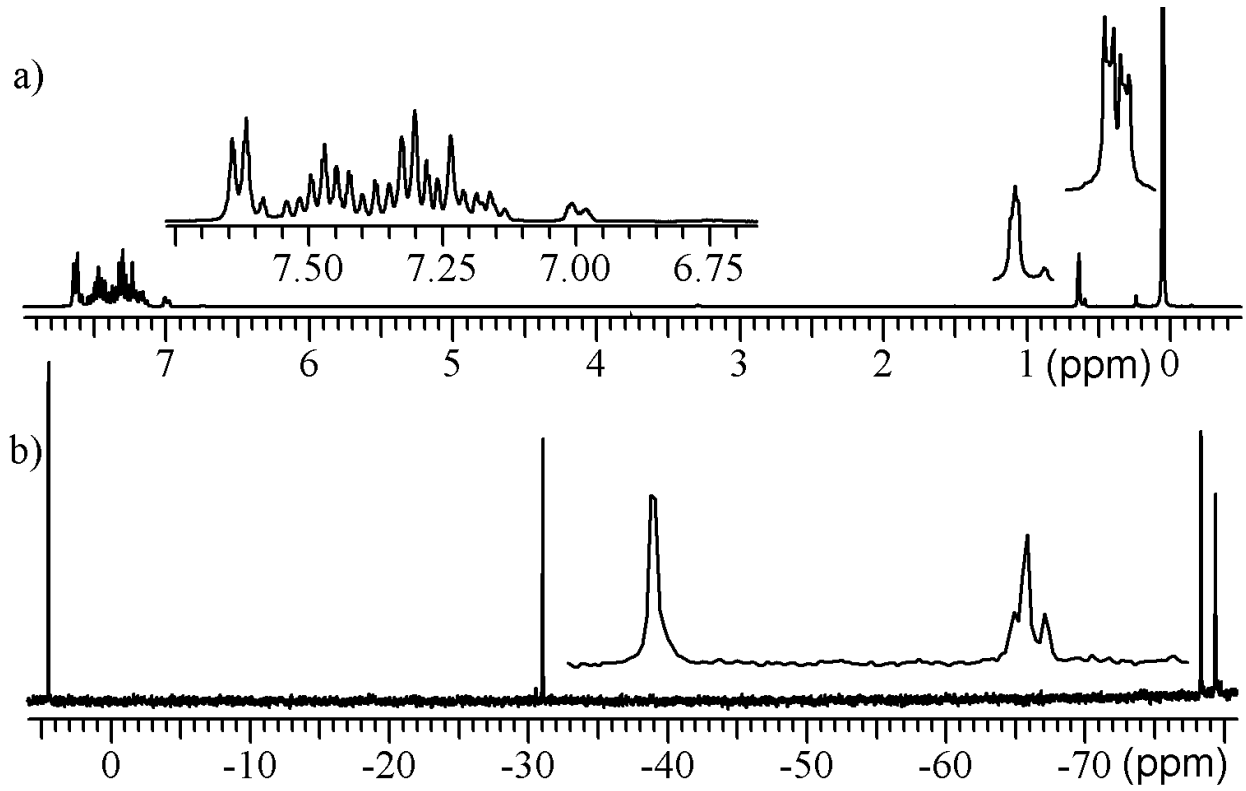

Figure B-4. N-silylated amines (a) ^{1}H NMR spectrum and (b) ^{29}Si NMR spectrum.

B.4 Analyzing NMR spectra of compound 3d

Compound **3d**, was comprised of an AP moiety with a combination of meta- and para-isomers. However, the synthetic procedure is anticipated to form 25 % compound **3a** (all meta), 25 % compound **3c** (all para), and 50 % compound **3d** (one side meta and one side para), based on statistics. The ^{1}H NMR spectrum of compound **3d** appears to be too convoluted to quantify the AP moieties, and additionally to quantify the ratio of *cis* and *trans* isomers in a sample using the methods from chapter 4 (Figure B-5). The location of the resonances unique to the meta- and para- AP moieties is observed in the ^{1}H NMR spectrum. However, it cannot be determined whether the meta-AP moiety is attached to a DDSQ with another meta-AP moiety, or a para-AP moiety since there is theoretically 50 % meta- and 50 % para-AP moieties. Furthermore, the

location of the meta- or para-resonance does not appear to be affected by the other AP moiety within the same structure. To clarify, a structure that is comprised of both meta- and para-AP appears to have the same ^{1}H NMR chemical shifts for each meta- and para- AP since there are no additional resonances in the ^{1}H NMR spectrum.

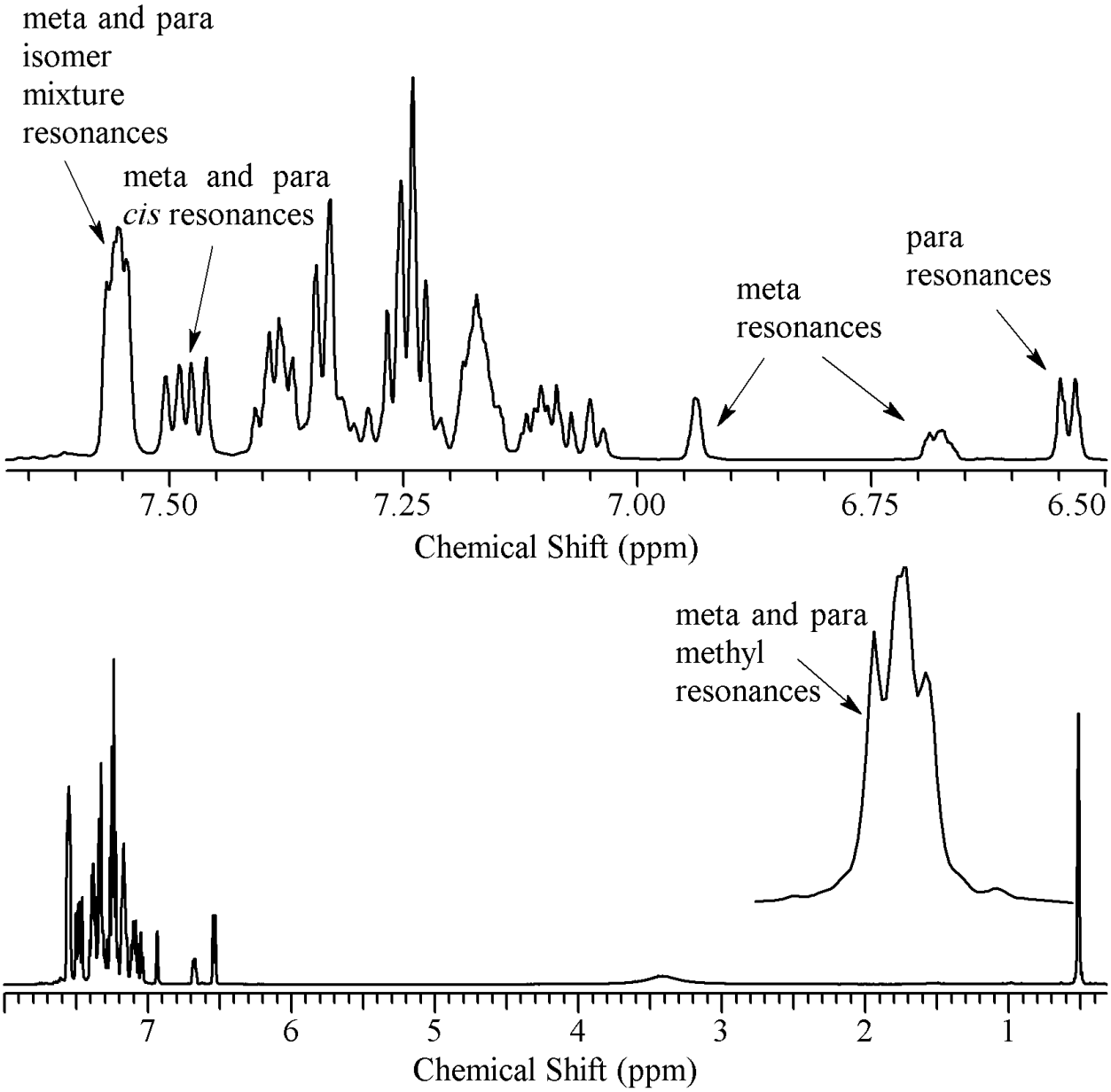

Figure B-5. ^{1}H NMR spectrum of compound **3d**.

The ^{29}Si NMR spectrum of compound **3d** was also examined in more detail (Figure B-6). From this spectrum, it is apparent that compound **3d** was produced. There are four resonances within the range unique to D-group silicon atoms, δ: -29.96, -29.99, -30.58, and -30.61 (Figure B-6a). According to the ^{29}Si NMR spectra in chapter 4, there is only one resonance representative for the D-group silicon atoms for compound **3a** (δ: -30.57) and one resonance for compound **3c** (δ: -29.73). For the ^{29}Si NMR spectrum of compound **3d**, there are two resonances in each of these areas. This indicates that there are two distinct D-group silicon atoms for each para- and meta- AP moiety in this range. Therefore, the D-group silicon atoms that have meta-moieties on both sides of the DDSQ (**3a**) are represented by one resonance (2 Si), and the D-group silicon atoms that have para-moieties on both sides of the DDSQ (**3c**) are represented by one resonance (2 Si). The D-group silicon atoms that have one para- *and* one meta-moiety on each side of the DDSQ (**3d**) are represented by two distinct resonances; one for the D-group silicon atom attached to the para-moiety and one for the D-group silicon atom attached to the meta-moiety. Each of these resonances would be equivalent to 1 Si, which is half as many as the ^{29}Si NMR resonances for compounds **3a** and **3c** in this region. However, since there is twice as much of compound **3d** statistically, all four resonances are anticipated to integrate to the same relative value. From the ^{29}Si NMR spectrum, it is apparent that all four regions are near equivalent, thus it can be said that compound **3d** was produced.

The region of the ^{29}Si NMR spectrum that represents the T-group silicon atoms appears to be more convoluted (Figure B-6b). There are two resonances representative of the external T-group silicon atoms (δ: -78.38 and -78.49). For compounds **3a** and **3c**, there is only one

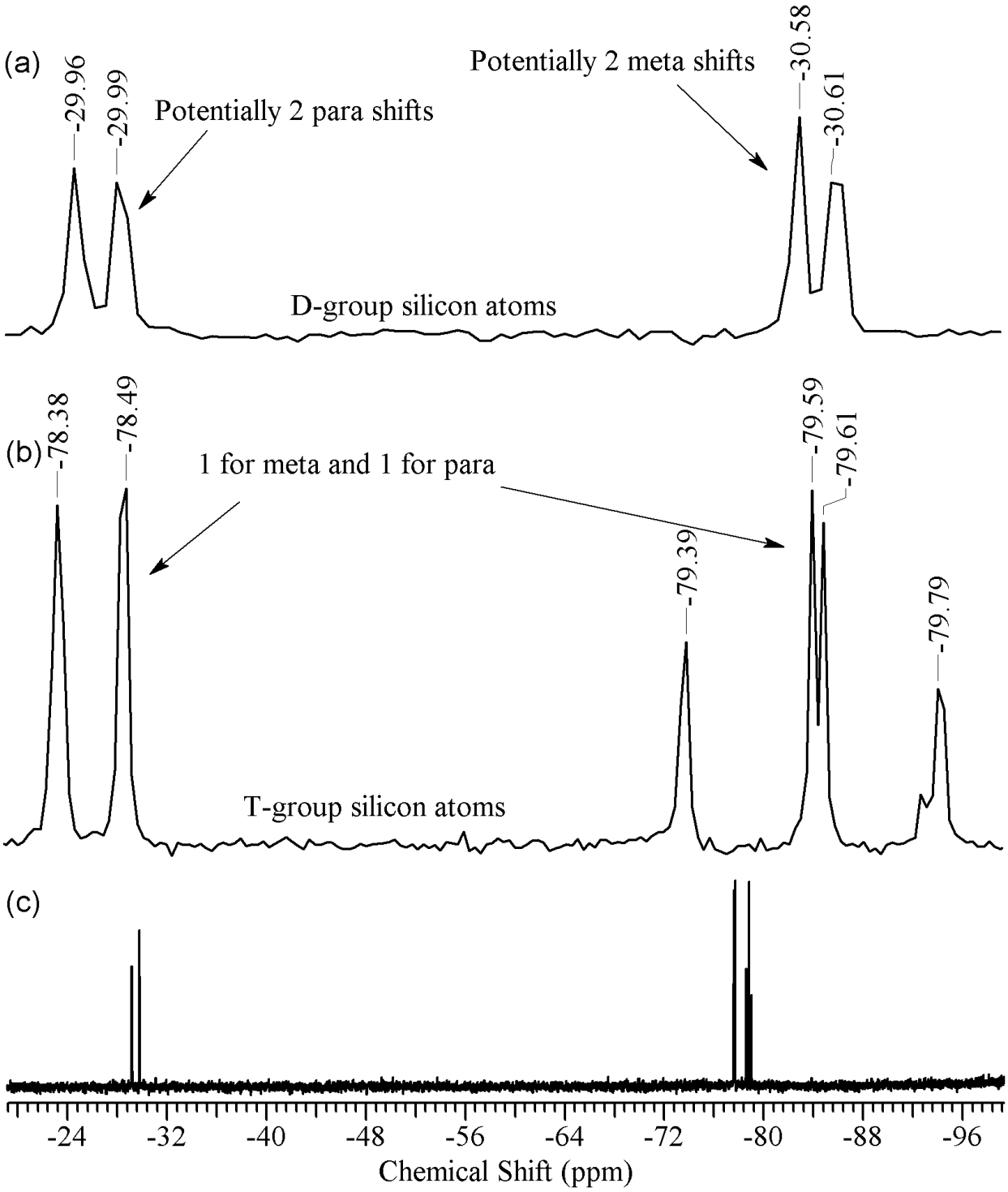

Figure B-6. ^{29}Si NMR spectrum of compound **3d**; (a) D-group silicon atoms, (b) T-group silicon atoms, and (c) whole spectrum.

resonance in this region for each compound (δ: -78.38 and -78.24, respectively). Therefore, there are two feasible scenarios for the resonances in this region of compound **3d**. The first being that one resonances is indicative of all external T-group silicon that are near a meta-moiety and the other resonances is indicative of all external T-group silicon that are near a para-moiety. It is equally possible that one of these resonances is indicative of the external T-group silicon of *both* compounds **3a** and **3c**, while the other resonance is indicative of the external T-group silicon of compound **3d**. The same argument can be made for the internal T-group silicon atoms representing the *trans*-isomers, δ: -79.59 and -79.61 (Figure B-6b). From the ^{29}Si NMR resonances representative of the internal T-group silicon atoms, it is apparent that the silicon atoms that are further from the para- or meta- moieties exhibit less deconvolution for these resonances (they are closer together). Moreover, there is little to none deconvolution of the resonances associated with the *cis*-isomers (δ: -79.39 and -79.79). The quantity and correlation of these resonances with the ^{1}H NMR spectrum has not been determined. However, it is apparent from the convolution of the ^{1}H NMR, that this task would be very difficult. Additionally, no new resonances were easily observed in the ^{1}H NMR spectrum, this makes correlating what may be Si-atoms associated with **3d** particularly challenging.

B.5 Quantifying 3d using Liquid-chromatography/mass spectroscopy (LC/MS)

Since, the ^{1}H and ^{29}Si NMR spectra of compound **3d** appear to be too convoluted to determine the exact ratio of regio- and geometrical isomers in the sample, LCMS was used. Solvents used for liquid chromatography-mass spectroscopy were aqueous ammonium acetate and acetonitrile, obtained as HPLC-grade from Sigma Aldrich and used as received. Mass spectrometry analyses were conducted using a Waters Xevo G2-S QToF (Waters, USA) mass

spectrometer equipped with Acquity UPLC chromatography system. All mass spectrometric analyses and data processing were accomplished using MassLynx v. 4.1 software.[1]

LC/MS analysis was used to characterize isomers. Analytes were separated using an Ascentis Express C18 column (5 cm×2.1 mm; 2.7 μm particles) with a reversed phase binary gradient. Solvent A was 10 mM aqueous ammonium acetate and solvent B was acetonitrile. Total solvent flow was maintained at 0.25 mL/min, and gradient elution was performed using the following solvent compositions: initial, 1 % B, held for 1 min; linear gradient to 99 % B at 15 min and hold at this composition until 17 min; sudden decrease to 1 % B at 17.01 min and hold at this composition until 20 min. Injection volume and column temperature were 5 μL and 40 °C. Four peaks are seen in the m/z spectrum for compound **3d**; extracted in chromatograms for ions with m/z 1336.17 shows four peaks at 15.96, 16.12, 16.22 and 16.39. There are two peaks for each the all meta- (**3a**) and all para- (**3c**) structures (Figure B-7). Each of the two peaks in the spectra for compounds **3a** and **3c** are anticipated to be representative of individual *cis* and *trans* isomers. Therefore, six peaks would be anticipated for the spectra of compound **3d**, but only four are visualized. The peak at 15.96 is also apparent in the spectrum of compound **3c**. Additionally, peaks at 16.22 and 16.39 are apparent in the compound **3a** spectrum, and also overlap the peak on the right hand side of the compound **3c** spectrum. There is one definitive peak (16.12) that is not accounted for in the other spectra, which may be indicative of compound **3d**, but it is difficult to tell if this is representative of *trans*- and/or *cis*- isomers. Overall, these studies address that it is possible to quantify and separate the different regio-isomers that are produced in the synthesis of compound **3d**, but additional LCMS studies to further deconvolute the spectrum need to be carried out.

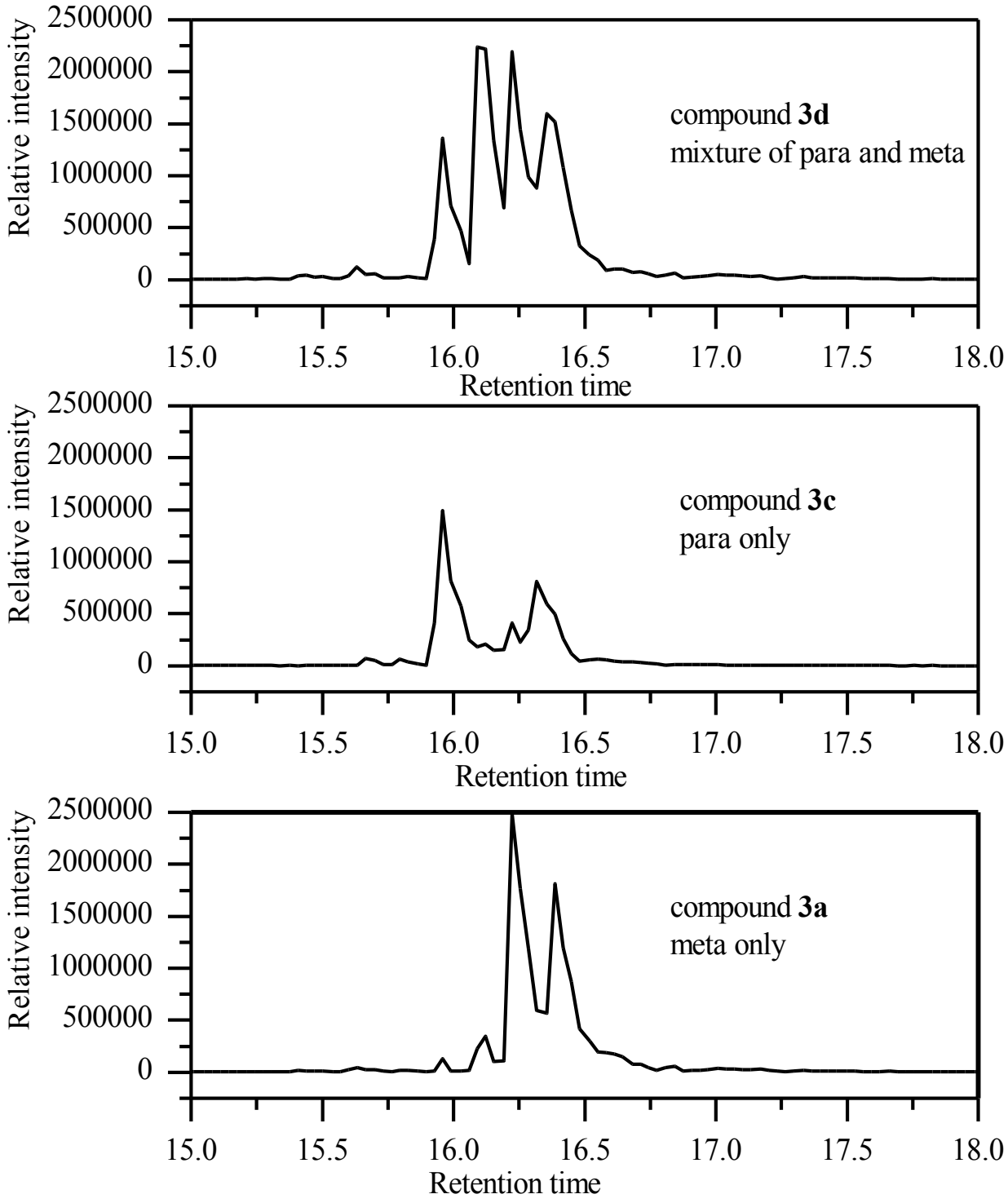

Figure B-7. LCMS spectra of compound **3d** (top), **3c** (middle), and **3a** (bottom).

REFERENCES

REFERENCES

(1) MassLynx v. 4.1 software, Waters Corporation, **2012**, USA

APPENDIX C.

SOLUBILITY BEHAVIOR

This appendix addresses the following key features that were not covered in chapter 5: (1) total mass balance of each isomer for the solubility studies, (2) R_F values associated with chromatography, and (3) the computational program that was designed for solubility modeling.

C. Solubility behavior

C.1 Total mass balance

Table C-1 summarizes the results of performing a total mass balance on the *cis* and *trans* isomers for the solubility studies. An example of the mass balance can be seen in equation C-1:

$$yield\ (\%\ cis) = \frac{(P1) * \left(\frac{1 - ppt1}{100}\right) + P2\ \left(\frac{ppt2}{100}\right)}{SM_{cis}} \qquad (C-1)$$

where *yield (% cis)* is the recovery of the *cis* isomer, *P1* and *P2* are the total masses (mg) of the products associated with ppt1 and ppt2, respectively, and *ppt1* is % *trans* isomers in *P1* and *ppt2* is the % *cis* isomers present in *P2*. Approximately 96 ± 8 % of the *cis* isomer is recovered for **3a**, 101 ± 10 % for **3b** and 86 ± 6 % for **3c**. For the *trans* isomer, approximately 96 ± 15 % is recovered for **3a**, 79 ± 24 % for **3b** and 90 ± 29 % for **3c**. Material balances that provide > 100 % yield, are mostly a result of the large % RE associated with that sample, and is majorly a result of the error associated with ^{1}H NMR (± 5 % confidence interval). Specifically, several of the *trans* isomer samples have > 100 % yield; since the quantity of *trans* isomer is so small that it is near or below the detection limit of ^{1}H NMR spectroscopy. Additionally, if the material did not fully dry, the mass could potentially be higher; specific examples follow.

Compound **3a**, experiment number 17 has a *yield* = 148 % *trans*. For this value, *ppt2* = 85 % *cis*. When *ppt2* = 90 % *cis*, which is within the ^{1}H NMR confidence interval (± 5 %), then the *yield* = 110 % *trans*. Although, 110 % is still high and relatively unrealistic, it shows that this experiment is within the error associated with ^{1}H NMR. Additionally, several other factors can be used to reinforce that this MB, although > 100 % is within experimental error. From chapter

5, it was determined that RE_{trans} = 33 % for experiment 17. Most of this error is a direct result of the mass of the SM (20 mg *trans*), which is lower than all the other SM for *trans*. Furthermore,

Table C-1. Total mass balance of the *cis* and *trans* isomers for compounds **3a**, **3b**, and **3c**.

Compound	Exp.	SM[a] (mg *cis*)	SM[a] (mg *trans*)	ppt1 (% *trans*)	ppt2 (% *cis*)	P1[c] (mg)	P2[d] (mg)	Yield (% *cis*)	Yield (% *trans*)	Overall Yield %
3a	1	551	477	84	90	450	512	97	90	94
	2	390	338	90	95	279	392	102	80	92
	3	237	255	58	86	427	58	97	100	99
	4	238	257	59	92	404	72	97	95	96
	5	342	368	96	99	369	327	99	97	98
	6[b]	525	520	85	77	423	470	81	90	85
	7[b]	533	575	93	83	496	549	92	97	94
	8[b]	279	425	95	75	350	328	94	97	96
	9[b]	66	337	97	31	163	220	110	92	95
	10[b]	178	738	96	60	545	457	115	108	109
	11[b]	29	417	99	16	298	136	84	98	97
	12[b]	583	505	91	93	429	586	100	86	93
	13	505	89	35	86	8	559	96	91	96
	14	376	77	20	91	267	157	95	88	94
	15	249	39	12	89	5	257	94	74	91
	16	879	167	15	85	448	569	98	91	97
	17	265	20	7	85	104	151	85	148	89
	18	429	76	33	84	20	455	92	105	94
3b	1	219	103	36	84	47	257	113	56	95
	2	188	48	31	86	113	117	95	107	97
	3	217	51	15	91	58	194	104	51	94
	4	142	80	29	73	86	128	109	74	96
	5	146	26	20	85	104	46	84	108	87
3c	1	199	133	71	99	161	131	89	87	88
	2	200	133	68	95	164	125	86	88	87
	3	433	289	78	96	323	322	88	92	89
	4[b]	214	142	82	87	130	193	90	93	91
	5[b]	211	141	88	86	129	193	86	100	91
	6[b]	86	211	92	71	159	86	85	81	82
	7[b]	93	227	92	63	202	105	89	99	96
	8[b]	144	337	93	39	177	286	86	101	96
	9	224	25	8	87	138	38	71	64	71
	10	322	36	3	88	263	73	99	47	94
	11	290	32	7	92	244	27	87	60	84
	12	493	55	32	97	268	217	80	168	88

[a] starting material; *cis:trans* ratio, [b] undersaturated *cis*, [c] P1 = product 1 (ppt1),
[d] P2 = product 2 (ppt2)

ppt1 has the lowest % *trans* of all the other experimental points. The same argument can be used for compound **3b**, experiment 5. For compound **3c**, experiments 7-12 a very similar argument can be made. The SM is approximately 90 % *cis*, which provided the values seen in Table C-1. If the SM were 95 % *cis*, then the following would be the reported *yield* % (Table C-2). Thus, overall, the material balances of the *cis* an *trans* isomers for compounds **3a-c** confirm that the solubility experiments were accurate.

Table C-2. The affect of the isomeric ratio in the SM on the MB of the *cis* and *trans* isomers for compound **3c**.

Compound	Exp.	SM[a] (mg *cis*)	SM[a] (mg *trans*)	ppt1 (% *trans*)	ppt2 (% *cis*)	P1[b] (mg)	P2[c] (mg)	Yield (% *cis*)	Yield (% *trans*)	Overall Yield %
3c	9	237	12	8	87	138	38	68	128	71
	10	340	18	3	88	263	73	94	93	94
	11	306	16	7	92	244	27	82	120	84
	12	521	27	32	97	268	217	75	337	88

[a] starting material in a ratio of *cis:trans*, [b] P1 = product 1 (ppt1), [c] P2 = product 2 (ppt2)

C.1 Retardation Factor (R_F)

The retardation factor (R_F) provides information on the ability for the compounds to move through a chromatography column. Experiments to determine the R_F for *cis* and *trans* isomers of compounds **3a-c** are accomplished with TLC plates. Mixtures of *cis* and *trans* isomers for each compound were dissolved in dichloromethane and a spot of each solution was place on a TLC plate similar to the procedure in chapter 5. The R_F values were determined by the ratio of the distance that the sample spot traveled up the TLC plate relative to the distance the solvent traveled (Equation II-2) and are summarized in Table C-3:

$$R_F = \frac{distance\ the\ sample\ traveled}{distance\ solvent\ traveled} \qquad (C-2)$$

Table C-3. Retardation factor determined from equation C-2, using TLC plates with spots of compounds **3a-c** dissolved in dichloromethane.

Compound	R_F *trans*	R_F *cis*	R_F *trans* - R_F *cis*
3a	0.563	0.438	0.125
3b-1	0.867	0.733	0.133
3b-2	0.533	0.667	0.133
3c	0.556	0.389	0.167

A smaller R_F value indicates that the material will move slower through the column. However, this can be dependent on the concentration of the sample. Thus, the actual R_F value of each isomer is not as important as the difference in the R_F values for the *cis* and *trans* isomers (R_F *cis* - R_F *trans*). A larger difference indicates that the isomers exhibit a larger degree of separation. As expected, the difference in the R_F values for compound **3c** is the largest and this compound exhibited the largest partitioning threshold of its isomers in terms of solubility, as seen in chapter 5. All values of R_F that are reported in Table C-3 are for a near equivalent mixture of *cis* and *trans* isomers. To see if the ratio of isomers affects the difference in the isomer R_F values, another sample of **3b** was used with a slightly higher *cis* isomer fraction. R_F *cis* - R_F *trans* = 0.133 for both, thus the isomer ratio does not have an affect on the difference in isomer R_F values.

C.3 Solubility modeling

Matlab[1] was used for the modeling portion of chapter 5. The functions that were programmed are below. Anything after a "%" is a comment.

```
function [xc,gc,parms]=ZcD
```

```
% xc are the calculated mole fractions, gc are the calculated activity coefficients, parms are the
calculated binary parameters, and ZcD is the program name

xtrans=[x1 x2 x3 x4;]; % values of the experimental data, can be as many rows as needed

xcis=[x1 x2 x3 x4;];

ntrans = size(xtrans,1); % size of the vectors, ntrans is the number of rows
ncis = size(xcis,1);
ntotal = ntrans + ncis;

dHv=[27*1472.2352 20*1472.2352]; % J/mol
Tmv=[265+273.15 250+273.15];          % K
temp=298.15;     % K
R=8.314;         % J/mol*K

% optimize parameters
parms = lsqnonlin(@calcobj,[3.5 -1],[-2 -4],[5.5 5.5]);
% calls calcobj function (see below) to optimize parameters

% set range of n1on2, extend calcs slightly beyond expt range
llim = min(xtrans(:,1)./xtrans(:,2)) - 0.2;
```

```
ulim = max(xtrans(:,1)./xtrans(:,2)) + 0.5;

% set up vector with 11 pts for n2on1 and n4on2 and initialize vectors
npts = 11;
n1on2v = linspace(llim,ulim,npts);

xc = zeros(npts,3);
gc = zeros(npts,3);
xc = zeros(npts,4);
gc = zeros(npts,4);

for j = 1:npts
   xc(j,2) = 1/(1 + n1on2v(j)); % material balances to find new x, g
   xc(j,1) = 1 - xc(j,2);
   [xc(j,:) gc(j,:)] = findx4(xc(j,:),j,dHv(1),dHv(2),Tmv(1),Tmv(2),parms);
end % for j
% now make a comparison plot
n1on2ex = xtrans(:,1)./xtrans(:,2);
semilogy(n1on2ex,xtrans(:,3),'o');
hold on
n1on2ex = xcis(:,1)./xcis(:,2);
semilogy(n1on2ex,xcis(:,4),'or');
```

```
% plot model
semilogy(n1on2v,xc(:,3),'b');
semilogy(n1on2v,xc(:,4),'-r');

xlabel('ratio of solvents, n1/n2')
ylabel('mole fraction of POSS at solubility limit')

hold off

hold off

%----------------------------
    function obj = calcobj(guessvalues)
        disp('---------------------')
        guessvalues;
        obj = zeros(ntotal,1);
        % parameters to adjust are in guessvalues(1) and guessvalues(2)
        for k = 1:ntotal
            k;
            dH = dHv(1);
            dH2= dHv(2);
            Tm = Tmv(1);
            Tm2= Tmv(2);
```

```
        if k<= ntrans
            x(k,:) = xtrans(k,:);
            [xc(k,:) gc(k,:)]= findx3(x(k,:),k,dH, dH2, Tm, Tm2, guessvalues);
            obj(k) = abs(log(xc(k,3)/x(k,3)));
        else
            x(k,:) = xcis(k-ntrans,:);
            % saturated with cis and trans
            [xc(k,:) gc(k,:)]= findx4(x(k,:),k, dH, dH2, Tm, Tm2, guessvalues);
            obj(k) = abs(log(xc(k,3)/x(k,3)))+abs(log(xc(k,4)/x(k,4)));
        end %if

    end %for
  end %function calcobj
%-------------------------
  function [xcrow gcrow ]= findx3(xrow, k, dH, dH2, Tm, Tm2, guessvalues)
    % find x based on saturation to fit only x(3)
    xold = 2; % force a step
    gcrow(3) = 1; % assume ideal solution
    gcrow(4) = 1;
    n1on2 = xrow(1)/xrow(2);
    n4on2 = xrow(4)/xrow(2);
    k;
    xcrow(3) = (exp((-dH/(R*temp))*(1-(temp/Tm))))/gcrow(3);
```

```
    xcrow(2) = (1-xcrow(3))/(1+n1on2+n4on2);
    xcrow(4) = xcrow(2)*n4on2;
    xcrow(1) = xcrow(2)*n1on2;
    gcrow = AAANRTL3(xcrow, temp, guessvalues(1),guessvalues(2));
    c=0;
    res=abs((xold - xcrow(3))/(xcrow(3)));

    while (res > 0.0001)
       gcrow = AAANRTL3(xcrow, temp, guessvalues(1),guessvalues(2));
       xcrow(3) = (exp((-dH/(R*temp))*(1-(temp/Tm))))/gcrow(3);
       xcrow(2) = (1-xcrow(3))/(1+n1on2+n4on2);
       xcrow(4) = xcrow(2)*n4on2;
       xcrow(1) = xcrow(2)*n1on2;
       c=c+1;
       res=abs((xold - xcrow(3))/(xcrow(3)));
       xold = xcrow(3);
    end  %while
  end %function findx3
%-------------------------
  function [xcrow gcrow ]= findx4(xrow, k, dH, dH2, Tm, Tm2, guessvalues)
    %function to fit x(3) and x(4)
    xold = [2 2];
    gcrow(3) = 1;
```

```
gcrow(4) = 1;
n1on2 = xrow(1)/xrow(2);
k;
xcrow(3) = (exp((-dH/(R*temp))*(1-(temp/Tm))))/gcrow(3);
xcrow(4) = (exp((-dH2/(R*temp))*(1-(temp/Tm2))))/gcrow(4);
xcrow(2) = (1 - xcrow(3)-xcrow(4))/(1 + n1on2);
xcrow(1) = 1 - xcrow(2) - xcrow(3)-xcrow(4);
gcrow = AAANRTL3(xcrow, temp, guessvalues(1),guessvalues(2));
c=0;

res=abs((xold(1) - xcrow(3))/(xcrow(3)))+abs((xold(2) - xcrow(4))/(xcrow(4)));

while (res > 0.0001)
   gcrow = AAANRTL3(xcrow, temp, guessvalues(1),guessvalues(2));
   xcrow(3) = (exp((-dH/(R*temp))*(1-(temp/Tm))))/gcrow(3);
   xcrow(4) = (exp((-dH2/(R*temp))*(1-(temp/Tm2))))/gcrow(4);
   xcrow(2) = (1 - xcrow(3)-xcrow(4))/(1 + n1on2);
   xcrow(1) = 1 - xcrow(2) -xcrow(3)-xcrow(4);

   c=c+1;
   res=abs((xold(1) - xcrow(3))/(xcrow(3)))+abs((xold(2) - xcrow(4))/(xcrow(4)));
   xold = [xcrow(3) xcrow(4)];
```

```
        end  %while
    end %function findx4
%-------------------------


end %USElsq




function gamma=AAANRTL3(moleFracs, temp, A13, A23)

%Row vector [Hexanes, THF, POSS]

x=moleFracs;

%this function defines the number of components
nComp=length(x);

%this will create a matrix with all the rows equal to the vector of
%compositions
Y = kron(x,ones(nComp,1));



%binary parameters for NRTL
```

```
aij=[0     0    A13   A13;
    0     0    A23   A23;
    A13   A23  0     0
    A13   A23  0     0;  ];

bij=[0          -15.0959    0      0;
    233.6258   0           0      0;
    0          0           0      0
    0          0           0      0;];

cij=[0     0.3   0.   0;
    0.3   0     0.   0;
    0.    0.    0    0
    0     0     0    0;];

%See Aspen reference for NRTL model
%tau is truncated after second term
%alpha is truncated after first term
tau=aij+bij/temp;
alpha=cij;
G=exp(-alpha.*tau);

term1=x*(tau.*G);
```

```
term2=x*G;

inverseterm2 = (1./term2);

squareinverseterm2=inverseterm2.^2;


part1=(term1./term2);

%part2=x*(tau.*G)'./term2

part2=inverseterm2*((Y.*tau.*G)');

%part3=-((x.*term1)*G')./(term2.^2);

part3=(term1.*squareinverseterm2)*((Y.*G)');


%logGamma=(term1./term2) + (x*(tau.*G)')./term2 - ((x.*term1)*G')./(term2.^2);

logGamma = part1 + part2 - part3;

gamma=exp(logGamma);


gamma(isnan(gamma))=1;

end
```

REFERENCES

REFERENCES

(1) MATLAB version R2011a; The Mathworks Inc.: Natick, Massachusetts, 2011.

APPENDIX D.

CRYSTAL STRUCTURES AND PHASE DIAGRAMS

This appendix addresses the following key features that were not covered in chapter 6:
(1) the tables and figures associated with the crystal structures and (2) the computation program used for modeling.

D. Crystal structures and phase diagrams

D.1 Crystal structures

Crystallographic data for all compounds are reported in Table D-1 through Table D-3. All structures are shown in Figures 6-8. Phenyl moieties and hydrogen atoms are not shown for simplicity.

Table D-1. Crystallographic data of compounds **3c**.

Compound	*trans*-**3c**	*cis*-**3c**
Empirical formula	$C_{62}H_{58}N_2O_{14}Si_{10}$	$C_{62}H_{58}N_2O_{14}Si_{10}$
FW (g/mol)	1336	1336
Crystal system	Monoclinic	Triclinic
Space group	P 2(1) / n	P-1
a (Å)	10.0493(9)	13.7676(14)
b (Å)	43.567(4)	17.5029(18)
c (Å)	14.5921(13)	27.499(3)
a (°)	90	87.1100(10)
b (°)	91.6600(10)	79.161(2)
g (°)	90	87.3850(10)
V ($Å^3$)	6386	6495.6
Z	4	4
ρ_{calcd} (Mg/m^3)	1.39	1.366
μ (mm-1)	0.272	0.267
F (0 0 0)	2784	2784
Crystal size (mm^3)	0.72 x 0.13 x 0.10	0.39 x 0.15 x 0.15
θ range (°)	1.47 - 25.42°	1.55 - 25.46°
Reflections collected	52876	23931
Independent reflections	11749	23931
Data / restr. / param.	11749 / 0 / 795	23931 / 0 / 1585
R(int)	0.0725	0
Final R_1 [$I > 2\sigma(I)$]	0.0495	0.0654
Final wR (F^2) [$I > 2\sigma(I)$]	0.106	0.1454
Final R_1 (all data)	0.0931	0.1264
Final wR (F^2) (all data)	0.1278	0.1655
Completeness to:	25.42° = 99.7%	25.46° = 99.3%
G-O-F on F^2	1.021	1.063
Lg. diff. peak/hole (e / $Å^3$)	0.9741 and 0.8272	0.9610 and 0.9029

Table D-2. Crystallographic data of compounds **3a**.

Compound	*trans*-**3a** Polymorph A	*trans*-**3a** Polymorph	*cis*-**3a**
Empirical formula	C_{62} H_{58} N_2 O_{14} Si_{10}	C_{62} H_{58} N_2 O_{14} Si_{10}	C_{62} H_{58} N_2 O_{14} Si_{10}
FW (g/mol)	1336	1336	1336
Crystal system	Triclinic	Triclinic	Monoclinic
Space group	P -1	P -1	C 2 / c
a (Å)	10.4549(6)	9.911(2)	20.8538(9)
b (Å)	12.7243(7)	13.532(3)	17.7674(7)
c (Å)	13.2241(8)	14.086(3)	17.6323(8)
a (°)	100.5230(10)	65.100(2)	90
b (°)	90.8660(10)	72.134(2)	95.9742(3)
g (°)	112.7660(10)	70.678(2)	90
V ($Å^3$)	1587.72(16)	1585.8(6)	6500.3(5)
Z	1	1	4
ρ_{calcd} (Mg/m^3)	1.397	1.399	1.365
μ (mm-1)	0.274	0.274	0.267
F (0 0 0)	696	696	2784
Crystal size (mm^3)	0.44 x 0.28 x 0.25	0.24 x 0.04 x 0.04	0.42 x 0.41 x 0.28
θ range (°)	1.77 – 25.28	1.63 – 25.32°	1.51 – 25.42°
Reflections collected	17266	18911	28342
Independent reflections	5763	5756	5974
Data / restr. / param.	5763 / 0 / 398	5756 / 0 / 398	5974 / 0 / 399
R(int)	0.0223	0.1235	0.035
Final R_1 [I > 2 σ (I)]	0.0316	0.0729	0.0503
Final wR (F^2) [I > 2 σ (I)]	0.0839	0.1787	0.1311
Final R_1 (all data)	0.036	0.1475	0.0653
Final wR (F^2) (all	0.0874	0.2145	0.1452
Completeness to:	25.28 ° = 99.8 %	25.32 ° = 99.7 %	25.42 ° = 99.4 %
G-O-F on F^2	1.049	1.034	1.047
Lg. diff. peak/hole ($e / Å^3$)	0.397 and -0.317	0.656 and -0.513	0.499 and -0.437

Table D-3. Crystallographic data of compounds **3b**.

Compound	*trans*-**3b** *Polymorph*	*trans*-**3b** Polymorph B	*trans*-**3b** Polymorph C
Empirical formula	C_{72} H_{74} N_2 O_{14} Si_{10}	C_{72} H_{74} N_2 O_{14} Si_{10}	C_{72} H_{74} N_2 O_{14} Si_{10}
FW (g/mol)	1472	1472	1472
Crystal system	Monoclinic	Triclinic	Triclinic
Space group	P 2(1) / c	P-1	P-1
a (Å)	13.8808(12)	11.4196(7)	10.9653(9)
b (Å)	20.5920(18)	12.2071(8)	12.9878(11)
c (Å)	14.3386(13)	14.5294(9)	14.4400(12)
a (°)	90	70.9960(10)	67.8970(10)
b (°)	117.9000(10)	76.2550(10)	81.1680(10)
g (°)	90	74.0800(10)	74.6940(10)
V ($Å^3$)	3622.07	1816.91	1834.37
Z	2	1	1
ρ_{calcd} (Mg/m^3)	1.35	1.346	1.33
μ (mm-1)	0.247	0.246	0.244
F (0 0 0)	1544	772	772
Crystal size	0.20 x 0.17 x 0.15	0.29 x 0.20 x 0.14	0.34 x 0.33 x 0.26
θ range (°)	1.66 - 25.33°	1.81 - 25.39°	1.74 - 25.41°
Reflections collected	29155	25277	30213
Independent reflections	6617	6689	6767
Data / restr. /	6617 / 0 / 442	6689 / 1018 / 612	6767 / 990 / 597
R(int)	0.0465	0.0405	0.0269
Final R_1 [I > 2 σ (I)]	0.051	0.084	0.0529
Final wR (F^2) [I > 2 σ (I)]	0.1313	0.2578	0.1643
Final R_1 (all data)	0.0729	0.1180	0.0612
Final wR (F^2) (all data)	0.1443	0.2943	0.1772
Completeness to:	25.33° = 99.8 %	25.39° = 99.9 %	25.41° = 99.8 %
G-O-F on F^2	1.03	1.038	0.87
Lg. diff. peak/hole ($e / Å^3$)	0.582 and -0.406	0.873 and -0.538	1.210 and -0.568

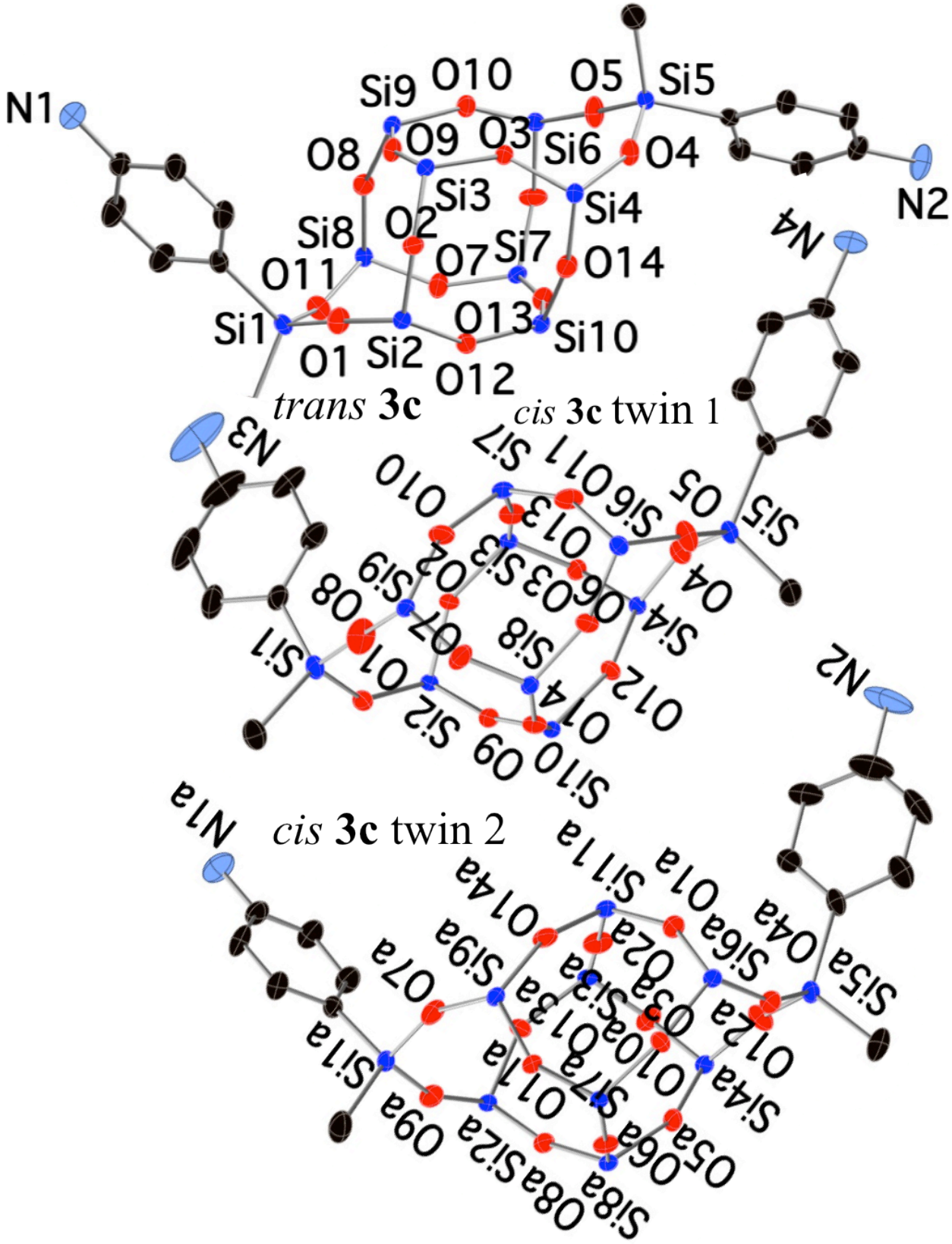

Figure D-1. Crystal structures for compound **3c**.

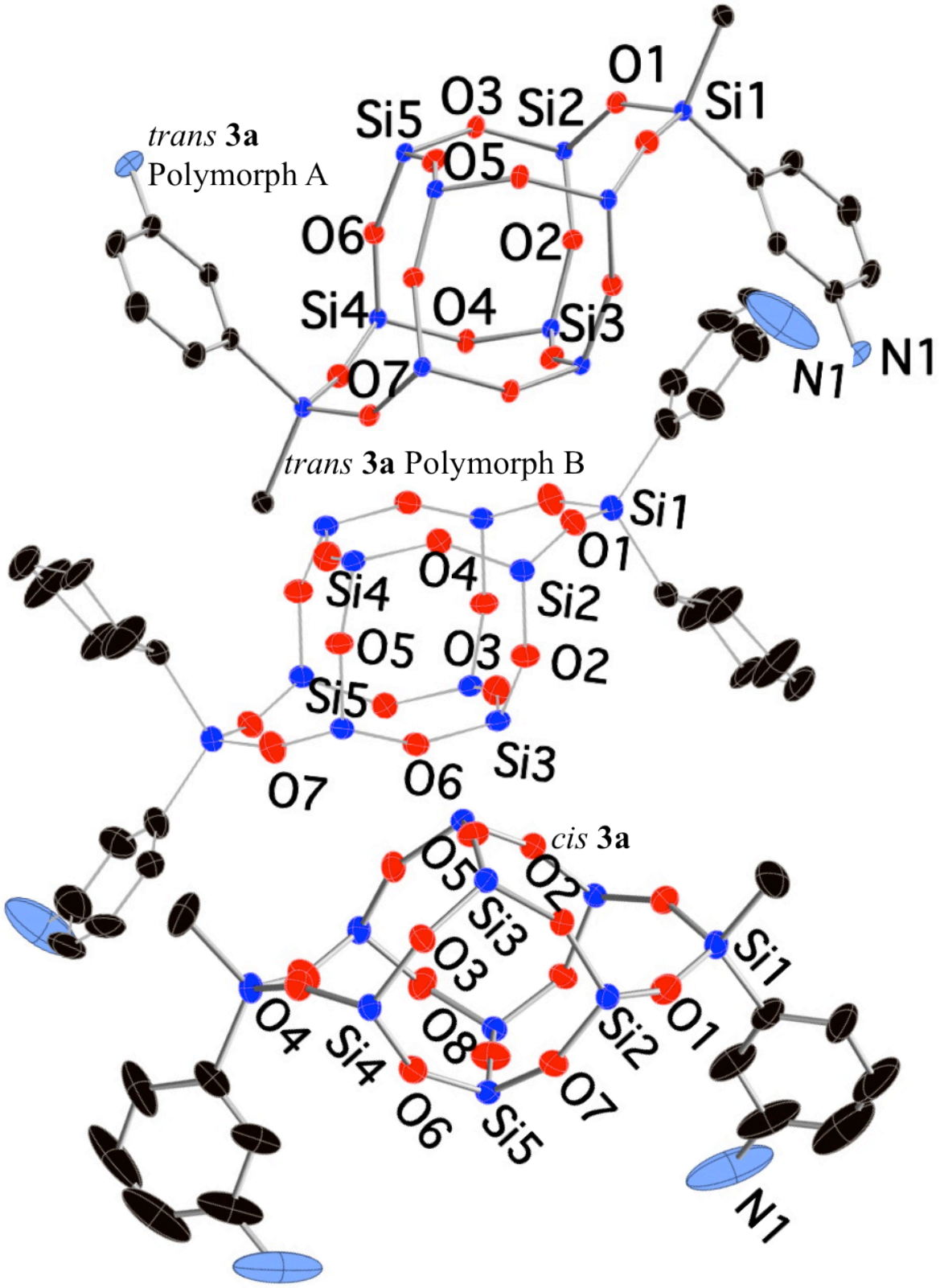

Figure D-2. Crystal structures for compound **3a**.

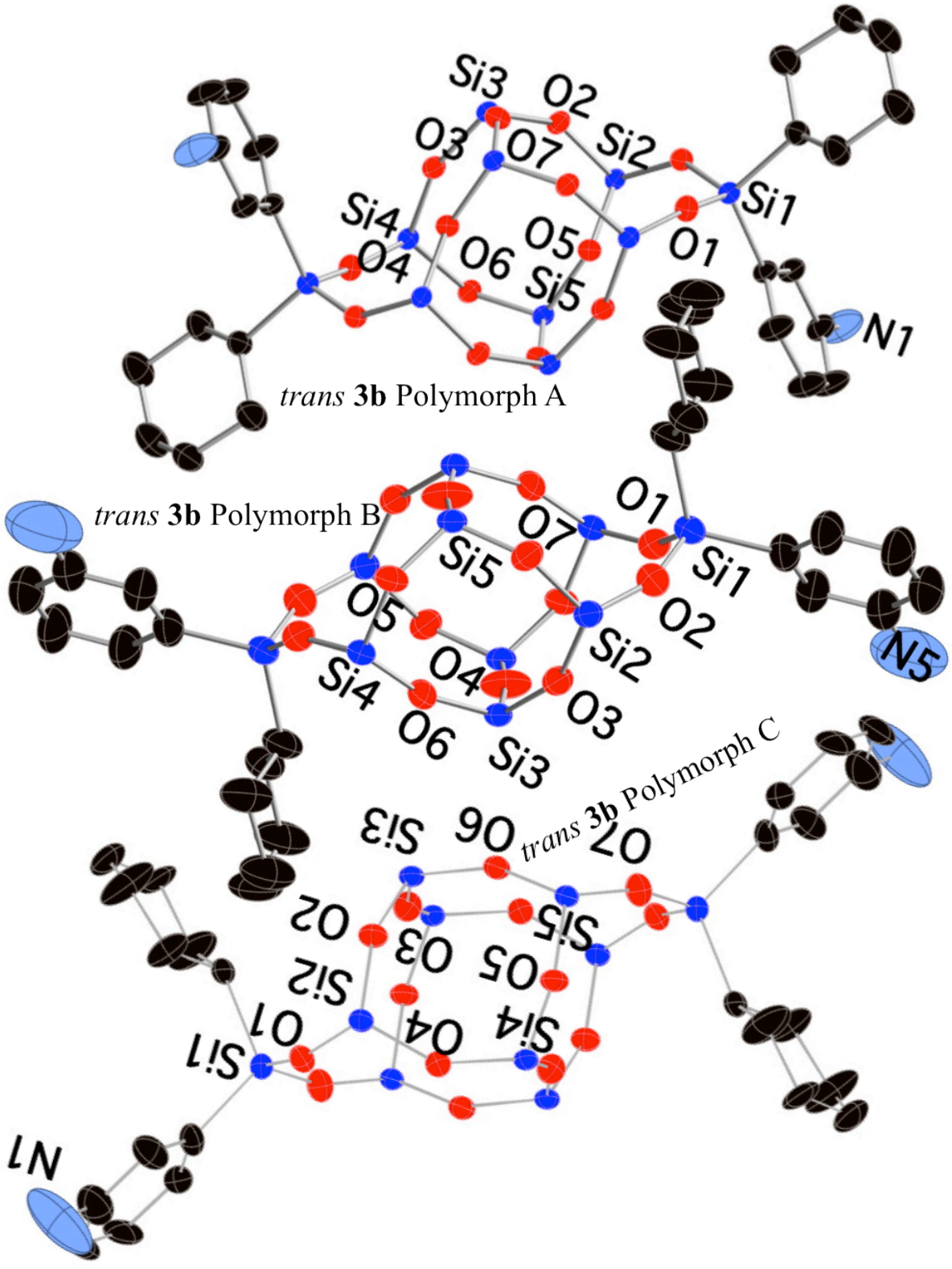

Figure D-3. Crystal structures for compound **3b**.

D.2 Phase diagram modeling

In order to fit the experimental data, a Matlab program, which was very similar to the one in the previous appendix was written and is shown below.

```
function [xcurve,gcurve,xcurve2, gcurve2, parms,temps,temps2]=tc1c5L


% This file has cis also.
%%
global ntotal dH dH2 Tm Tm2 x1 x2 temp R xc gc


%% These are the values of the mole fraction and the temperature.
db = load('fix1c.mat');


x1 = db.fixx(:,1);
temp = db.fixx(:,2) + 273.15; %K
x2 = 1-x1;


ntotal = size(x1,1);


dHv=[55000 38000]; %J/mol
Tmv=[310.6+273.15 275.7+273.15]; % K
R=8.314;        %J/mol*K


dH = dHv(1);
```

```
dH2 = dHv(2);


Tm = Tmv(1);
Tm2 = Tmv(2);


options = optimset('Display','iter');
% The parms are the initial guesses for the NRTLDSC file (A12 and A21).
parms = lsqnonlin(@calcobjtc1c5,[-0.03 3.35 100 100], [], [],options);


xcOUT = xc;
gcOUT = gc;


% Corresponding temperatures for trans.
 llim = 150; %C
 ulim = 310.6; %C
%
% % New temperature values
 temps = linspace(llim+273.15,ulim+273.15,100);
 npts = length(temps);
%
 for j = 1:npts
     [xcurve(j,:),gcurve(j,:)] = findx123(temps(j),dH, Tm, parms);
 end % for j
```

```
% Corresponding temperatures for cis.
 llim2 = 150; %C
 ulim2 = 275.7; %C

 % New temperature values
 temps2 = linspace(llim2+273.15,ulim2+273.15,100);
 npts2 = length(temps2);

 for j = 1:npts2
     [xcurve2(j,:),gcurve2(j,:)] = findx223(temps2(j),dH2, Tm2, parms);
 end % for j

figure(1)
%plot all experimental values
ph(1) = plot(x1(:,1),temp,'bo'); hold on;
%plot values from findx1 function, using trans dH and Tm
ph(2) = plot(xcurve(:,1),temps,'r-'); hold on;
%plot values from findx2 function, using cis dH and Tm
ph(3) = plot((1-xcurve2(:,1)),temps2,'r-'); hold off;


set(gcf,'Color',[1 1 1],'Position',[1000 600 1000 700],'InvertHardcopy','off');
```

```
set(gca, ...
  'Color'       , [0.8 0.8 0.8], ...
  'FontName'    , 'Times New Roman'   , ...
  'FontSize'    , 20       , ...
  'FontWeight'  , 'bold'    , ...
  'TickDir'     , 'in'      , ...
  'TickLength'  , [.02 .02] , ...
  'XMinorTick'  , 'on'      , ...
  'YMinorTick'  , 'on'      , ...
  'XGrid'       , 'on'      , ...
  'YGrid'       , 'on'      , ...
  'LineWidth'   , 1         );
ylabel('Temp','Interpreter','latex');
xlabel('XcNEW','Interpreter','latex');
legend(ph,{'xcNEW','x1'});



end


function obj = calcobjtc1c5(guessvalues)
global dH dH2 Tm Tm2 ntotal x1 x2 xc gc temp

    %disp('----------------------');
```

```
    obj = zeros(ntotal,1);
    xc = zeros(ntotal,2);
    gc = zeros(ntotal,2);


    for k = 1:ntotal
       if k < 7
       [xc(k,:), gc(k,:) ]= findx123(temp(k),dH, Tm, guessvalues);
       obj(k) = xc(k,1) - x1(k);
       else
       [xc(k,:), gc(k,:) ]= findx223(temp(k),dH2, Tm2, guessvalues);
       obj(k) = xc(k,2) - x2(k);
       end
    end

end

function [xcrow, gcrow ]= findx123(temp, dH, Tm, guessvalues)
    global R
    activity = (exp((-dH/(R*temp))*(1-(temp/Tm))));

    xcrow = fzero(@iterx,[1 0]);
```

```
    %xcrow(2) = 1-xcrow(1);

    function obj = iterx(x1c)
        gcrow = NRTLDSCa([x1c 1-x1c], temp,
guessvalues(1),guessvalues(2),guessvalues(3),guessvalues(4));
        obj = x1c*gcrow(1) - activity;
    end

end %function findx1

function [xcrow, gcrow ]= findx223(temp, dH2, Tm2, guessvalues)
    global R
    activity2 = (exp((-dH2/(R*temp))*(1-(temp/Tm2))));

    xcrow = fzero(@iterx,[0 1]);

    function obj = iterx(x2c)
        gcrow = NRTLDSCa([1-x2c x2c], temp,
guessvalues(1),guessvalues(2),guessvalues(3),guessvalues(4));
        obj = x2c*gcrow(2) - activity2;
    end

end %function findx2
```

```
function gamma=NRTLDSCa(moleFracs, temp, A12, A21,B12,B21)

%Row vector [Hexanes, THF, POSS]

x=moleFracs;

%this function defines the number of components
nComp=length(x);

%this will create a matrix with all the rows equal to the vector of
%compositions
Y = kron(x,ones(nComp,1));



%binary parameters for NRTL
aij=[0   A12    ;
    A21       0    ;  ];

bij=[0  B12     ;
    B21    0          ;];

cij=[0     0.3   ;
```

```
    0.3   0     ;];

%See Aspen reference for NRTL model
%tau is truncated after second term
%alpha is truncated after first term

% I took bij out because of the varying temp. I will need to fix this later

tau=aij+bij/temp;
alpha=cij;
G=exp(-alpha.*tau);

term1=x*(tau.*G);
term2=x*G;
inverseterm2 = (1./term2);
squareinverseterm2=inverseterm2.^2;

part1=(term1./term2);
%part2=x*(tau.*G)'./term2
part2=inverseterm2*((Y.*tau.*G)');
%part3=-((x.*term1)*G')./(term2.^2);
part3=(term1.*squareinverseterm2)*((Y.*G)');
```

```
%logGamma=(term1./term2) + (x*(tau.*G)')./term2 - ((x.*term1)*G')./(term2.^2);
logGamma = part1 + part2 - part3;
gamma=exp(logGamma);


gamma(isnan(gamma))=1;
end
```

REFERENCES

REFERENCES

(1) MATLAB version R2011a; The Mathworks Inc.: Natick, Massachusetts, 2011.

APPENDIX E.

APPLICATIONS

This appendix addresses the following key features regarding the following that were not covered in chapter 7:

(1) polyimide thermosets and (2) aromatic polyamides.

E. Applications

E.1 Polyimide thermoset

E.1.1 Synthesis of 5b

Cis and *trans* [(meta- phenylethynylphthalimide)cyclohexyl silyl]-bridged-(phenyl)$_8$-double-decker silsesquioxane, DDSQ(m-PEPI)(Cy)-**5b**, was also synthesized, but due to its highly crystalline nature, optimization of the product was not pursued. Under a nitrogen atmosphere, a well-stirred solution of Ph$_8$bisaniline-POSS (0.164 g, 0.093 mmol) and PEPA (0.051 g, 0.19 mmol) in anhydrous THF (2 mL) and anhydrous toluene (2 mL) was stirred at room temperature (25 °C) for one hour. After which, it was heated to 60 °C 2 h and then to 115 °C and refluxed for 20 h. Solvent was removed under vacuum until a white precipitate appeared. Methanol was added until no more precipitation occurred, and the product was filtered, and dried in a vacuum oven at 125 °C for 24 h. ^{1}H NMR, δ: 8.1-7.1 (64 H's, overlapping multiplets), 1.28-0.87 (10 H's).

E.1.2 General synthesis

It was determined that using a large excess of PEPA (> 100 % excess) in the reaction provided an optimized yield. When not enough excess is used, it is most noticeable in the ^{29}Si NMR spectrum. Figure E-1 depicts a *trans* **5c** with additional resonances in the region between -78 and - 80 ppm. It is anticipated that the most common impurity would be product that is not fully immidized (Figure E-2). During the reaction, THF and Toluene form an azeotrope with the water that is produced through the condensation reaction, allowing the imidization to occur and pushing the reaction towards completion. However, as depicted in Figure E-1, refluxing was not

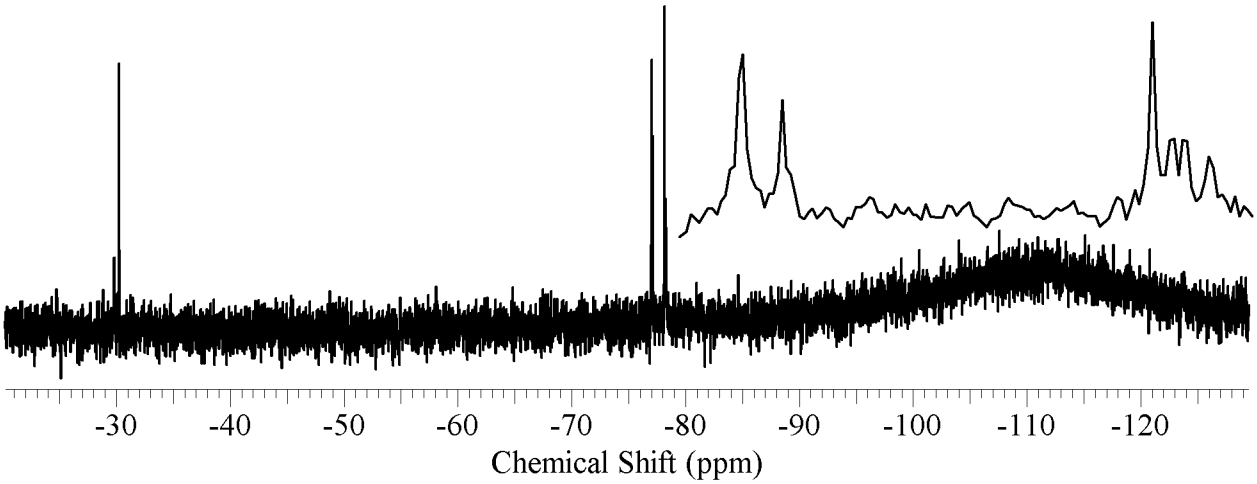

Figure E-1. ^{29}Si NMR spectrum of *trans* **5c** that is not a pure product.

enough to drive the product to completion. To ensure the imidization does occur, molecular sieves were added to the reaction flask, the yield improved, and ^{29}Si spectra did not contain additional resonances. When the reaction is driven to completion, the yield is generally > 80 %.

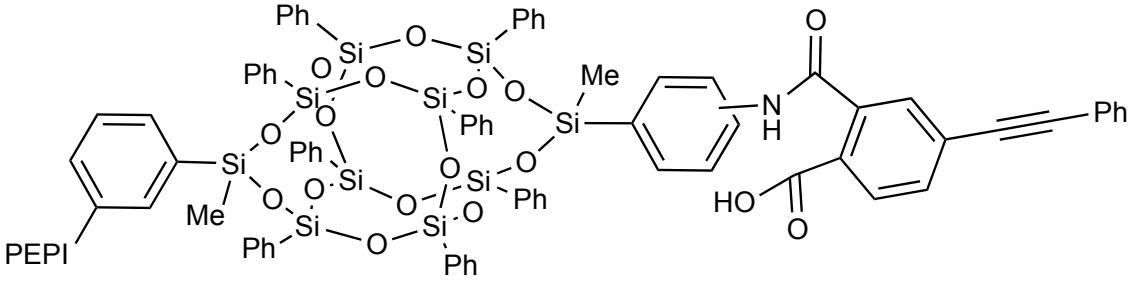

Figure E-2. Anticipated impurity in the synthesis of **5**.

E.1.2 Spectroscopy of 5d

The ^{29}Si NMR spectrum of compound 5d (Figure E-3) was distinctly different than the spectrum of compound **3d**. The D-group silicon region that previously showed four resonances in the spectrum of compound **3d** only shows two resonances in the spectrum of compound **5d**. Additionally, there are now four resonances in the region representing the external T-group silicon, while there were previously only two. The argument that was made for the four ^{29}Si

NMR resonances in the region of the D-group silicon in appendix B can also be made for the external T-group silicon here. The most noticeable difference is in the region of the internal T-group silicon, which is representative of the *cis* and *trans* isomers. For compounds **5a** and **5c**, these resonances appear in the order: *cis trans cis*. For compound **5a**, the distance from *cis* to *cis* (peak to peak) is approximately 0.2 ppm, and for compound **5c** it is 0.4 ppm. For the ^{29}Si NMR spectrum of compound **5d**, there are nine total resonances in this region (δ: -78.80, -78.87, -78.93, -78.98, -79.02, -79.07, -79.14, -79.17, -79.19). The resonance at -79.02 may actually be two overlapping resonances (which would make 10 resonances), similar to the two overlapping resonances representative of the *trans* isomer in the ^{29}Si NMR spectrum of compound **3d**. Three regions are circled on the spectrum in Figure E-3. Each of these regions appears to have the *cis trans cis* pattern, where the summation of the integration for both *cis* resonances is equivalent to the integration for one *trans* resonance. If this were accurate, then each region would be representative for **5a**, **5c**, or **5d**. However, according to the *cis* to *cis* distance that was mentioned previously, this is unlikely. Figure E-3 also shows the typical spacing of compounds **5a** and **5c**, on the spectrum for compound **5d**. Clearly, these can be the resonances depicting the all meta- and all para- DDSQ, and the remaining resonances (δ: -78.87, -78.98, -79.07, -79.17) could be representative of compound **5d**. The resonances in regions 1 and 3 may represent *cis* isomers, which suggests that the shifts at δ: -78.87 and -79.17 are associated with *cis* **5d**. There is twice as much **5d** as **5a** and **5c** due to the statistics of the synthetic procedure, and according to the ^{29}Si NMR, these resonances appear to fit that ratio. The resonances in region 2 (δ: -78.98 and -79.07) represent *trans* **5d**, and it is anticipated that each resonance is representative of a specific regio-environment; silicon atoms near the meta- and para-moieties.

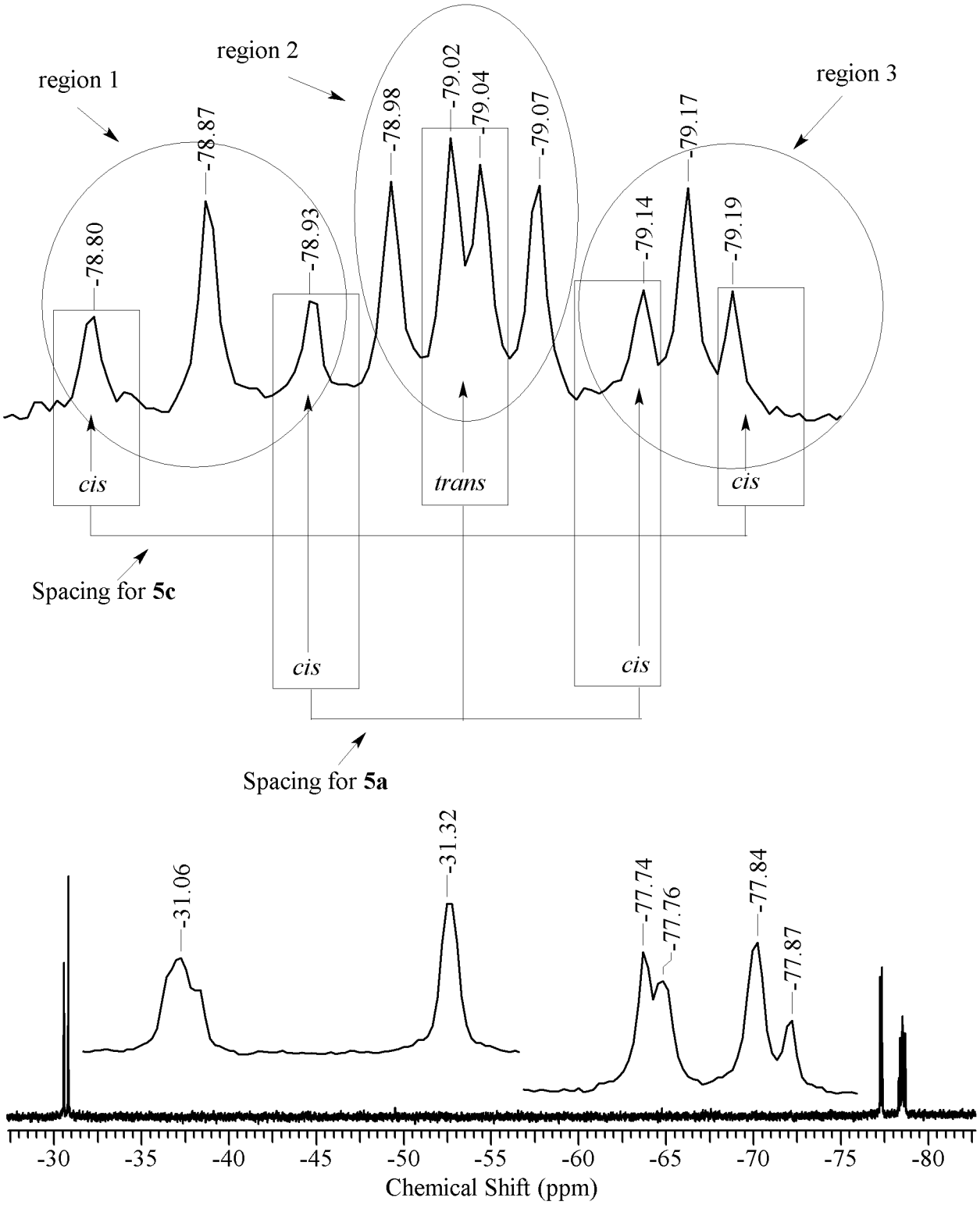

Figure E-3. ^{29}Si NMR spectrum of compound **5d**.

E.2 Polyaramide thermoplastic

Before the polyaramid synthesis, a model reaction with N-(trimethylsilyl)aniline with benzoyl chloride was investigated (Scheme E-1).[1] The silylated amine had to be synthesized first

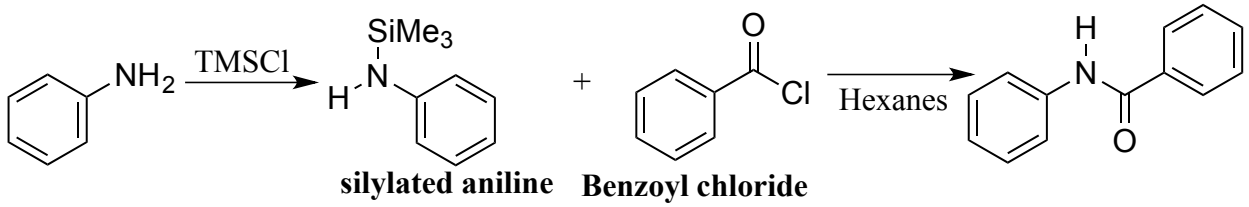

Scheme E-1. Model reaction for Nomex.

E.2.1 Silylated aniline

Under a nitrogen atmosphere, chlorotrimethylsilane (14.30 g, 0.132 mole) was added dropwise to a stirring solution of aniline (10.22 g, 0.1097 mole) and triethylamines (33.30 g, 0.329 mmole) at 60 °C. After 20 hours, solvent was removed by vacuum and the product was isolated by fractional distillation (T_{BP} = 40 – 49 °C, P = 435 – 444 mTorr) (14.0 g, 0.0847 mole, 77 % yield). ^{1}H NMR δ: 7.28 (2 H, t, J = 7.9 Hz), 6.85 (1 H, t, J = 7.4 Hz), 6.79 (2 H, d, J = 8.5 Hz), 3.54 (1H, NH, broad singlet), 0.41 (9 H, singlet) (Figure E-4).

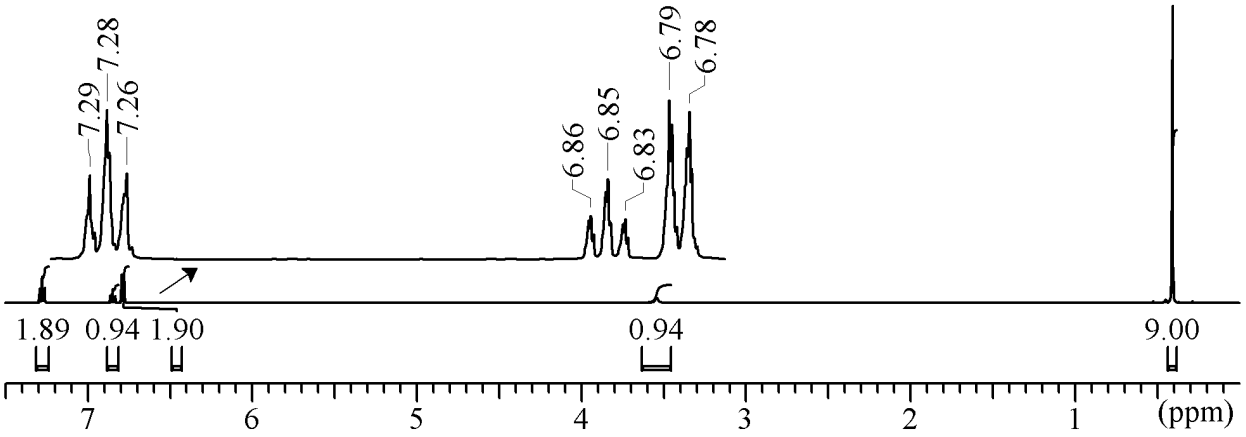

Figure E-4. ^{1}H NMR spectrum of silylated aniline.

E.2.2 Model Nomex

Under a nitrogen atmosphere a solution of benzoyl chloride (1.7 g, 0.012 mmole), was added dropwise to a stirring solution of silylated amines (2 g, 0.012 mmole) and hexanes (25 mL) at 25 °C. The product formed a white precipitate and was washed with hexanes and isolated by filtration (1.98 g, 0.011 mmole, 90 % yield). The IR spectrum showed characteristic absorptions at 3340 (NH) and 1655 (C=O) cm^{-1}.

REFERENCES

REFERENCES

(1) Oishi, Y.; Kakimoto, M. A.; Imai, Y. *Macromolecules* **1988**, *21*, 547.

APPENDIX F.

FUTURE WORK

This appendix addresses ideas for future work in this area.

F. Future work

F.1 Separate meta/para mixtures

One area of research that can easily be expanded upon would be evaluating the synthesis for compound **3d** such that the all meta-structures could be separated from the all para-structures and the one side meta- one side para-structure as shown again in Figure F-1. This could potentially be accomplished using further 2D NMR spectroscopy studies, or the LCMS analysis provided in appendix II.

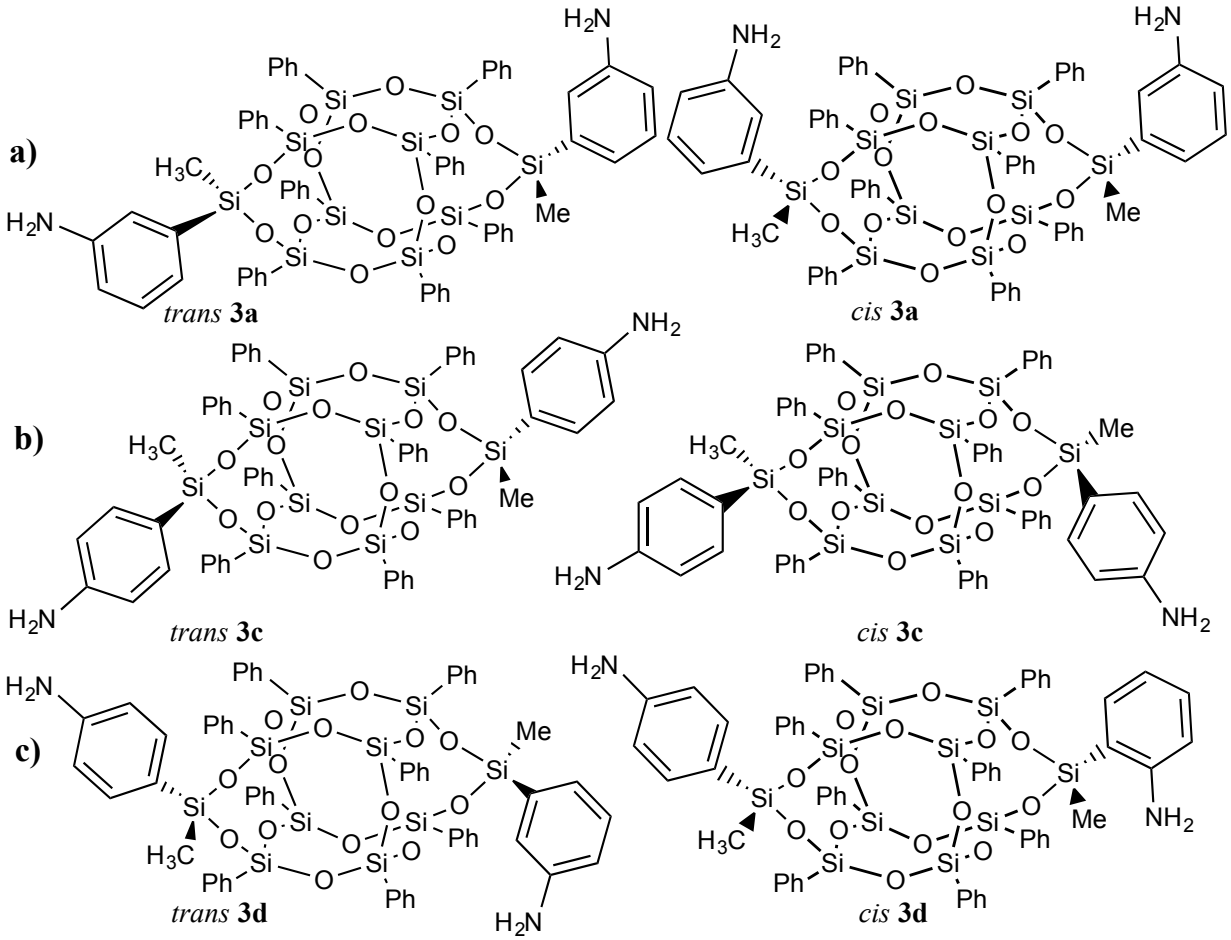

Figure F-1. Compound (a) **3a**-all meta-structure, (b) **3c**-all para-structure, and (c) **3d**-one side meta- and one side para-structure.

F.2 X-moiety = propylamine

Substituting the X-moiety for a propylamine as opposed to an aminophenyl (Figure F-2) moiety may provide evidence of why compound **3b**, with a cyclohexyl moiety, is an isomorphous solution. It has been suggested that since the cyclohexyl moiety is similar in size and shape to the aminophenyl moiety, the *cis* and *trans* isomers are not as different, thus providing similar crystal structures. Since a linear, propylamine, is more similar to the methyl moiety, this can be used to evaluate this theory. Additionally, determining the crystal structure for *cis* **3c** is also relevant to this future work section.

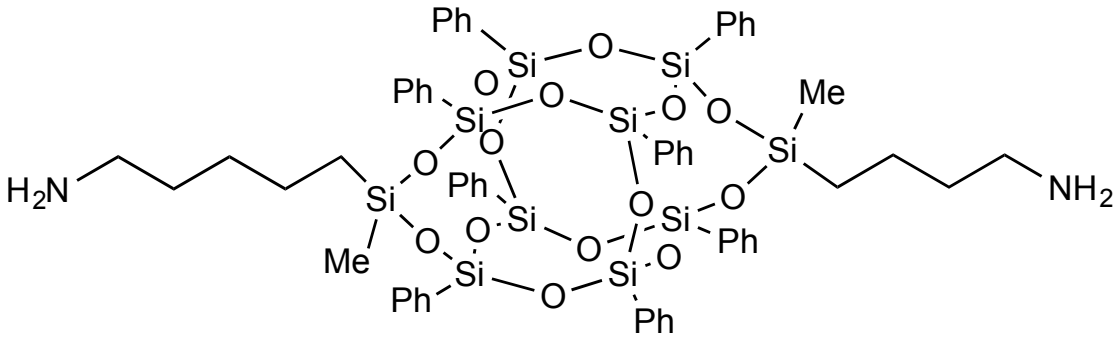

Figure F-2. DDSQ(propylamine)(Me).

F.3 Additional applications

Developing additional applications, or expanding upon the ones developed in this dissertation, that incorporate the distinctive features of the *cis* and *trans* isomers is central to the future of this research. Since a detailed analysis of the chemical and physical features of these *cis* and *trans* isomers has been established, the next step would be to apply this knowledge to the development of novel materials whose properties can be adjusted according to the quantity of *cis* and *trans* isomers used.